DYNAMIC MODELING OF STRUCTURAL JOINTS

A THESIS SUBMITTED TO
THE GRADUATE SCHOOL OF NATURAL AND APPLIED SCIENCES
OF
MIDDLE EAST TECHNICAL UNIVERSITY

BY

ŞERİFE TOL

IN PARTIAL FULFILLMENT OF THE REQUIREMENTS
FOR
THE DEGREE OF MASTER OF SCIENCE
IN
MECHANICAL ENGINEERING

MAY 2012

Approval of the thesis:

DYNAMIC MODELING OF STRUCTURAL JOINTS

submitted by **ŞERİFE TOL** in partial fulfillment of the requirements for the degree of **Master of Science in Mechanical Engineering Department, Middle East Technical University** by,

Prof. Dr. Canan Özgen _____
Dean, Graduate School of **Natural and Applied Sciences**

Prof. Dr. S. Suha Oral _____
Head of Department, **Mechanical Engineering**

Prof. Dr. H. Nevzat Özgüven _____
Supervisor, **Mechanical Engineering Dept., METU**

Examining Committee Members:

Prof. Dr. Samim Ünlüsoy _____
Mechanical Engineering Dept., METU

Prof. Dr. H. Nevzat Özgüven _____
Mechanical Engineering Dept., METU

Assist. Prof. Dr. Gökhan O. Özgen _____
Mechanical Engineering Dept., METU

Assist. Prof. Dr. Ender Ciğeroğlu _____
Mechanical Engineering Dept., METU

Prof. Dr. Yavuz Yaman _____
Aerospace Engineering Dept., METU

Date: 31.05.2012

I hereby declare that all information in this document has been obtained and presented in accordance with academic rules and ethical conduct. I also declare that, as required by these rules and conduct, I have fully cited and referenced all material and results that are not original to this work.

Name, Last name : Şerife TOL

Signature :

ABSTRACT

DYNAMIC MODELING OF STRUCTURAL JOINTS

Tol, Şerife
M.Sc., Department of Mechanical Engineering
Supervisor: Prof. Dr. H. Nevzat Özgüven

May 2012, 183 pages

Complex systems composed of many substructures include various structural joints connecting the substructures together. These mechanical connections play a significant role in predicting the dynamic characteristics of the assembled systems accurately. Therefore, equivalent dynamic models of joints that consist of stiffness and damping elements should be developed and the joint parameters should be determined for an accurate vibration analysis. Since it is difficult to estimate joint parameters accurately by using a pure analytical approach, it is a general practice to use experimental measurements to model joints connecting substructures. In this study an experimental identification method is suggested. In this approach the frequency response functions (FRFs) of substructures and the coupled structure are measured and FRF decoupling method is used to identify equivalent dynamic characteristics of bolted joints. Since rotational degrees of freedom (RDOF) in connection dynamics is very important, a structural joint is modeled with translational, rotational and cross-coupling stiffness and damping terms. FRF synthesis and finite-difference formulations are used for the estimation of unmeasured FRFs and RDOF related FRFs, respectively. The validity and application of the proposed method are demonstrated both numerically and experimentally. In simulation studies, simulated experimental values are used, and it

is seen that the identification results are prone to high errors due to noise in measurement and the matrix inversions in the identification equations. In order to reduce the effect of noise, it is proposed to extract the joint properties by taking the average of the results obtained at several frequencies in the frequency regions sensitive to joint parameters. Yet, it is observed in practical applications that experimental errors combine with the measurement noise and the identification results still may not be so accurate. In order to solve this problem, an update algorithm is developed. In the approach proposed, the identified dynamic parameters are used as initial estimates and then optimum dynamic parameters representing the joint are obtained by using an optimization algorithm. The application of the proposed method is performed on a bolted assembly. It is shown with experimental studies that this method is very successful in identifying bolted joint parameters. The accuracy and applicability of the identification method suggested are illustrated by using a dynamically identified bolt in a new structure, and showing that the calculated FRFs in which identified joint parameters are used, match perfectly with the measured ones for the new structure. In this study, the effects of bolt size and quality of bolts, as well as the bolt torque on the joint properties are also studied by making a series of experiments and identifying the joint parameters for each case.

Keywords: joint parameter identification, estimation of joint properties, dynamics of bolted connections, joint modeling

ÖZ

YAPISAL BAĞLANTILARIN DİNAMİK OLARAK MODELLENMESİ

Tol, Şerife
Yüksek Lisans, Makine Mühendisliği Bölümü
Tez Yöneticisi: Prof. Dr. H. Nevzat Özgüven

Mayıs 2012, 183 sayfa

Birçok parçadan oluşan karmaşık yapılar bu parçaları birbirine bağlayan çeşitli mekanik bağlantılar içermektedir. Bu mekanik bağlantılar, birleştirilmiş sistemlerin dinamik karakterlerinin doğru olarak tespit edilmesinde önemli bir rol oynamaktadır. Bundan dolayı, bağlantıların direngenlik ve sönüm elemanları içeren eşdeğer dinamik modelleri geliştirilmelidir ve doğru bir titreşim analizi için bağlantı parametreleri tespit edilmelidir. Sadece analitik bir yöntem kullanarak bağlantı parametrelerinin elde edilmesi zor olduğu için deneysel ölçümler kullanarak parçaları birleştiren bağlantıların modellenmesi genel bir uygulamadır. Bu çalışmada deneysel tanılama yöntemi önerilmiştir. Bu yaklaşımda parçaların ve tüm yapının frekans tepki fonksiyonları (FTF'leri) ölçülmüş ve ayrıştırma yöntemi kullanılarak cıvatalı bağlantıların eşdeğer dinamik karakteristiği saptanmıştır. Dönme serbestlik dereceleri bağlantı dinamiğinde çok önemli olduğu için; cıvatalı bağlantı; ötelenme, dönme ve çapraz bağlantılı direngenlik ve sönüm terimleri ile modellenmiştir. FTF sentezi ve sonlu-fark formülleri ölçülmemiş FTF'lerin ve dönme serbestlik dereceli FTF'lerin hesaplanmasında kullanılmaktadır. Önerilen yöntemlerin geçerliliği ve uygulaması sayısal ve deneysel çalışmalarla gösterilmiştir. Simülasyon

çalışmalarında teorik olarak hesaplanan değerler deneysel veriler olarak kullanılmış ve ölçümdeki gürültü ve denklemlerdeki matris ters alma işlemlerinden dolayı hesaplanan değerlerde yüksek hatalar oluştuğu görülmüştür. Gürültü etkisinin azaltılması için bağlantı parametrelerinin, bağlantı parametrelerine hassas olan frekans bölgelerinde birçok frekansta saptanmış olan sonuçlarının ortalaması alınarak elde edilmesi önerilmiştir. Yine de, gerçek deneysel uygulamalarda, deneysel hataların ölçüm gürültüsüyle birleşmiş olduğu ve hesaplanan değerlerin çok doğru olmayabileceği gözlenmiştir. Bu problemi çözmek için bir güncelleme algoritması geliştirilmiştir. Önerilen bu yaklaşımda, saptanan bağlantı parametreleri ilk tahmin olarak alınmış ve sonra bağlantıyı temsil eden en uygun dinamik parametreler bir optimizasyon algoritmasıyla elde edilmiştir. Önerilen yöntemin uygulaması cıvatalı bir yapı üzerinde gerçekleştirilmiştir. Deneysel çalışmalarla bu yöntemin cıvata bağlantı parametrelerini saptamakta oldukça başarılı olduğu gösterilmiştir. Sunulan tanılama yönteminin hassasiyeti ve uygulanabilirliği, dinamik olarak tanılanmış olan cıvatanın yeni bir sistemde kullanılması ve tanılanmış bağlantı parametreleri kullanılarak hesaplanan FTF'lerin yeni yapı için ölçülenler ile tam olarak örtüştüğünün gösterilmesi ile gösterilmiştir. Bu çalışmada, cıvata boyutu ve kalitesinin yanı sıra, sıkma torkunun da bağlantı dinamiği üzerinde etkisi, bir seri deneysel çalışma yapılarak ve her durum için bağlantı parametreleri hesaplanarak gösterilmiştir.

Anahtar kelimeler: bağlantı parametresi saptama, bağlantı özellikleri tahmini, cıvatalı bağlantıların dinamiği, bağlantı modellemesi

to my father, my mother and Evren

ACKNOWLEDGEMENTS

I would like to express my genuine appreciation to my supervisor Prof. Dr. H. Nevzat Özgüven for his guidance and contributions. His vision, style of thinking and knowledge contributed not only this study but also my understanding and future plans.

I am very grateful to my company ASELSAN Inc. and my colleagues. For their effort in supporting me with their technical knowledge, I must thank to İ. Furkan Lüleci and Deniz Mutlu. This thesis study could not have been finalized without their support and contributions. I am especially thankful to all my dear friends. They always shared my happiness and sadness and tried to help me.

I would like to thank to TÜBİTAK (The Scientific and Technological Research Council of Turkey) for the generous support through my graduate studies.

I would like to thank to my father, Ahmet Tol and to my mother, Selbi Tol for their love, support and encouragement in every stage of my life. I know that my achievements make them happier than me. I also would like to thank to my brothers, Eray Tol and Erhan Tol whom I always take as my model. I feel very confident in my life, since I have such brothers.

Evren, my fiancé, has always been with me even when there is overseas between us. He encourages me to reveal my self-confidence in my desperate times. Without his delicate support, I would feel so lonely. It is very simple to express my feelings to him: *"I love you just because of you"*.

Şerife

TABLE OF CONTENTS

LIST OF FIGURES

FIGURES

LIST OF TABLES

TABLES

NOMENCLATURE

A_{pqr}	: residue for response location p, reference location q, at mode r
E_o	: elastic modulus of sticking
E_t	: tangent modulus describing the slope of slip motion
F	: input force
F_c	: friction force
F_N	: normal load
$H(\omega)$	: frequency response function; when no ambiguity exist H is used instead of $H(\omega)$
$H_{pq}(\omega)$	: frequency response function for response location p, reference location q; when no ambiguity exist H_{pq} is used instead of $H_{pq}(\omega)$
$[H_{est}]$	: estimated FRFs
$[K^*(\omega)]$	: complex stiffness matrix
LA_{pq}	: Lower residual term (residual mass)
N	: number of modes
N_{inc}	: incomplete number of modes
$\overline{R}_{pq}(\omega)$	: residual terms
$[T_{2c}]$	: second-order-central transformation matrix
UA_{pq}	: Upper residual term (residual stiffness)
U_{pr}	: mode shape coefficients for response location p, reference location q, of mode r
a_r	: complex scaling constant
c_{Fy}	: Translational damping
$c_{F\theta}$	: Cross-coupling damping
$c_{M\theta}$	: Rotational damping

$\{f\}$: force vector

h :threshold forces

k : elastic spring

k_{Fy} : Translational stiffness

$k_{F\theta}$: Cross-coupling stiffness

$k_{M\theta}$: Rotational stiffness

j : $\sqrt{-1}$

m_r : modal mass for mode r

p : output, or response point (subscript)

q : input, or reference point (subscript)

r : mode number (subscript)

s : constant spacing

$\{x\}$: displacement vector

μ : friction coefficient

x : displacement in physical coordinates

υ : velocity difference between the sliding surfaces

κ :parameter controlling the influence of micro-slip

σ_0 : parameter indicating the stick limit equivalent to yield stress

ϕ_{pr} : scaled p^{th} response of normal modal vector for mode r

ζ : damping ratio

ζ_r : damping ratio for mode r

$\alpha_{1,2}$: roots of the characteristic equation

λ_r : pole value for mode r

λ_r^* : complex conjugate of the pole value for mode r

ω : variable of frequency (rad/sec)

ω_r : imaginary part of the system pole, or damped natural frequency, for mode r (rad/sec)

$\omega_r = \Omega_r\sqrt{1-\zeta_r}$

CHAPTER 1

INTRODUCTION

1.1 GENERAL OVERVIEW AND MOTIVATION FOR THE STUDY

Nowadays many finite element (FE) packages are widely used in structural dynamics problems due to the ease of access to commercial software and the recent advances in FE methods. Their accuracy of modeling a solid structure is usually satisfactory. However, most of the engineering structures exist in the form of assemblies of several components or substructures. Modeling and predicting the dynamics of assembled structures are far from the required accuracy and reliability. The results obtained from the actual test is usually differ from those of FE analysis, and this discrepancy is believed to be due to the uncertainty in material properties, joint characteristics, boundary conditions, etc. as well as the non-linearities that might exist. Among these, the characteristics of mechanical joints have large effect on system responses. As pointed out by Beards (1983), up to 60% of the deformation and 90% of the damping in an assembled structure can arise from various joints. Neglecting these effects can make the prediction on the property of the whole structure inaccurate or even unreasonable. Complex systems composed of many substructures include various mechanical joints such as bolts, welds, rivets and bearings connecting the substructures together. For these systems equivalent models of the joints that consist of masses, springs, and dampers should be developed. Therefore, the identification of joint parameters such as the stiffnesses and the damping coefficients play a significant role in predicting the dynamic characteristics of mechanical systems, which are very important for aerospace

structures, weapon systems, automotive applications, machine tools, and many other structural systems.

For instance, the nonlinear influence of structural connections causes the nonlinear transfer behavior of an assembled structure such as a large lightweight space structure. When designing an active control system, it is crucial to understand how the non-linear system parameters change with amplitude and frequency. According to Moon and Li (1990), small amounts of play in the joints could lead to chaotic dynamics in the response of the structure under periodic excitation. Then, this chaotic dynamics in space structures may impose some difficulties in the design of active control systems to damp out transient dynamics. In weapon systems, on the other hand, the constitutive behavior of mechanical joints is largely responsible for the energy dissipation and vibration damping with the characteristics of the overall structure. Furthermore, in automobile industry, noise, vibration and harshness characteristics of sheet metal structures such as vehicle frames are significantly affected by welded or adhesive joints and interfaces. Kamal and Wolf (1982) found that local compliances in automotive frames associated with structural joints are important. They recommended the addition of static rotational stiffness elements in linear finite element models, since such elements effectively model the slope discontinuities associated with structural joints. This improved the accuracy of their models by as much as 50%. In automotive systems, the joint mechanics problem is of interest not only from the structural acoustics standpoint, but also from the standpoint of static or fatigue analyses, impact strength and durability. For instance, the following noise and vibration control problems are found to be controlled by joints: a. Variation in elastic modes of deformation and their couplings with acoustic cavities, b. Influence of the joining process on perceived vehicle quality (Young et al., 2007). Moreover, contact dynamics at the spindle-holder and holder-tool interfaces influence the tool point frequency response function (FRF) considerably (Özşahin et al., 2009). Using the tool point FRF, the stability lobe diagrams for predicting regenerative chatter vibrations can be obtained. Since the contact stiffness and damping values alter the frequencies and peak values of dominant modes,

respectively, accurate identification of contact dynamics is very important in predicting the dynamic behavior and chatter stability of spindle-tool assemblies in machining centers.

1.2 OBJECTIVE

The aim of this thesis is to characterize structural joints dynamically. Since it is not always possible to derive accurate theoretical models of joints by using a purely analytical approach, FRF based joint identification method is proposed in this study. As it will be further explained in Chapter 2, there are several methods developed for the identification of joint parameters, but almost all of them are restricted to some particular applications and cannot easily be generalized. In this study it is aimed to provide a systematic approach to the identification of linear dynamic parameters of structural joints. One of the common problems of FRF based-methods is the incompleteness of the measured FRFs. In this study, it is intended to use a practical approach by employing FRF synthesis method for the unmeasured FRFs. The applicability of the method suggested is demonstrated with modal tests performed. Furthermore, the importance of rotational degrees of freedom (RDOF) in connection dynamics is clarified and a bolted joint is modeled with translational, rotational and cross-coupling stiffness and damping terms. The FRF decoupling method is further improved with respect to the practical aspects of the implementation of the method. Then, it is aimed to demonstrate the validity and applicability of the proposed method in various case studies performing several simulated and real experiments. The application of this method is intended to be performed on a bolted assembly. Furthermore, in this study, it is also intended to study the effect of different size and quality of bolts, as well as the bolt torque on the joint properties by making a series of experiments and identifying the joint parameters for each case. After identifying the joint parameters, the ultimate goal of this thesis is to incorporate the joint model into a FE model of a structure.

1.3 SCOPE OF THE THESIS

The outline of the thesis is presented as follows:

Chapter 2 reviews the relevant literature. A detailed survey on the problem of identification for linear and nonlinear joints is presented. The analytical models and experimental approaches used for the dynamic characterization of joints are explained.

Chapter 3 provides the basic theory of joint identification method. First, the general procedure of substructure uncoupling method is introduced. Then, the importance of the RDOF in joint modeling is explained and the estimation methods for FRFs are presented.

In Chapter 4, several simulation studies are given to verify and illustrate the application of the suggested method. Firstly, the joint properties are extracted in terms of stiffness and damping matrices for various cases. The importance of the rotational degrees of freedom is demonstrated with bolted beams, and different approaches in using the decoupling method are explained. Then, the effects of measurement noise on the identification results are studied and the error analysis is presented.

Chapter 5 gives several experimental studies to illustrate the real life application of the suggested method. Aluminum beams including M10x16 and M8x16 bolts and steel beams including M10x35, M8x35 and M6x30 bolts are tested and the equivalent dynamic properties of the bolted connections are determined. Then, with the identified joint parameters, receptances of new structures are obtained and these FRFs are compared with the measured FRFs of the new assemblies. Furthermore, the effect of different size and quality of bolts, as well as the bolt torque on the joint properties are studied in this chapter by first identifying joint parameters for each case from experimental measurements and then by comparing identified parameters.

Finally, general conclusions and recommendations for future research are presented in Chapter 6.

CHAPTER 2

LITERATURE REVIEW

This chapter is divided into three sections. Section 2.1 introduces identification problem of linear and nonlinear joints. In section 2.2, a brief overview of analytical models based on joint friction is provided. Finally, section 2.3 explains the experimental approaches for the identification of joint properties.

2.1 IDENTIFICATION OF LINEAR AND NONLINEAR JOINT PROPERTIES

Many engineering structures are assembled from components by using a variety of connections; such as bolted, riveted, welded and bonded joints. Due to the effect of joints on the dynamic behavior of assembled structures, the importance of joint modeling or the identification of joint dynamic properties has become more and more significant. Modeling methods which have been reported in literature can be basically classified into two categories: nonlinear joint models and linear joint models. The nonlinear joint models are used for the connections which include friction related nonlinearities in the interface surfaces. Due to the complex mechanism (macro-slip and micro-slip behavior) of frictional joints, the nonlinear models require a strong understanding and analytical description of the joints and interface. Furthermore, their applicability in experimental studies and validity in practical applications are not fully satisfactory. On the other hand, linear joint models including constant mass, stiffness and damping properties represent the firmly fastened connections. With the experiments performed on a bolted assembly under different excitation levels, Liu (2000) showed that, in normal working conditions,

fastened or tightened joints are in the stuck state and the structures are dominated by linear performance. However, it should be noted that the significance of joint nonlinear effect to the dynamic behavior of structures may change from case to case. In addition, for the low levels of excitation, a friction joint behaves like a linear component. Therefore, for the identification of joints whether it is linear or nonlinear, it is appropriate to start with developing methods for linear identification. After a full understanding of linear joint is gained, the method may be extended to identify nonlinear joints, or a new method, based on the understanding of linear joint identification, can be developed to deal with the problem of the nonlinear joint modeling (Ren, 1992).

2.2 ANALYTICAL APPROACH WITH JOINT FRICTION MODELS

Friction force in structural joints causes energy dissipation between contacting surfaces experiencing relative motion. During this relative motion shear and torsional forces arise between the parts. Tension in the bolt and the friction coefficient determines the degree of energy dissipation (Ibrahim and Pettit, 2005). The tension in the bolt changes due to relaxation of the bolt preload. Chesson and Munse (1964) reported that most of the loss occurs within a day after tightening up. They measured the variation of the bolt tension with time using strain gage load cell within the grip in relaxation tests and showed that after 21 days percent loss of the applied preload is 5%, however 90% percent of this loss is occurred in the first day. On the other hand, the friction coefficient is also not constant. It depends on the properties of contact surfaces which change during slip, and on the magnitude of the clamping pressure exerted by bolts (Groper and Hemmye, 1983). Bolted joints may slide and result in energy dissipation under dynamic loading. Groper (1985) defined two stages of loading for high strength friction grip bolted joints, namely micro-slip and macro-slip. The former occurs when the regions away from the hole experience slip while those close to the hole do not slip and the latter takes place for tangential loading causing slip over the entire contact surface. The basic models of friction for bolted

joints are classified into phenomenological and constitutive by Gaul and Nitsche (2001).

2.2.1 Phenomenological Description

Phenomenological models are based on the experimental observations and provide description of the relationship between the friction force and relative displacement in the frictional interface of the joint connection. The friction force acts as internal force in the tangential direction of the contacting surfaces. In static case, the frictional force balances net force tending to cause motion and prevents motion between surfaces. According to Coulomb's law there is a threshold value called traction for frictional force and above this motion would start. This phenomenon is described with static friction models regarding friction as a function of the velocity difference υ between the sliding surfaces. The static friction models include Signum-Friction Models and Elasto Slip Model.

Signum-Friction Models

This model describes the friction force with signum notation which is only valid in case of sliding. The friction force F is given by:

$$F = F_c sgn(\upsilon) = \mu F_N sgn(\upsilon) \tag{2.1}$$

where F_c is the friction force level which is proportional to the normal load F_N and μ is the friction coefficient. The relation between friction force and velocity is depicted in Figure 2.1.

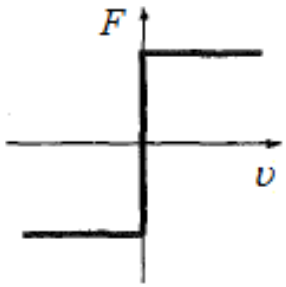

Figure 2.1 Signum-Friction Model (Gaul and Nitsche, 2001)

Elasto Slip Models

Sgn-based friction models do not account for deformation that can occur prior to the slip at the interface so sticking must be treated separately. For that reason, elasto slip models are developed and a set of spring-slider elements (so called Jenkins- or Masing- Elements) are used to model joint interface with an elastic spring k_i in series with an ideal Coulomb element with threshold forces h_i. A generalized model including Jenkins-Elements in parallel is seen in Figure 2.2.

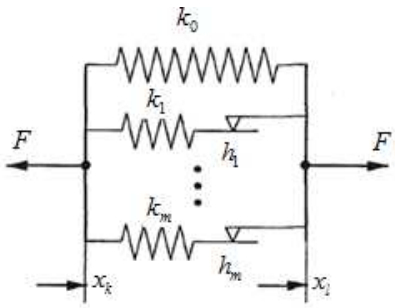

Figure 2.2 Generalized Elasto-Slip Model (Gaul and Nitsche, 2001)

The relation between force and velocity (depicted in Figure 2.3) is formulated as:

$$F(x,\dot{x}) = k_0 x + \sum_{i=1}^{m} \begin{cases} r_i(t) & |r_i(t)| < h_i \\ h_i \operatorname{sgn}(\dot{x}) \end{cases} \tag{2.2}$$

$$x = x_k - x_l, \quad |r_i(t)| = |k_i(x - x^+) - h_i \operatorname{sgn}(\dot{x}^+)|$$

where $x+$ denotes the displacement prior to velocity reversal.

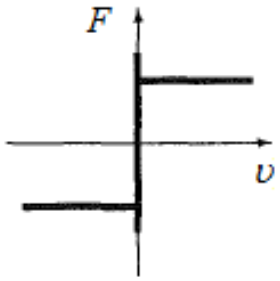

Figure 2.3 Elasto-Slip Model (Gaul and Nitsche, 2001)

Mayer and Gaul (2007) have implemented this approach to model contact interfaces of joints in finite element analysis (FEA). Using Masing model, they include the nonlinear influence of frictional micro-slip which results in frictional hysteresis in the contact interface of joints.

Segalman et al. (2003) depicted the stiffness model obtained with the parallel system of Jenkins elements (or sometimes called parallel-series Iwan model) as shown in Figure 2.4. The slope of the hysteresis curve gives the parameter of the joint which is the total stiffness of the contact patch. A detailed description of this model and its formulation can be found in Segalman (2000).

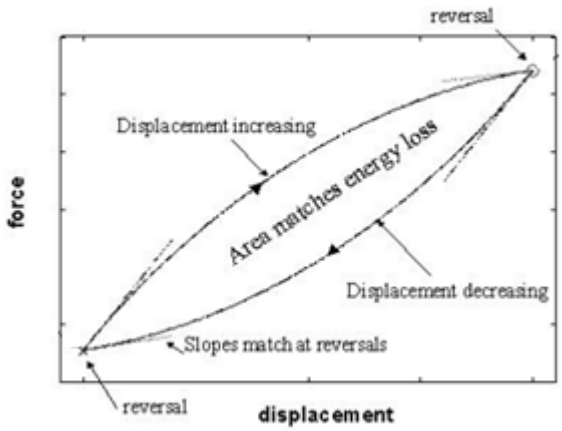

Figure 2.4 Stiffness Model (Segalman et al., 2003)

These static friction models do not always sufficiently describe joint friction concept, so by slightly modifying the static models dynamic models are obtained. The dynamic friction models include LuGre Model and Valanis Model.

LuGre (*Lu*nd-*Gre*noble) Model

In LuGre Model the friction interface is visualized as contact between bristles. The force generated in the contact surfaces is the starting point of the model derivation, as shown in Figure 2.5 (for simplicity the bristles of the lower part are assumed to be rigid). Due to the irregularities of the surfaces at the microscopic level, they make contact at a number of asperities which can be thought of as a contact through elastic bristles. With the application of a tangential force, the bristles deflect like springs and give rise to the friction force. If the force is sufficiently large, some of the bristles deflect so much that they slip of each other and new contacts are then formed. This process goes on as the two surfaces continue to move.

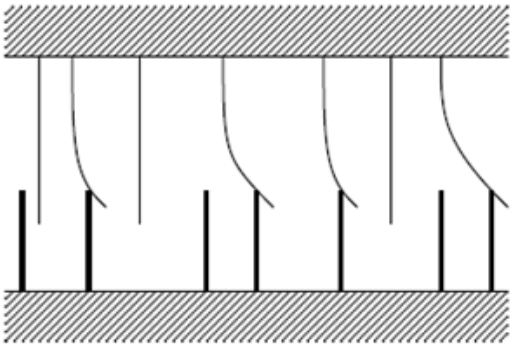

Figure 2.5 Model of the Friction Interface (Olsson, 1996)

Due to the irregular shape of the surfaces, contact phenomena are highly random. Therefore the model is based on the average behavior of the bristles that make up the contact, which is depicted in Figure 2.6. This friction model, used to describe nonlinear load and moment transfer behavior of joints (Gaul and Nitsche, 2000), makes it possible to describe pre-sliding displacement, stick-slip motion and other rate dependent friction phenomena. A detailed description of the model and its formulation can be found in Olsson (1996) and Canudas de Wit et al. (1995).

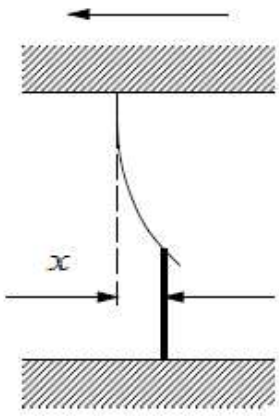

Figure 2.6 A Single Bristle Representing the Average Deflection of the Bristles (Olsson, 1996)

Valanis Model

In the study of Lenz and Gaul (1995); the Valanis Model, known from plasticity, is adopted in order to model the nonlinear transfer behavior of an isolated joint connection. Their aim was to obtain a single model containing the joint behavior in the local slip regime (micro-slip) and the global slip regime (macro-slip) experimentally. By having x as the relative displacement in the friction interface and F as the friction force, the constitutive equation for this model is stated as:

$$\dot{F} = \frac{E_0 \dot{x}\left[1 + \frac{\lambda}{E_0}\operatorname{sgn}(\dot{x})(E_t x - F)\right]}{1 + \kappa \frac{\lambda}{E_0}\operatorname{sgn}(\dot{x})(E_t x - F)} = \dot{F}(x, \dot{x}, F) \tag{2.3}$$

The physical meanings of the parameters in (2.3) are as follows: E_o is the elastic modulus of sticking, E_t is the tangent modulus describing the slope of slip motion, κ is the parameter controlling the influence of micro-slip (note that, high values of κ correspond to small influence of micro-slip) and σ_0 is the parameter indicating the stick limit equivalent to yield stress. These parameters can be identified from a measured hysteresis as shown in Figure 2.7.

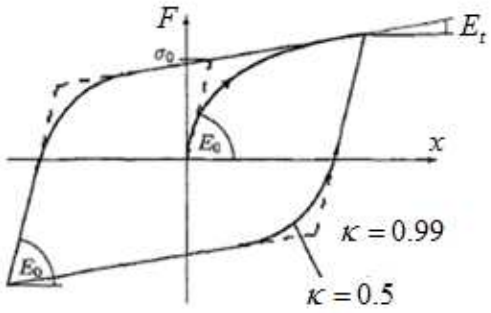

Figure 2.7 Closed Hysteresis of the Valanis Model (Gaul and Nitsche, 2001)

Furthermore, Gaul and Lenz (1997) have developed a finite element (FE) module to simulate micro-slip and macro-slip in the joint interfaces of the assembled structures by implementing the Valanis model as a nonlinear substructure module into a FE program. Hence, with this FE-module it becomes possible to predict the response of assembled structures in the design stage or to predict the influence of structural modifications.

2.2.2 Constitutive Description

Constitutive models deal with interface physics in the contact area and establish relationship between stress and displacement fields in a local manner. The finite-element method is often used for the description of local behavior in the contact surfaces. Contact mechanics with statistical surface roughness description (Willner and Gaul, 1995) and fractal characterization of surface roughness in joints (Majundar and Bhushan, 1991) are included in the constitutive description in order to obtain joint behavior.

In the analysis of structures with frictional joints three common solution techniques in terms of harmonic balance method, the time integration technique and exact solution technique are applied. For example, Ren et al. (1998) utilized the harmonic balance method for the identification of dynamic characteristics of nonlinear joints. Oldfield et al. (2005) and Ouyang et al. (2006) used Jenkins-element model for the friction torque in the joint and they reproduced the hysteresis loops using time integration technique.

In fact, the friction models of joints are not limited to those mentioned in this chapter, but these are the most widely used ones. The common point of all friction models is to obtain hysteresis curve and estimate parameters in the constitutive relations describing the transfer behavior of a joint connection. The other studies can be briefly explained as follows:

Manchu (2006) calculated the energy loss per cycle using the hysteresis curve and saw that energy loss per cycle increases with increasing the force amplitude. On the other hand, at the lower force levels the system behaves like a linear system and the equivalent viscous damping ratio is same. With increasing forcing amplitude, system becomes nonlinear and viscous damping ratio increases. The interesting point is that, when the force is increased further, behavior of the system is again linear in which case the viscous damping ratio remains constant for all force levels.

2.2.3 Modal Updating Methods

In literature there are several work using modal updating techniques for the dynamic characterization of assembled structures including joints. Magneval et al. (2007) estimated parameters of hysteresis elements using harmonic input. They tested a structure connected with a bolted joint and excite this system with different forcing levels. Using the linear FRFs obtained from the low level excitation, they calculated the nonlinear FRF analytically. From the difference between the measured and analytic nonlinear FRFs they update the parameters in their analytical model using a minimization algorithm. However, this method fails in the prediction of the FRF of the actual system at high levels of excitation.

Böswald and Link (2005) used a similar approach in their work. They developed a nonlinear modal updating algorithm using the equivalent stiffness and damping obtained in the harmonic balance method.

Ahmadian and Jalali (2007a) modeled the bolted lap joint as a combination of linear and nonlinear springs with a viscous damper representing the energy dissipation of the joint. They identified these parameters by minimizing the discrepancies between the calculated and the measured frequency response functions. Later a generic element formulation consisting of a generic stiffness and a generic damping matrix to model the nonlinear behavior of bolted lap joints was presented by the same authors (Ahmadian and Jalali, 2007b). They used this generic element used in a FE model of

a jointed beam structure and obtained the analytical nonlinear frequency response functions utilizing the incremental harmonic balance method. By minimizing the difference between analytical nonlinear frequency response curves with their experimental counterparts, they identified the joint parameters.

Jalali et al. (2007) represented the bolted lap joint with a linear viscous damper and cubic stiffness. They identified these parameters for different excitation levels using steady state response of the structure and employing force state mapping technique. They updated a FE model of a beam with linear joint, hence, eliminated the need for the direct force and displacement measurements at the joint.

2.3 EXPERIMENTAL APPROACH

The dynamic properties of joints are difficult to model analytically. Experimental approach is used as an alternative approach for establishing a mathematical model for a joint. The main parameters considered in structural dynamics are stiffness and damping of a joint. Hence, the aim of the experimental approach is to identify joint properties in terms of stiffness and damping values.

2.3.1 Modal Based Identification Methods

In the past, several techniques have been developed in order to estimate the joint properties by using modal parameters obtained from modal test. Yuan and Wu (1985) used condensation technique for the FE model with incomplete mode shapes and identified the joint parameter matrices. Similarly, Kim et al. (1989) combined the FE model of a structure with the results of experimental modal analysis to investigate the joint stiffness and damping characteristics of a tool-holder system with a taper joint. Wang and Sas (1990) used the natural frequency and damping ratio information obtained from modal testing and characterized the bolted joints in a beam. Due to the fact that the measured resonance frequencies are much more

accurate than the measured damping ratios in experimental modal analysis, their formulation predicted stiffness more accurately than damping. Since it is difficult to extract accurate modal parameters in the case of high modal density and large damping, the joint properties cannot be estimated accurately by using modal based methods. In order to overcome these problems, Frequency Response Functions (FRFs) of the assembled system and its substructures were directly used.

2.3.2 FRF Based Identification Methods

FRF-based joint identification methods are usually more advantageous than modal-based methods due to the following reasons (Nobari, 1991):

- relative ease in handling damping problem,
- simplicity of the FRF-based coupling techniques,
- in the case of a pure experimental analysis, there is no need for modal analysis when using an FRF-based identification method,
- having measured FRFs for a limited frequency range, the effect of out-of-range modes is already reflected in the measured data, and
- usually, the amount of information measured in the frequency domain is large and this provides the flexibility of selecting proper data points for an identification analysis.

Ren (1992) pointed out another advantage of FRF based methods. Such methods give the identification results in frequency domain, so the FRF data at one frequency is enough for the identification. However, for a nonlinear joint due to change of its properties with frequency, it is not possible to find a linear joint to represent the nonlinear joint over a whole range of frequencies. Yet, at one frequency or in a narrow frequency range, the properties of the nonlinear joints can be represented by an equivalent linear joint. So the FRF based identification is more attractive than the modal based identification methods for nonlinear joint studies, as well. For example, Kashani and Nobari (2010) used an identification method based on optimum

equivalent linear FRF and extracted the dynamic parameters of the nonlinear elements in the system.

In the past decade, several researches were focused on the identification of joint properties using FRF based methods. These identification techniques are based on the fact that if the properties of the structure without joints (which is referred to as the substructure system) and the structure with joints (which is referred to as the assembled system) are known (experimentally/analytically), from the difference between the dynamic properties of the substructure and assembled systems, the joint properties can be identified. However, due to the inherent noise in measurements and different sensitivities of the formulations to noise, accuracy of the identification results differs. The reason for this sensitivity and ways of coping with it are investigated in several studies.

Tsai and Chou (1988) formulated the joint parameter identification based on the substructure FRF synthesis method. In their method, mass of the joint is neglected due to the dominance of the stiffness and damping in dynamic properties, hence, only the stiffness and damping of the bolted joint are considered. However, it is seen from the experimental results that the method had some problems due to the unavoidable noise in the FRFs measured.

Wang and Liou (1991) extended the work of Tsai and Chou (1988). They modeled joints with diagonal matrices and developed an algorithm to reduce the noise effect. In their algorithm, the inversion of the FRF matrix is avoided, so the redistribution and amplification of the measured noise are prevented. Hence, the problem caused by ill-conditioned FRF matrix (especially when the orders of magnitude of the elements of the FRF matrices are very different) is avoided as well. They used least squares method in the joint parameters identification. Due to the nature of this method, the smaller parameter in the identification is calculated with a larger percentage error. They overcame this difficulty by identifying the damping coefficient, which is too small in comparison with the stiffness, separately.

Wang and Chuang (2004) developed a new identification algorithm to improve the identified results of Wang and Liou (1991). With the new algorithm, they used error functions and tried to solve the problem of the measured noise with non-Gaussian distribution in FRFs.

Hwang (1998) identified the stiffness parameter of a connection by subtracting the inverted FRF matrices of the structure without joints from those of the structure with joints. His identification formulation is similar to the formulation of Wang and Liou (1991). However, he used an averaging process excluding the FRF near the resonance zones in order to reduce the noise effect. For the estimation of joint parameters, these methods require or use the measured FRFs related to the joint interface degrees of freedoms (dofs) which are not easy to be obtained in real structures.

Yang et.al (2003) improved the methods of Tsai and Chou (1988) and Wang and Liou (1991) by eliminating the need for joint related FRFs, and derived the identification equations for joints using substructure synthesis method with measured FRFs. Their joint model is composed of a coupled stiffness matrix including translational and rotational springs, which is given in Figure 2.8.

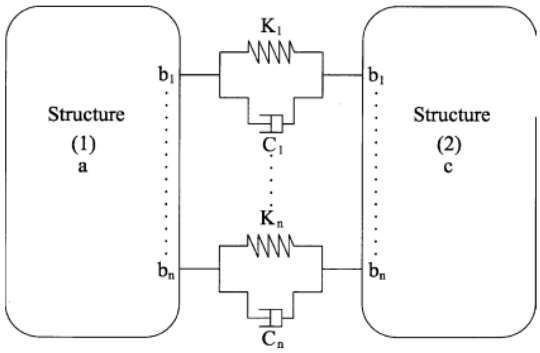

Figure 2.8 Substructures and Joints (Yang et.al, 2003)

In order to obtain the FRFs related to the rotational degrees of freedom (RDOF), they utilized finite element analysis. In the solution of the identification equations singular value decomposition (SVD) technique is used to reduce the noise effect. Their results seem to be promising; however, damping parameters of the joint is not included in their work. Furthermore, they assumed one of the substructures as rigid and simplified their model as seen in Figure 2.9. Since the application of their formulation is useful only when one of the substructures is rigid, their approach does not provide a general identification method. Later, Hu et al. (2009) used the same method for the identification of dynamic stiffness matrix of a bearing joint region.

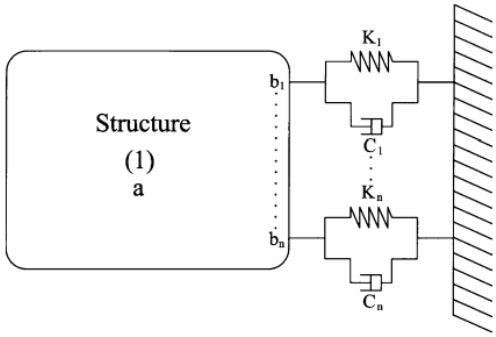

Figure 2.9 Joints at the Boundary of the Structure (Yang et.al, 2003)

Yang and Park (1993) employed an iterative approach in the joint identification. They obtained the FRFs of the assembled structure experimentally and developed a new method (for the cases in which measurement of FRFs related to joint coordinates is not practical) to estimate unmeasured FRFs from the measured ones. After one column of the FRF matrix is obtained from partly estimated and partly measured FRFs, joint parameters are identified iteratively with the minimization of loss function. With the developed method, besides the joint related FRFs, FRFs including RDOF can be calculated. They proposed and evaluated the validity of three different joint models in terms of translational parameters only, translational and rotational

parameters, and translational and rotational parameters with cross-coupling terms. In order to reduce the effect of identification errors, they used weighting techniques.

Ren and Beards (1995a) developed a new physically and mathematically generalized receptance coupling method and implemented this coupling process in a single step for multiple connections. They identified the mass, stiffness and damping parameters of the joint with this method (Ren and Beards, 1995b). They used least squares solution which is dominated by the equations with larger coefficients. To scale equations a weighting technique was used, hence better solution was obtained with proper consideration of information at all frequencies and all locations. However, in the experimental verification, they used exponential window in measuring the response signal which introduced artificial damping into the FRFs and resulted in incorrect identification of damping parameter. In another work, they eliminated stiff joints in the identification process, hence, avoiding the singular or ill-conditioned matrix in the identification formulation (Ren and Beards, 1998).

Silva et al. (1996) presented uncoupling method and in order to avoid direct use of data with experimental errors, they regenerated the FRFs from a mathematical model using the modal parameters obtained from the experimental data. Later, Maia et al. (1998) utilized this uncoupling technique for the dynamic characterization of joints. Despite this process brought with some difficulties, it has the advantage of eliminating the need for the measurement of FRFs at the joint coordinates. However, it is seen that the identification results deteriorates when the differences between the responses of the coupled structure and substructure are very small.

Liu and Ewins (2002) developed a new FRF coupling analysis method called generalized joint describing method. Actually, they improved the method used in the work at Ren and Beards (1998). The new method, in respect of the substructure coupling analysis, lies in the joint description and synthesis with substructures.

The FRF-based methods described above are direct methods in which the joint parameters are directly obtained using the measured/calculated FRFs. Due to the inverse matrix operations in the formulations; the results are prone to error. Hence, Lee and Hwang (2007) developed a new optimization technique which is regarded as an indirect method to improve results. While reducing the noise effect through indirect formulation, their method maintains the advantages of FRF-based methods.

Čelič and Boltežar (2008) improved the work of Ren and Beards (1995, 1998) with the addition of RDOF. A more detailed and clear formulation of their method is given in their later work (Čelič and Boltežar, 2009). They used the FRF estimation technique (Yang and Park, 1993) to obtain the unmeasured FRFs at the RDOF coordinates from the measured FRFs including translational degrees of freedom (TDOF). Using the partly measured and partly estimated FRFs, they identified the joint properties in terms of mass, stiffness and hysteretic damping.

Batista and Maia (2011) improved the methods of Ren and Beard (1995a) and Maia et al. (1998) and compared the identification results through numerical examples. They proposed addition of local inertial elements to deal with the ill-conditioning problems, from which most substructure synthesis methods suffer. However, their approach has not been validated with experimental data yet.

The FRF-based substructuring methods are so versatile that they were used in several studies for the joint identification of modular tools (Özşahin et al., 2009; Park and Chae, 2008; Mao et al., 2010). For instance, Özşahin et al. (2009) implemented the elastic coupling method in a reverse manner, and they identified the contact parameters between spindle-holder and tool. In identification they used the measured FRFs of the spindle-holder-tool assembly (which can be regarded as a coupled structure), and the calculated/ measured FRFs of the cutting tool and spindle-holder (which can be regarded as substructures).

De Klerk et al. (2008) presented a brief overview about the experimental dynamic substructuring. They discussed the main difficulties and proposed solutions. First, the truncation errors in the experimental modal analysis cause problems in modal based methods and the inclusion of the residual terms is the remedy. Secondly, the RDOF is another source of difficulty, because measurement of the rotational FRFs is not easy and practical. In order to tackle this problem, estimation methods using the translational FRFs were proposed in literature (Yang and Park, 1993 and Duarte and Ewins, 2000). Finally, the experimental errors affect the response of the coupled system. These experimental errors include random measurement noise which can be overcome by averaging.

From the literature discussed above, the other major concerns about the implementation of the substructure synthesis or substructure coupling methods can be summarized as:

- incompleteness of the FRF measurements,
- inaccessibility of the measurement at the joints,
- and adequacy of the joint model.

CHAPTER 3

DYNAMIC CHARACTERIZATION OF STRUCTURAL JOINTS

In this chapter, dynamic characterization of structural joints is analyzed. In section 3.1, how substructure uncoupling method for the identification of joint parameters is represented in literature and in this study is explained and different approaches are compared. Finally, in section 3.2 the importance of the RDOF in joint modeling is explained and the estimation methods for FRFs are presented.

3.1 SUBSTRUCTURE UNCOUPLING

Frequency response function coupling is one of the most widely used methods in the literature in order to couple two structures elastically. Consider substructures A, B and their assembly (structure C) obtained by coupling them with a flexible element as shown in Figure 3.1.

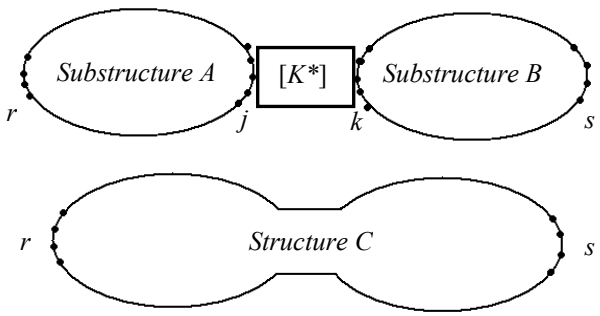

Figure 3.1 Coupling of Two Substructures with Elastic Joints

The coordinates *j* and *k* represent joint degrees of freedoms (DOFs), while *r* and *s* are the ones that belong to the selected points of substructures A and B, respectively, excluding joint DOFs. Let us partition the receptance matrices of substructures A and B:

$$[H_A(\omega)] = \begin{bmatrix} [H_{rr}(\omega)] & [H_{rj}(\omega)] \\ [H_{jr}(\omega)] & [H_{jj}(\omega)] \end{bmatrix} \quad [H_B(\omega)] = \begin{bmatrix} [H_{kk}(\omega)] & [H_{ks}(\omega)] \\ [H_{sk}(\omega)] & [H_{ss}(\omega)] \end{bmatrix} \tag{3.1}$$

and receptance matrix of the coupled structure C:

$$[H_C(\omega)] = \begin{bmatrix} [H^C_{kk}(\omega)] & [H^C_{ks}(\omega)] \\ [H^C_{sk}(\omega)] & [H^C_{ss}(\omega)] \end{bmatrix} \tag{3.2}$$

For substructure A, the relationship between the force vector and displacement vector can be written as:

$$\{x_r\} = [H_{rr}(\omega)]\{f_r\} + [H_{rj}(\omega)]\{f_j\} \tag{3.3}$$

$$\{x_j\} = [H_{jr}(\omega)]\{f_r\} + [H_{jj}(\omega)]\{f_j\} \tag{3.4}$$

And similarly, for substructure B:

$$\{x_k\} = [H_{kk}(\omega)]\{f_k\} + [H_{ks}(\omega)]\{f_s\} \tag{3.5}$$

$$\{x_s\} = [H_{sk}(\omega)]\{f_k\} + [H_{ss}(\omega)]\{f_s\} \tag{3.6}$$

Assuming no external forces and moments are acting on joints, the equations representing equilibrium of the forces and compatibility of displacements at connection DOFs can be written as:

$$\{f_j\} + \{f_k\} = 0 \tag{3.7}$$

$$[K^*(\omega)]\left(\{x_j\} - \{x_k\}\right) = \{f_k\} \tag{3.8}$$

where [*K*(ω)*] is complex stiffness matrix representing the joint dynamics and consists of the stiffness and damping elements that are to be identified.

Using equations (3.4) and (3.5) in equation (3.8) yields,

$$[H_{jr}(\omega)]\{f_r\} + [H_{jj}(\omega)]\{f_j\} = [H_{kk}(\omega)]\{f_k\} + [H_{ks}(\omega)]\{f_s\} + [K^*(\omega)]^{-1}\{f_k\} \tag{3.9}$$

Using equations (3.7) in equation (3.9) and rearranging the equation, we obtain,

$$\begin{aligned}\{f_j\} = &\left[H_{jj}(\omega) + [H_{kk}(\omega)] + [K^*(\omega)]^{-1}\right]^{-1}[H_{ks}(\omega)]\{f_s\} - \ldots \\ &\ldots\left[H_{jj}(\omega) + [H_{kk}(\omega)] + [K^*(\omega)]^{-1}\right]^{-1}[H_{jr}(\omega)]\{f_r\}\end{aligned} \tag{3.10}$$

Then, employing the equation (3.10) in equation (3.3) gives,

$$\begin{aligned}\{x_r^C\} = &\left[[H_{rr}(\omega)] - [H_{rj}(\omega)]\left[H_{jj}(\omega) + [H_{kk}(\omega)] + [K^*(\omega)]^{-1}\right]^{-1}[H_{jr}(\omega)]\right]\{f_r\} + \ldots \\ &\ldots[H_{rj}(\omega)]\left[H_{jj}(\omega) + [H_{kk}(\omega)] + [K^*(\omega)]^{-1}\right]^{-1}[H_{ks}(\omega)]\{f_s\}\end{aligned} \tag{3.11}$$

where, $\{x_r^C\}$ represents the displacement vector of the coordinates shown with *r* in the assembly (structure C).

From equation (3.11), two of the assembly receptance matrices can be extracted as follows (the frequency dependency of the formulation is not included for simplification):

$$\left[H_{rr}^{C}\right]=\left[H_{rr}\right]-\left[H_{rj}\right].\left[\left[H_{jj}\right]+\left[H_{kk}\right]+\left[K^{*}\right]^{-1}\right]^{-1}.\left[H_{jr}\right] \tag{3.12}$$

$$\left[H_{rs}^{C}\right]=\left[H_{rj}\right].\left[\left[H_{jj}\right]+\left[H_{kk}\right]+\left[K^{*}\right]^{-1}\right]^{-1}.\left[H_{ks}\right] \tag{3.13}$$

To obtain the remaining two receptance matrices of the assembly, equation (3.7) can be used and equation (3.10) can be written as

$$\begin{aligned}\left\{f_k\right\}=&-\left[H_{jj}(\omega)+\left[H_{kk}(\omega)\right]+\left[K^{*}(\omega)\right]^{-1}\right]^{-1}\left[H_{ks}(\omega)\right]\left\{f_s\right\}+\ldots\\ &\ldots\left[H_{jj}(\omega)+\left[H_{kk}(\omega)\right]+\left[K^{*}(\omega)\right]^{-1}\right]^{-1}\left[H_{jr}(\omega)\right]\left\{f_r\right\}\end{aligned} \tag{3.14}$$

Now, employing equation (3.14) in equation (3.6) we obtain,

$$\begin{aligned}\left\{x_s^{C}\right\}=&\left[H_{sk}(\omega)\right]\left[H_{jj}(\omega)+\left[H_{kk}(\omega)\right]+\left[K^{*}(\omega)\right]^{-1}\right]^{-1}\left[H_{jr}(\omega)\right]\left\{f_r\right\}+\ldots\\ &\ldots\left[\left[H_{ss}(\omega)\right]-\left[H_{sk}(\omega)\right]\left[H_{jj}(\omega)+\left[H_{kk}(\omega)\right]+\left[K^{*}(\omega)\right]^{-1}\right]^{-1}\left[H_{ks}(\omega)\right]\right]\left\{f_s\right\}\end{aligned} \tag{3.15}$$

Finally, from equation (3.11), the receptance submatrices of the assembly can be written as follows (the frequency dependency of the formulation is not included for simplification):

$$\left[H_{sr}^{C}\right]=\left[H_{sk}\right].\left[\left[H_{jj}\right]+\left[H_{kk}\right]+\left[K^{*}\right]^{-1}\right]^{-1}.\left[H_{jr}\right] \tag{3.16}$$

$$\left[H_{ss}^{C}\right]=\left[H_{ss}\right]-\left[H_{sk}\right].\left[\left[H_{jj}\right]+\left[H_{kk}\right]+\left[K^{*}\right]^{-1}\right]^{-1}.\left[H_{ks}\right] \tag{3.17}$$

Hence, the receptance matrix of the coupled structure C is obtained.

By using the equations (3.12), (3.13), (3.16) and (3.17) it is possible to decouple and thus calculate the complex stiffness matrix representing joint stiffness and damping as shown below (the frequency dependency of the formulation is not included for simplification):

$$[K^*] = \left[[H_{jr}] . \left[[H_{rr}] - [H_{rr}^C] \right]^{-1} . [H_{rj}] - [H_{jj}] - [H_{kk}] \right]^{-1} \tag{3.18}$$

$$[K^*] = \left[[H_{ks}] . [H_{rs}^C]^{-1} . [H_{rj}] - [H_{jj}] - [H_{kk}] \right]^{-1} \tag{3.19}$$

$$[K^*] = \left[[H_{jr}] . [H_{sr}^C]^{-1} . [H_{sk}] - [H_{jj}] - [H_{kk}] \right]^{-1} \tag{3.20}$$

$$[K^*] = \left[[H_{ks}] . \left[[H_{ss}] - [H_{ss}^C] \right]^{-1} . [H_{sk}] - [H_{jj}] - [H_{kk}] \right]^{-1} \tag{3.21}$$

If FRF matrices of the substructures and that of the coupled structure at any frequency are available, joint identification can be achieved by using any of the above equations and, theoretically speaking, it does not make any difference which one of the equations are used in the extraction of the joint properties. However, due to the identification of rotational and cross-coupling elements, the performance of each equation was observed to be different and the most accurate results were obtained when equation (3.18) was used as will be demonstrated later. Furthermore, again theoretically, the identification equation can be used with FRFs measured at any frequency. However, as will be discussed in the case studies given in Chapter 4, the effects of joint dynamics on system response are almost negligible at several frequencies, but very much pronounced at certain other frequencies. Therefore, it is not easy, if not impossible, to use these equations to identify system properties at several frequencies where the equation will be very sensitive to noise which is unavoidable in practical applications. Yet, if these equations are used at a frequency

in a mode where joint properties affect the system response considerably, the computations will be less sensitive to measurement noise. This point will be discussed further in Chapter 4. Note that, here we can use any number of points in either of the substructures to take FRF measurements. Thus, orders of the submatrices in equations (3.18)-(3.21) can be kept very small. This will be further explained and illustrated with case studies in Chapter 4.

After calculating the complex joint stiffness matrix, the stiffness and damping values representing the joint dynamics are obtained from the real and imaginary parts of the matrix elements, respectively. Different joint models can be used. Then, depending on the model used the number of identified elements will change. The models used for a joint can be classified in three groups.

Joint Model 1

Only translational joint parameters are considered in this model:

$$\left[K^*(\omega)\right] = \left[k_{Fy} + j\omega c_{Fy}\right] \tag{3.22}$$

If more than one joint element is used in the connection, the joint stiffness matrix including only translational properties can be given as:

$$\left[K^*(\omega)\right] = \begin{bmatrix} k_{Fy1} + j\omega c_{Fy1} & & & \\ & k_{Fy2} + j\omega c_{Fy2} & & \\ & & \ddots & \\ & & & k_{FyN} + j\omega c_{FyN} \end{bmatrix} \tag{3.23}$$

Note that, N represents the number of connection points at the joint interface.

Joint Model 2

This model includes both translational and rotational joint parameters:

$$\left[K^*(\omega)\right]=\begin{bmatrix} k_{Fy}+j\omega c_{Fy} & 0 \\ 0 & k_{M\theta}+j\omega c_{M\theta} \end{bmatrix} \tag{3.24}$$

If N joints are used in the connection, the second joint model can be represented with:

$$\left[K^*(\omega)\right]=\begin{bmatrix} k_{Fy1}+j\omega c_{Fy1} & & & & & \\ & k_{M\theta 1}+j\omega c_{M\theta 1} & & & & \\ & & . & & & \\ & & & . & & \\ & & & & k_{FyN}+j\omega c_{FyN} & \\ & & & & & k_{M\theta N}+j\omega c_{M\theta N} \end{bmatrix} \tag{3.25}$$

Joint Model 3

In Model 3, joint is represented with translational, rotational and cross-coupling joint elements:

$$\left[K^*(\omega)\right]=\begin{bmatrix} k_{Fy}+j\omega c_{Fy} & k_{F\theta}+j\omega c_{F\theta} \\ k_{My}+j\omega c_{My} & k_{M\theta}+j\omega c_{M\theta} \end{bmatrix} \tag{3.26}$$

If N joints are used in the connection, the third joint model will be:

$$\left[K^*(\omega)\right]=\begin{bmatrix} k_{Fy1}+j\omega c_{Fy1} & k_{F\theta 1}+j\omega c_{F\theta 1} & & & & \\ k_{My1}+j\omega c_{My1} & k_{M\theta 1}+j\omega c_{M\theta 1} & & & & \\ & & . & & & \\ & & & . & & \\ & & & & k_{FyN}+j\omega c_{FyN} & k_{F\theta N}+j\omega c_{F\theta N} \\ & & & & k_{MyN}+j\omega c_{MyN} & k_{M\theta N}+j\omega c_{M\theta N} \end{bmatrix} \tag{3.27}$$

This approach has been used in the work of Özşahin et al. (2009) for the identification of contact parameters between spindle-holder and tool from the measured FRFs of the spindle-holder-tool assembly (which can be regarded as a coupled structure) and the calculated/ measured FRFs of the cutting tool and spindle-holder (which can be regarded as substructures) (Figure 3.2).

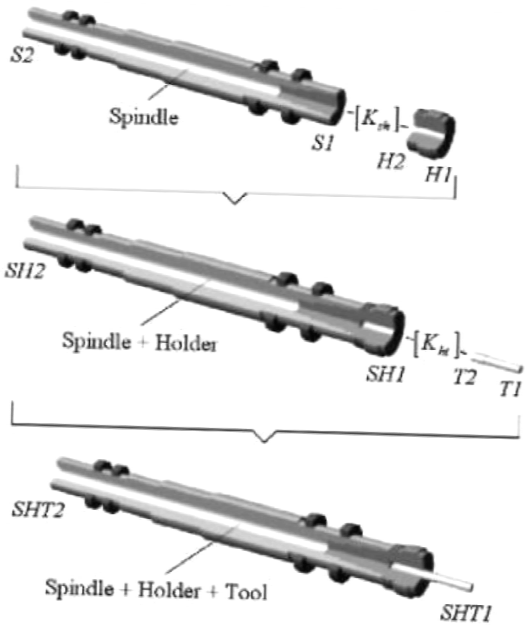

Figure 3.2 Components of Spindle-Holder-Tool Assembly and the Complex Stiffness Matrices of Spindle-Holder and Holder-Tool Interfaces (Özşahin et al., 2009)

3.2 ESTIMATION OF FRFS

Analytically, all elements of an FRF matrix can be calculated easily. However, in real life applications, measuring all the elements of an FRF matrix experimentally is very time consuming and expensive; besides, it may not be possible for all cases. Usually, only one column of an FRF matrix can be obtained by exciting the structure

from a single point and measuring responses at all the points we are interested in. Furthermore, the measurement of FRFs related to RDOFs is very difficult and requires special equipment. Therefore, in experimental studies it is a general practice to obtain accurate and fast solutions for the estimation of unmeasured FRFs.

3.2.1 Unmeasured FRF Estimation

In the method proposed we need the full receptance matrix for the DOFs we are interested in. In order to obtain complete FRF matrix, the structure should be excited from all points we are interested in. However, in testing usually only one column of the FRF matrix is obtained by exciting the structure from a single point and measuring responses at all other points we are interested in. Then, the incomplete data (in any of the FRF matrices we need to use) can be obtained by using FRF synthesis after extracting modal parameters by modal testing (Silva et al., 2000). This process is briefly explained below.

For N degrees of freedom, viscously damped system the receptance matrix of frequency response functions $H_{pq}(\omega)$ relating the response at a given coordinate p to an excitation force applied at a given coordinate q can be written as:

$$H_{pq}(\omega) = \sum_{r=1}^{N} \frac{\phi_{pr}\phi_{qr}}{(\omega_r^2 - \omega^2 + j2\zeta_r\omega_r\omega)} \tag{3.28}$$

where ϕ_{jr} and ϕ_{kr} are the p^{th} and q^{th} elements, respectively, of the mass-normalized modal vector of the r^{th} mode, ω is the excitation frequency, ω_r and ζ_r are the r^{th} mode natural frequency and viscous damping ratio, respectively. Equation (3.28) can be alternatively written as follows:

$$H_{pq}(\omega) = \sum_{r=1}^{N} \frac{{}_r\overline{A}_{pq}}{(\omega_r^2 - \omega^2 + j2\zeta_r\omega_r\omega)} \tag{3.29}$$

where

$$ {}_r\overline{A}_{pq} = \phi_{pr}\phi_{qr} \tag{3.30} $$

is the modal constant for coordinates p and q, and mode r. Since the receptance matrix is symmetric, from the reciprocity principle, the following relation can be written:

$$ H_{pq}(\omega) = H_{qp}(\omega) \tag{3.31} $$

Then, the modal constants obey the following relationships known as the modal constants consistency equations:

$$ {}_r\overline{A}_{pq} = \phi_{pr}\phi_{qr} \qquad {}_r\overline{A}_{pp} = \phi_{pr}^2 \qquad {}_r\overline{A}_{qq} = \phi_{qr}^2 \tag{3.32} $$

From equations (3.31) and (3.32), it is clear that when a full column (or row) of the receptance matrix $\left[H(\omega)\right]$ is known, and then the complete matrix can be calculated. However, in practical applications due to the limitation of the frequency range of the experimental measurement, only a limited number of modes can be included in the analysis. Therefore, the response model will be truncated and contain errors due to omission of the out-of-range modes. In order to minimize the consequences of using such a model, residual terms ($\overline{R}_{pq}(\omega)$) are included in the response equation, accounting for the contribution of the out-of-range modes, i.e.:

$$ H_{pq}(\omega) = \sum_{r=1}^{N_{inc}} \frac{{}_r\overline{A}_{pq}}{(\omega_r^2 - \omega^2 + j2\zeta_r\omega_r\omega)} + \overline{R}_{pq}(\omega) \tag{3.33} $$

where $N_{inc} < N$ is the incomplete number of modes included in the analysis.

Actually, mode truncation, without including the residuals in the synthesis, generally has a negligible effect on the response at resonance frequencies, but does shift the anti-resonances upward in frequency (Campbell and Hambric, 2004).

In the experimental part of this study, LMS SCADAS modal test system is used and the modal parameters (natural frequency, damping ratio, modal constant, lower and upper residues) are extracted from the LMS software. Then the required FRFs are synthesized by using the identified parameters and the equation given in the technical report of LMS Theory and Background (LMS Int., 2000). Although the expression used is different in appearance it can be obtained from equation (3.33), which is given below.

Let us first write the FRF formula more explicitly by expressing the mass normalized modal vectors. Mass normalized modal vector elements ϕ_{pr} and ϕ_{qr} can be written as

$$\phi_{pr} = \frac{U_{pr}}{\sqrt{m_r}} \qquad \phi_{qr} = \frac{U_{qr}}{\sqrt{m_r}} \tag{3.34}$$

where U_{pr} and U_{qr} are the elements of modal vector corresponding to response DOF *p* of mode *r* and reference DOF *q* of mode *r*, respectively and m_r is the modal mass of mode *r*.

Substituting equation (3.34) in equation (3.28), we obtain:

$$H_{pq}(\omega) = \sum_{r=1}^{N} \frac{\dfrac{U_{pr}U_{qr}}{m_r}}{(-\omega^2 + j2\zeta_r\omega_r\omega + \omega_r^2)} \tag{3.35}$$

Using partial-fraction decomposition, equation (3.35) is decomposed into its polynomial fractions,

$$\frac{\frac{U_{pr}U_{qr}}{m_r}}{(-\omega^2 + j2\zeta_r\omega_r\omega + \omega_r^2)} = \frac{A}{\omega - \alpha_1} + \frac{B}{\omega - \alpha_2} \tag{3.36}$$

where α_1 and α_2 are the roots of the system characteristic equation and calculated as follows,

$$\alpha_{1,2} = j\zeta_r\omega_r \pm \omega_r\sqrt{1-\zeta_r^2} \tag{3.37}$$

Substituting equation (3.37) into equation (3.36), we obtain,

$$\frac{A}{\omega - \alpha_1} + \frac{B}{\omega - \alpha_2} = \frac{Aj}{j\omega - (-\zeta_r\omega_r + j\omega_r\sqrt{1-\zeta_r^2})} + \frac{Bj}{j\omega - (-\zeta_r\omega_r - j\omega_r\sqrt{1-\zeta_r^2})} \tag{3.38}$$

Let's call the term,

$$\lambda_r = -\zeta_r\omega_r + j\omega_r\sqrt{1-\zeta_r^2} \tag{3.39}$$

as the pole value for mode *r*, λ_r. Then equation (3.36) can be simplified into,

$$\frac{\frac{U_{pr}U_{qr}}{m_r}}{(-\omega^2 + j2\zeta_r\omega_r\omega + \omega_r^2)} = \frac{Aj}{j\omega - \lambda_r} + \frac{Bj}{j\omega - \lambda_r^*} \tag{3.40}$$

Note that * designates complex conjugate.

Multiplying both sides of equation (3.40) by the common denominator of $(j\omega - \lambda)(j\omega - \lambda_r^*)$ we obtain

$$\frac{U_{pr}U_{qr}}{m_r} = Aj(j\omega - \lambda_r^*) + Bj(j\omega - \lambda_r) \tag{3.41}$$

After multiplication, the ω terms and the constant terms can be grouped as shown below:

$$0 = -\omega(A + B) \tag{3.42}$$

$$\frac{U_{pr}U_{qr}}{m_r} = j(-A\lambda_r^* - B\lambda_r) \tag{3.43}$$

Knowing that $B = -A$, from equation (3.42), and substituting equation (3.39) into equation (3.43) we obtain,

$$\frac{U_{pr}U_{qr}}{m_r} = 2j\omega_r\sqrt{1-\zeta_r^2}\,Aj \tag{3.44}$$

Then the numerators on the right hand side of the equation (3.40) can be found as,

$$Aj = \frac{U_{pr}U_{qr}}{2jm_r\omega_r\sqrt{1-\zeta_r^2}} \tag{3.45}$$

$$Bj = -Aj = -\frac{U_{pr}U_{qr}}{2jm_r\omega_r\sqrt{1-\zeta_r^2}} = \left(\frac{U_{pr}U_{qr}}{2jm_r\omega_r\sqrt{1-\zeta_r^2}}\right)^* \tag{3.46}$$

Complex scaling constant, a_r is the term below:

$$a_r = \frac{1}{2jm_r\omega_r\sqrt{1-\zeta_r^2}} \tag{3.47}$$

and numerators on the right hand side of the equation (3.40) is given as follows:

$$r_{pqr} = a_r U_{pr} U_{qr} \tag{3.48}$$

In the LMS software the value of the complex scaling constant is determined by the scaling of the mode shapes. Note that mode shape coefficients can be either real (normal mode shapes) or complex.

Then substituting equations (3.45)-(3.48) into equation (3.40), we obtain:

$$H_{pq}(\omega) = \sum_{r=1}^{N} \left(\frac{r_{pqr}}{(j\omega - \lambda_r)} + \frac{r_{pqr}^{*}}{(j\omega - \lambda_r^{*})} \right) \tag{3.49}$$

which is the exact relation for FRFs given in the technical report of LMS Theory and Background (LMS Int., 2000).

The parameters of each mode are determined separately in the analysis band and this approach is called the single degree of freedom (sDOF) assumption which is illustrated in Figure 3.3. Then, in order to compensate for the modes in the neighborhood of the analysis band, the upper and lower residual terms are included in the equation (3.34). The upper and lower residuals are illustrated in Figure 3.4.

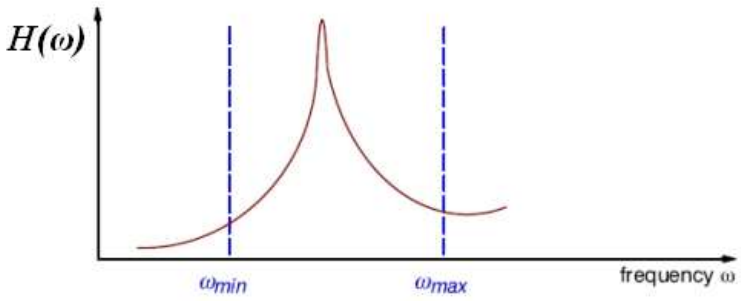

Figure 3.3 The Single Degree of Freedom System Assumption

$$H_{pq}(\omega)=\sum_{r=1}^{N}\left(\frac{r_{pqr}}{(j\omega-\lambda_r)}+\frac{r_{pqr}^{\ *}}{(j\omega-\lambda_r^{\ *})}\right)+UA_{pq}-\frac{LA_{pq}}{\omega^2} \tag{3.50}$$

where

UA_{pq} : Upper residual term (residual stiffness) used to approximate the modes at frequencies above $\omega_{\max}$.

LA_{pq} : Lower residual term (residual mass) used to approximate the modes at frequencies above $\omega_{\min}$.

Finally, after obtaining the modal parameters from modal testing, the complete FRF matrix can be generated as:

$$H_{pq}(\omega)=\sum_{r=1}^{N}\left(\frac{\frac{1}{j2\omega_r\sqrt{1-(\zeta_r)^2}}U_{pr}U_{qr}}{\omega_r\zeta_r+j(\omega-\omega_r\sqrt{1-(\zeta_r)^2})}+\frac{(\frac{1}{j2\omega_r\sqrt{1-(\zeta_r)^2}}U_{pr}U_{qr})^*}{\omega_r\zeta_r+j(\omega+\omega_r\sqrt{1-(\zeta_r)^2})}\right)+... \tag{3.51}$$

$$...UA_{pq}-\frac{LA_{pq}}{\omega^2}$$

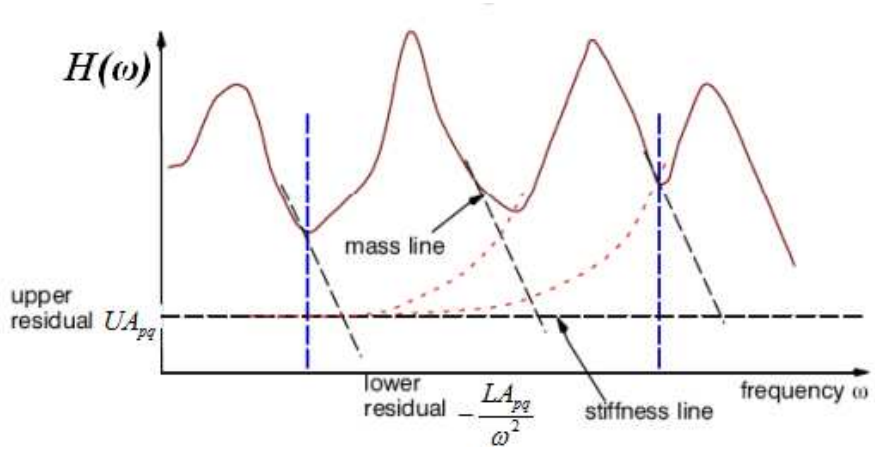

Figure 3.4 Upper and Lower Residuals (LMS Int., 2000)

In FRF measurements, mostly, accelerometers and force transducers are used to measure the dynamic response of the structure. Hence, we measure directly accelerance $A(\omega)$ instead of receptance $H(\omega)$. Before performing FRF synthesis, accelerance should be converted to receptance by integrating the accelerometer data twice, or equivalently:

$$H(\omega) = \frac{A(\omega)}{-\omega^2} \tag{3.52}$$

3.2.2 RDOF Estimation

In order to obtain a full description of system dynamics, rotational degrees of freedom information plays a significant role. The effect of including RDOF related FRFs in the identification of joint parameters will be examined in this study in Chapter 4. There are various methods developed for the measurement of RDOFs directly and indirectly. Duarte and Ewins (2000) classified them as: the block, the finite difference, the estimation, the angular transducers and the laser technique. Among these approaches only the estimation techniques based on expansion method are not purely experimental techniques, because they require a FE model of the structure (Avitable and O'Callahan, 2003). Hence, they are not practical for the present study. The block techniques have several problems associated with them and the most susceptible errors using this technique are caused by the functions related to moment excitations (Duarte, 1996). Furthermore, angular response transducers and the laser technique may not be always available due to their high cost. On the other hand, finite-difference technique (also known as the close accelerometers method) provides a simple and versatile way of deriving experimentally the required DOFs. So in the current study, this approach is used to obtain rotational information from the translational measurements. The close accelerometers method is performed with the three (or two) accelerometers which are placed close to each-other in a constant spacing (s), as illustrated in Figure 3.5.

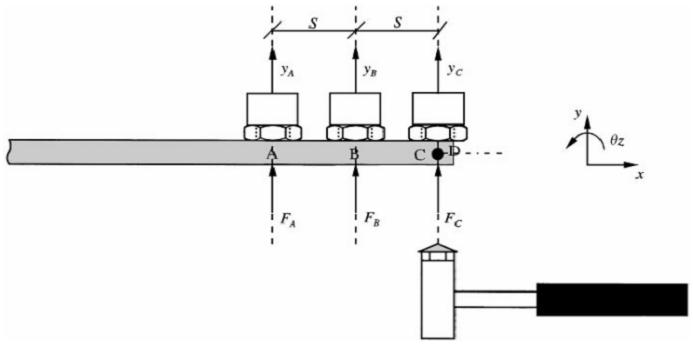

Figure 3.5 Close-Accelerometers Method for RDOF Measurements (Duarte and Ewins, 2000)

The number of measurement points is governed by the desired accuracy of the results. The order of accuracy is one less than the number of measurement points when the traditional finite difference formulae are employed. For example, first order accuracy requires the measurement of FRFs for two locations; second order requires three locations, and so on. Another important thing related to the accuracy of this technique is the spacing between the measurement points. It is vital for the correct estimation of rotational-related FRFs to control this parameter carefully and keep as small as possible.

Three different formulas can be employed depending on the accelerometer position and coordinate system position. A summary of the finite-difference transformation matrices is given in Table 3.1. The choice between these transformation matrices depends on whether the location, where the rotational information is desired, is an inside, middle or outside location, or on whether it is on the positive or negative end of the global axis. Indeed, the same order forward-, central- and backward-difference transformation matrices are of equivalent accuracy. A more detailed explanation can be found in Duarte (1996).

In the current study, second order central approximation which requires three measurement points (points A, B and C in Figure 3.5) is utilized because it is better for deriving FRFs or residual-related parameters.

Table 3.1 First and Second Order Finite Difference Transformation Matrices (Duarte, 1996)

	First Order	Second Order
Forward	$\begin{bmatrix} 0 & 1 \\ 1/s & -1/s \end{bmatrix}$	$\frac{1}{2s}\begin{bmatrix} 0 & 0 & 2s \\ -1 & 4 & -3 \end{bmatrix}$
Central	NA	$\frac{1}{2s}\begin{bmatrix} 0 & 2s & 0 \\ -1 & 0 & 1 \end{bmatrix}$
Backward	$\begin{bmatrix} 0 & 1 \\ -1/s & 1/s \end{bmatrix}$	$\frac{1}{2s}\begin{bmatrix} 0 & 0 & 2s \\ 1 & -4 & 3 \end{bmatrix}$

Then, rotational FRF at point B is calculated by using the second-order-central transformation matrix:

$$[T_{2c}] = \frac{1}{2s}\begin{bmatrix} 0 & 2s & 0 \\ -1 & 0 & 1 \end{bmatrix} \tag{3.53}$$

as follows:

$$[H_{est}] = \begin{bmatrix} H_{yy} & H_{y\theta} \\ H_{\theta y} & H_{\theta\theta} \end{bmatrix} = [T_{2c}].[H_{meas}].[T_{2c}]^T \tag{3.54}$$

where $[H_{est}]$ represents the estimated FRFs in y and θ directions at point B, and $[H_{meas}]$ denotes the measured translational FRFs at points A, B and C, and is defined as:

$$[H_{meas}] = \begin{bmatrix} H_{AA} & H_{AB} & H_{AC} \\ H_{BA} & H_{BB} & H_{BC} \\ H_{CA} & H_{CB} & H_{CC} \end{bmatrix} \tag{3.55}$$

CHAPTER 4

JOINT IDENTIFICATION - SIMULATION STUDIES

In this chapter, three case studies are given to verify and illustrate the application of the method suggested. In section 4.1, connection in a discrete system is identified. Then, in section 4.2, two case studies of two beams bolted to each other are considered and the bolted joint properties in terms of stiffness and damping matrices are extracted. In the first case study with bolted beams given in section 4.2.1, the importance of the rotational degrees of freedom is demonstrated, while in the second case study with bolted beams given in section 4.2.2 different approaches in the utilization of decoupling method are explained. Finally, in section 4.3 simulation of experimental data with different noise contamination procedures is given, and then the effects of measurement noise on the identification results are evaluated and error analysis is presented.

4.1 LUMPED PARAMETER MODEL

In the first case study, two 2 DOF discrete systems connected with a damped elastic element is used in order to demonstrate and validate the joint identification method. Here, joint complex stiffness is modeled with a translational stiffness and a viscous damping element as illustrated in Figure 4.1 and Figure 4.2.

$$k* = (k + j\omega c) \tag{4.1}$$

Properties of the substructures and joints are tabulated in Table 4.1.

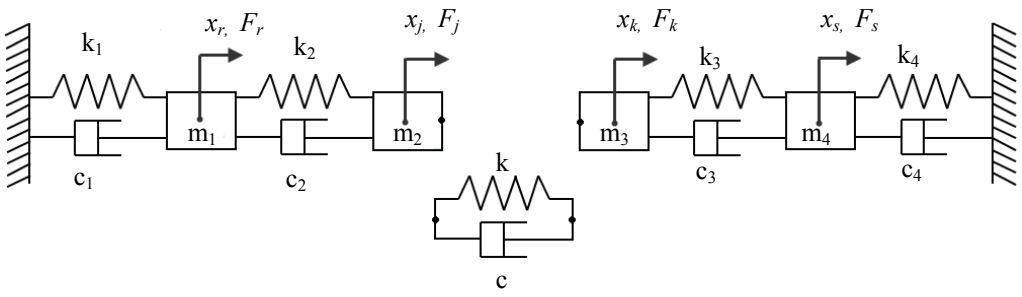

Figure 4.1 Two Subsystems and Elastic Coupling Element

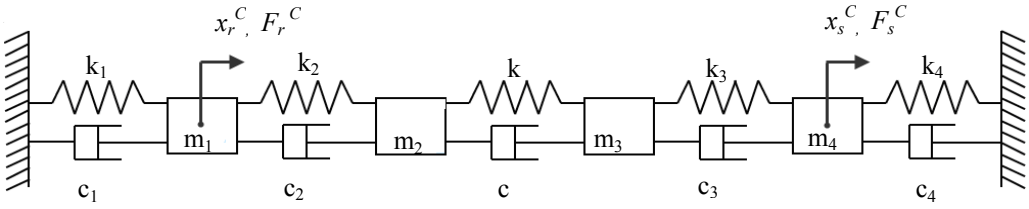

Figure 4.2 Coupled System

Table 4.1 Dynamic properties of the lumped coupled system

Index	Mass, *m* [kg]	Stiffness, *k* [N/m]	Damping, *c* [N.s/m]
1	5	2500	3
2	3	3500	4
3	4	2000	2
4	2	2500	1
joint	-	2000	3

After calculating all required FRFs for identification (FRFs of subsystems and of the coupled system), FRFs of the coupled system are polluted with 5% noise to simulate experimental measurements. The noise is generated with the "normrnd" function of MATLAB with zero mean, normal distribution and standard deviation of 5% of the maximum amplitude of the system response. Thus, the response of the system is polluted with randomly distributed noise. Then by taking the Fast Fourier Transform (FFT) of the response and dividing it by the FFT of the forcing, the polluted receptance is obtained. With this procedure, the noise becomes more effective when the response of the structure is low. Therefore, it is believed that this is a more realistic way of simulating noise in FRF measurements. This issue will be further investigated in section 4.3. The receptances of the coupled system at the 1st DOF (shown in Figure 4.3) are used in equation (3.18) for the identification of joint properties.

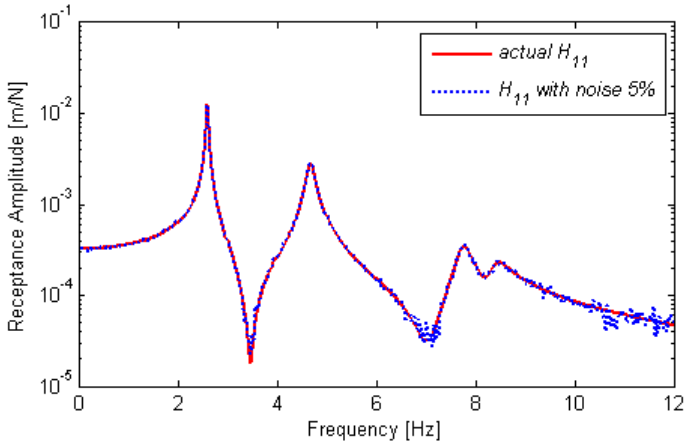

Figure 4.3 H_{11} for the Coupled Structure

The joint identification can be made by using the related equations at any frequency in the range. Theoretically, it is expected to find the exact values of the stiffness and damping in each case. However, due to noise in measurements and the system

response having different sensitivity to the joint properties at different frequencies, the calculated values deviate from the actual values considerably at some frequencies.

The identified joint stiffness (k) and joint damping (c) values obtained by employing FRFs measured at each frequency in the range covering all four modes are given in Figure 4.4 and Figure 4.5, respectively.

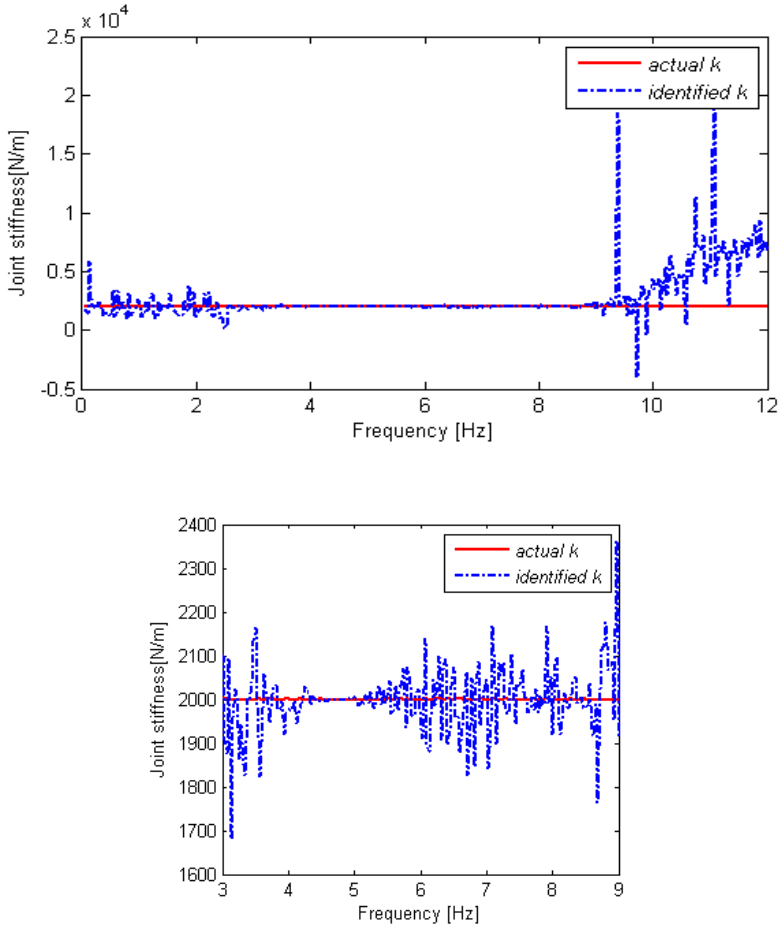

Figure 4.4 Identified Stiffness of the Joint - Average Value Between 3-9Hz is 2008 N/m

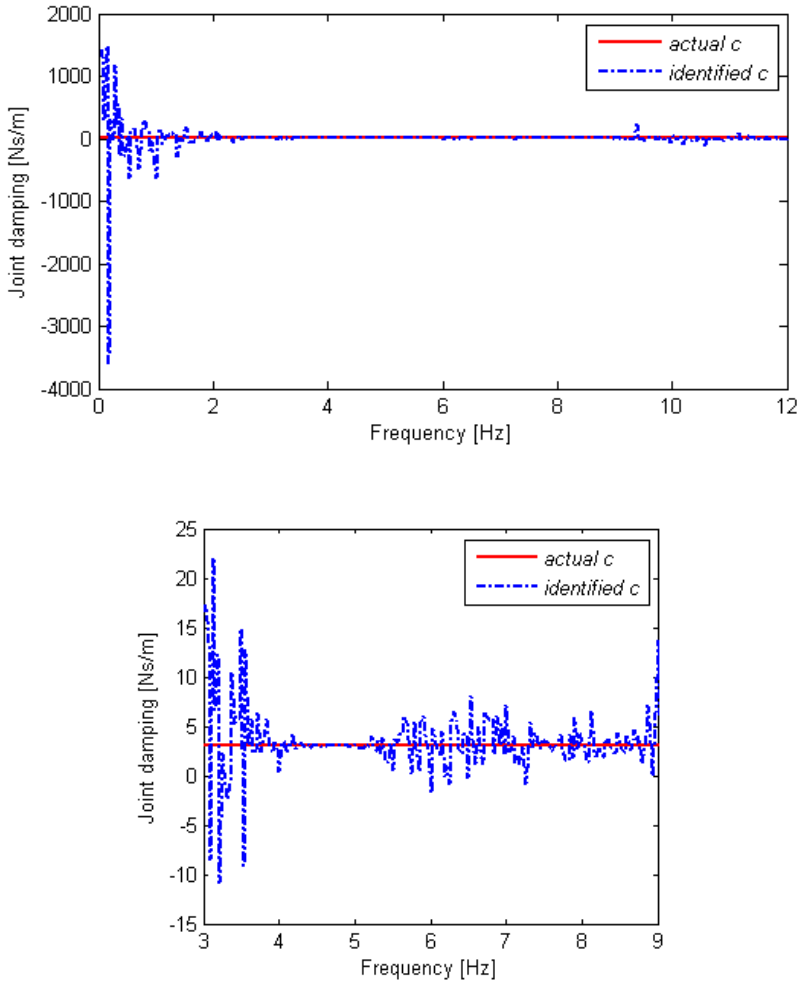

Figure 4.5 Identified Damping of the Joint - Average Value Between 3-9Hz is 3.52 N.s/m

It is observed that exact values are calculated for joint stiffness and damping when the exact FRF values are used for the coupled system. However, when polluted FRFs are used, although very accurate values are obtained at some frequencies, the results are deteriorated and deviations from the actual values are drastic at some other frequencies. In order to demonstrate the reason for this behavior, the sensitivity of the receptance of the coupled system to the joint properties is investigated. It can be seen from Figure 4.6 that, the joint stiffness is effective in the second, third and fourth modes. The receptance values are not affected from the change in joint

stiffness, approximately up to 2~3Hz and after 9 Hz. Hence, it does not make any sense to use the identification results calculated by using the FRFs measured in these regions. The results show that the FRF decoupling method works well in the sensitive frequency range, which is between 3-9 Hz for this case. When the average stiffness and damping of the values identified in the frequency range of 3-9 Hz are calculated, the identification results are found to be 2008 N/m for stiffness and 3.52 N.s/m for damping (deviations from the actual values are 0.4% and 17%, respectively).

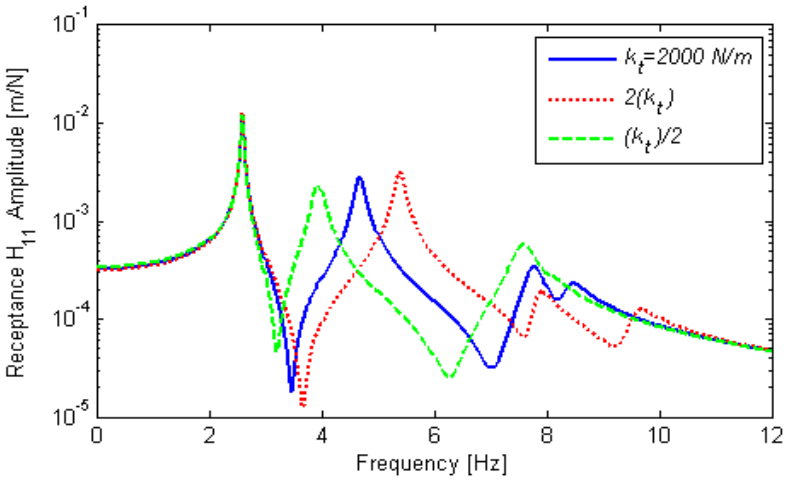

Figure 4.6 Sensitivity of the Receptance to the Joint Stiffness

By using the identified joint parameters, receptance of the coupled system at the 1st DOF is regenerated and compared with the actual receptance in Figure 4.7. It can be seen from the comparison of the actual and regenerated FRFs that the FRF regenerated by using the joint parameters perfectly matches with the actual FRF.

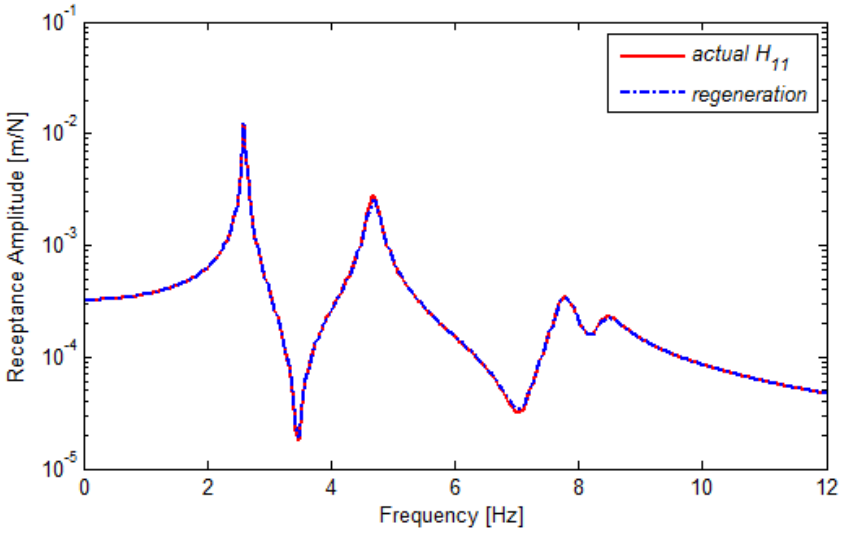

Figure 4.7 Regenerated FRF of the Coupled Structure at the 1st DOF

Thus it is concluded that, in the identification of the joint properties, FRFs measured at frequencies where connection stiffness has less effect on the response of the coupled system should be avoided. Instead, any set of FRFs, measured at any frequency in the modes at which connection dynamics affect coupled system dynamics considerably, can be used and very accurate identification can be made as can be seen from Figure 4.4 and Figure 4.5. Since it is not known in advance at which mode the joint dynamics will affect the coupled system dynamics considerably, it is the best to identify joint properties in a range of frequency and take the average of the values in a region where deviations from a constant value is minimum.

In order to compare the performances of four decoupling equations (equations (3.18)-(3.21)), the joint identification is performed using each equation by following the procedure described above, and the accuracies of the joint parameters identified from each equation are compared. The joint parameters identified by using each equation and the percentage differences from the actual values are given in Table 4.2

(Equations (3.19) and (3.20) are the same). (Note that the identification results using equation (3.18) are illustrated schematically, while the results obtained from the other decoupling equations are compared in a table format.) As it can be seen from the table the best performance is obtained from equation (3.18).

Table 4.2 Joint Parameters Identified by Using Different Decoupling Equations (Equations (3.18), (3.19) and (3.21))

	k [N/m]	*% Error*	c [N.s/m]	*% Error*
Actual values	2000	-	3	-
Identified values (3.18)	2008	*0.4*	3.52	*0.4*
Identified values (3.19)	2016	*0.8*	2.73	*-9*
Identified values (3.21)	2020	*1.0*	2.80	*-6.7*

4.2 BOLTED BEAMS

4.2.1 Case Study 1

In this case study, two identical beams; substructure A having fixed-free boundary condition and substructure B having free-free boundary condition, are coupled elastically with a joint as shown in Figure 4.8. Each substructure is modeled with beam elements using finite element method (FEM). The elemental mass and stiffness matrices are given in equations (4.3) and (4.4), respectively. In the dynamic modeling of beams, displacements at each node are represented with one translational and one rotational DOF.

$$[m_e] = \frac{ml}{420}\begin{bmatrix} 156 & 22l & 54 & -13l \\ 22l & 4l^2 & 13l & -3l^2 \\ 54 & 13l & 156 & -22l \\ -13l & -3l^2 & -22l & 4l^2 \end{bmatrix} \tag{4.3}$$

$$[k_e] = \frac{EI}{l^3}\begin{bmatrix} 12 & 6l & -12 & 6l \\ 6l & 4l^2 & -6l & 2l^2 \\ -12 & -6l & 12 & -6l \\ 6l & 2l^2 & -6l & 4l^2 \end{bmatrix} \tag{4.4}$$

Here, m is the mass per unit length of the beam, E is the modulus of elasticity of beam element, I is the moment of inertia of the cross-sectional area, and l is the length of the beam element.

The following data are used for the beams:
Beam length: $L=0.3\ m$; modulus of elasticity: $E=2.07\ 10^{11}\ N/m^2$; moment of inertia of the cross-sectional area: $I=1.0667\ 10^{-9}\ m^3$; mass per unit length of the beams: $m=1.5094\ kg/m$. Damping of the beams is taken structural damping with a loss factor of 0.05.

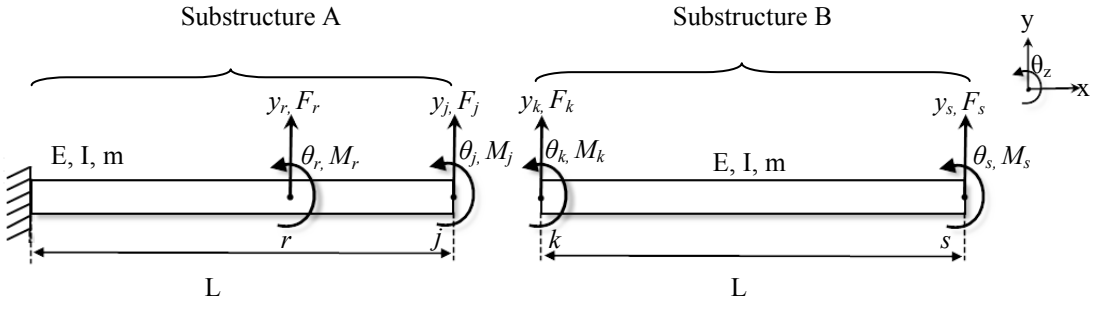

Figure 4.8 Coupling of Two Beams with Bolted Joint

Here, it is assumed that the bolted joint can be modeled with a complex stiffness matrix, as shown below:

$$[K^*] = \begin{bmatrix} k_{Fy} + j\omega c_{Fy} & k_{F\theta} + j\omega c_{F\theta} \\ k_{My} + j\omega c_{My} & k_{M\theta} + j\omega c_{M\theta} \end{bmatrix} \tag{4.5}$$

where k_{Fy} is the force-to-linear displacement stiffness, c_{Fy} is the force-to-linear displacement damping, $k_{F\theta}$ is the force-to-angular displacement stiffness, $c_{F\theta}$ is the force-to-angular displacement damping, k_{My} is the moment-to-linear displacement stiffness, c_{My} is the moment-to-linear displacement damping, $k_{M\theta}$ is the moment-to-angular displacement stiffness and $c_{M\theta}$ is the moment-to-angular displacement damping of the joint, ω is the excitation frequency and j is the unit imaginary number. Hence, in this case study fully populated form of the complex stiffness matrix is used. The other joint models will be examined in the next section. The data used for the joint is given in Table 4.3.

Table 4.3 Joint Parameters of the Bolted Connection

k_{Fy} : Translational stiffness *[N/m]*	10^6
c_{Fy} : Translational damping *[N.s/m]*	*25*
$k_{F\theta}$: Cross-coupling stiffness *[N/rad]*	10^4
$c_{F\theta}$: Cross-coupling damping *[N.s/rad]*	*8*
k_{My} : Cross-coupling stiffness *[N.m/m]*	10^4
c_{My} : Cross-coupling damping *[N.m.s/m]*	*8*
$k_{M\theta}$: Rotational stiffness *[N.m/rad]*	10^3

$c_{M\theta}$: Rotational damping *[N.m.s/rad]*	5

Before the identification process, for simulating experimental data, the calculated FRFs of the coupled structure are contaminated with 5% noise as described in the previous case study. The noise contaminated translational FRFs of the coupled structure at the coordinates *r* and *s* are shown in Figure 4.9 to Figure 4.12.

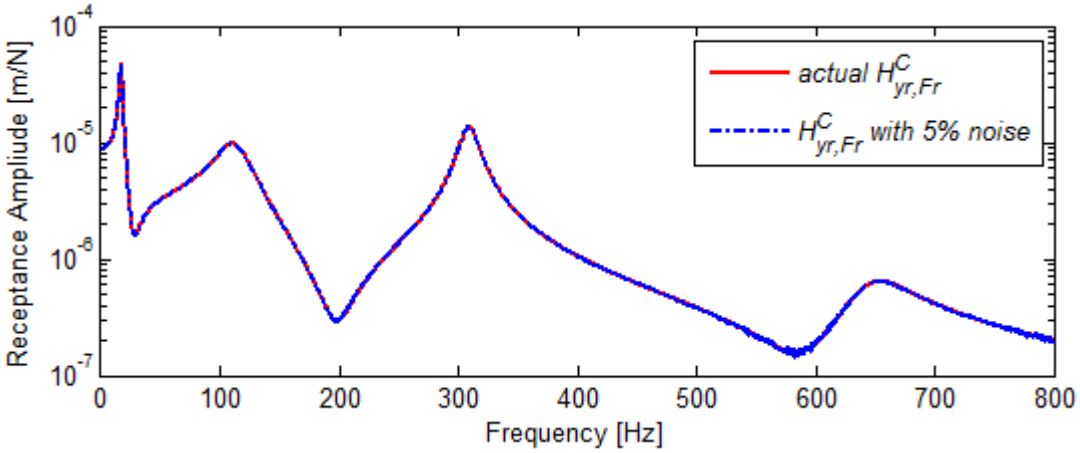

Figure 4.9 Translational Receptance of the Coupled Structure at r^{th} Coordinate

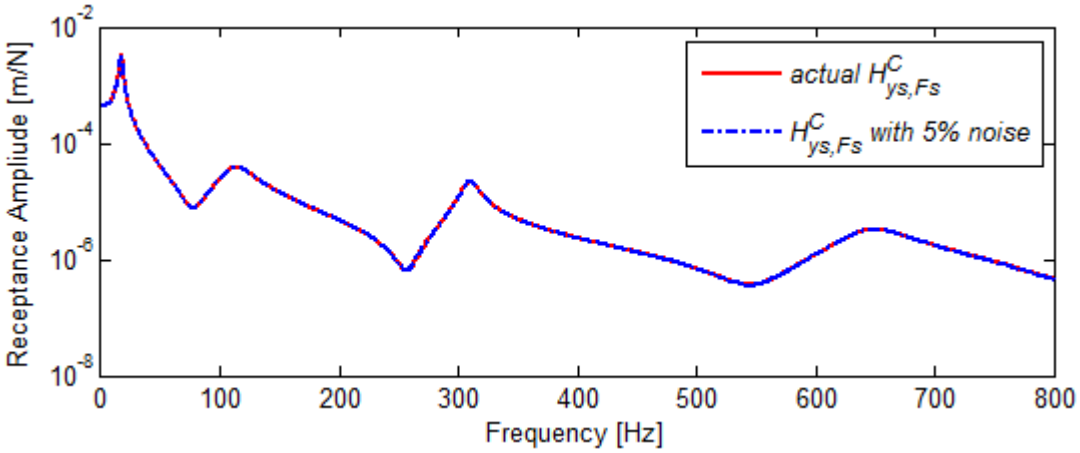

Figure 4.10 Translational Receptance of the Coupled Structure at s^{th} Coordinate

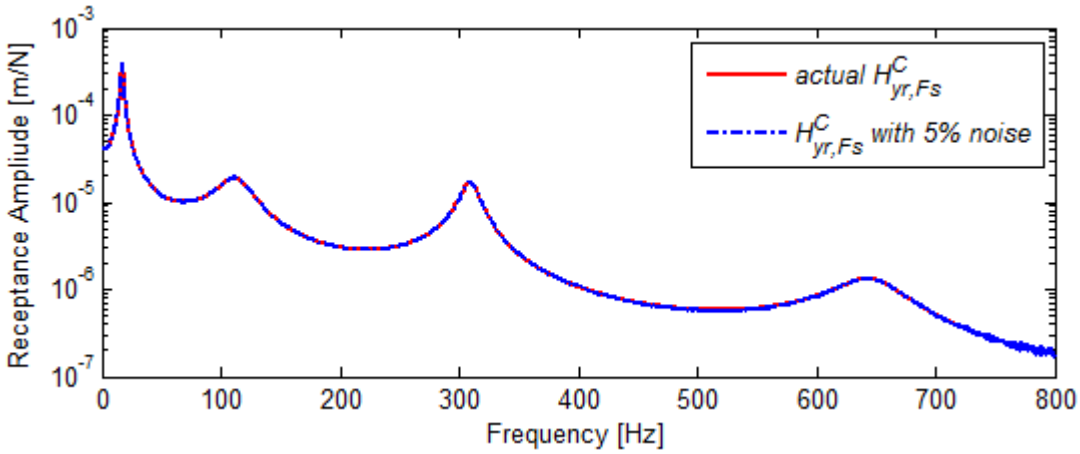

Figure 4.11 Translational Receptance of the Coupled Structure between *r-s*

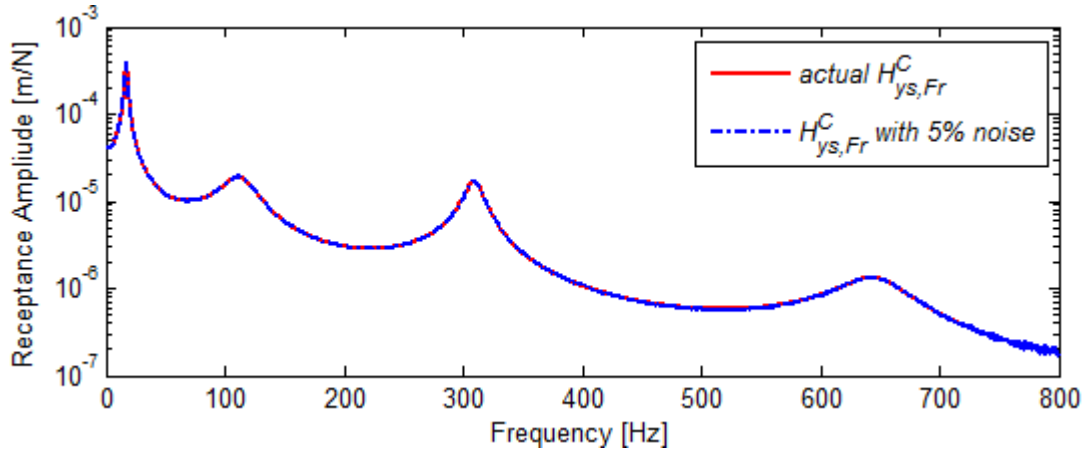

Figure 4.12 Translational Receptance of the Coupled Structure between *s-r*

In order to compare the performances of four decoupling equations (equations (3.18) to (3.21)), the joint identification is performed using each equation by following the procedure described in theory, and the accuracy of the joint parameters identified from each equation are compared. The joint parameters identified by using each equation and the percentage differences from the actual values are given in Table 4.4. As it can be seen from the table the best performance is obtained from equation (3.18).

Table 4.4 Joint Parameters Identified by Using Different Decoupling Equations (Equations (3.18), (3.19) and (3.21))

	k_{Fy} *[N/m]*	$k_{M\theta}$ *[N.m/rad]*	$k_{F\theta}$ *[N/rad]*	c_{Fy} *[N.s/m]*	$c_{M\theta}$ *[N.m.s/rad]*	$c_{F\theta}$ *[N.s/rad]*
Actual values	10^6	10^3	10^4	25	5	8
Identified values (3.18)	$1.01*10^6$	$1.11*10^3$	$9.03*10^3$	25.2	4.83	5.60
Error (%)	*1.3*	*11*	*-9.7*	*0.8*	*-3.4*	*-30*
Identified values (3.19)	$9.91*10^5$	178	$8.60*10^3$	43.2	3.52	8.19
Error (%)	*-1*	*-82*	*-14*	*72*	*-30*	*3*
Identified values (3.21)	$9.02*10^6$	$9.66*10^2$	$2.38*10^4$	76.3	3.36	13.5
Error (%)	*10*	*-4*	*138*	*205*	*-32*	*68*

It should be noted that, in the identification of joint parameters, FRFs for RDOF can be taken either from the computational model (thus, it can be assumed that in real life applications they will be directly measured), or else they can be estimated from three translational FRF values. Here, both approaches are used separately and thus the effect of estimating FRFs for RDOF is studied. In the latter approach, simulated experimental values for translational FRFs around node *r* with a spacing of 0.02m are used in equation (3.43) in order to find FRFs related with RDOF as illustrated inFigure 4.13 and the resulting estimation is shown in Figure 4.14 to Figure 4.17. In the figures, the blue curve gives the results of the estimation process when there is no

noise in the translational FRFs around node *r*. In the identification of the joint properties, when the estimated FRFs with 5% noisy data are used, from the figures it is seen that, prediction of $H^C_{\theta r,Mr}$ is worse than that of $H^C_{\theta r,Fr}$, and the noise effect is higher in the low frequency range. This is due to using the second-order approximation as noted by Duarte and Ewins (2000).

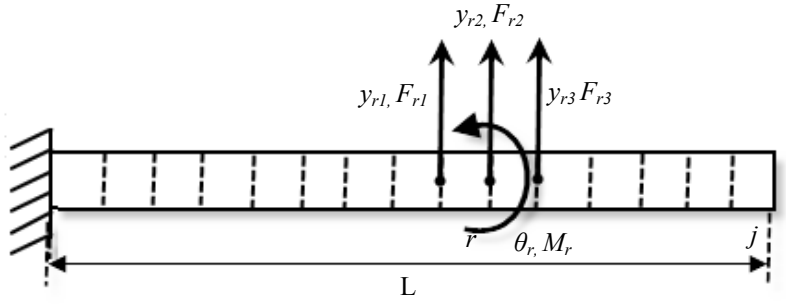

Figure 4.13 Substructure A –RDOF Estimation at the r^{th} Coordinate

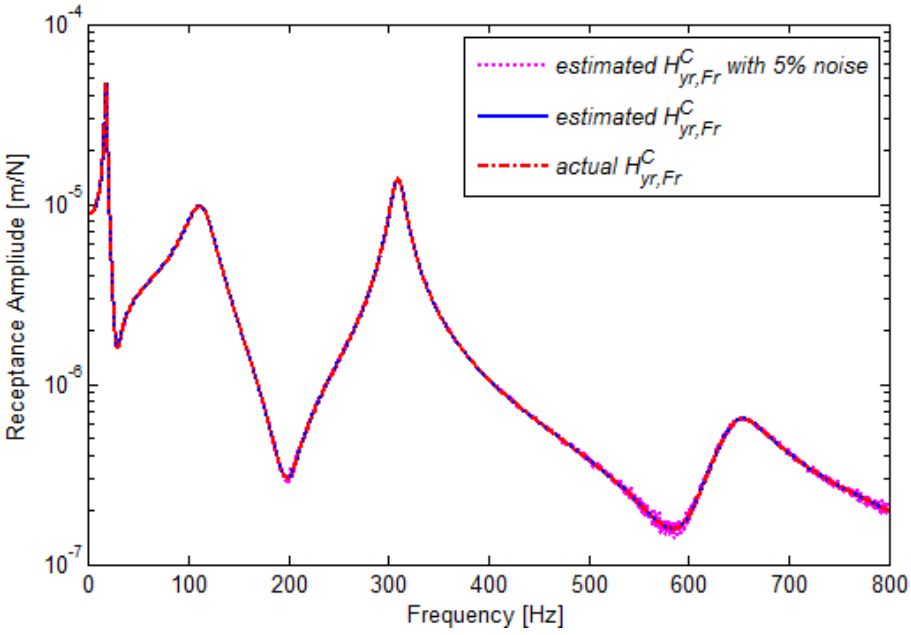

Figure 4.14 Translational Receptance of the Coupled Structure at the r^{th} Coordinate

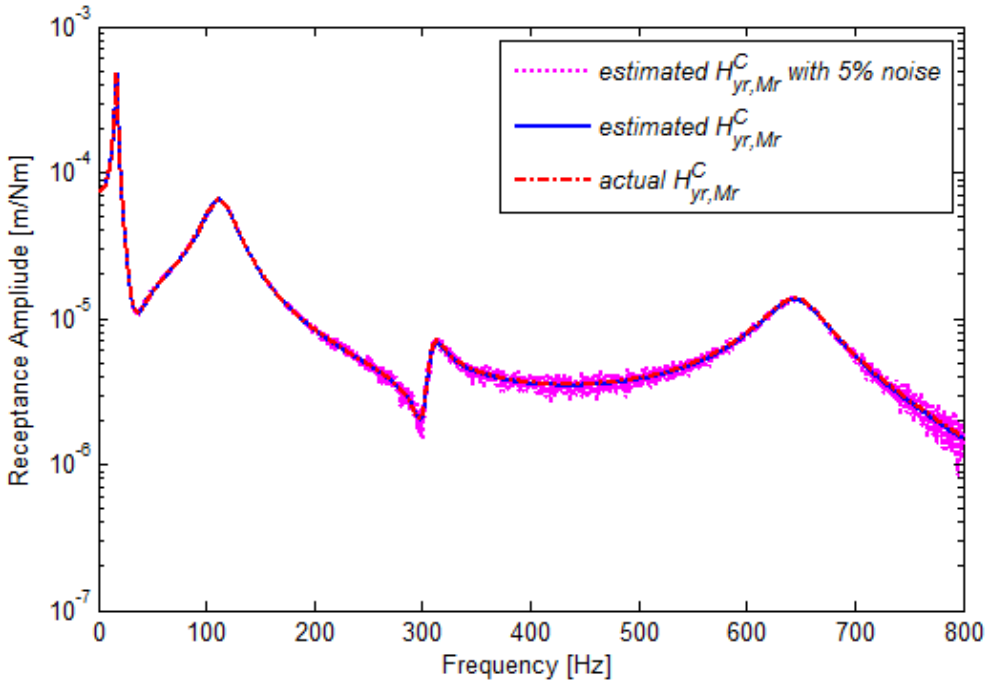

Figure 4.15 Translation/Moment Receptance of the Coupled Structure at the r^{th} Coordinate

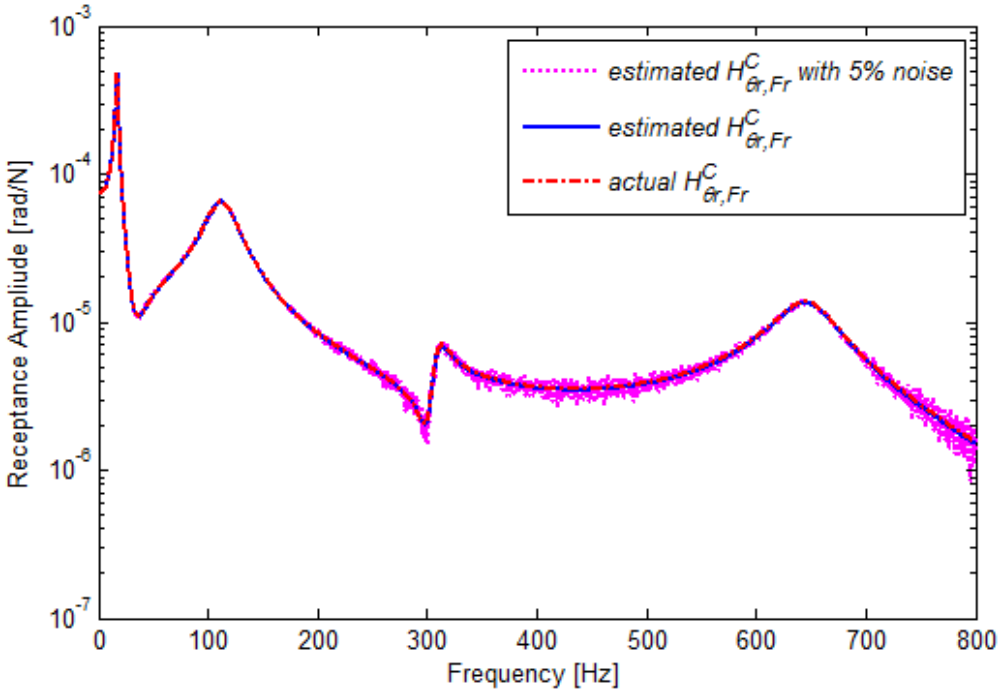

Figure 4.16 Rotation/Force Receptance of the Coupled Structure at the r^{th} Coordinate

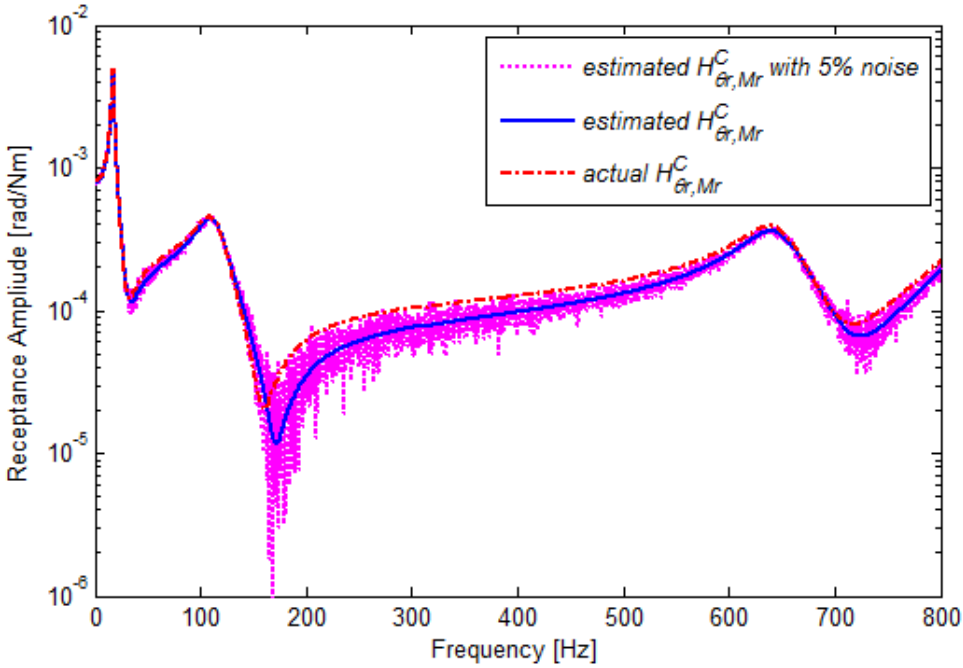

Figure 4.17 Rotational Receptance of the Coupled Structure at the r^{th} Coordinate

Identified joint stiffness and damping values are given in Figure 4.18 to Figure 4.20 and Figure 4.21 to Figure 4.23, respectively. In these figures, *identification 1* represents the identified joint parameters by using simulated measurements for RDOF related FRFs; *identification 2* represents the identified joint parameters by using estimated RDOF related FRFs.

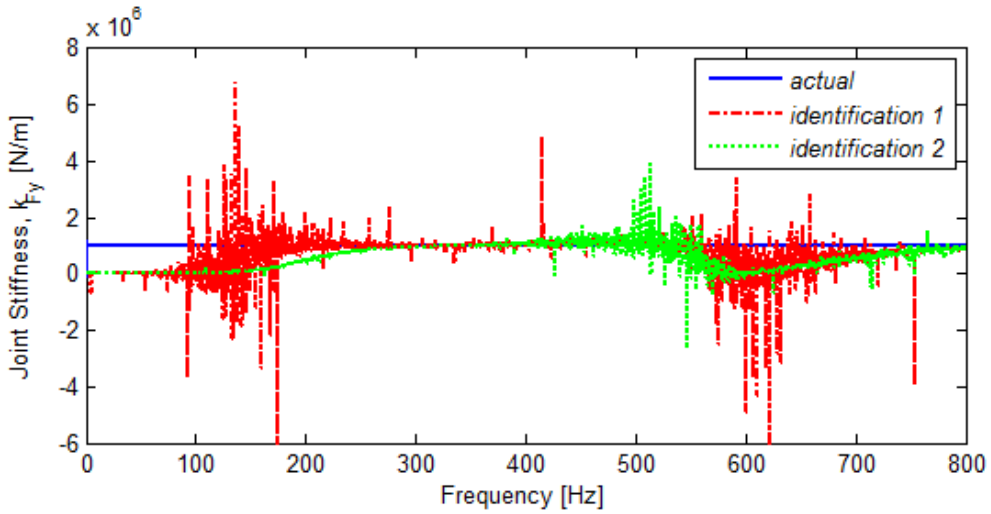

Figure 4.18 Identification of Translational Joint Stiffness

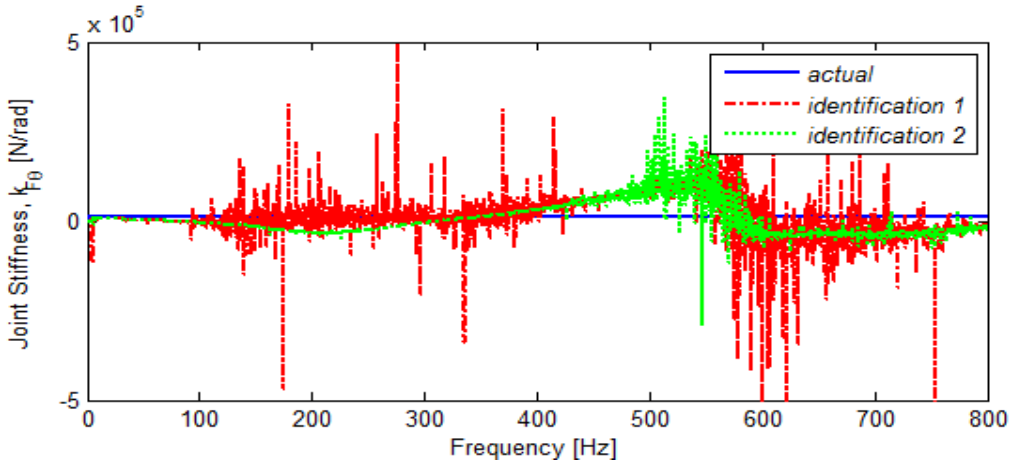

Figure 4.19 Identification of Cross-coupling Joint Stiffness

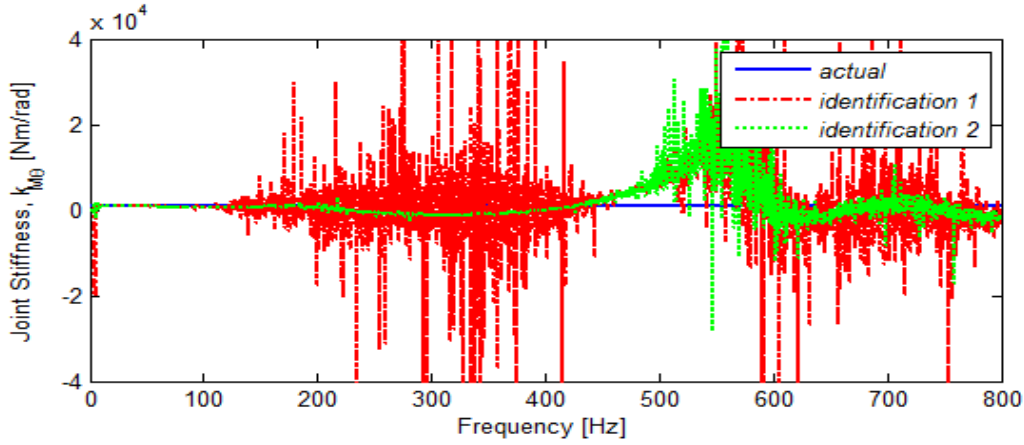

Figure 4.20 Identification of Rotational Joint Stiffness

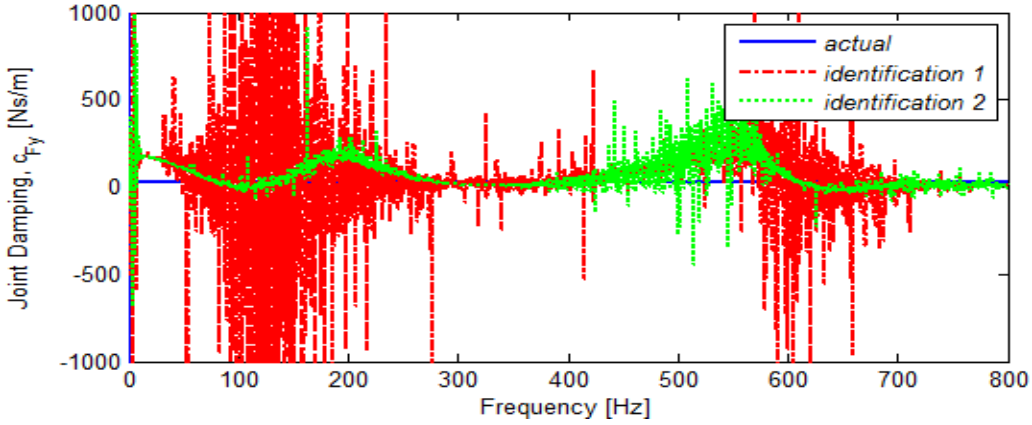

Figure 4.21 Identification of Translational Joint Damping

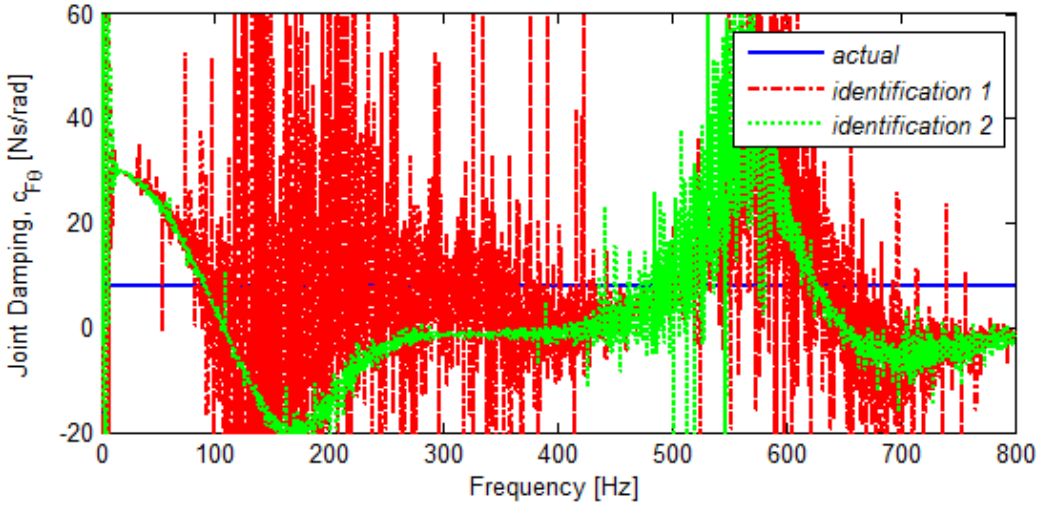

Figure 4.22 Identification of Cross-coupling Joint Damping

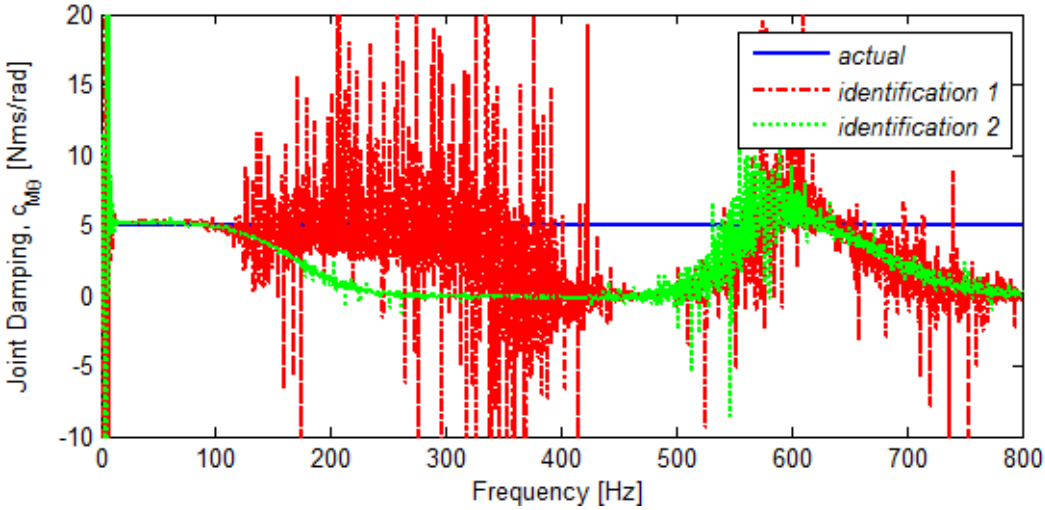

Figure 4.23 Identification of Rotational Joint Damping

As discussed above, at frequencies where the connection parameters have less effect on the response of the coupled system, the identified values deviate from the actual values considerably. Although it is not known in advance at which mode the joint dynamics will affect the coupled system dynamics considerably, the joint properties are identified in a range of frequency and the average of the values are taken in a region where deviations from a constant value is minimum. In this case study, the following ranges are used in the identification of the joint properties: 200-400 Hz for the translational joint properties, 15-300 Hz for the rotational joint properties and 150-310 Hz for the cross-coupling joint properties as shown in Figure 4.24. As it will be further illustrated with the experimental studies, due to the measurement errors (including errors in the estimation of FRFs) and numerical errors associated with matrix inversion, the best frequency range to determine the joint properties may not be obvious. In order to obtain the joint properties accurately, an optimization algorithm is developed, which will be explained in more detail in Chapter 5.

Note that, the damping properties are prone to noise much more than the stiffness properties, since their effects on the coupled system dynamics is much less than those of joint stiffness values. For the damping terms, the frequency ranges used for identification of stiffness values are employed as shown in Figure 4.25.

The average values of the identification results in these ranges are given in Table 4.5. Note that when cross-coupling terms are identified as negative values, they are taken as zero.

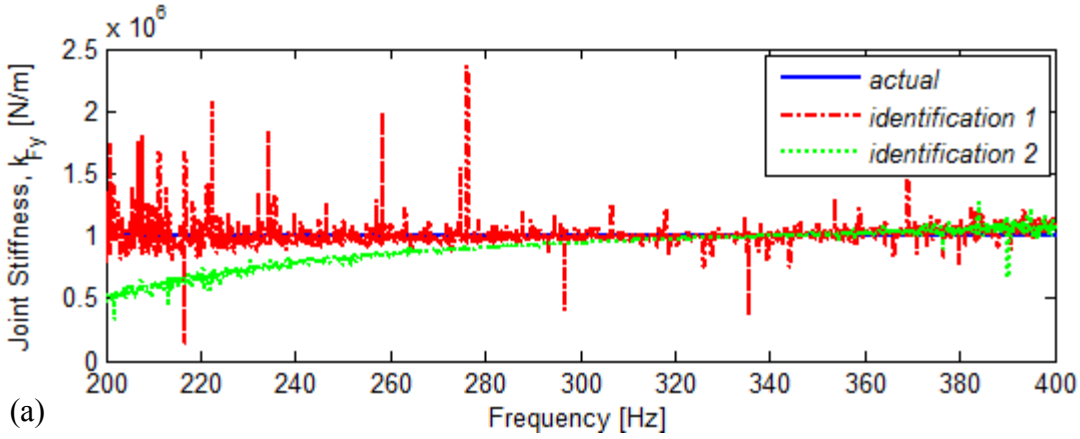

(a)

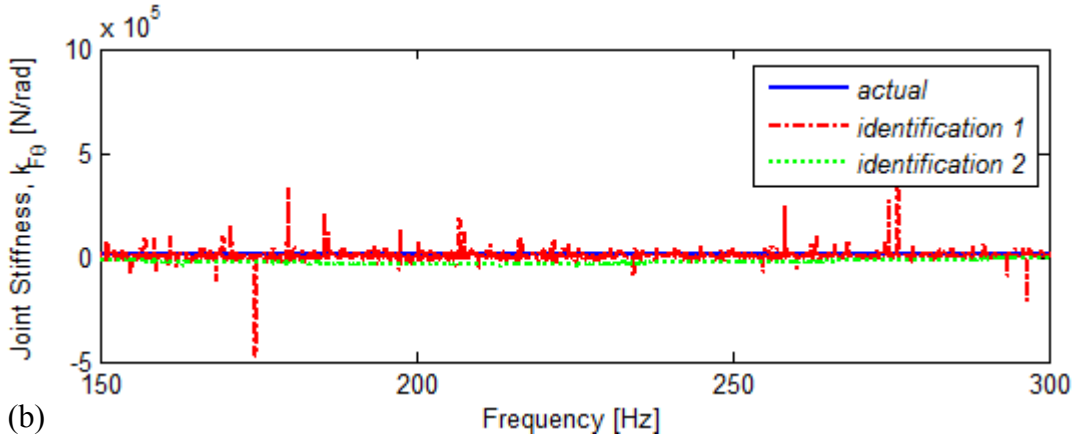

(b)

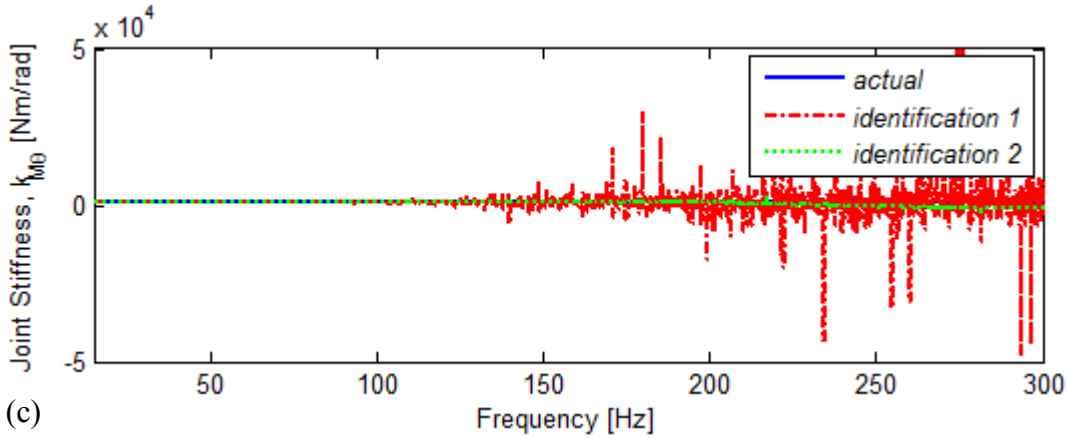

(c)

Figure 4.24 Identification of Joint Stiffness (a) Translational Joint Stiffness, (b) Cross-coupling Joint Stiffness, (c) Rotational Joint Stiffness

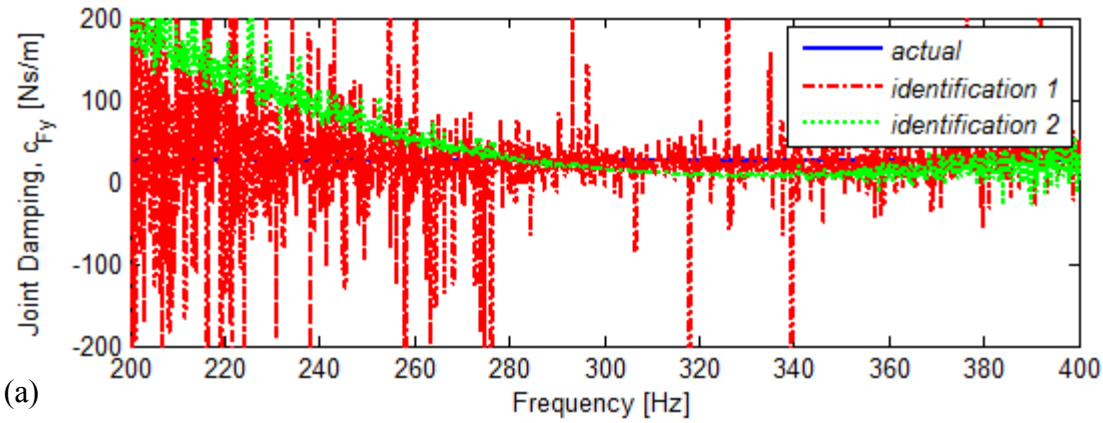

(a)

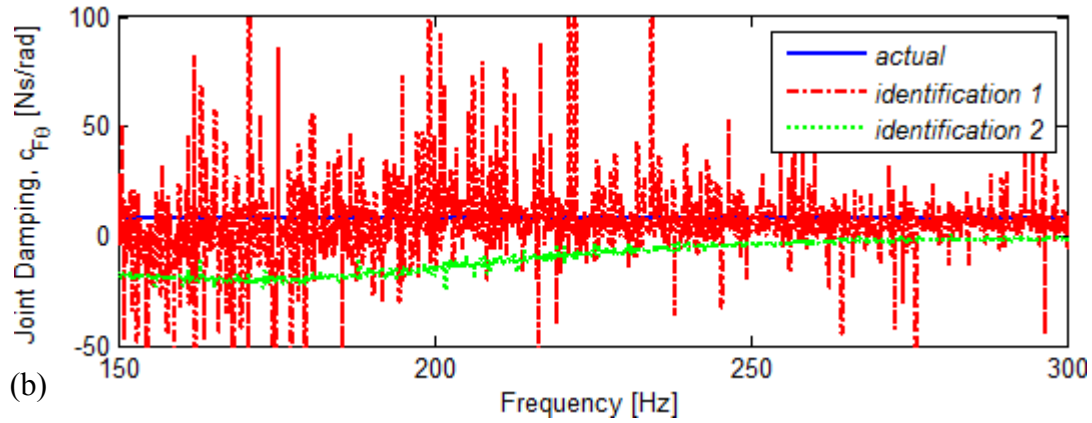

(b)

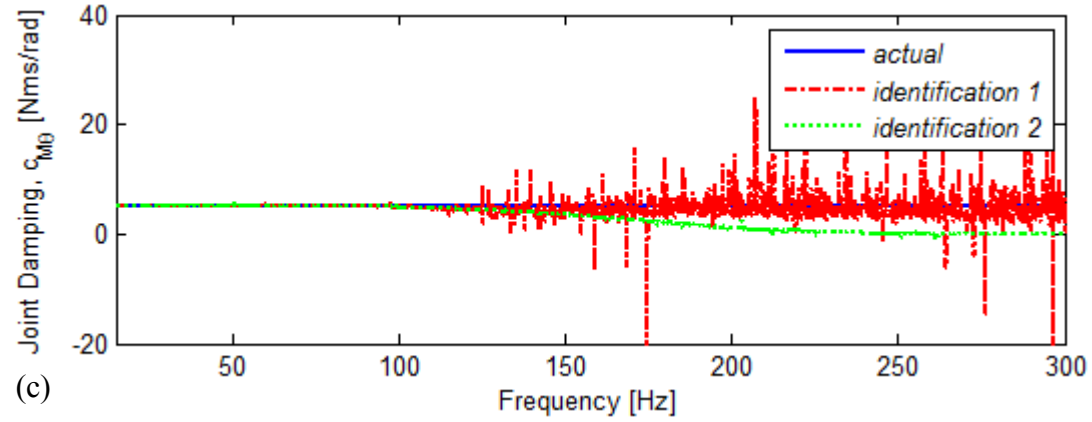

(c)

Figure 4.25 Identification of Joint Damping (a) Translational Joint Damping, (b) Cross-coupling Joint Damping, (c) Rotational Joint Damping

Table 4.5 Identified Joint Properties and Percentage Errors in These Values

	k_{Fy} *[N/m]*	$k_{M\theta}$ *[N.m/rad]*	$k_{F\theta}$ *[N/rad]*	c_{Fy} *[N.s/m]*	$c_{M\theta}$ *[N.m.s/rad]*	$c_{F\theta}$ *[N.s/rad]*
Actual values	10^6	10^3	10^4	25	5	8
Identification1	$1.01*10^6$	$1.11*10^3$	$9.03*10^3$	25.2	4.83	5.60
Error (%)	*1.3*	*11*	*-9.7*	*0.8*	-3.4	-30
Identification2	$9.02*10^5$	$5.30*10^2$	0	47.6	2.79	0
Error (%)	*-9.8*	*-47*	*-100*	90	-44	-100

From Table 4.5 it can be observed that when the simulated measurement values for RDOF related FRFs are used in the identification, the maximum error in the identified translational stiffness and damping values does not exceed 1.3%. The error in rotational and/or cross-coupling stiffness and damping values can reach to -30%. However, when the estimated RDOF related FRFs are used in the identification, the error in identified translational stiffness and damping values reaches to about -10% and 90%, respectively, whereas the error in rotational and cross-coupling values can be completely erroneous. At this stage, it may be concluded that using estimated FRFs will yield unacceptable errors. However, before reaching to such a conclusion, the effect of the errors in the identified properties of the joints on the regenerated response of the system is to be studied. It is quite possible that major effect of the joint dynamics on system response is represented by the translational stiffness of which identified value deviates from the actual one less than -10% in the worst case in this case study. For this purpose, firstly the sensitivity of system response to each joint parameter is investigated. Figure 4.26 shows the sensitivity of the receptance $H_{yr,Fr}$ of the coupled structure to joint stiffness values.

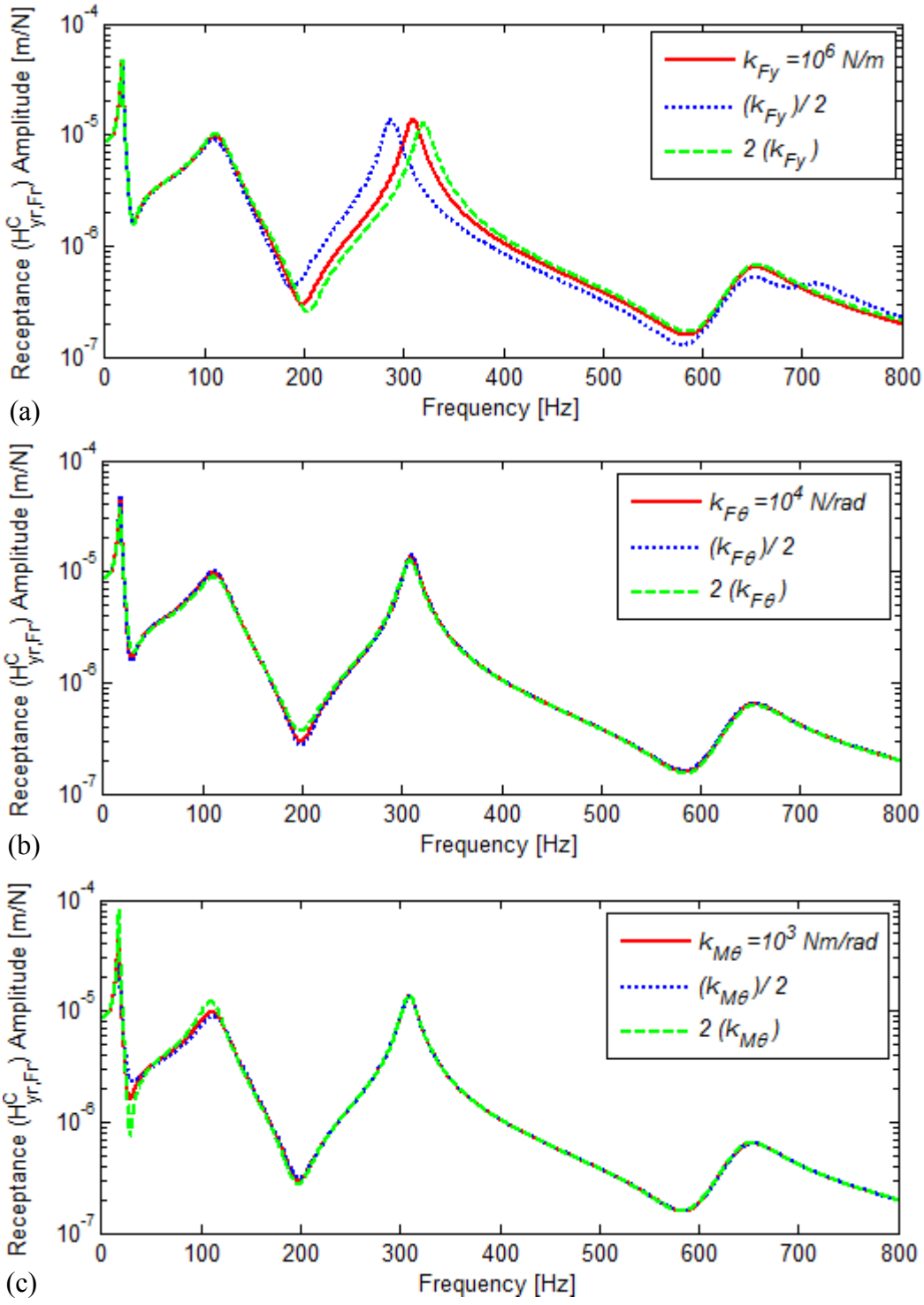

Figure 4.26 Sensitivity of the Receptances of the Coupled Structure to: (a) Translational, (b) Cross-coupling, (c) Rotational Joint Stiffness

It is observed that, the translational joint stiffness is very effective at the third and fourth modes and rotational joint stiffness has some effect at the second mode, while the cross-coupling joint stiffness has negligible effect on the receptance of the coupled system. Hence, it can be concluded for this case study that having large errors in the identified values of rotational and especially cross-coupling joint stiffness values will not deteriorate the mathematical model for the joint, as long as translational stiffness of the joint is accurately identified.

Secondly, by using the two sets of identified joint parameters, FRFs of the assembled system are regenerated and they are compared with the actual FRFs in Figure 4.27. It can be seen from the comparison that the FRFs regenerated by using the joint parameters obtained from *identification 1* perfectly match with the actual FRFs. On the other hand, the FRFs regenerated by using the joint parameters obtained from *identification 2* have some slight deviations from the actual FRFs, especially at the second and fourth modes. Thus, it can be concluded that although the accuracy of the identified values for some joint parameters are not so good (when estimated FRFs for RDOF are used), their effect on the system dynamics is not so significant, and therefore the identification method proposed in this study can be used in practical applications for the identification of joint dynamics by using only translational FRF measurements.

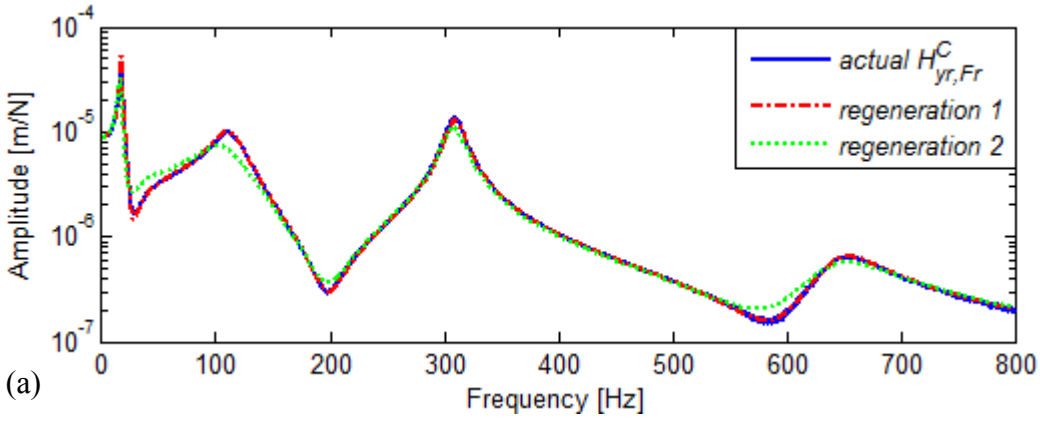

(a)

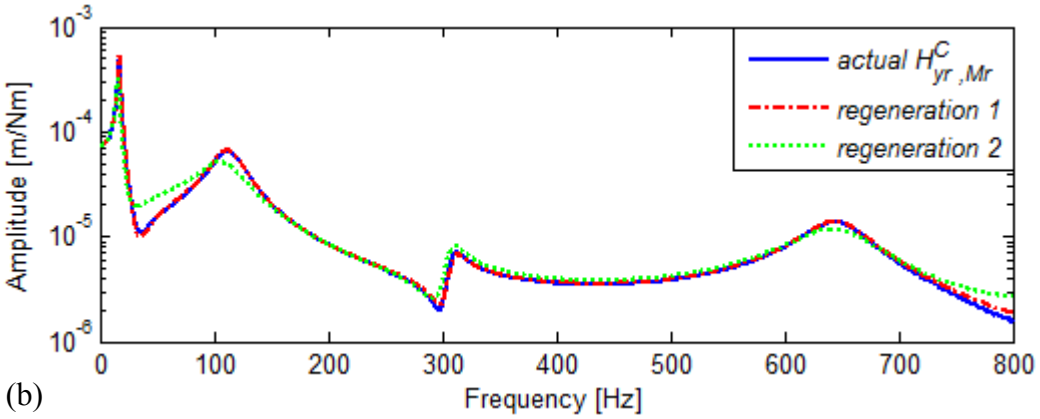

(b)

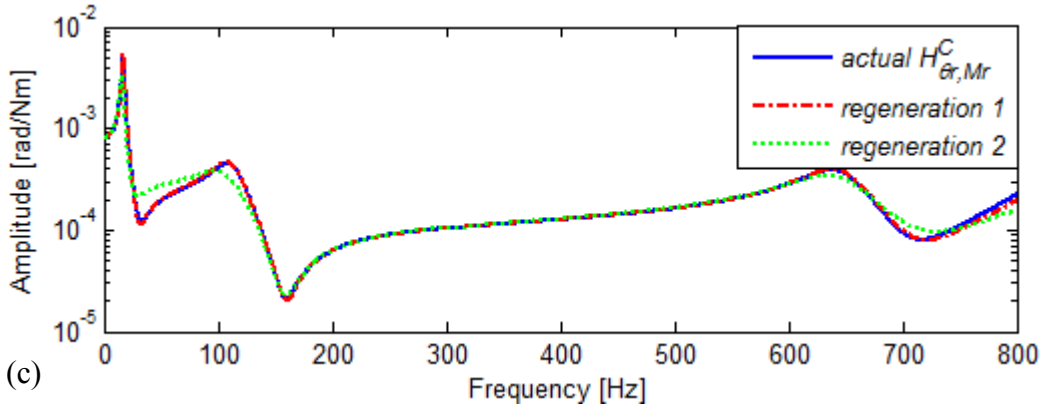

(c)

Figure 4.27 Regenerated FRFs of the Coupled Structure by Using Identified Joint Properties (a) $H^C_{yr,Fr}$, (b) $H^C_{yr,Mr}$ (or $H^C_{\theta r,Fr}$), (c) $H^C_{\theta r,Mr}$

4.2.2 Case Study 2

The aim of this case study is to show the importance of using rotational stiffness values in a joint model, and identify joint properties by using different decoupling equations. Although the most accurate results are obtained with equation (3.18), from practical application point of view, joint parameters are estimated by using decoupling equation given by equation (3.21), because as it will be explained in more detail in Chapter 5, among the decoupling equations the most practical one is equation (3.21) from the experimental applicability point of view. In this case study, in order to make the identification more practical for real experiments, rather than using RDOF related FRFs of the coupled structure, only TDOF related ones are measured and used in the identification equation. Hence, in the identification process, the need for the estimation of RDOF related FRFs belonging to the coupled structure is eliminated while keeping joint model (consisting of translational, rotational and cross-coupling elements) unchanged. This approach is also expected to increase the accuracy of the identification. As illustrated in Figure 4.28, substructure A having fixed-free boundary condition and substructure B having free-free boundary condition. Each substructure is modeled with 5mm length beam elements using finite element method (FEM).

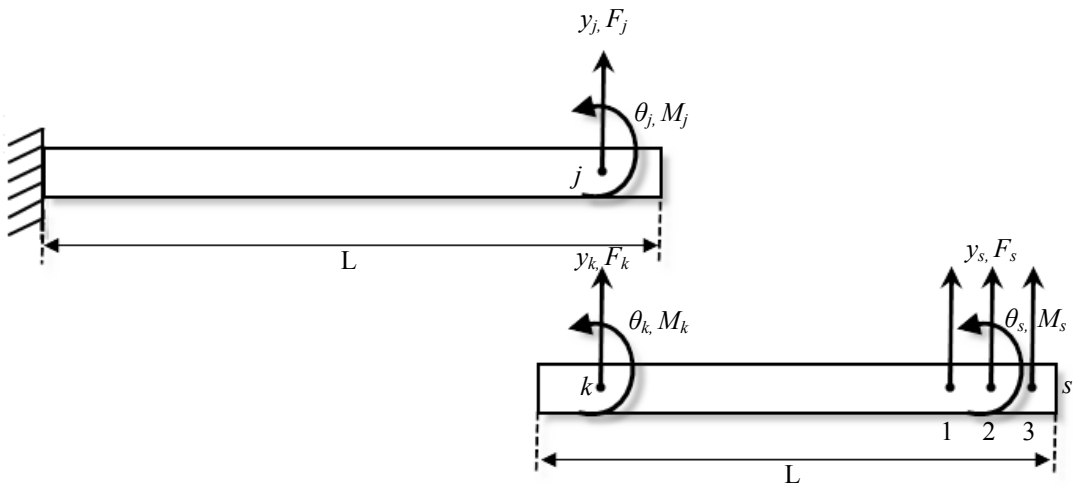

Figure 4.28 Substructures Coupled with a Joint

The following data are used for the beams:

Length of substructure A: $L=0.3\ m$; Length of substructure B: $L=0.225\ m$; modulus of elasticity: $E=67\ 10^{9}\ N/m^{2}$; moment of inertia of the cross-sectional area: $I=4.5\ 10^{-10}\ m^{3}$; mass per unit length of the beams: $m=0.4050\ kg/m$; constant damping ratio for beams: $\zeta=0.01$.

Coupled Structure with Joint Model 1

Only translational joint parameters are included in Model 1, hence this model couples the translational DOFs at the connection interface of the two beams.

$$[K^{*}(\omega)]=[10\text{ ^ }5+j\omega 5] \tag{4.6}$$

FRF of the coupled structure at the tip point obtained with coupling of two beams with a pure translational joint model is given in Figure 4.29.

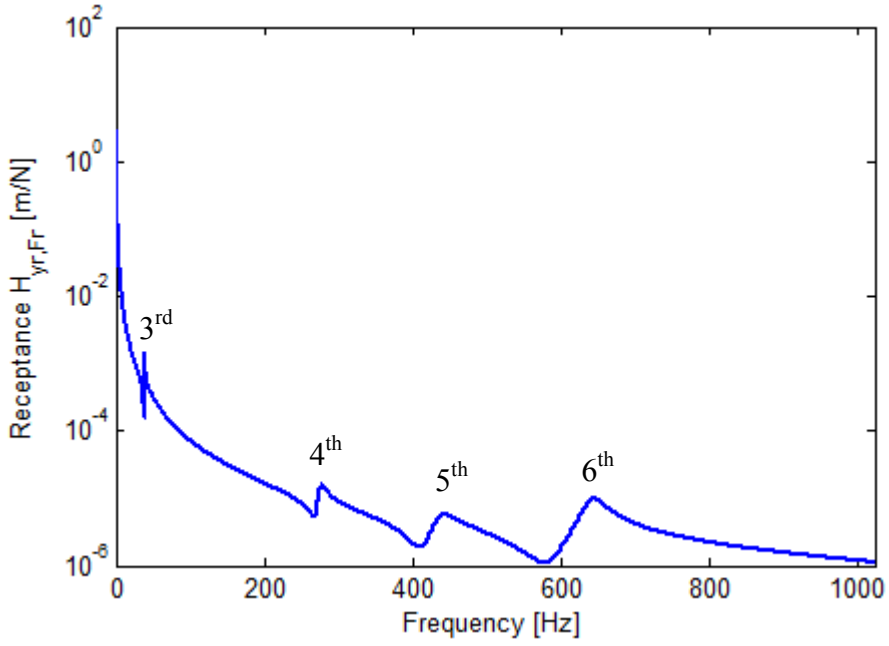

Figure 4.29 Coupled Structure Translational FRF at Point 2

The coupling theory in this system is verified with the simulations performed in ANSYS and the mode shapes of the coupled structure obtained are shown in Figure 4.30. Note that, the connection is modeled with "*combin14*" element from the element library of ANSYS.

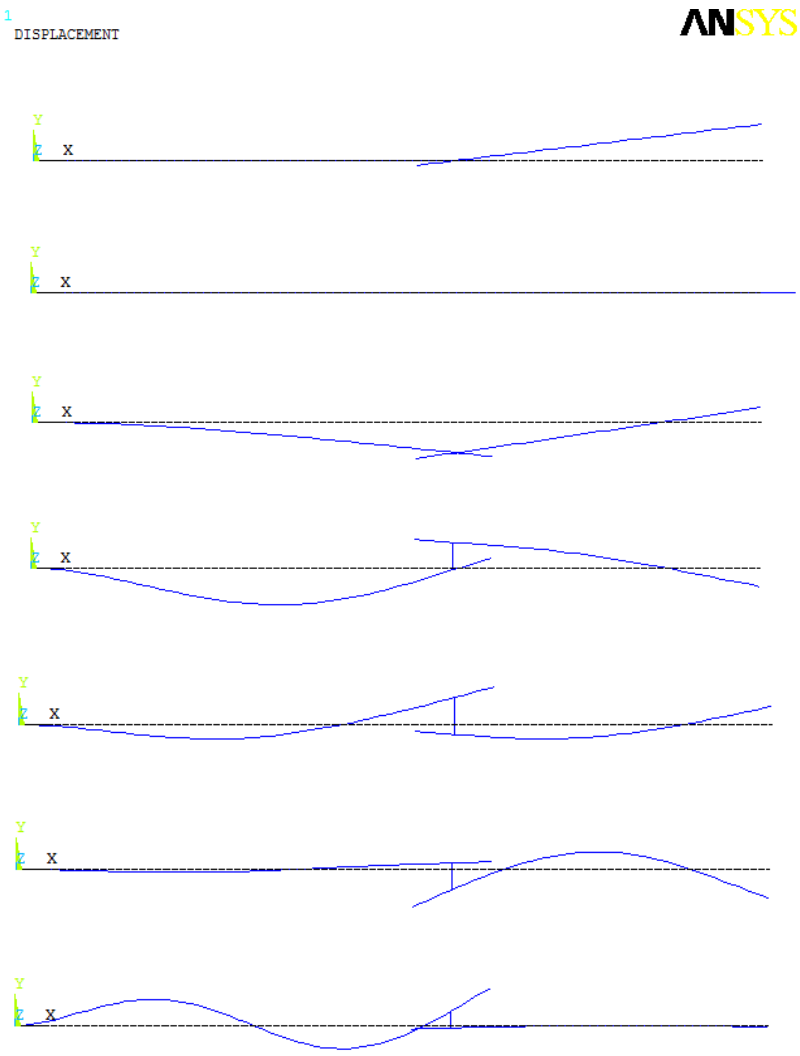

Figure 4.30 Mode Shapes of the Coupled Structure, 1st & 2nd Modes: 0Hz, 3rd Mode: 39.5Hz, 4th Mode: 278.3Hz, 5th Mode: 442Hz, 6th Mode:645.5Hz

It can be seen from the mode shapes that coupling two beams via only one translational joint is not realistic. Actually, the mode shapes are expected to be similar to the case for a cantilever beam. Hence, it can be inferred that using only one translational joint does not fully simulate the real case because it lacks of coupling the RDOFs at the connection interface of the beams. For that purpose, in the next case Model 2 including RDOF joint property is used in the coupling analysis.

Coupled Structure with Joint Model 2

In this model, a rotational joint parameter is added in the joint matrix. Hence this model couples both the translational and rotational DOFs at the connection interface of the two beams.

The joint model including the translational and rotational joint parameters is given as follows:

$$[K^*(\omega)] = \begin{bmatrix} 10^5 + j\omega 5 & 0 \\ 0 & 10^3 + j\omega 0.05 \end{bmatrix} \qquad \begin{bmatrix} N/m & \\ & Nm/rad \end{bmatrix} \tag{4.7}$$

FRF of the coupled structure is given in Figure 4.31.

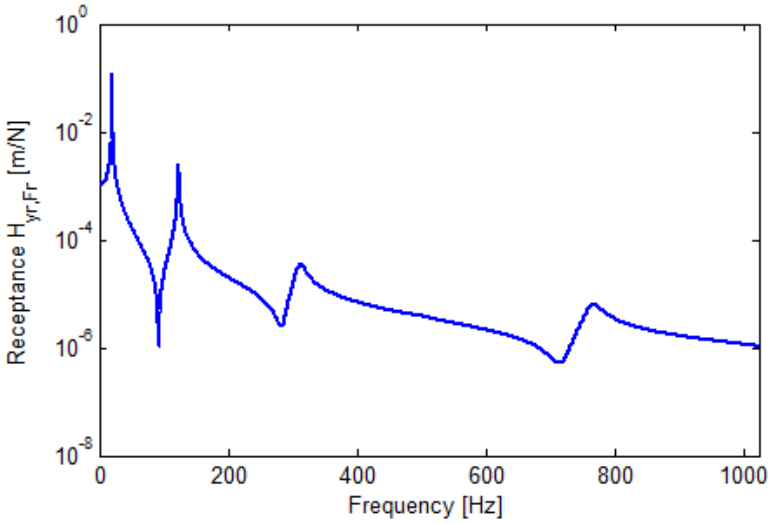

Figure 4.31 Translational FRF of the Coupled Structure at Point 2

Again, this system is modeled in ANSYS to see the behavior of the coupled structure response at different modes. In order to simulate the rotational joint, another "*combin14"* element with freedom in rotation is used. The mode shapes obtained are shown in Figure 4.32. It can be seen that mode shapes of the coupled beam resembles the mode shapes of the cantilever beam. Hence it can be concluded that rotational joint parameters are very important for beam type structures in order to simulate the coupled structure behavior in a correct fashion.

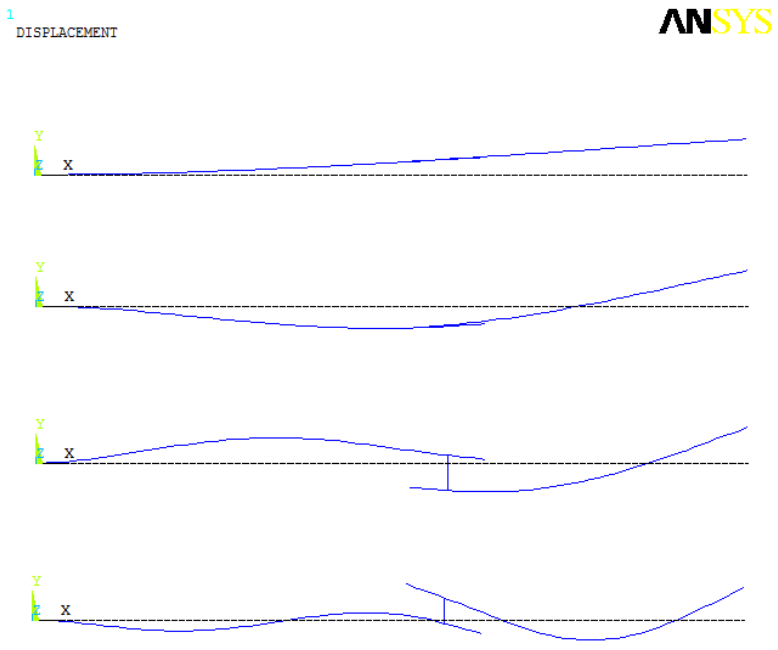

Figure 4.32 Mode Shapes of the Coupled Structure, 1st Mode: 20.4Hz, 2nd Mode: 123.8Hz, 3rd Mode: 312.5Hz, 4th Mode: 767.5Hz

Joint model 3 can also be considered in joint modeling, which is given in the previous case study in section 4.2.1. Hence, in order not to duplicate that work, it is not given here.

Before the identification of joint parameters, the sensitivity of FRFs to joint stiffness in different frequency regions is determined as shown in Figure 4.33 and Figure 4.34.

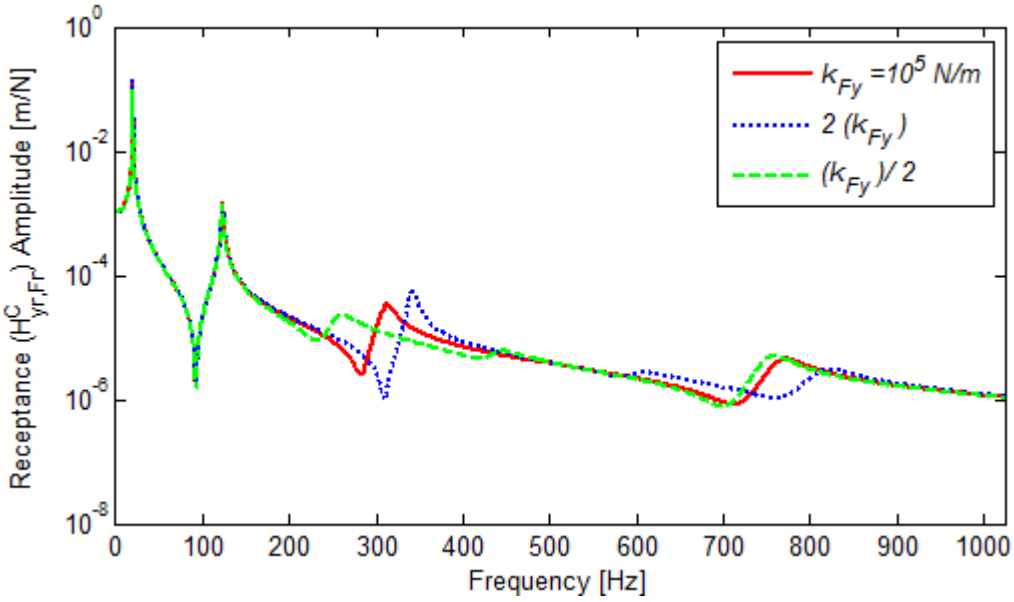

Figure 4.33 Sensitivity of the Coupled Structure Receptance toTranslational Joint Stiffness

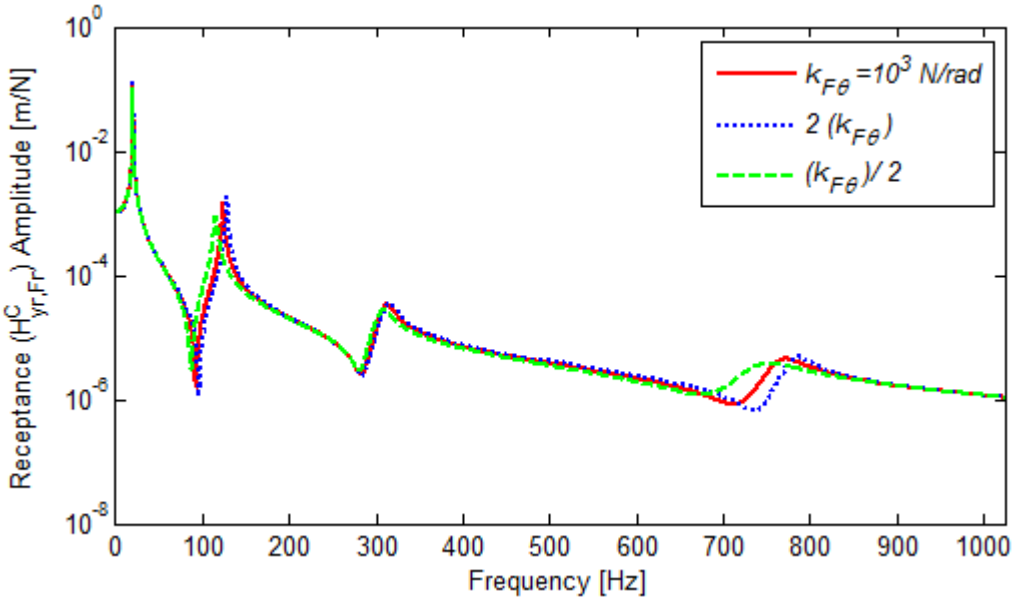

Figure 4.34 Sensitivity of the Coupled Structure Receptance to Rotational Joint Stiffness

In this case study, as it is mentioned before, different approaches are tried to increase the accuracy of the identification. After simulating the experimental data by contaminating the calculated FRFs of the coupled structure, which is connected via joint model 2, with 1% noise as described in the previous case studies, joint identification is performed with equation (3.21). In this part of the study 1% noise contamination is preferred, since the applicability of the identification theory is already verified in previous case studies including 5% noise levels. As, the aim here is to show the differences of the identification approaches, there will not be any problem using 1% noise level. However, a noise study will be given with more detail in section 4.3.

In all the identification approaches the same joint, which is modeled with translational and rotational stiffness and damping terms, will be identified.

Identification Approach 1

This is the classical approach in which the translational and rotational FRFs at the tip point (point 2s) of the coupled structure are used in the decoupling equations. This approach requires the RDOF related FRFs at the tip point. All the FRF matrices used in the identification (equation 4.8) are of size 2 by 2.

$$\underset{(2x2)}{[K^*]} = \underset{(2x2)}{\left[\underset{(2x2)}{[H_{ks}]}.\left[\underset{(2x2)}{[H_{ss}]} - \underset{(2x2)}{\left[H_{ss}^C\right]}\right]^{-1}}.\underset{(2x2)}{[H_{sk}]} - \underset{(2x2)}{[H_{jj}]} - \underset{(2x2)}{[H_{kk}]}\right]^{-1} \tag{4.8}$$

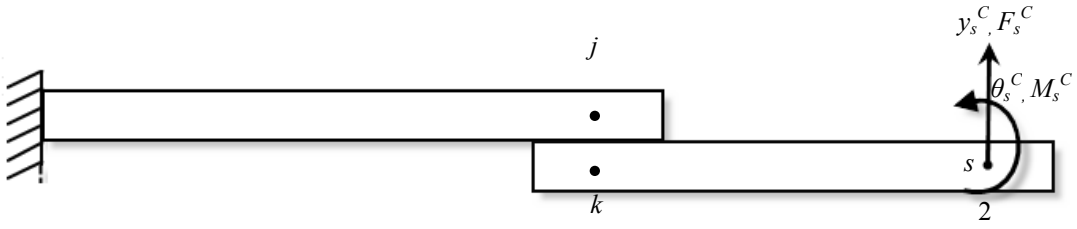

Figure 4.35 Coupled Structure with a Bolted Joint

Identification Approach 2

In this approach only the translational FRFs at the tip point (point 2s) of the coupled structure is used in the decoupling equation. The matrix dimensions can be written as follows:

$$\underset{(2x2)}{[K^*]} = \underset{(2x2)}{\left[\underset{(2x1)}{[H_{ks}]}.\left[\underset{(1x1)}{[H_{ss}]} - \underset{(1x1)}{\left[H_{ss}^{C}\right]}\right]^{-1}.\underset{(1x2)}{[H_{sk}]} - \underset{(2x2)}{[H_{jj}]} - \underset{(2x2)}{[H_{kk}]}\right]^{-1}} \tag{4.9}$$

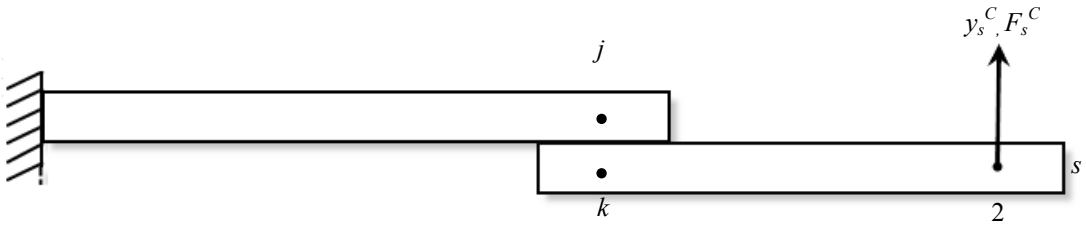

Figure 4.36 Coupled Structure with a Bolted Joint

Identification Approach 3

In this approach two of the translational FRFs at the tip point (points 2s and 3s) of the coupled structure are used in the decoupling equation. In that case all FRF matrices used in the identification (equation 4.10) are of size 2 by 2. Note that, this approach differs from the classical approach by using only the translational FRFs of the coupled structure.

$$\underset{(2x2)}{[K^*]} = \underset{(2x2)}{\left[\underset{(2x2)}{[H_{ks}]}.\left[\underset{(2x2)}{[H_{ss}]} - \underset{(2x2)}{\left[H_{ss}^{C}\right]}\right]^{-1}.\underset{(2x2)}{[H_{sk}]} - \underset{(2x2)}{[H_{jj}]} - \underset{(2x2)}{[H_{kk}]}\right]^{-1}} \tag{4.10}$$

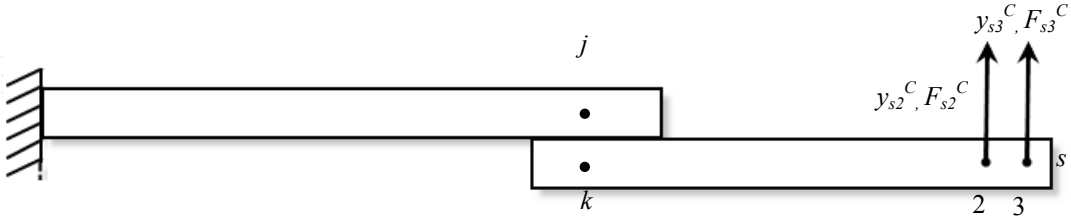

Figure 4.37 Coupled Structure with a Bolted Joint

Identification Approach 4

In this approach three of the translational FRFs at the tip point (points 1s, 2s and 3s) of the coupled structure are used in the decoupling equation. The matrix dimensions can be written as follows:

$$\underset{(2x2)}{[K^*]} = \underset{(2x3)}{\left[H_{ks}\right]} . \left[\underset{(3x3)}{\left[H_{ss}\right]} - \underset{(3x3)}{\left[H_{ss}^C\right]} \right]^{-1} . \underset{(3x2)}{\left[H_{sk}\right]} - \left[\underset{(2x2)}{\left[H_{jj}\right]} - \underset{(2x2)}{\left[H_{kk}\right]} \right]^{-1} \tag{4.11}$$

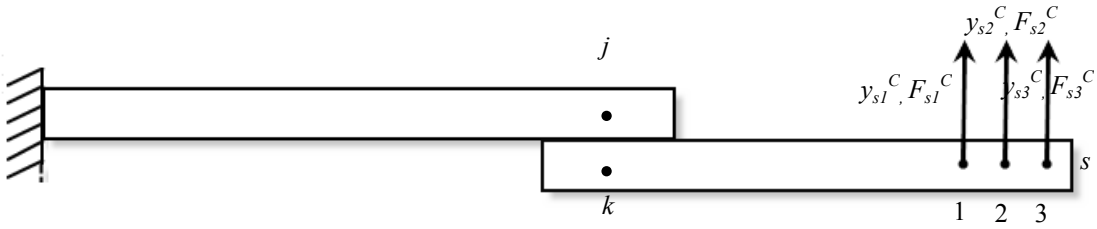

Figure 4.38 Coupled Structure with a Bolted Joint

In this case study, the following ranges are used in the identification of the joint properties: 200-300 Hz for the translational joint properties, 60-180 Hz for the rotational joint properties as shown in Figure 4.39.

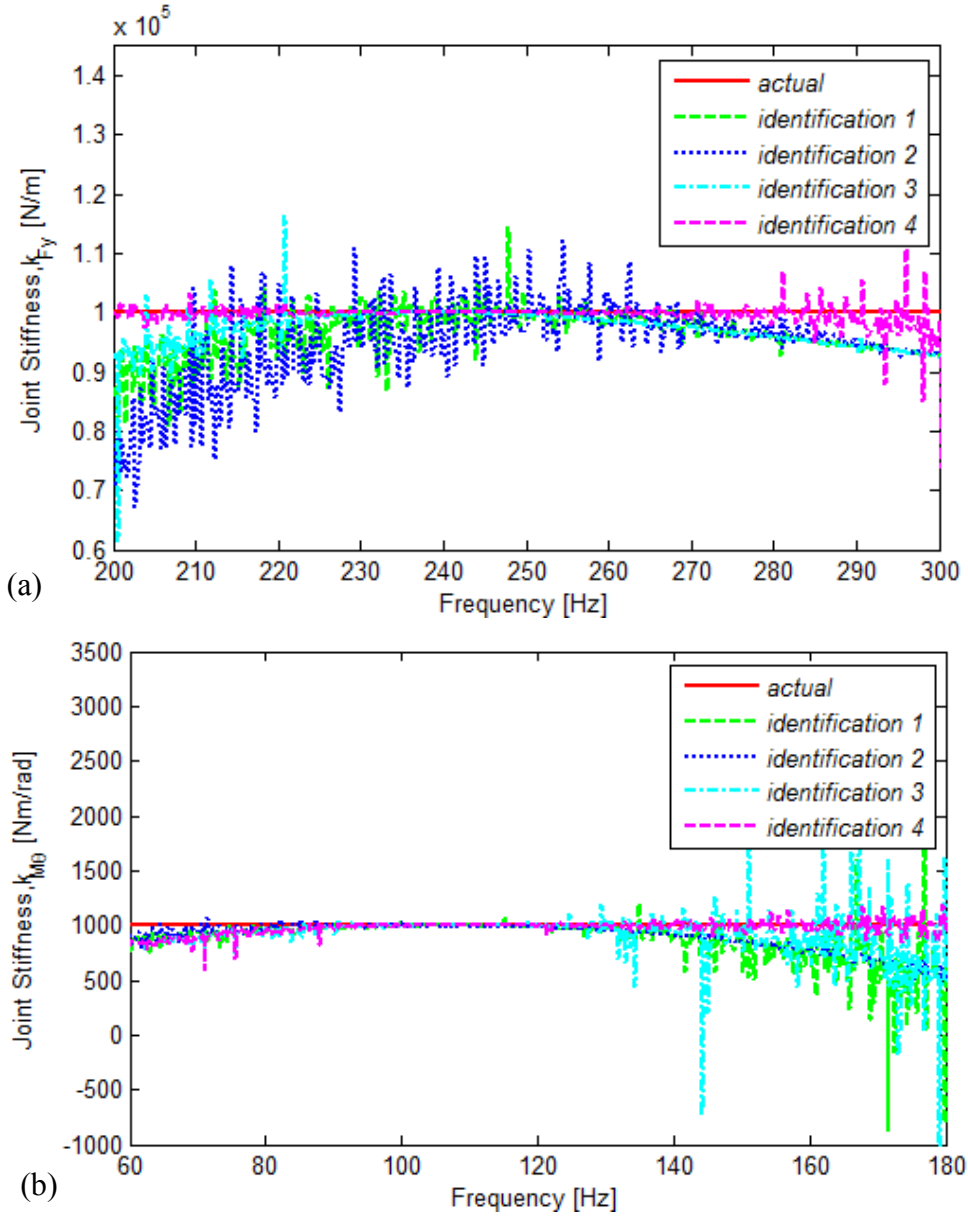

Figure 4.39 Identification of Joint Stiffness (a) Translational Joint Stiffness, (b) Rotational Joint Stiffness

For the damping terms, the frequency ranges used for identification of stiffness values are employed as shown in Figure 4.40. In the figures; *identification 1* corresponds to the identified joint parameters using identification approach 1, *identification 2* corresponds to the identified joint parameters using identification

approach 2, *identification 3* corresponds to the identified joint parameters using identification approach 3 and *identification 4* corresponds to the identified joint parameters using identification approach 4.

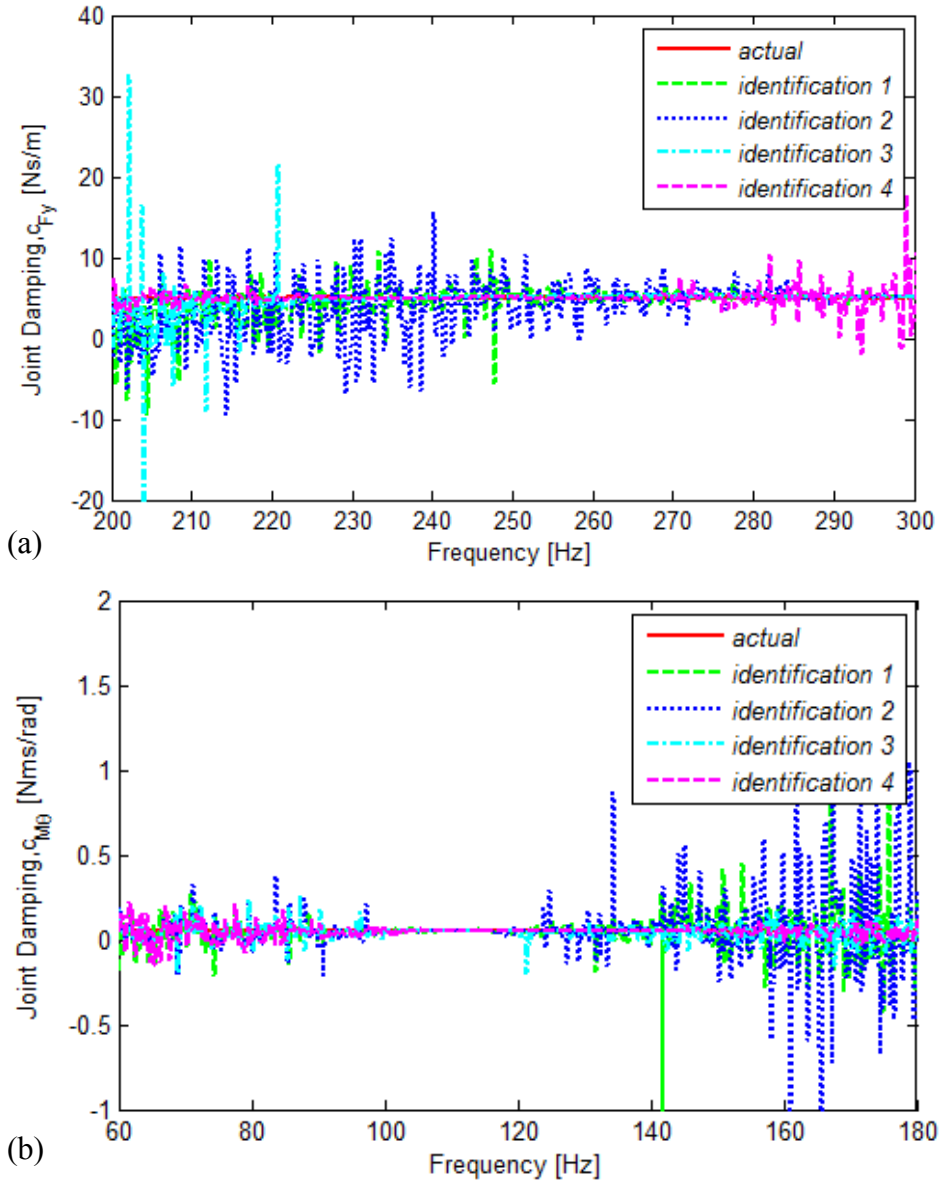

Figure 4.40 Identification of Joint Damping (a) Translational Joint Damping, (b) Rotational Joint Damping

The average values of the identification results in these ranges are compared in Table 4.6.

Table 4.6 Identified Joint Properties and Percentage Errors in These Values

	k_{Fy} *[N/m]*	$k_{M\theta}$ *[N.m/rad]*	c_{Fy} *[N.s/m]*	$c_{M\theta}$ *[N.m.s/rad]*
Actual values	10^5	10^3	5	0.05
Identification 1	$9.68*10^4$	$8.77*10^2$	4.6	0.047
Error (%)	*-3.2*	*-12*	*-7.5*	-5.3
Identification 2	$9.51*10^4$	$9.04*10^2$	4.1	0.055
Error (%)	*-4.9*	*-10*	-18.8	9.7
Identification 3	$9.75*10^4$	$9.20*10^2$	4.8	0.046
Error (%)	*-2.5*	*-8*	*-4.5*	-7.5
Identification 4	$1.00*10^5$	$9.78*10^2$	5	0.049
Error (%)	*0.03*	*-2*	-0.1	-2.3

From the table it can be observed that when the simulated measurements for RDOF related FRFs are used in the identification, the maximum error in the identified translational stiffness and damping values is -7.5%. The error in rotational stiffness and damping values can reach to -12%. However, when only the TDOF related FRFs are used in the identification, the error in identified translational and rotational stiffness and damping values reaches to -18.8% and -10%, respectively. At this stage, when the number of TDOF related FRFs is increased, the identification results get better. For example, when TDOF related FRFs at two points are used, the error in translational stiffness and damping values decreases from -4.9% to -2.5% and -10% to -8%, respectively. Similarly, the error decreases from -18.8% to -4.5% for rotational stiffness and 9.7% to -7.5% for rotational damping. Finally, the most

accurate results are obtained for the case when three translational measurements are taken at the tip point of the coupled structure. The maximum error in the identified translational stiffness and damping values does not exceed -0.1%. The error in rotational stiffness and damping values can reach to -2.3%. Then it can be concluded that as the number of measurement points in the non-joint region is increased, the accuracy of the identification results increase. For this case study, the translational joint stiffness is identified with an error less than 1%. Furthermore, from the experimental point of view, three translational FRF measurements are essential for the estimation of RDOF related FRF at the tip point. In order to eliminate the errors caused by this estimation procedure, using the identification approach 4 instead of identification approach 1 is much better. In this approach, it is also seen from the results that the deviations of the identified values from the exact value are very small for the whole frequency band, except some regions.

In this case study an important conclusion can be drawn about the frequency region where the joint parameters are to be extracted by taking the average of the identified values. As it can be seen from the sensitivity plots given in Figure 4.33 and Figure 4.34, the translational joint properties are effective in the second mode of the system, between 200-400Hz, but in this case study the frequency band taken for the identification of translational joint properties is limited to the band 200-300 Hz. It is due to the fact that, the resonant frequency of the substructure, which is at 336.3Hz, affects the identification results by causing larger errors around this frequency. This can be best observed from the comparison of the substructure resonant frequencies shown in Figure 4.41 with the identification result for the cross-coupling joint stiffnesses given in Figure 4.42. In fact, this joint model does not include cross-coupling terms, so they should be identified as zero. However, it is seen that around the natural frequencies of the substructure, the identified values deviate drastically from zero. This trend happens for the other joint parameters as well. Hence, it is important to avoid the substructure natural frequencies when selecting frequency range for the identification.

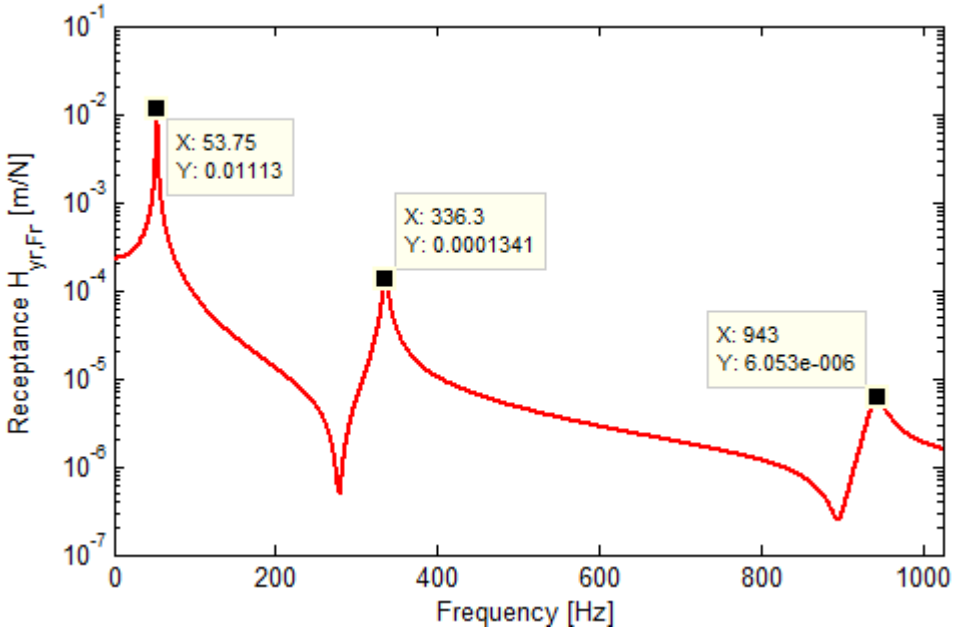

Figure 4.41 TDOF Related Receptance of Substructure A

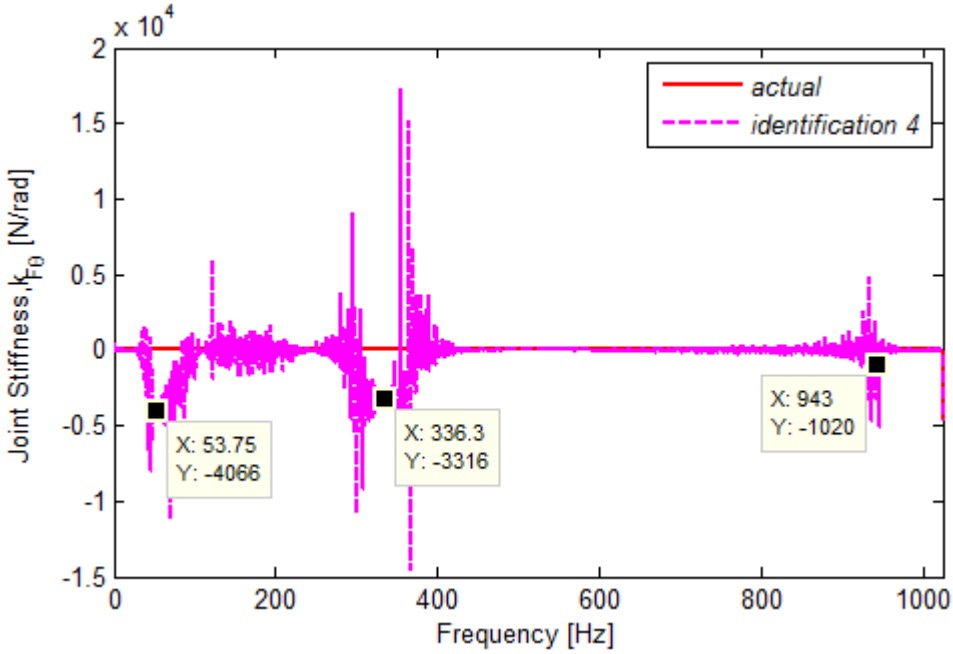

Figure 4.42 Identification of Cross-coupling Joint Stiffness

Then, by using the four sets of identified joint parameters, FRFs of the assembled system are regenerated and they are compared with the actual FRFs in Figure 4.43.

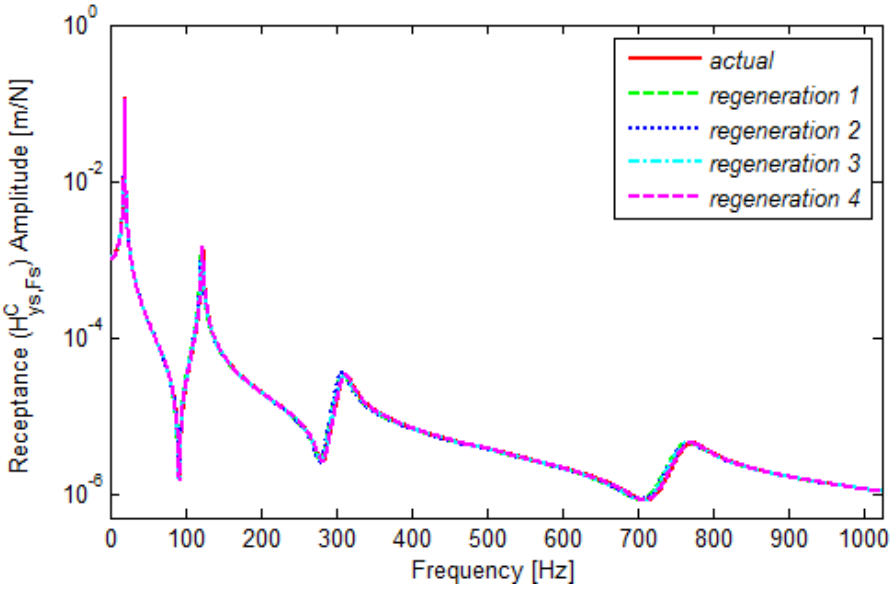

(a)

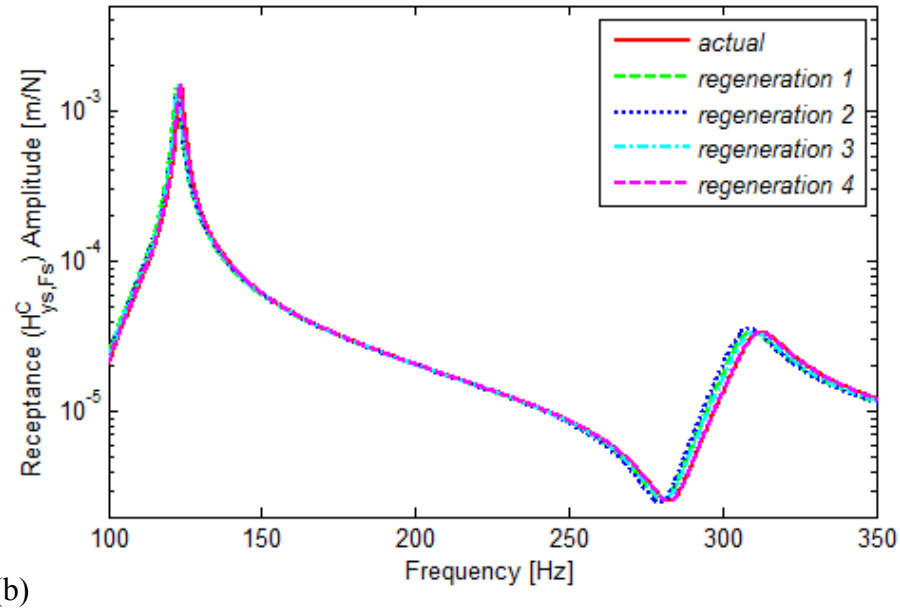

(b)

Figure 4.43 Regenerated Translational FRF of the Coupled Structure by Using Identified Joint Properties (a) Whole Frequency Range, (b) Zoomed Between 100-350Hz

Using only the translational FRFs of the coupled structure is very practical from the experimental point of view. As it can be seen from the regenerated FRFs this approach gives very promising results. Furthermore, by using this approach, one eliminates the need for estimating the RDOF related FRFs of the coupled structure.

4.3 ERROR ANALYSIS

In this section using the fourth identification approach, in which three translational FRFs of the coupled structure at the tip point are used, joint parameters are extracted from the coupled structure's FRFs contaminated with different levels of random noise, such as 1%, 3%, 5% and 10%. The simulation of experimental FRFs is performed with two different noise contamination methods, namely, FRF pollution and response pollution. The aim of this study is to show the effect of noise on the identification results and present the different noise contamination techniques for the simulation of measured FRFs.

4.3.1 Noise Contamination with FRF Pollution

In the first method, FRFs of the system are directly multiplied with randomly distributed data with a mean of 1 and different standard deviations. The noise is generated with the "normrnd" function of MATLAB with normal distribution and standard deviation of 1%, 3%, 5% and 10% around 1 as shown in Figure 4.44. In this approach, noise contamination is uniform in all regions of the FRF curve as in Figure 4.45 and Figure 4.46.

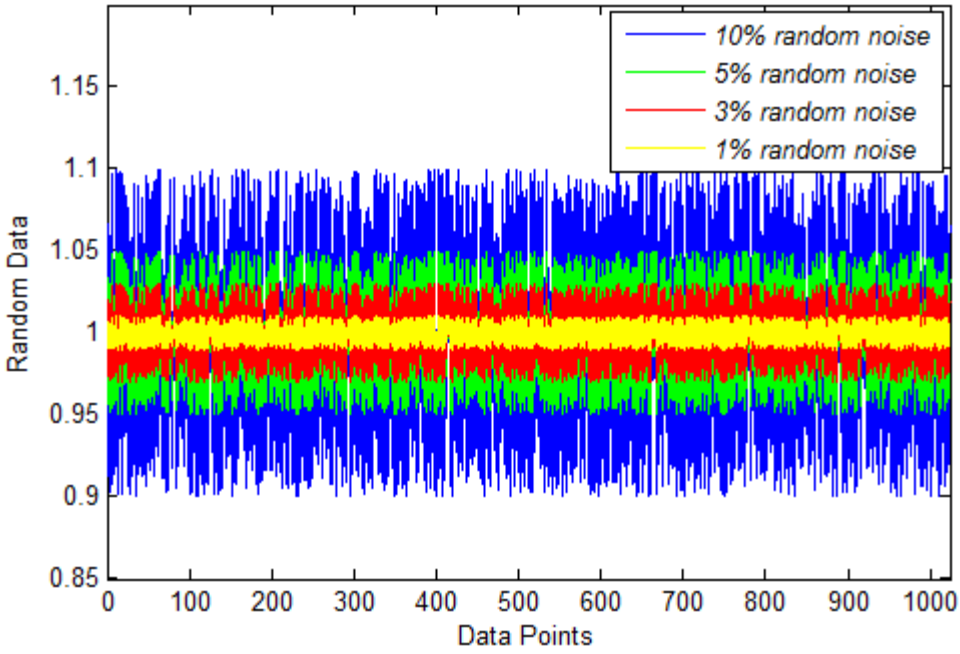

Figure 4.44 Random Data Generated with Different Levels

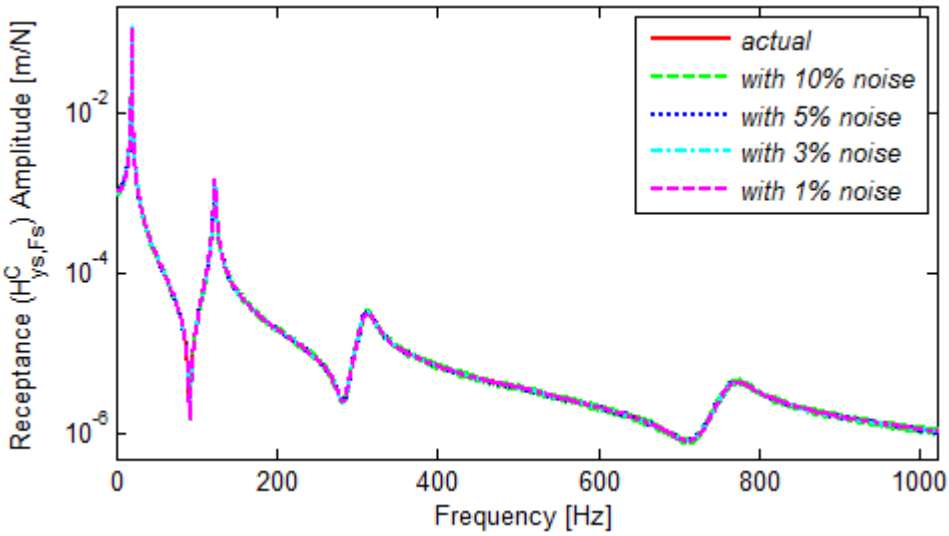

Figure 4.45 Translational Receptance of the Coupled Structure at Point 2

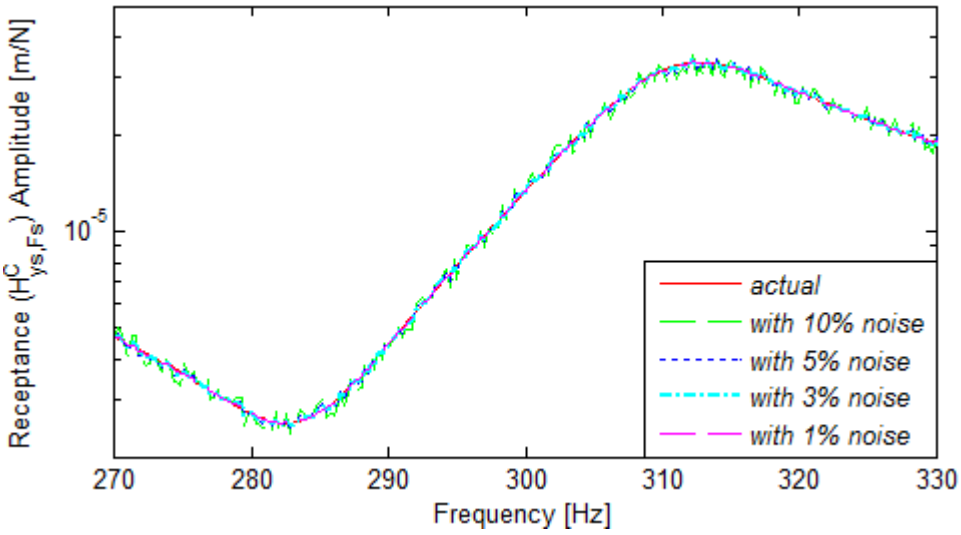

Figure 4.46 Translational Receptance of the Coupled Structure at Point 2-Zoomed View

Identified joint stiffness and damping values obtained by using these data are given in Figure 4.47 and Figure 4.48, respectively. In the figures, comparison of the identification results, which is obtained by using the FRFs simulated through different levels of noise, is illustrated.

The joint parameters identified by using different levels of contaminated FRFs and the percentage differences from the actual values are given in
Table 4.7. It can be seen from the table, the accuracy of the identification gets worse with an increase in noise levels. Rotational joint properties are more prone to noise when compared with the translational joint properties. This conclusion is in line with the conclusion drawn in section 4.2.1. Although rotational joint properties are important for the physical completeness of the coupled model, having large errors in the identified values of rotational joint stiffness values do not deteriorate the mathematical model for the joint, as long as translational stiffness of the joint is accurately identified. Furthermore, the sensitivity of the identification method to noisy data is due to the fact that the decoupling equation involves two inverse matrix operations. With small changes from the actual values of FRFs, the error is amplified

during these inversion operations. This causes some shifts or deviations from the actual values as seen in Figure 4.47and Figure 4.48. Furthermore, it can be concluded that the noise levels have less effect in the frequency regions which are sensitive to joint parameters.

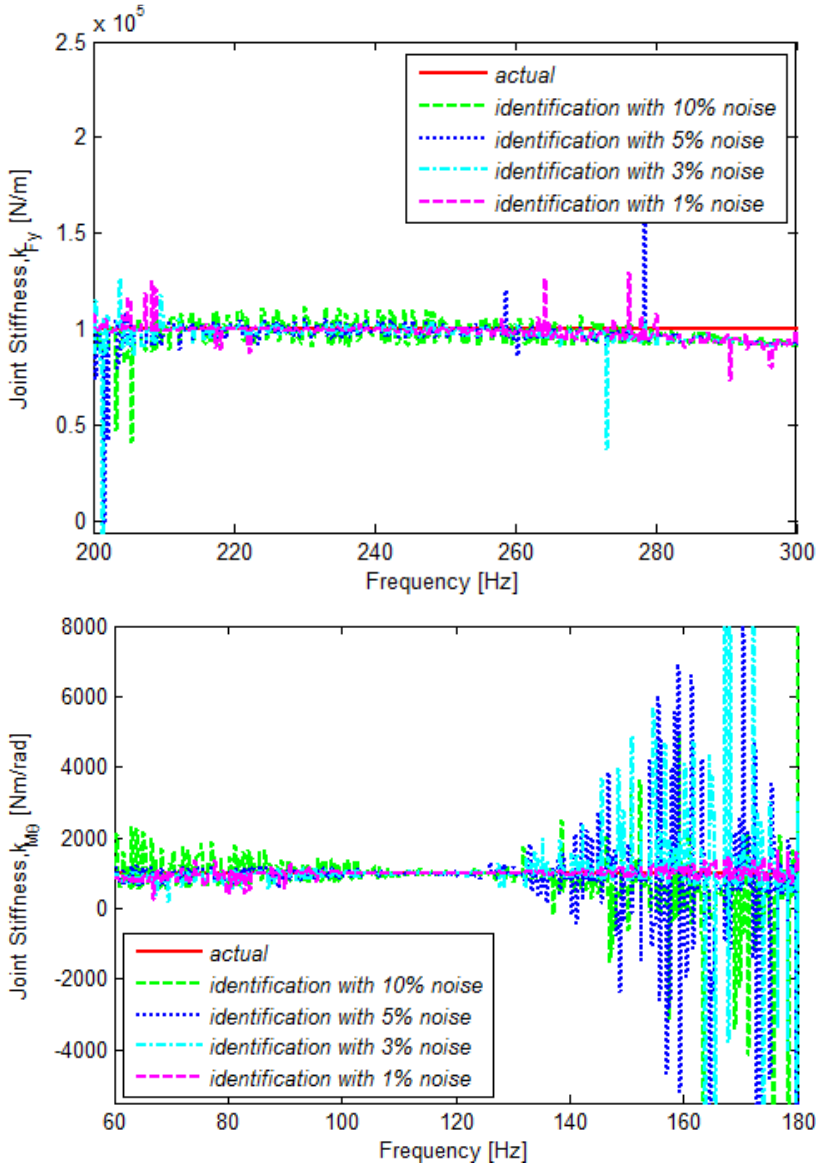

Figure 4.47 Identification of Joint Stiffness (a)Translational Joint Stiffness, (b) Rotational Joint Stiffness

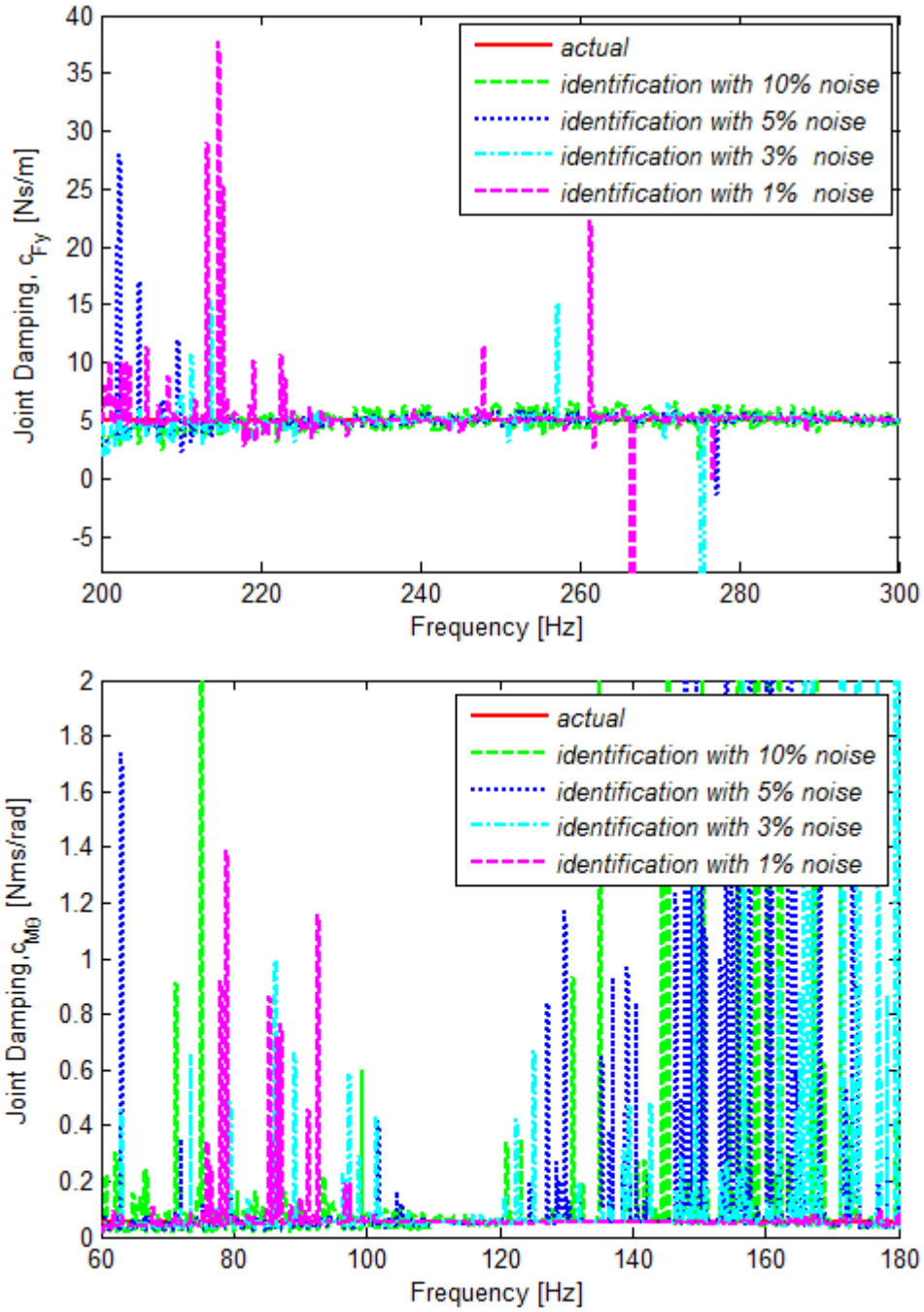

Figure 4.48 Identification of Joint Damping (a) Translational Joint Damping, (b) Rotational Joint Damping

Table 4.7 Identified Joint Properties and Percentage Errors in These Values

	k_{Fy} *[N/m]*	$k_{M\theta}$ *[N.m/rad]*	c_{Fy} *[N.s/m]*	$c_{M\theta}$ *[N.m.s/rad]*
Actual values	10^5	10^3	5	0.05
Identification with 10% Noise	$9.80*10^4$	$7.64*10^2$	5.29	0.218
Error (%)	*-2*	*-24*	*5.76*	*335*
Identification with 5% Noise	$9.79*10^4$	$8.44*10^2$	4.86	0.199
Error (%)	*-2.1*	*-16*	*-2.8*	*297*
Identification with 3% Noise	$9.79*10^4$	$1.06*10^3$	5.12	0.228
Error (%)	*-2.1*	*6*	*2.3*	*357*
Identification with 1% Noise	$9.89*10^4$	$9.93*10^2$	4.998	0.067
Error (%)	*-1.06*	*-0.7*	*-0.04*	*34*

4.3.2 Noise Contamination with Response Pollution

In the second noise contamination technique of FRFs, time response of the system under the harmonic loading is calculated and randomly distributed simulated error with different levels is added to time response and forcing. The noise is generated with the "normrnd" function of MATLAB with zero mean, normal distribution and standard deviations of 1%, 3%, 5% and 10% of the maximum amplitude of the system response. Then by taking the Fast Fourier Transform (FFT) of the response and dividing it by the FFT of the forcing, the polluted receptance is obtained. As the noise becomes more effective when the response of the structure is low, it is believed that this is a more realistic way of simulating noise in FRF measurements. In fact, in all measurement system there is some noise due to the cabling, sensors and data acquisition system. This noise is always in the data. The effect of noise is not much noticeable for high levels of system response, while for the lower levels of response the dominance of the noise increases, so that the response may be totally

contaminated with noise as shown in Figure 4.49. Therefore this type of noise contamination technique is considered to be more realistic for the simulation of an experimental data.

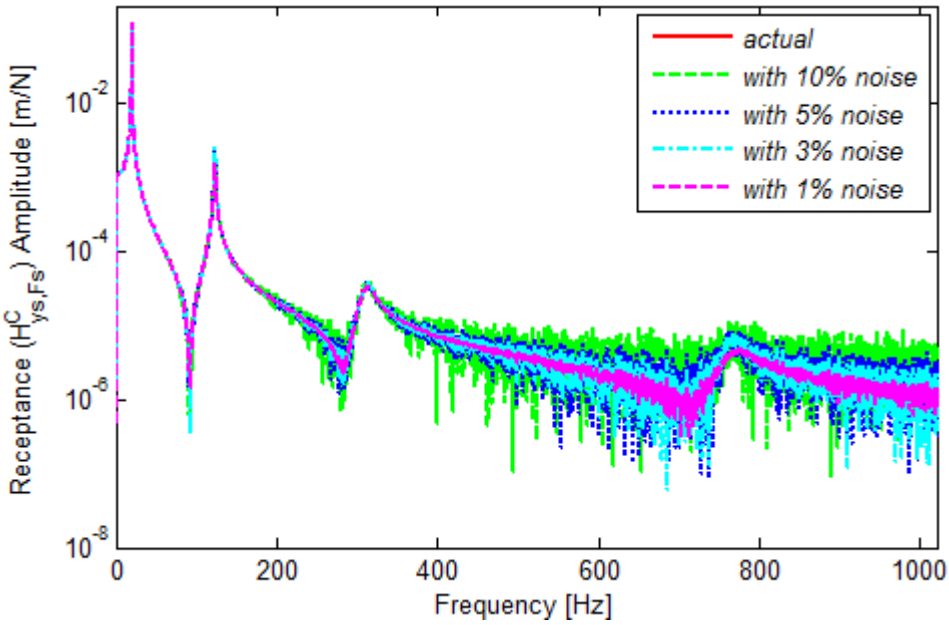

Figure 4.49 Translational Receptance of the Coupled Structure at 2^{nd} Point

Identified joint stiffness and damping values are given in Figure 4.50 and Figure 4.51, respectively. In the figures, comparison of the identification results, which are obtained by using different levels of noise contaminated FRFs, is given.

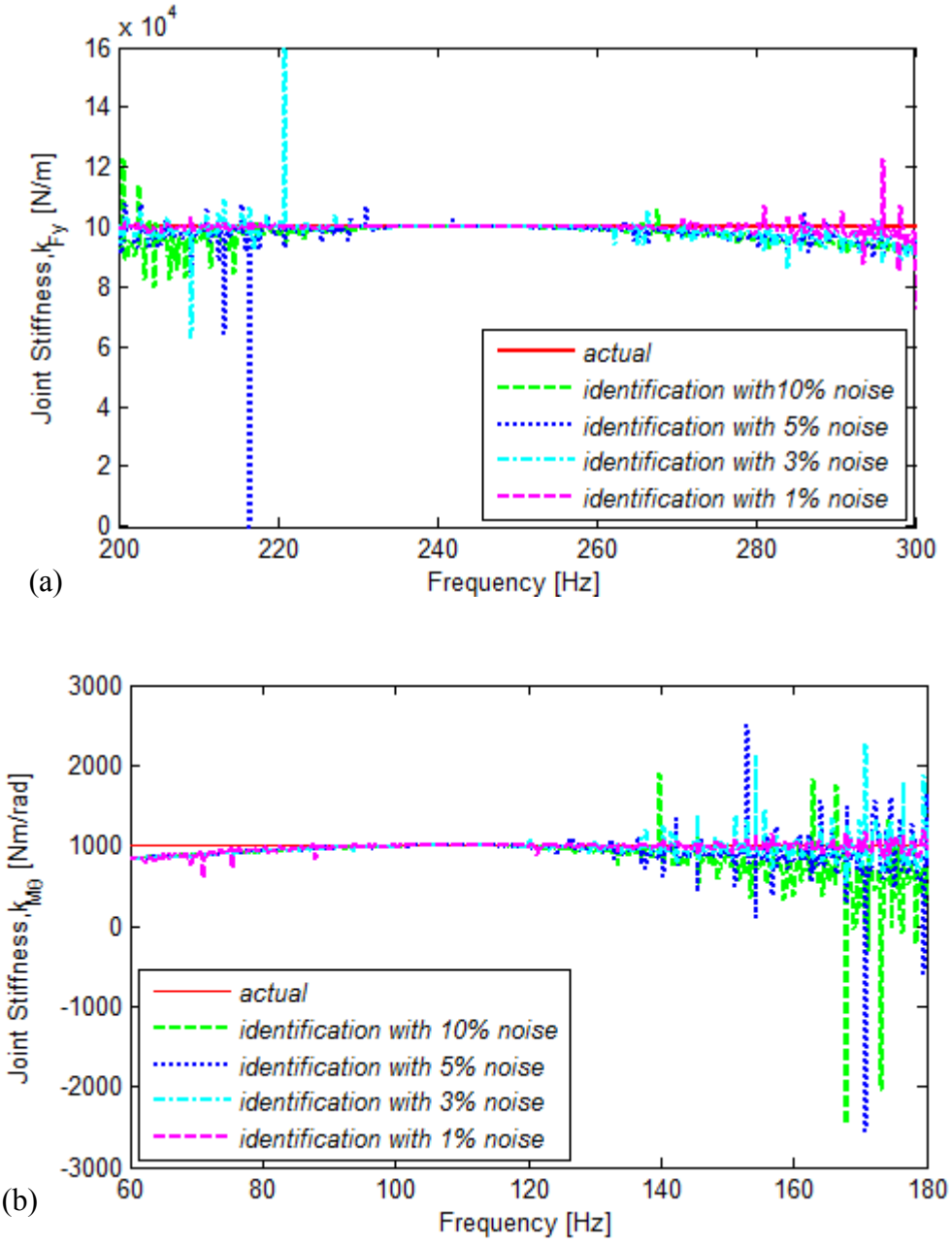

Figure 4.50 Identification of Joint Stiffness (a)Translational Joint Stiffness, (b) Rotational Joint Stiffness

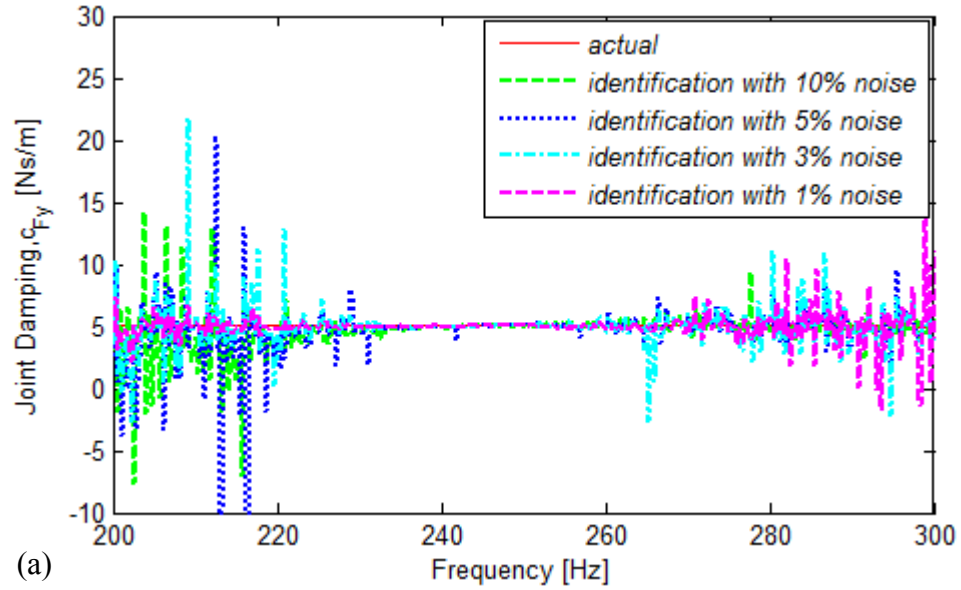

(a)

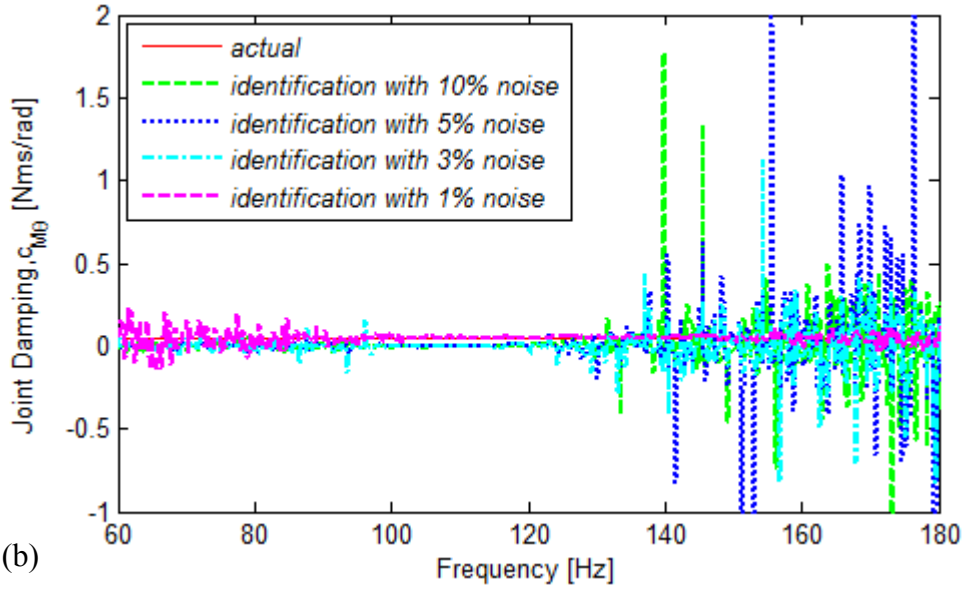

(b)

Figure 4.51 Identification of Joint Damping (a) Translational Joint Damping, (b) Rotational Joint Damping

The joint parameters identified by using FRFs with different levels of noise contamination, and the percentage differences from the actual values are given in Table 4.8.

Table 4.8 Identified Joint Properties and Percentage Errors in These Values

	k_{Fy} *[N/m]*	$k_{M\theta}$ *[N.m/rad]*	c_{Fy} *[N.s/m]*	$c_{M\theta}$ *[N.m.s/rad]*
Actual values	10^5	10^3	5	0.05
Identification with 10% Noise	$9.76*10^4$	$8.52*10^2$	4.71	-0.002
Error (%)	*-2.4*	*-15*	*-5.7*	*100*
Identification with5% Noise	$9.79*10^4$	$9.22*10^2$	4.56	0.006
Error (%)	*-2.1*	*-7.7*	*-8.9*	*-87*
Identification with 3% Noise	$9.89*10^4$	$9.70*10^2$	4.995	0.012
Error (%)	*-1*	*-3*	*-0.09*	*-75*
Identification with 1% Noise	$1.0003*10^5$	$9.78*10^2$	4.998	0.049
Error (%)	*0.03*	*-2.24*	*-0.03*	*-2.3*

It can be seen that with the increase in noise levels, the accuracy of the identification becomes worse. As it was mentioned in the previous case studies, again rotational joint properties are more prone to noise when compared with the translational joint properties. Then, it is seen that the conclusion drawn in section 4.2.1 is valid. Although rotational joint properties are important for the physical completeness of

the coupled model, having large errors in the identified values of rotational joint stiffness values will not deteriorate the mathematical model for the joint, as long as translational stiffness of the joint is accurately identified. Furthermore, the noise sensitivity of the identification method is due to the fact that the decoupling equation involves two inverse matrix operations. With small changes from the actual values of FRFs, the error is amplified during these inverse operations. This causes some shifts or deviations from the actual values as seen in Figure 4.50 and Figure 4.51. Furthermore, it can be concluded that the noise levels have less effect in the frequency regions sensitive to joint parameters.

4.3.3 Comparison of Experimental Simulations

As mentioned above, the response pollution technique is a more realistic way of simulating experimental data; in this part the two noise contamination methods with 1% noise levels will be compared. Figure 4.52 shows that for the response pollution the noise is more dominant at the anti-resonance regions of the FRF and at resonance frequencies the effect of noise is not very notable, while the FRF pollution has a more uniform noise distribution at both the resonance and anti-resonance regions.

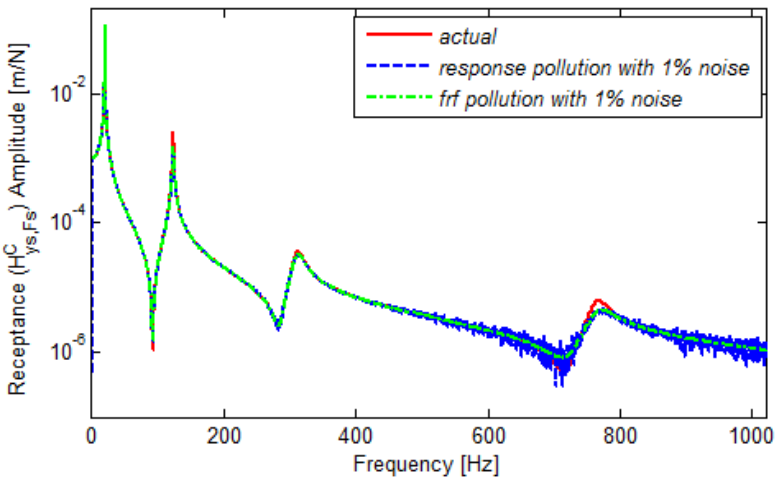

Figure 4.52 Translational Receptance of the Coupled Structure at 2^{nd} Point

Identified joint stiffness and damping values using 1% polluted FRFs via two noise contamination methods are compared in Figure 4.53 and Figure 4.54, respectively. In the figures, *identification (4.3.2)* corresponds to the identification results using the 1% noise contaminated FRFs from response pollution technique given in section 4.3.2, while *identification (4.3.1)* corresponds to the identification results using 1% noise contaminated FRFs with FRF pollution technique given in section 4.3.1.

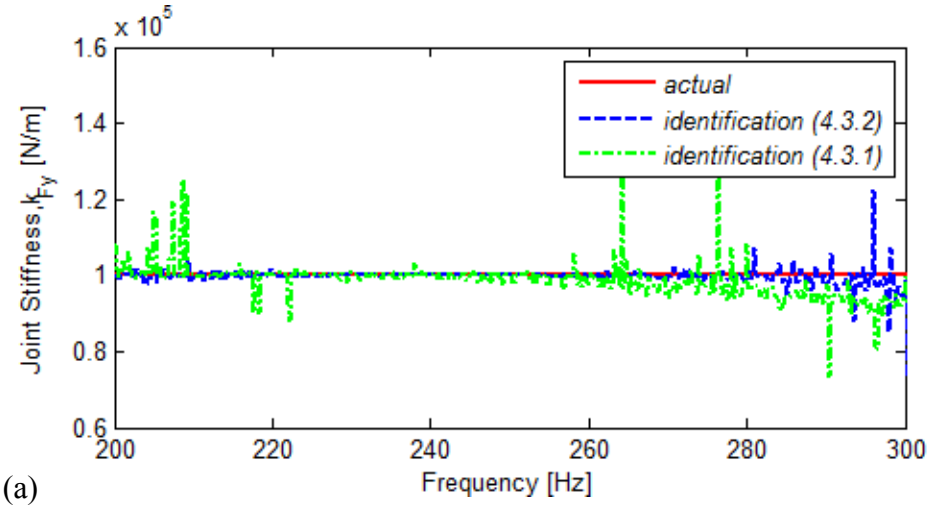

(a)

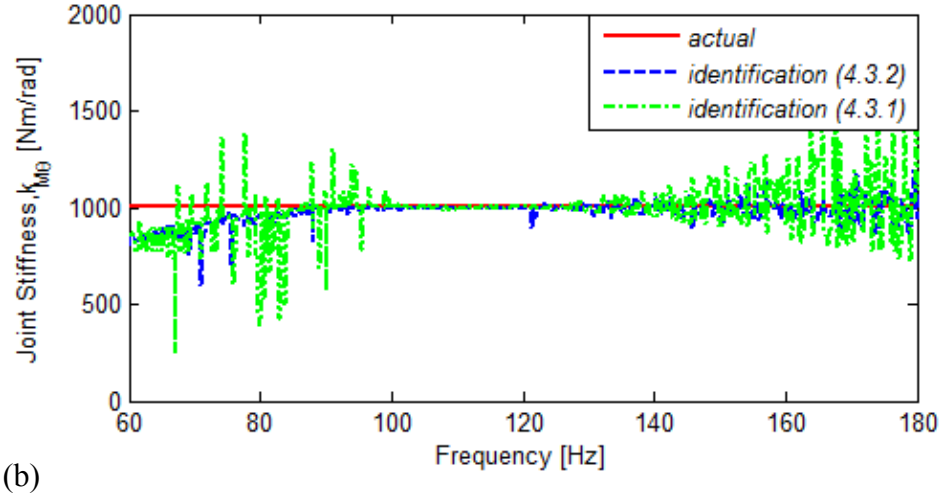

(b)

Figure 4.53 Identification of Joint Stiffness (a) Translational Joint Stiffness, (b) Rotational Joint Stiffness

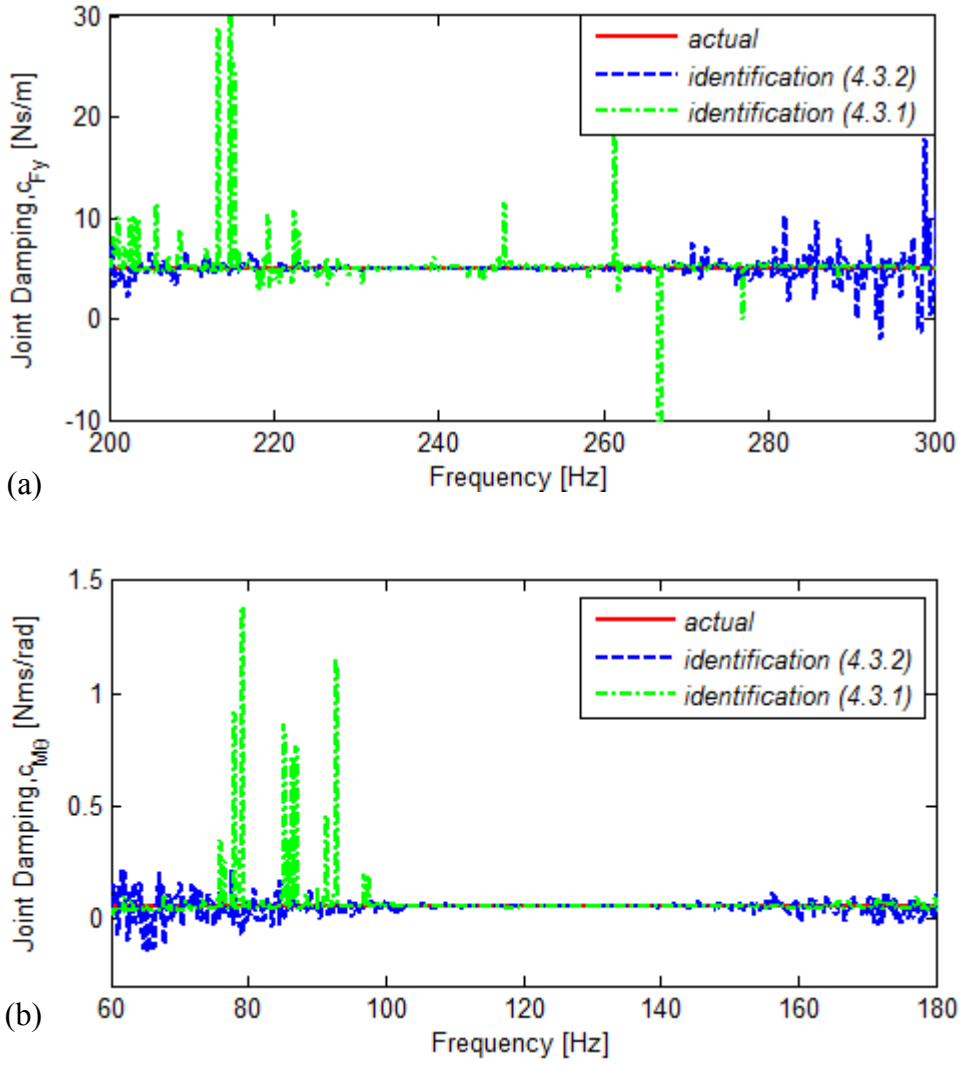

Figure 4.54 Identification of Joint Damping (a) Translational Joint Damping, (b) Rotational Joint Damping

The joint parameters identified by using two types of noise contamination techniques and the percentage differences from the actual values in the identification results are compared in Table 4.9. It can be seen that the error in the identified values using the simulated data from the FRF pollution technique is more, except the rotational joint stiffness. The accuracy of the identification results obtained from response pollution technique is quite well because in this technique, noise is much more effective in the

frequency regions where the response of the system is low and these regions should be avoided in identification of joint properties. Thus, it can be concluded that, while selecting the frequency region for identification, sensitive modes with higher amplitudes should be selected in order to reduce the effect of measurement noise.

Table 4.9 Identified Joint Properties and Percentage Errors in These Values

	k_{Fy} *[N/m]*	$k_{M\theta}$ *[N.m/rad]*	c_{Fy} *[N.s/m]*	$c_{M\theta}$ *[N.m.s/rad]*
Actual values	10^5	10^3	5	0.05
Identification (4.3.2)	$1.0003*10^5$	$9.78*10^2$	4.998	0.049
Error (%)	*0.03*	*-2.24*	*-0.03*	*-2.3*
Identification (4.3.1)	$9.89*10^4$	$9.93*10^2$	4.998	0.067
Error (%)	*-1.06*	*-0.7*	*-0.04*	*34*

CHAPTER 5

JOINT IDENTIFICATION - EXPERIMENTAL STUDIES

In this chapter, several experimental studies are given to illustrate the real life application of the method suggested. In section 5.1, an overview of the experimental set-up is given and the fundamental settings of the data acquisition software utilized in this study are explained. In section 5.2, M10x16 and M8x16 bolts with a quality of A2 70 are used in the connection of two aluminum beams and the equivalent dynamic properties of the bolted connections are determined. Then, in section 5.3, it is intended to identify the properties of joints with M10x35, M8x35 and M6x30 bolts in the connection of two steel beams. Moreover, different levels of tightening torque are used in the M8 bolted connection and the effect of torque on the connection of two coupled systems and the relation between the tightening torque and joint parameters are examined. Then, with the identified parameters of M8x35 bolt, a different substructure is coupled and with the identified parameters of M6x30 bolt, the receptance of the structure coupled with a multiple connection is obtained and the regenerated FRFs are compared with the measured FRFs of these new assemblies. Furthermore, different quality (A2 70 and A4 80 type) M6 bolts are used in the connection and the effect of quality of the bolts on the coupled system dynamics and joint parameters are examined. Finally, in section 5.4, results of the identification are summarized and conclusions obtained from the experimental studies are given.

5.1 EXPERIMENTAL SET-UP

In the experimental part of this study, LMS modal test system, PCB impact hammer, PCB miniature sensors and torque wrench are utilized as given in Table 5.1. In the

experiments frequency resolution is selected as 0.25Hz and the frequency range is set to 512Hz using soft tip of the impact hammer. Note that, for the free-free tests of the substructure the frequency range is set to 1024Hz using hard tip of the impact hammer. A sufficient pre-trigger level is selected and during the experiments it is assured that all pulses are captured.

Table 5.1 Components of the experimental setup

Component	**Brand**	**Function / Properties**
Modal Test System 	LMS SCADAS III	LMS Modal Analysis Software
Impact Hammer 	PCB	Sensitivity:1.126 mV/N
Miniature Sensors 	PCB	Range: 50g Sensitivity: 100.4mV/g Weight: 2.8 g,
Torque Wrench 	Matador	Capacity: 3-30Nm

In this study, no windowing is applied to the collected data. Actually, for lightly damped structures like the ones used in this study, exponential window is applied on the response data in order to avoid leakage. However, exponential windowing adds artificial damping in the data. Since one of the aims of this study is to identify the damping of the joint, no windowing is used for the response data. Instead, the amount of data acquisition time is increased up to when decaying of the structure is totally completed. Furthermore, 10 averages are taken for the measurements. A view from the acquisition set-up of the software is shown in Figure 5.1. Furthermore, in the experiments the coherence values are very good except the anti-resonance frequencies as shown in Figure 5.2.

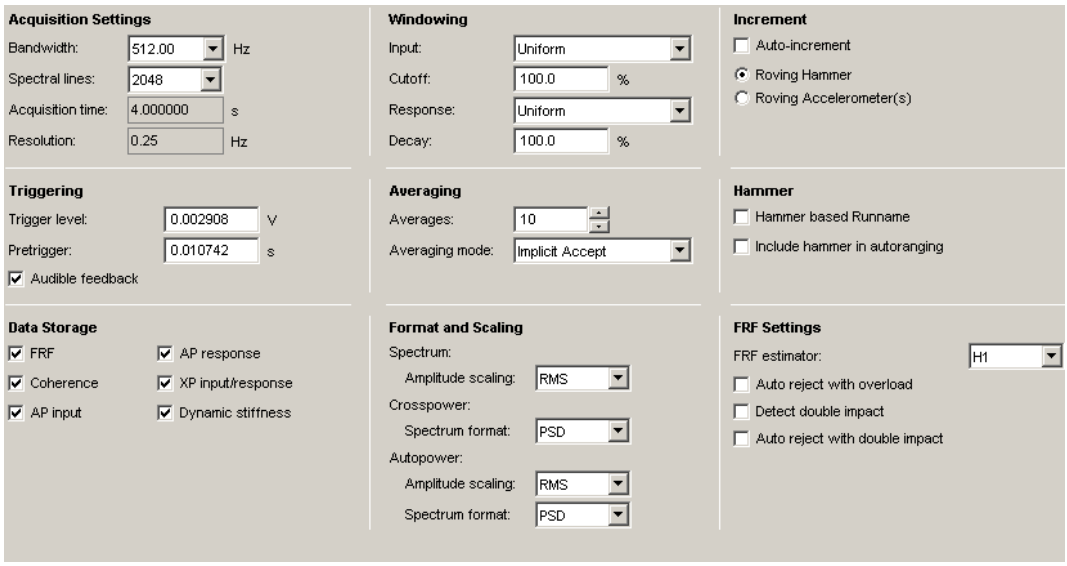

Figure 5.1 LMS Set-up for Data Acquisition

After acquiring test data, LMS modal analysis software is used for the system identification and the required parameters (the mode shapes, the damping ratio for each mode, undamped natural frequency, lower and upper residuals) for the FRF synthesis are obtained.

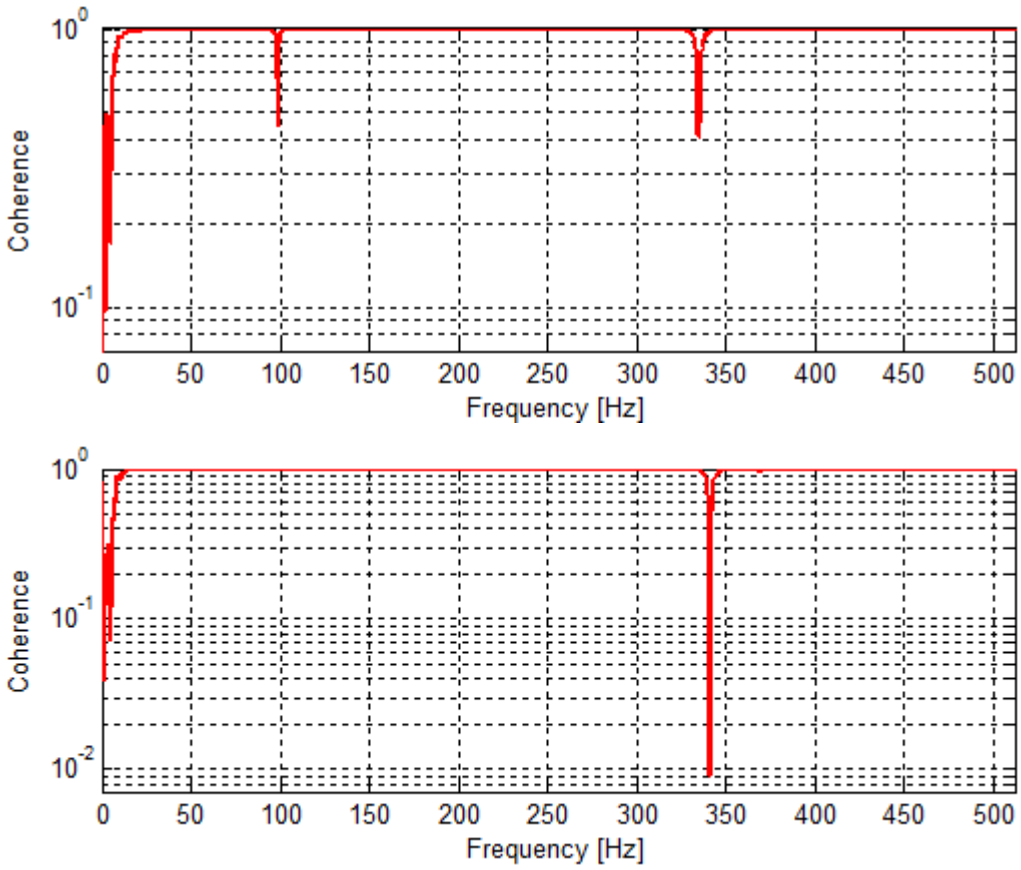

Figure 5.2 Measured Coherence: a) Coupled Structure, b) Substructure

As it was mentioned in Chapter 4, from the experimental point of view, among the decoupling equations the most practical one is equation (3.21). Equation (3.18) requires the measurements of FRFs belonging to the substructure A at the joint and as well as non-joint DOFs, which is very time consuming and expensive. Furthermore, when equation (3.18) is used it is not possible to obtain cross-coupling FRFs including RDOF information between joint and non-joint coordinates. On the other hand, when equation (3.21) is used, FRFs of the substructure B can be obtained theoretically and only the translational and rotational FRFs at the joint coordinate of the substructure A are required to be measured. Hence, it can be seen that the most practical decoupling equation is the last one (equation (3.21)) which is verified with simulation studies in Chapter 5.

5.2 BOLTED CONNECTION OF ALUMINUM BEAMS

In the first set-up a single bolt connects two aluminum beams as shown in Figure 5.3. The beams are produced from Al6061, and dimensions of the beams are as follows: Length of substructure A: L_A=*0.3 m*; Length of substructure B: L_B=*0.221 m*; width of the beams: *0.025 m*, height of the beams: *0.006 m*.

M10x16 and M8x16 bolts with a quality of A2 70 are used in the connection of the aluminum beams.

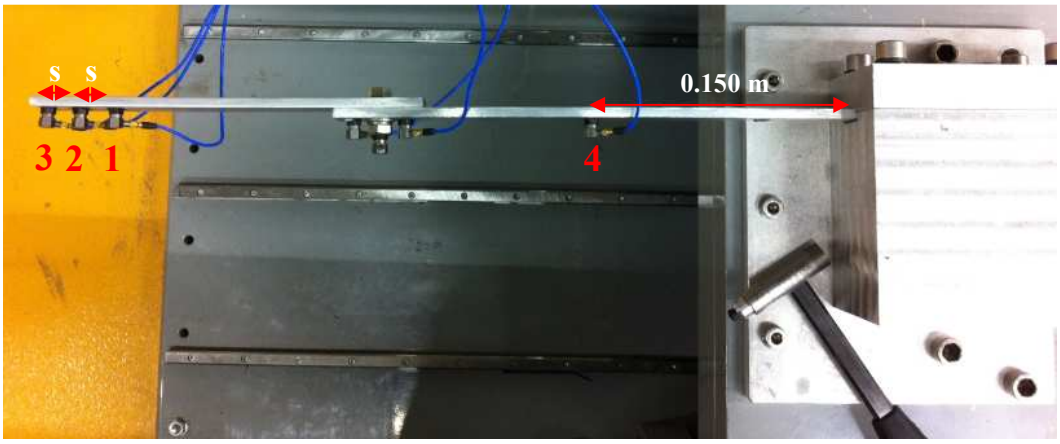

Figure 5.3 Bolted Connection of Aluminum Beams

In the experimental identification of the bolted joint, FRFs of the substructure A, which has fixed-free boundary conditions, is measured; while the FRFs of the substructure B, which has free-free boundary conditions, are obtained theoretically. For substructure B, experiments are conducted just to determine the modal properties. Then, FRFs are obtained theoretically, but by tuning the modal and structural parameters of the beam with the measured ones. In the testing of the substructure B, it is suspended with elastic cords as shown in Figure 5.4.

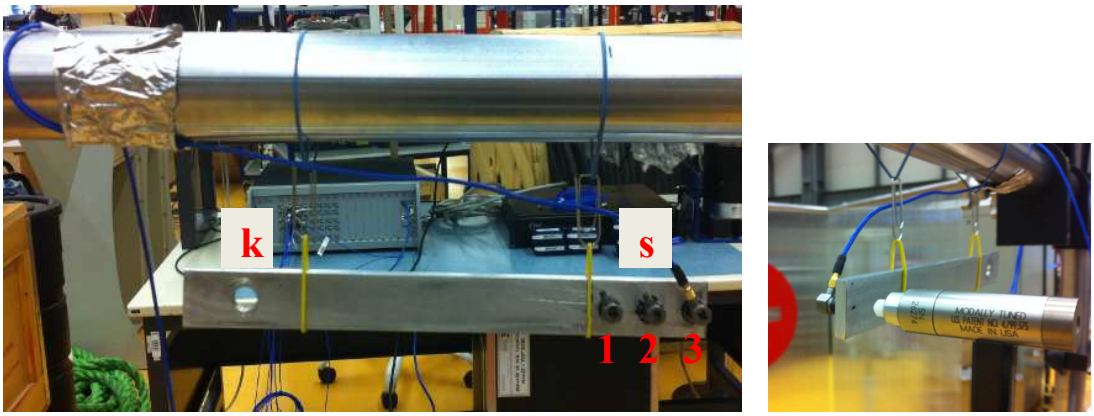

Figure 5.4 Testing of Substructure B

The substructure B is excited at the tip point and the tip point FRFs are obtained as shown in Figure 5.5 and the modal parameters are identified. According to the tests performed on the substructure B, the following data is used for the FE model of the free-free beam: elastic modulus $E=70\ 10^9\ N/m^2$; density $\rho=2700\ kg/m^2$. Also, the damping ratio for the first elastic mode is obtained from the tests as 0.0008. Then by using the modal properties determined, the FRFs of the substructure B, $[H_{kk}]$, $[H_{ks}]$, $[H_{sk}]$ and $[H_{ss}]$ are calculated accurately.

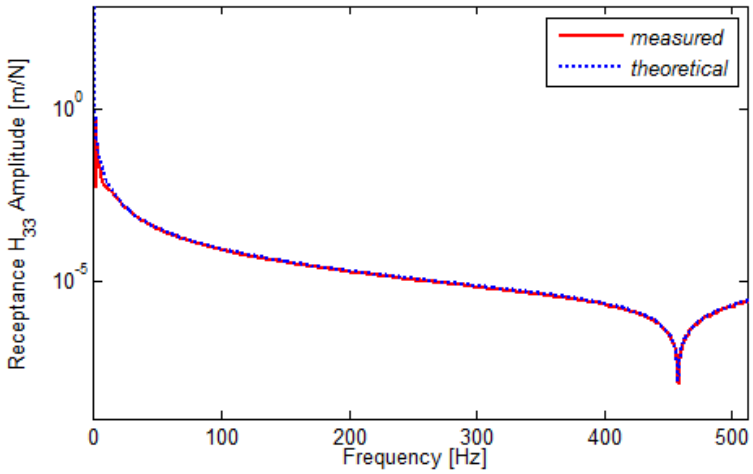

Figure 5.5 Tuning of the Substructure B FRF

5.2.1 Beams Connected with M10x16 Hexagonal Bolt

In this case study A2-70 M10x16 hexagon head bolt is used and the tightening torque is set to 30Nm.

5.2.1.1 Measurements and Estimation of FRFs

In order to estimate the RDOF related FRFs of substructure A, three accelerometer measurements are taken. The accelerometers are located with spacing, *s*, of 0.015m as shown in Figure 5.6.

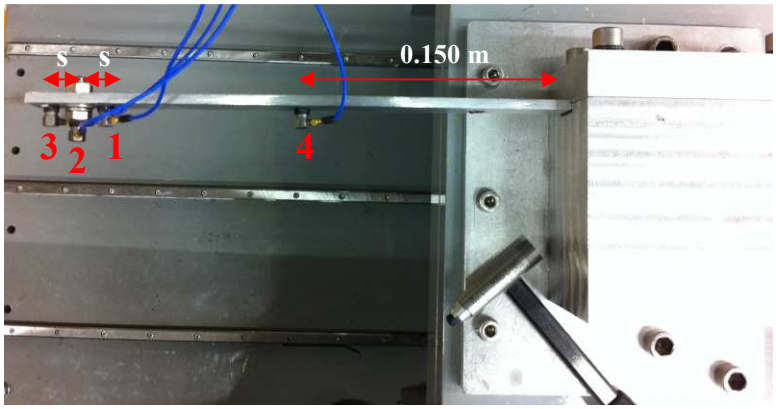

Figure 5.6 Close Accelerometers Method for Substructure A

In this study, substructure A is excited at point 4, because beyond this point double impacts are observed in the measurements. In order to avoid that, excitation is applied at point 4 and the tip point direct FRFs are obtained via FRF synthesis. In fact, for the impact testing the best location for impact is the tip point, because the structure is most excited by hitting the most deflecting point. However; due to the

very low damping of these structures, exciting the system at the tip point causes unavoidable double hits even multiple hits. Avitabile (2008) suggests that, the multiple impacts can be well used as an excitation technique. However, the key point is that, the overall measurement, including the frequency response and the coherence, must be checked along with the averaged spectrums for the measurement. Furthermore, care should be taken while the series of pulses are applied to structure. The impulses should be applied in a very incoherent fashion in terms of their timing and spacing. The pulses should also not to be applied for the entire sample period and the response should be totally observed within the sample interval so that no leakage will occur. By this technique, when the double hits are unavoidable, for some cases (for example if we use these FRFs directly in the decoupling equation as in the case given in section 5.2.2) the measured FRFs can still be used. However, if we use these data in the rotational FRF estimation, and then use these estimated rotational FRFs in the decoupling equations, identification results will not be accurate. Hence, for the accurate estimation of RDOF related FRFs the substructure is excited at point 4.

After completing the FRF measurements; system identification is performed using the LMS modal analysis software and using required parameters for the FRF synthesis (given in Appendix A), translational FRFs at the tip point of substructure A is obtained as shown in Figure 5.7.

As it can be seen from the figures the measured FRFs include very little noise levels at the resonant frequencies, while the noise is more effective at the anti-resonance frequencies. Furthermore in order to show the accuracy of the FRF synthesis method, the synthesized direct point FRF is compared with the measured direct point FRF at accelerometer location 3 in Figure 5.8.

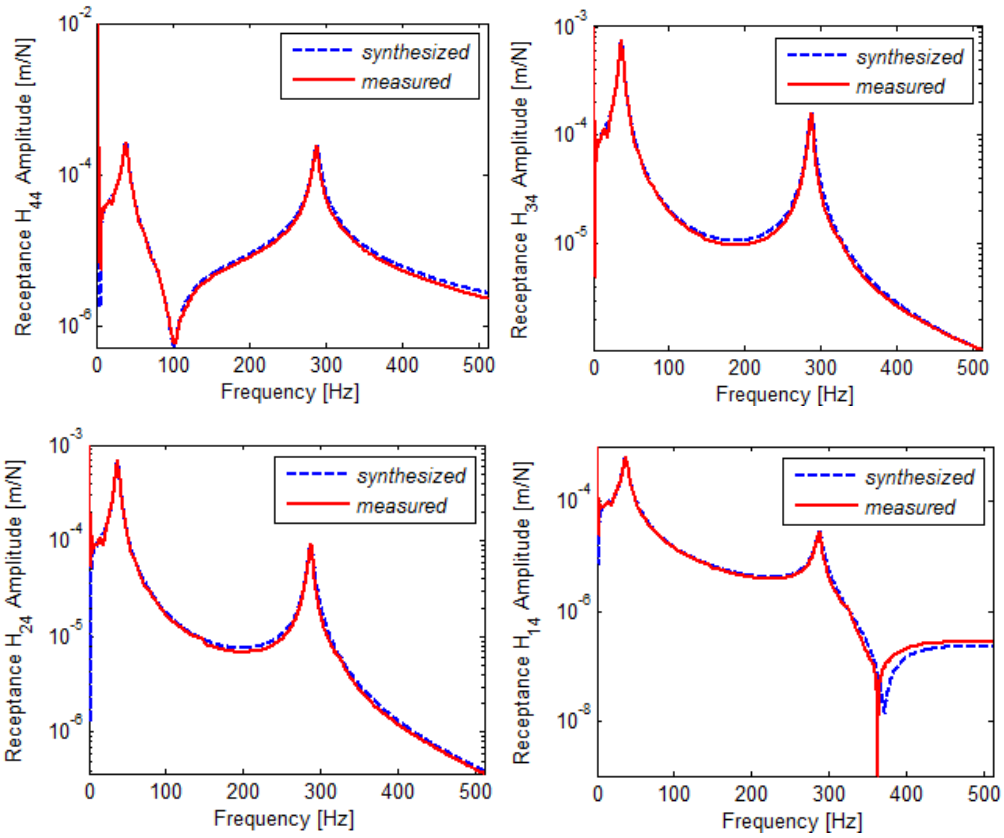

Figure 5.7 FRF Synthesis for Substructure A

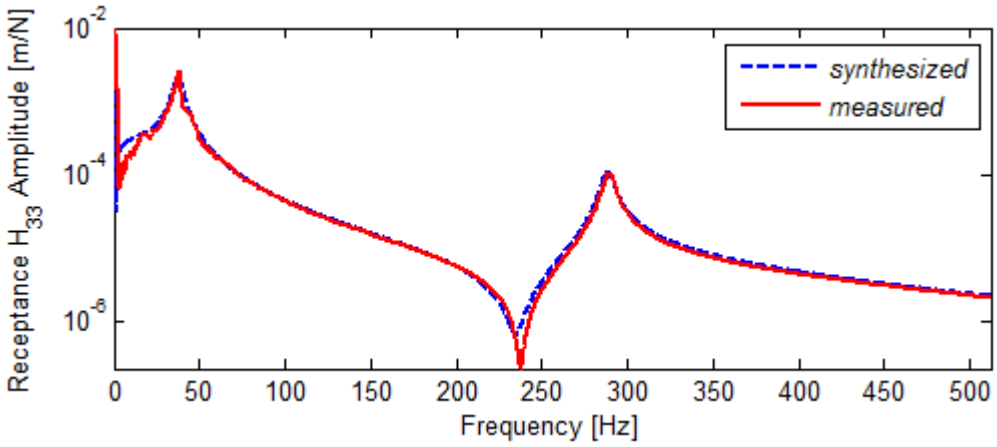

Figure 5.8 FRF Synthesis for Substructure A

It is seen that the FRF synthesis method provides an accurate and alternative solution for direct point FRF measurements when the double hit is unavoidable. After obtaining the translational FRFs at the tip point, using the second order finite difference formula rotational FRFs are estimated at point 2 as shown in Figure 5.9.

On the other hand, the coupled structure is excited at the three tip points (point1, point 2 and point 3) separately and responses are measured at these points. The FRFs measured (given in Figure 5.10) are directly used in the identification of joint properties.

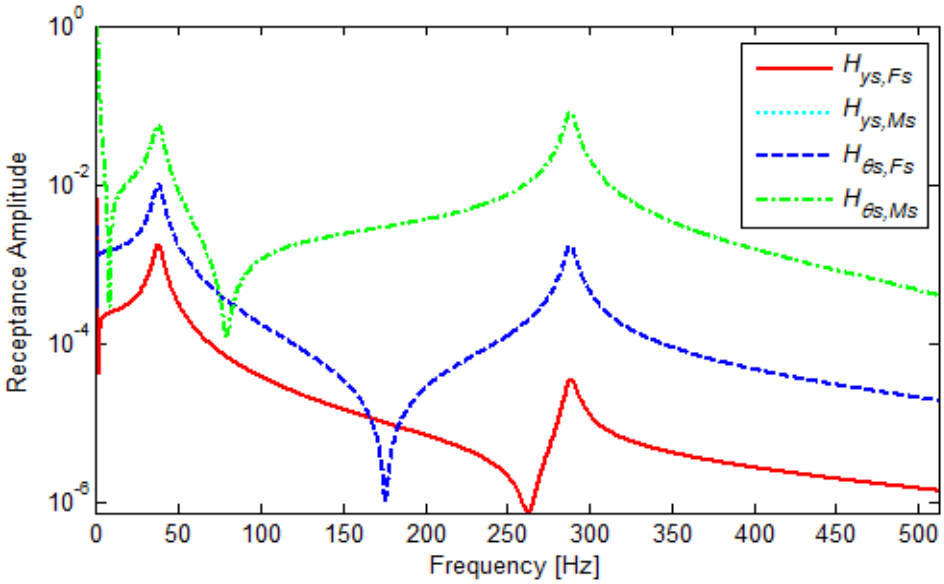

Figure 5.9 Rotational FRF Estimation for Substructure A

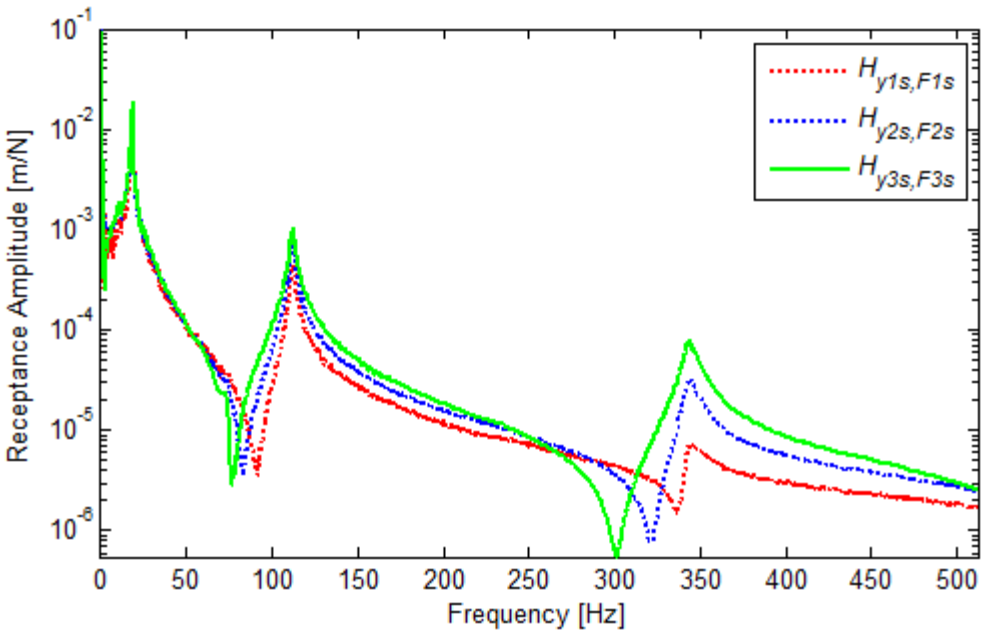

Figure 5.10 Measured FRFs of the Coupled Structure

5.2.1.2 Identification of Bolted Joint

In this case study the properties of the bolt are extracted with the identification approach 4, which gives the most accurate identification. In this approach the translational FRFs measured at the tip points of the structure are used. The identified joint stiffness and damping values are shown in Figure 5.11 and Figure 5.12, respectively.

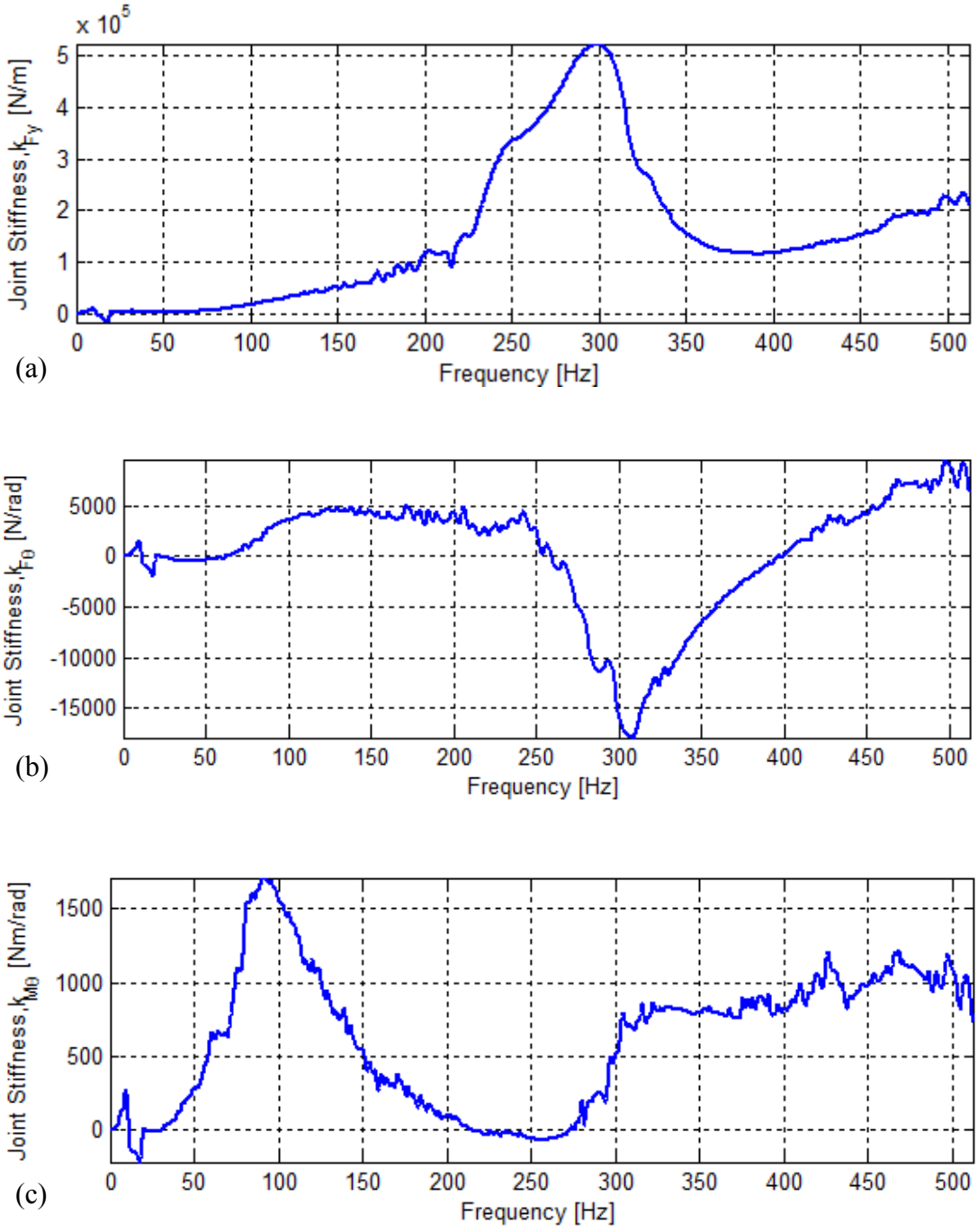

Figure 5.11 Identification of Joint Stiffness (a) Translational Joint Stiffness, (b) Cross-coupling Joint Stiffness, (c) Rotational Joint Stiffness

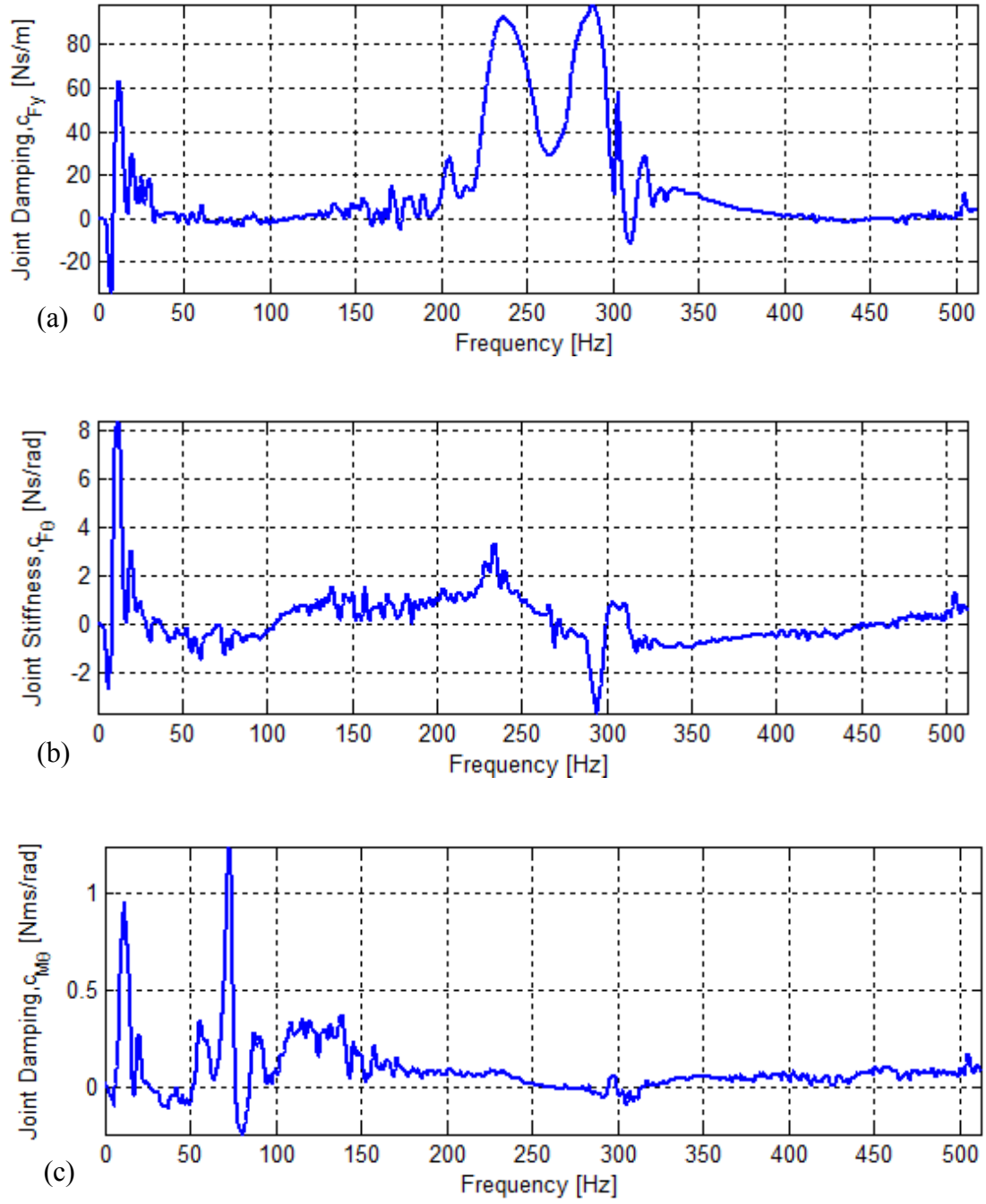

Figure 5.12 Identification of Joint Damping (a) Translational Joint Damping, (b) Cross-coupling Joint Damping, (c) Rotational Joint Damping

It is seen that the joint properties are changing with frequency and the best frequency range to determine the joint properties are not obvious. This could result from the measurement errors (including the errors in the estimation of FRFs) and numerical errors associated with matrix inversion. Young et al. (2007) proposed a solution for this problem by taking some fit values from the identification curve and using these values to redefine the joint stiffness matrix in a dynamic manner. However, they do not provide the enhanced results in their work.

In this case study with M10x16 bolts, when the identification results at some modes of the coupled structure, which are given in Table 5.2, are used in the coupling equations, regenerated FRFs of the coupled structure are found to be exactly the same with the measured FRFs at these modes as shown in Figure 5.13. However, the aim in this study is to obtain constant value for joint stiffness and damping. Then the joint properties should be optimized to match all the modes in the frequency region of interest. For that purpose an optimization algorithm is developed using "fminunc" command of MATLAB. Starting with initial estimates for the joint properties, this algorithm updates the joint parameters by minimizing the sum of the difference between the squares of the actual and regenerated receptance amplitudes calculated at each frequency. It is also referred to as unconstrained nonlinear optimization. The key point for the success of the optimization process lies in starting with a good initial estimate. In fact, one can obtain a set of joint parameters using some fictitious initial estimates and may calculate the actual FRF curve used in the optimization process. However when these values are used in a new assembly, the resulting FRFs will not be correct, due to the lacking of a physical basis of the initial estimates. Hence, in order to have a correct solution, after several attempts, it is seen that, initial estimates for the joint parameters should be selected from the identification results obtained with decoupling equations.

As it was mentioned in the simulation studies the frequencies at which FRFs are sensitive to joint dynamics are the best region for an accurate identification. Hence,

the sensitivity analysis given in Figure 5.14 is performed before deciding on the initial estimates of the joint update process.

Table 5.2 Identified Joint Properties using Decoupling Equation

	k_{Fy} *[N/m]*	$k_{F\theta}$ *[N/rad]*	$k_{M\theta}$ *[N.m/rad]*	c_{Fy} *[N.s/m]*	$c_{F\theta}$ *[N.s/rad]*	$c_{M\theta}$ *[N.m.s/rad]*
Identification @ 112.5Hz	$2.48*10^4$	$4.24*10^3$	$1.31*10^3$	0	0.43	0.28
Identification @ 344Hz	$1.71*10^5$	$-7.68*10^3$	$7.91*10^2$	10.8	-0.84	0.05

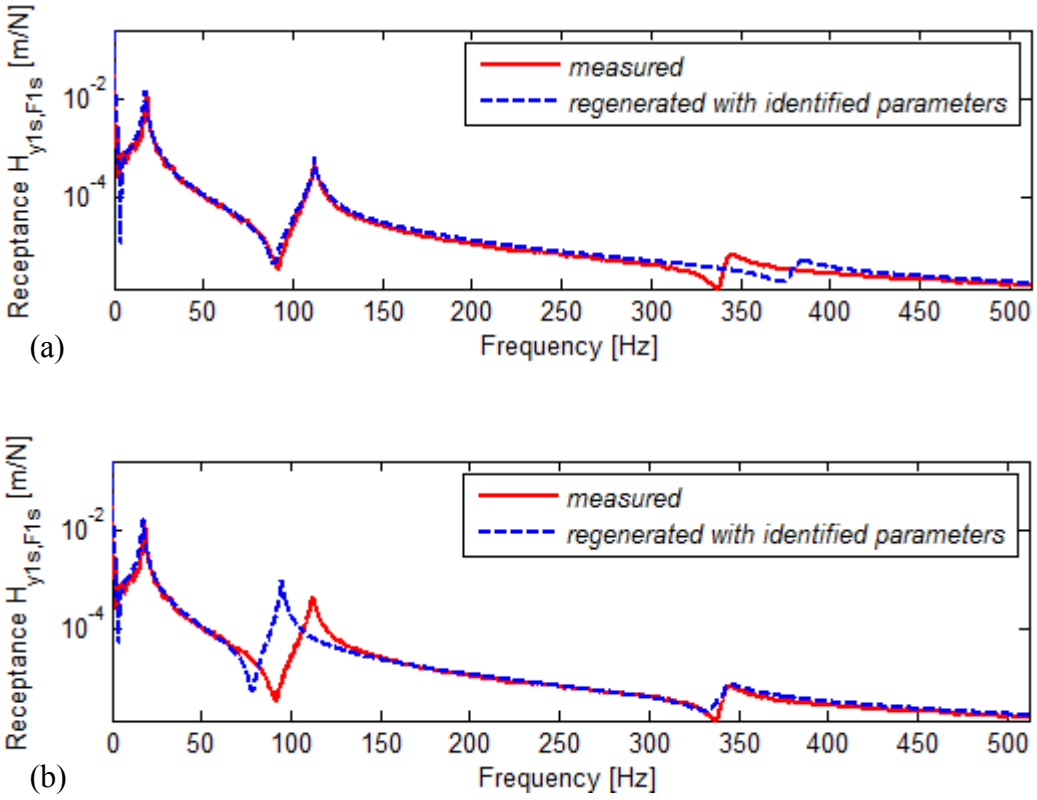

Figure 5.13 Regenerated FRFs of the Coupled Structure Using Identified Joint Properties: a) at 112.5 Hz, b) 344Hz

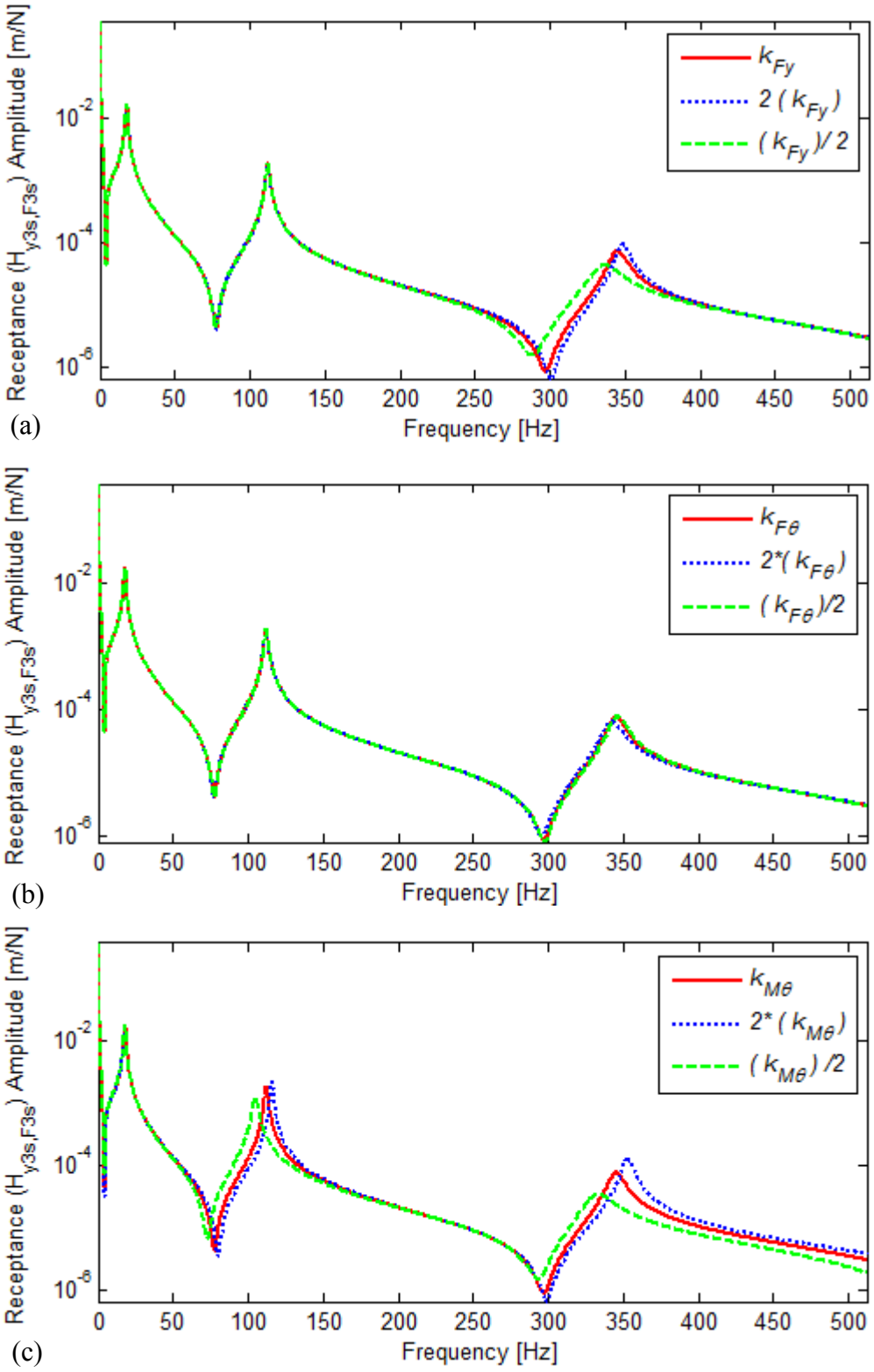

Figure 5.14 Sensitivity of the Receptances of the Coupled Structure to: (a) Translational, (b) Cross-coupling, (c) Rotational Joint Stiffness

It can be seen that, translational and cross-coupling joint stiffnesses are effective at the third mode, while rotational stiffness is effective at both second and third modes. As noted in Chapter 4, while selecting the frequency region for identification, sensitive modes with higher amplitudes should be selected in order to reduce the effect of measurement noise. Hence, the values of translational and cross-coupling joint stiffnesses and damping identified at the third mode, and rotational parameters identified at the second mode are used as initial estimates. Then, these values are updated with the algorithm mentioned above. The joint updating is performed in two steps; in the first step the stiffness parameters are tuned, and then in the second step with the updated joint stiffnesses joint damping parameters are tuned. The initial estimates and the identified joint properties by using optimization are given in Table 5.3. By using the updated joint parameters, FRFs of the assembled system are calculated and they are compared with the measured FRFs in Figure 5.15. It can be seen from the comparison that the FRFs calculated by using the updated joint parameters perfectly match with the actual FRFs.

Table 5.3 Updated Joint Properties for M10 Bolt

	k_{Fy} *[N/m]*	$k_{F\theta}$ *[N/rad]*	$k_{M\theta}$ *[N.m/rad]*	c_{Fy} *[N.s/m]*	$c_{F\theta}$ *[N.s/rad]*	$c_{M\theta}$ *[N.m.s/rad]*
Initial Estimates	$1.71*10^5$	$-7.68*10^3$	$1.31*10^3$	10.8	-0.84	0.28
Updated	$5.73*10^5$	$5.82*10^3$	$1.29*10^3$	10.83	-0.83	0.083

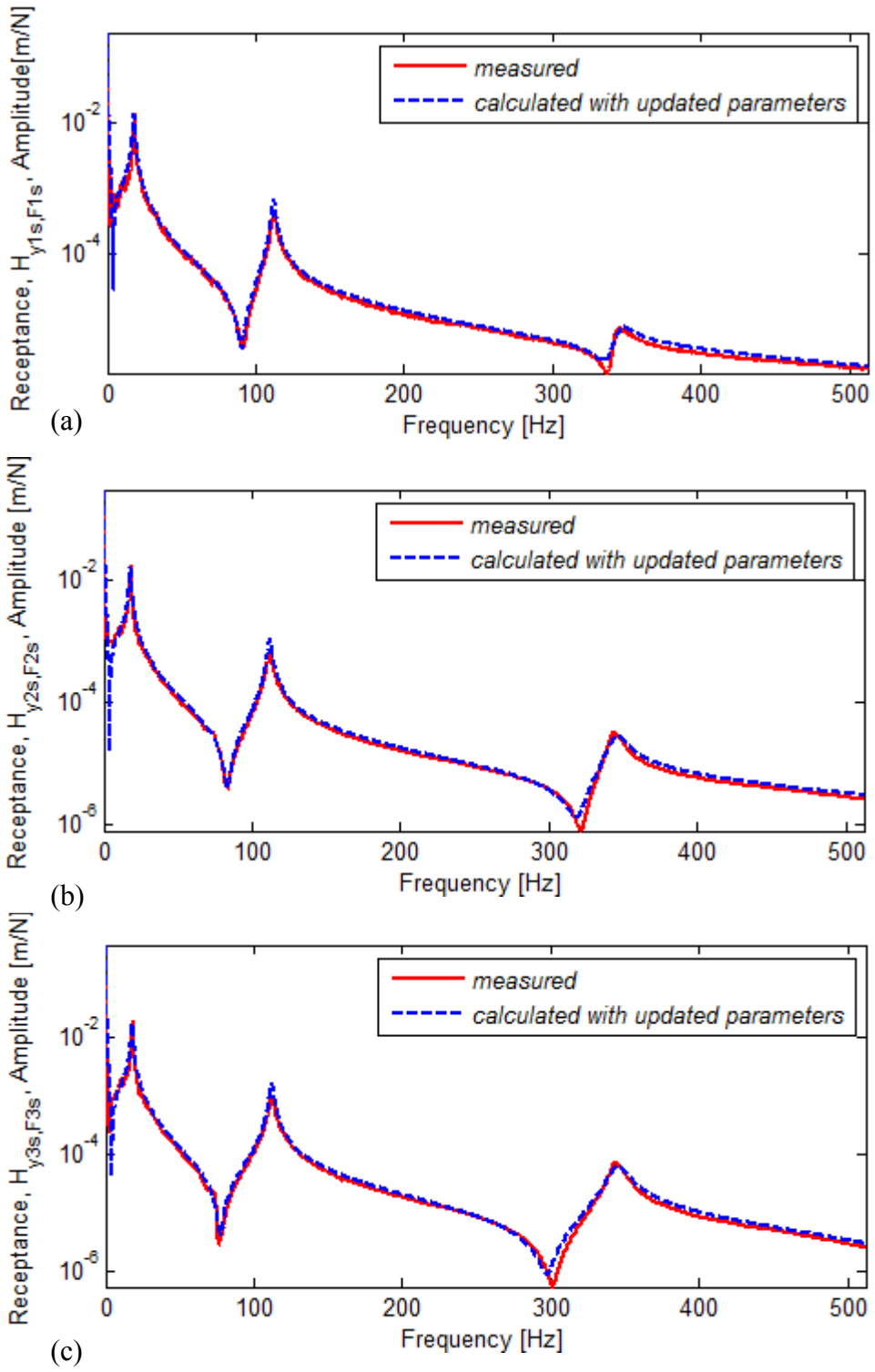

Figure 5.15 Calculated FRFs of the Coupled Structure Using Updated Joint Properties a) $H_{y1s.F1s}$, b) $H_{y2s.F2s}$, c) $H_{y3s.F3s}$

5.2.2 Beams Connected with M8x16 Hexagonal Bolt

In this case study, the stiffness and damping values of the connection with M8x16mm hexagon head bolt are to be determined.

5.2.2.1 Measurements and Estimation of FRFs

RDOF related FRFs of substructure A shown in Figure 5.16 are obtained with the same procedure explained in the previous case study. The required parameters for the FRF synthesis and the synthesized FRFs are given in Appendix A.

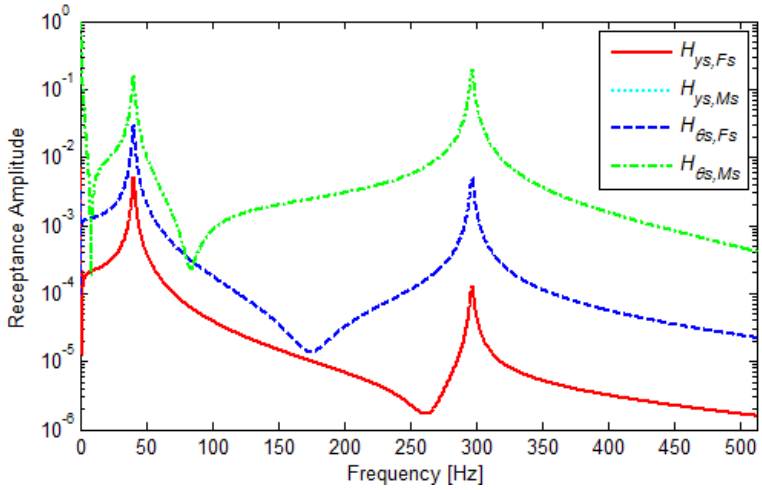

Figure 5.16 Rotational FRF Estimation for Substructure A

5.2.2.2 Identification of Bolted Joint

In this case study the properties of the bolted joint are extracted with the identification approach 2, in which only one of the translational FRF measured at the tip point (point 2 in this case) of the structure is directly used. The identified joint stiffness and damping are shown in Figure 5.17 and Figure 5.18, respectively.

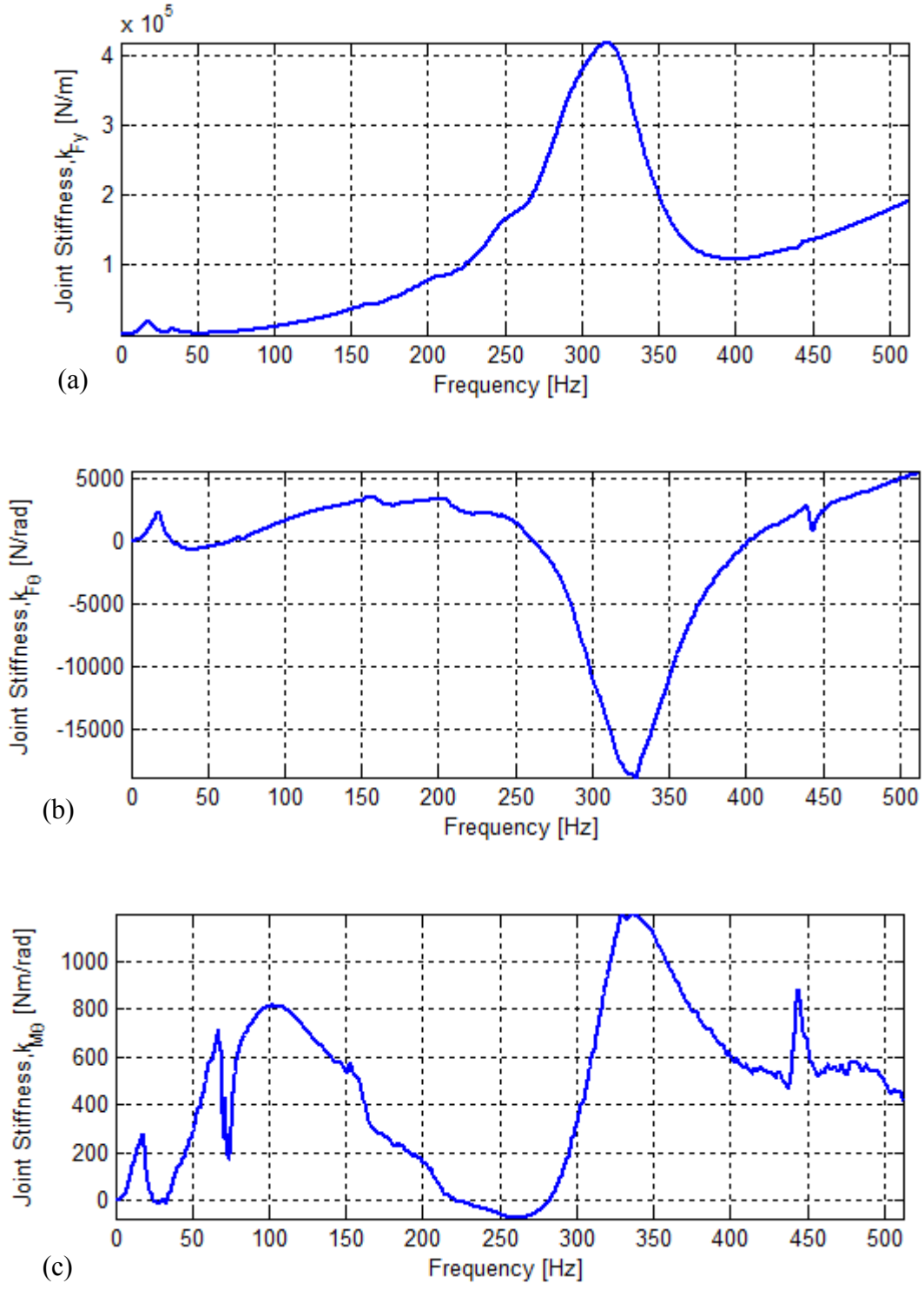

Figure 5.17 Identification of Joint Stiffness (a) Translational Joint Stiffness, (b) Cross-coupling Joint Stiffness, (c) Rotational Joint Stiffness

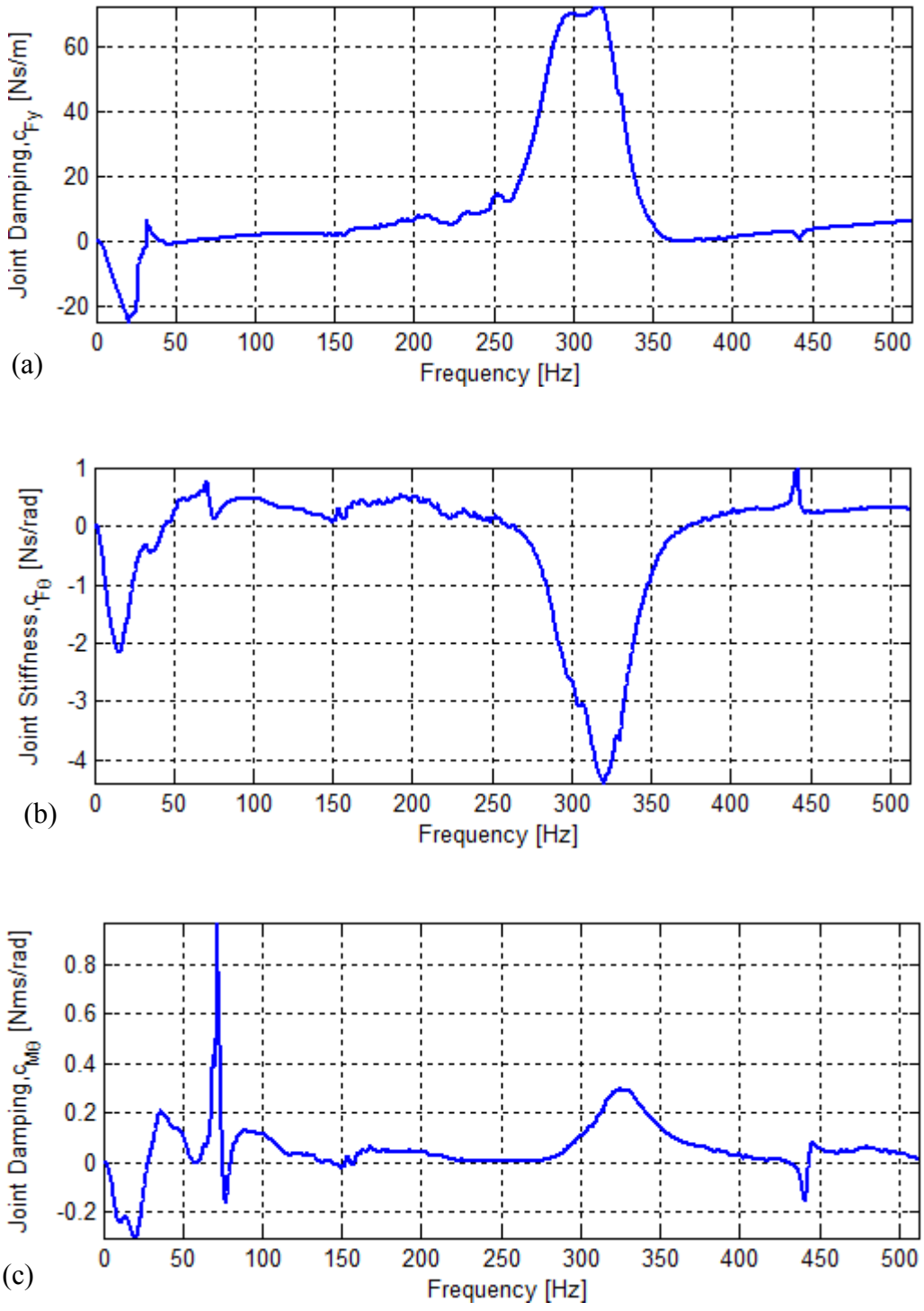

Figure 5.18 Identification of Joint Damping (a) Translational Joint Damping, (b) Cross-coupling Joint Damping, (c) Rotational Joint Damping

Starting with initial estimates from the identified results at the second mode for rotational parameters and the third mode for translational and cross-coupling parameters, the updated joint parameters are obtained as given in Table 5.4. By using the updated joint parameters, receptance of the assembled system is regenerated and they are compared with the measured receptance in Figure 5.19. It can be seen from the comparison that the receptance regenerated by using the updated joint parameters perfectly match with the measured FRFs.

Table 5.4 Joint Parameters of the M8x16 Bolted Connection

	k_{Fy} *[N/m]*	$k_{F\theta}$ *[N/rad]*	$k_{M\theta}$ *[N.m/rad]*	c_{Fy} *[N.s/m]*	$c_{F\theta}$ *[N.s/rad]*	$c_{M\theta}$ *[N.m.s/rad]*
Initial Estimates	$2.12*10^5$	$-1.17*10^4$	$7.80*10^2$	6.09	-0.978	0
Updated	$5.04*10^5$	$-1.21*10^4$	$1.22*10^3$	5.04	1.20	0

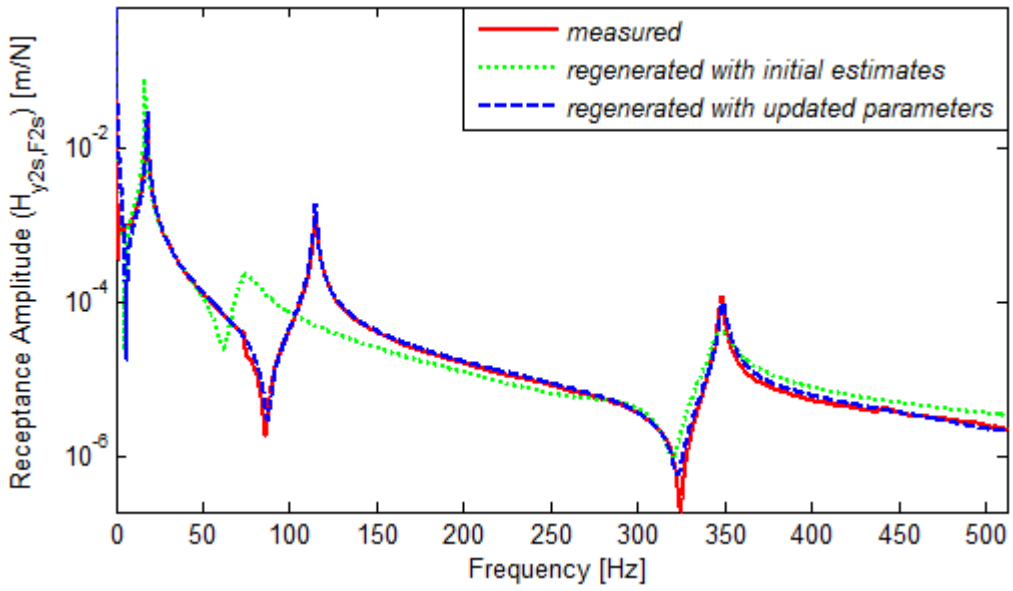

Figure 5.19 Regenerated FRF, $H_{y2s,F2s}$, of the Coupled Structure Using Updated Joint Properties

Furthermore, by using the updated joint parameters, the FRF of the coupled structure at Point 3, which is not used in the identification of joint properties, is obtained. It can be seen from Figure 5.20 that the receptance calculated by using the updated joint parameters perfectly match with the measured FRF. Hence, it can be concluded that, the joint properties are identified accurately.

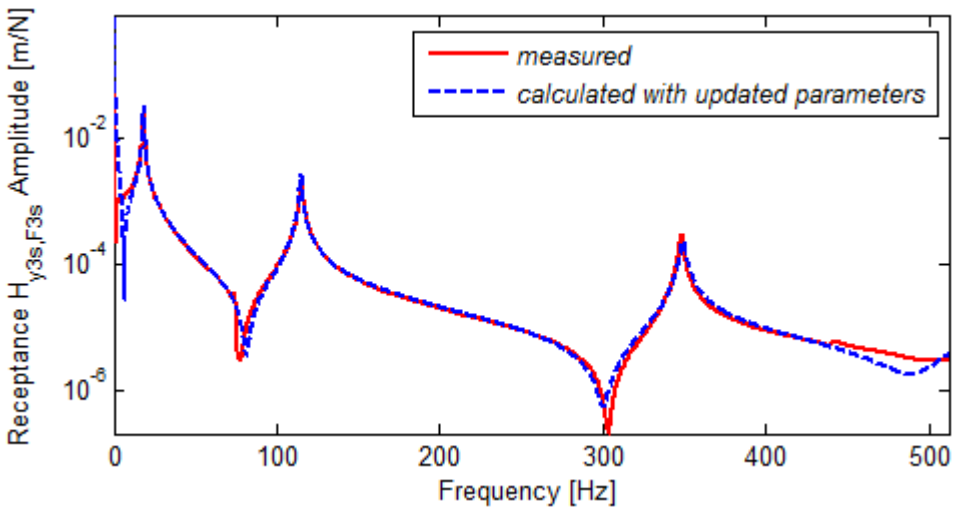

Figure 5.20 Calculated FRF, $H_{y3s.F3s}$, of the Coupled Structure Using Updated Joint Properties

5.3 BOLTED CONNECTION OF STEEL BEAMS

In the second set-up, again single bolt connection is used between two stainless steel beams as shown in Figure 5.21. Dimensions of the beams are given as follows: Length of substructure A: L_A=*0.3 m*; Length of substructure B: L_B=*0.335 m*; width of the beams: *0.015 m*, height of the beams: *0.010 m*.

In this section the aim is to identify the properties of the joints obtained by using M10x35, M8x35 and M6x30 bolts, respectively, in the connection of two steel beams, and examine the effect of material difference on the connection properties.

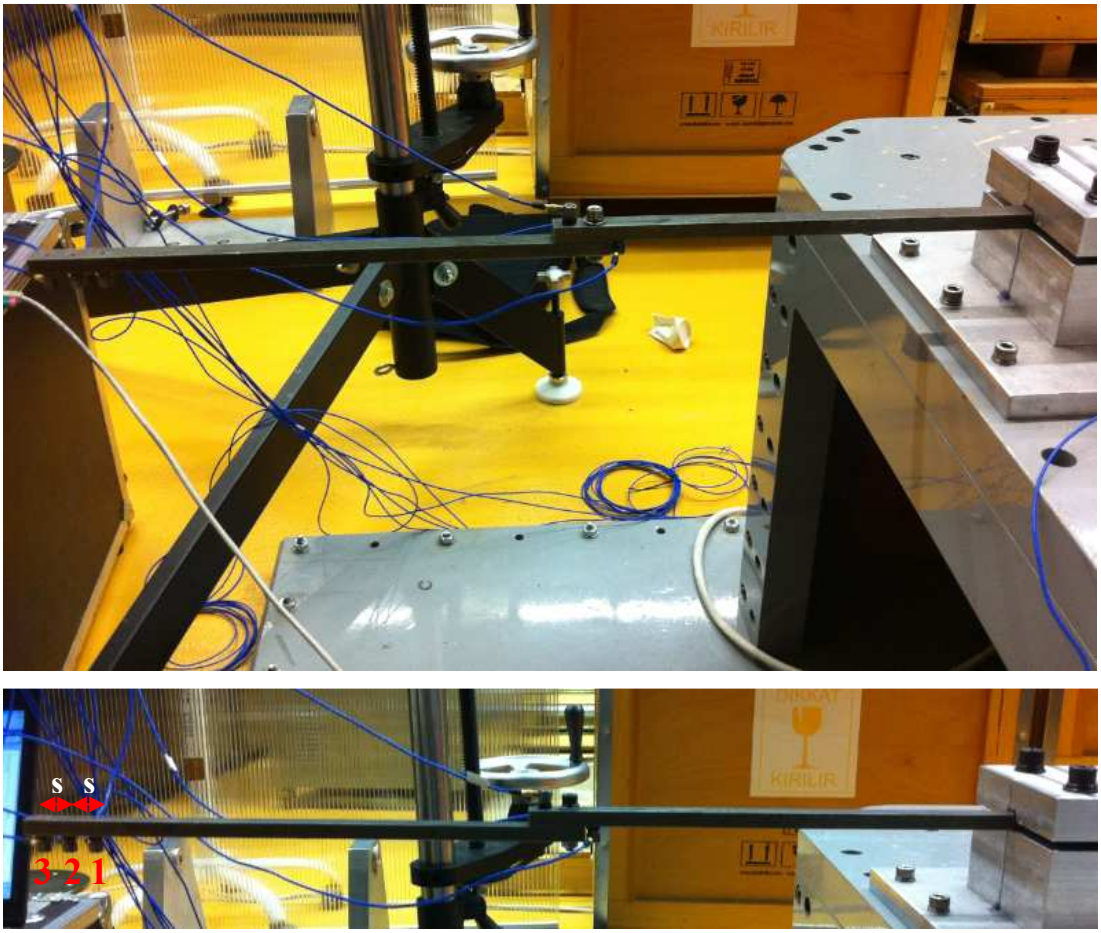

Figure 5.21 Single Bolt Connection

5.3.1 Beams Connected with M10x35 Hexagonal Bolt

In this case study A2-70 M10x35 hexagon head bolt is used and the tightening torque is set to 30Nm.

5.3.1.1 Measurements and Estimation of FRFs

In the experimental identification of the bolted joint, FRFs of substructure A, which has fixed-free boundary conditions, are measured; while the FRFs of substructure B, which has free-free boundary conditions, are obtained theoretically by tuning the modal and structural parameters of the beam with the measured ones as explained in section 5.2. In the testing of the substructure B, it is suspended with elastic cords as shown in Figure 5.22.

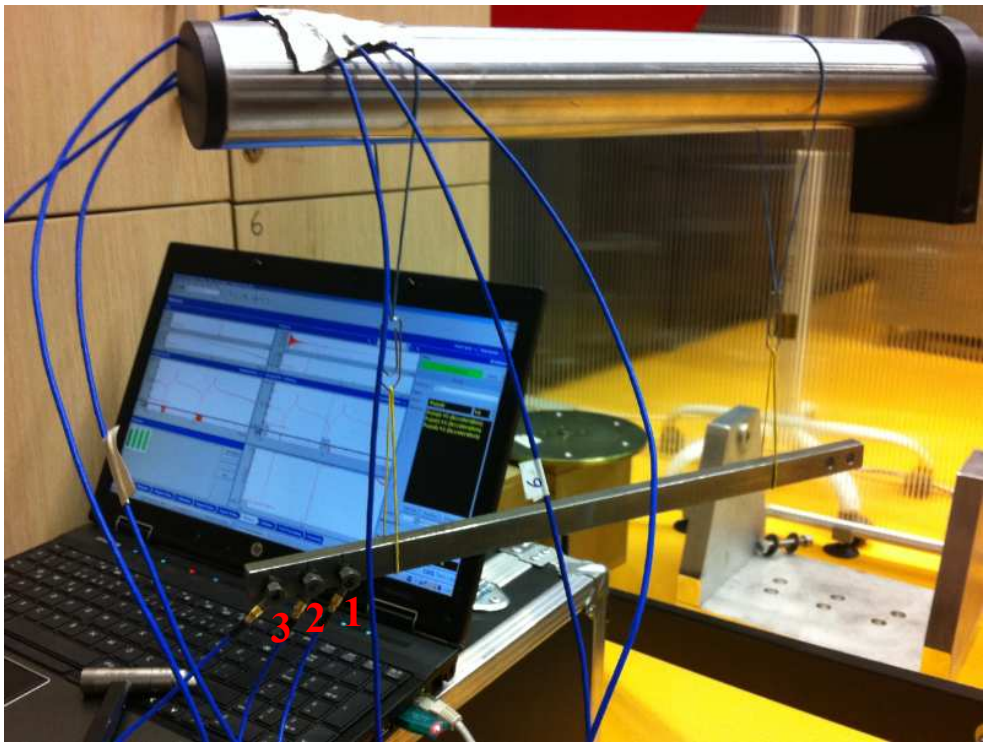

Figure 5.22 Testing of Substructure B

The structure B is excited at the tip point and the tip point FRFs are obtained as shown in Figure 5.23 and the modal parameters are identified. According to the tests performed on substructure B, the following data is used for the FE model of the free-free beam: the elastic modulus $E=1.92\ 10^{11}\ N/m^2$; density $\rho=7604\ kg/m^2$. Also, the damping ratio for the first elastic mode is obtained from the tests as 0.0005. Then by using the modal properties determined, the FRFs of the substructure B, $[H_{kk}]$, $[H_{ks}]$, $[H_{sk}]$ and $[H_{ss}]$ are calculated accurately.

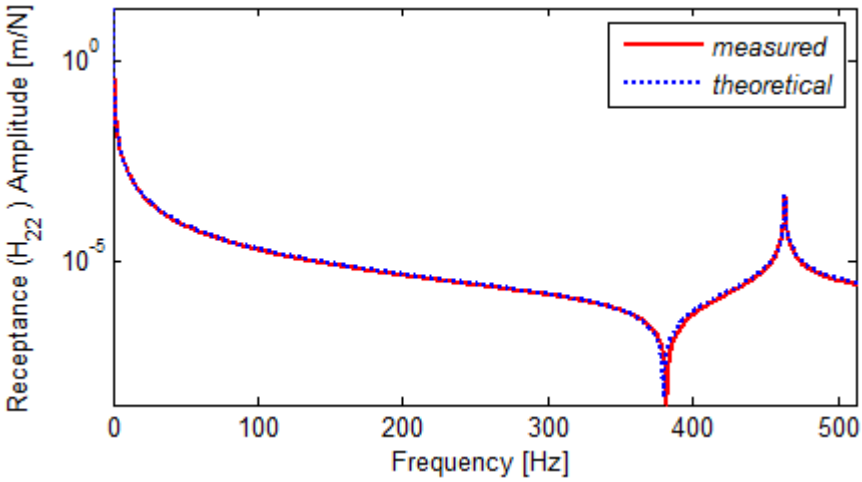

Figure 5.23 Tuning of the Substructure B FRF

In order to estimate the RDOF related FRFs of substructure A, three accelerometer measurements are taken. Since steel is more rigid than aluminum beam and the response time is longer than aluminum beam, it is possible to excite the structure at point 1 without making double hit. The accelerometers are located with spacing, s, of 0.015m as shown in Figure 5.24.

Figure 5.24 Close Accelerometers Method for Substructure A

After completing the FRF measurements, system identification is performed using the LMS modal analysis software and using required parameters for the FRF synthesis (the results are given in Appendix A), translational FRFs at the tip point of substructure A are obtained as shown in Figure 5.25.

After obtaining the translational FRFs at the tip point, using the second order finite difference formula, rotational FRFs are estimated at point 2 as shown in Figure 5.26.

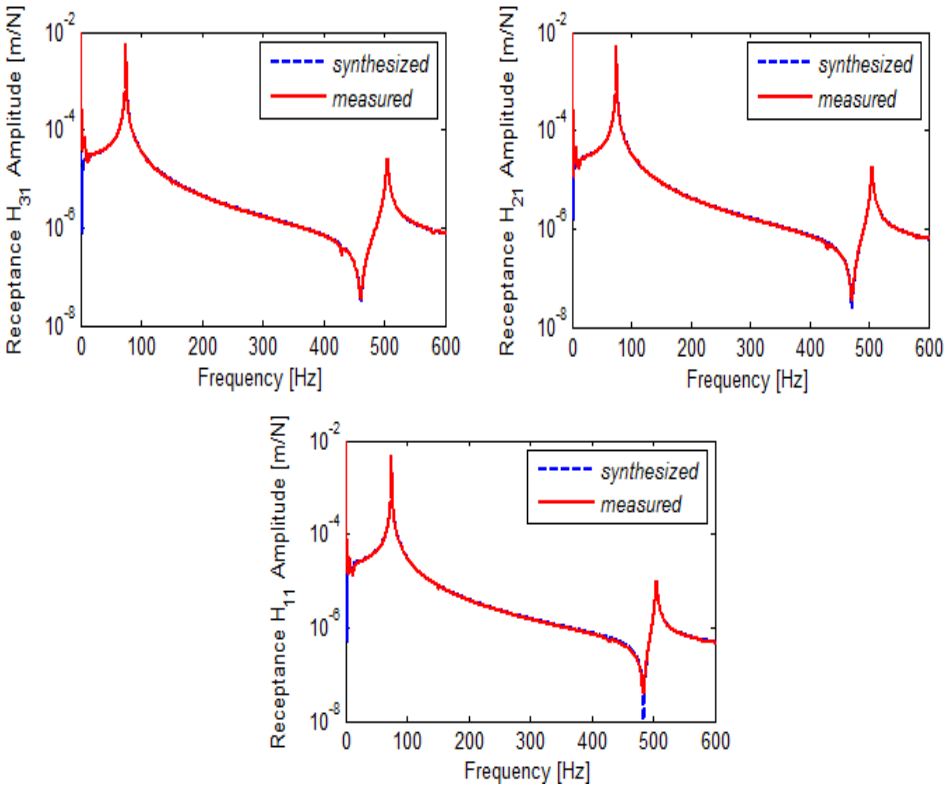

Figure 5.25 FRF Synthesis for Substructure A

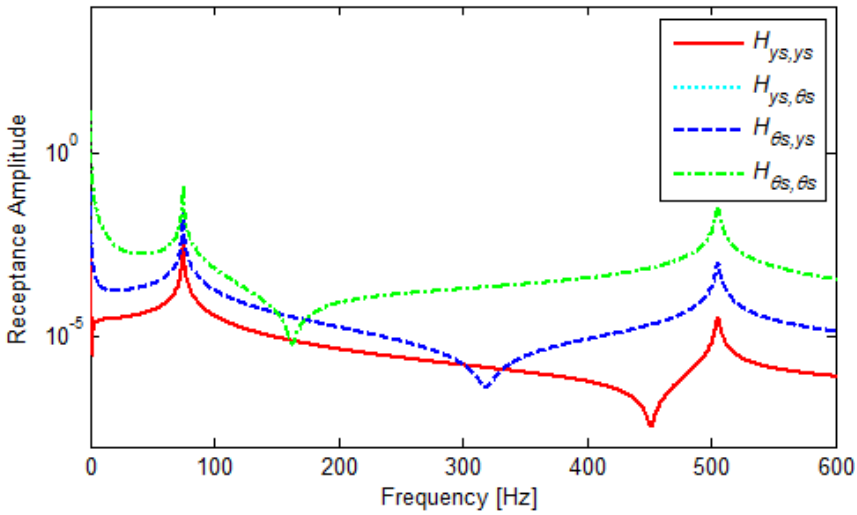

Figure 5.26 Rotational FRF Estimation for Substructure A

5.3.1.2 Identification of Bolted Joint

In this case study the properties of the bolted joint are extracted with the identification approach 2, in which only one of the translational FRF measured at the tip point 2 of the structure is directly used. The identified joint stiffness and damping values are shown in Figure 5.27 and Figure 5.28, respectively.

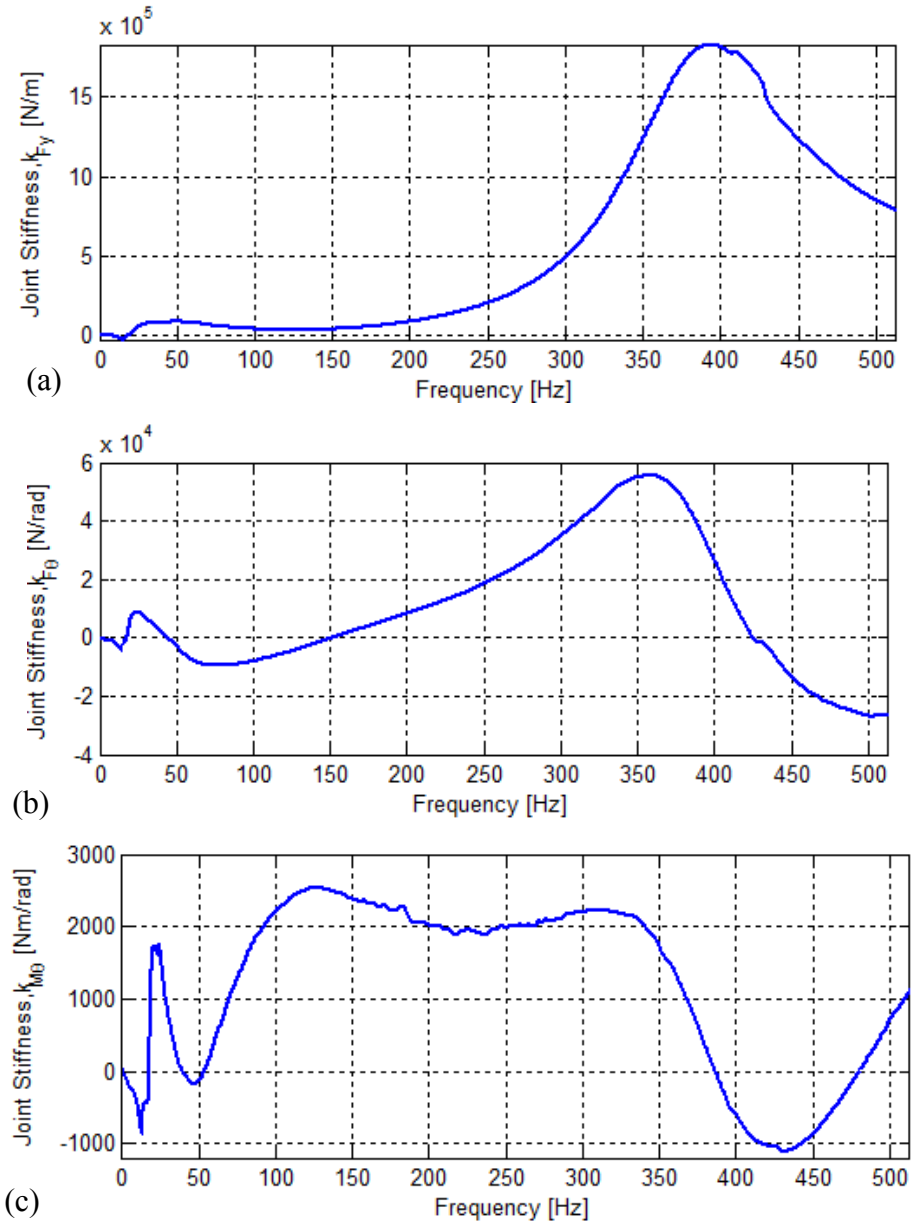

Figure 5.27 Identification of Joint Stiffness (a) Translational Joint Stiffness, (b) Cross-coupling Joint Stiffness, (c) Rotational Joint Stiffness

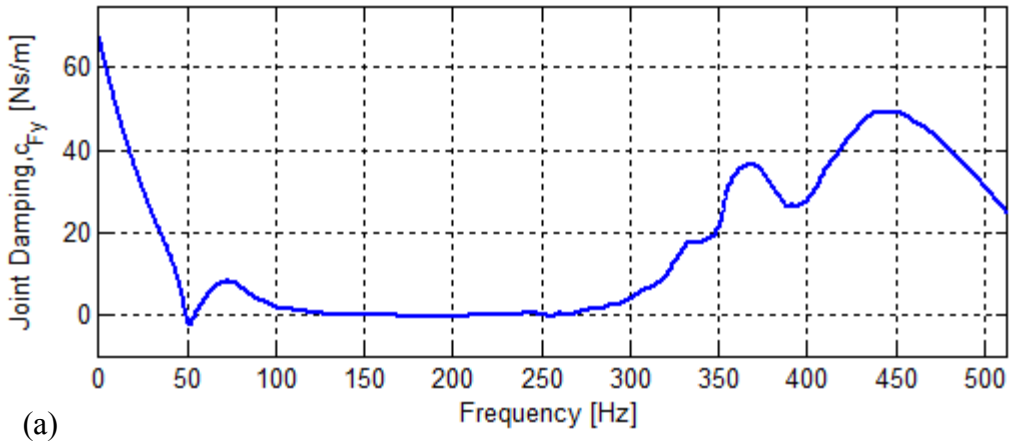

(a)

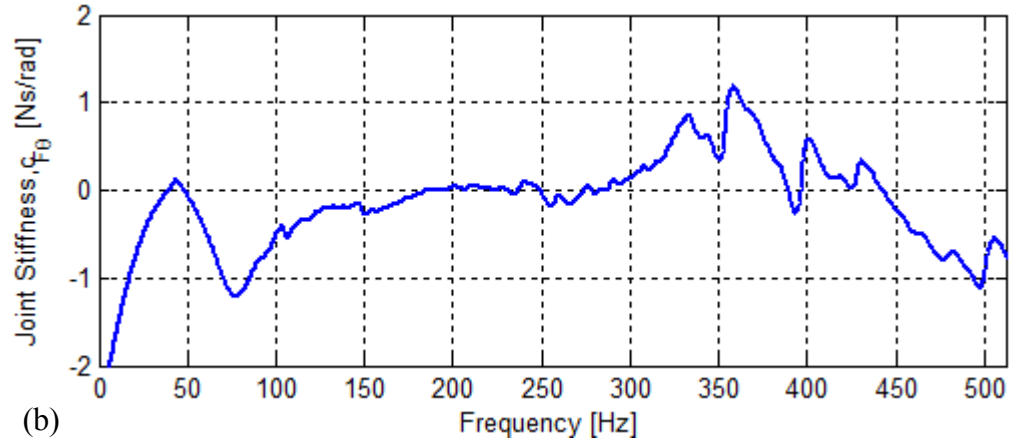

(b)

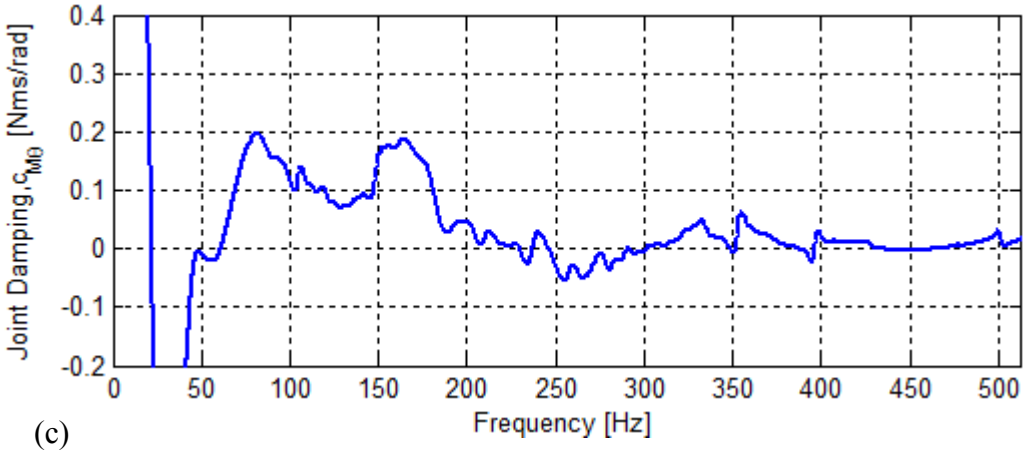

(c)

Figure 5.28 Identification of Joint Damping (a) Translational Joint Damping, (b) Cross-coupling Joint Damping, (c) Rotational Joint Damping

From the sensitivity analysis, it is again seen that, translational and cross-coupling joint stiffness is effective at the third mode, while rotational stiffness is effective at both second and third modes (Appendix C). Therefore, the values of translational and cross-coupling joint stiffness and damping identified at the third mode and rotational parameters identified at the second mode can be used as initial estimates. Then, these values are updated with the algorithm mentioned above. Starting with initial estimates from the identified results at the second mode for rotational parameters, the third mode for translational and cross-coupling parameters, the updated joint parameters are obtained as given in Table 5.5.

Table 5.5 Joint Parameters of the M10x35 Bolted Connection

	k_{Fy} *[N/m]*	$k_{F\theta}$ *[N/rad]*	$k_{M\theta}$ *[N.m/rad]*	c_{Fy} *[N.s/m]*	$c_{F\theta}$ *[N.s/rad]*	$c_{M\theta}$ *[N.m.s/rad]*
Initial Estimates	$1.71*10^6$	$5.12*10^4$	$2.5*10^3$	34.72	0.646	0.073
Updated	$2.02*10^6$	$2.47*10^4$	$2.8*10^3$	34.41	0.635	0.077

By using the updated joint parameters, receptances of the assembled system are regenerated and they are compared with the measured receptances in Figure 5.29. It can be seen from the comparison that the receptances regenerated by using the updated joint parameters perfectly match with the measured FRFs.

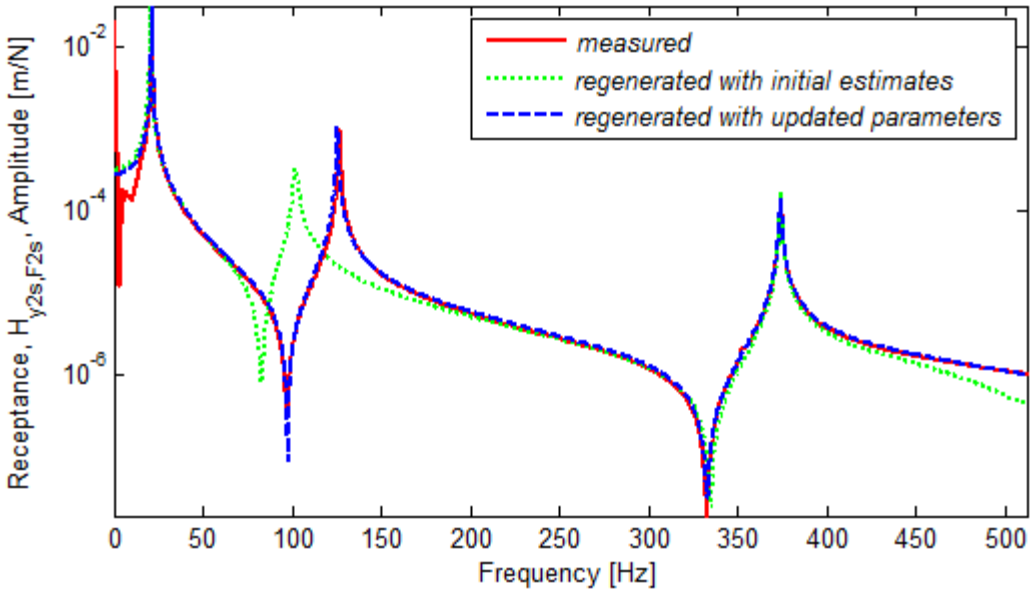

Figure 5.29 Regenerated FRF, $H_{y2s.F2s}$, of the Coupled Structure Using Updated Joint Properties

Furthermore, by using the updated joint parameters, the FRFs of the coupled structure at Point 1 and Point 3, which are not used in the identification of joint properties, are obtained. It can be seen from Figure 5.30 that the receptances calculated by using the updated joint parameters perfectly match with the measured FRFs. Hence, it can be concluded that, the joint properties are identified accurately.

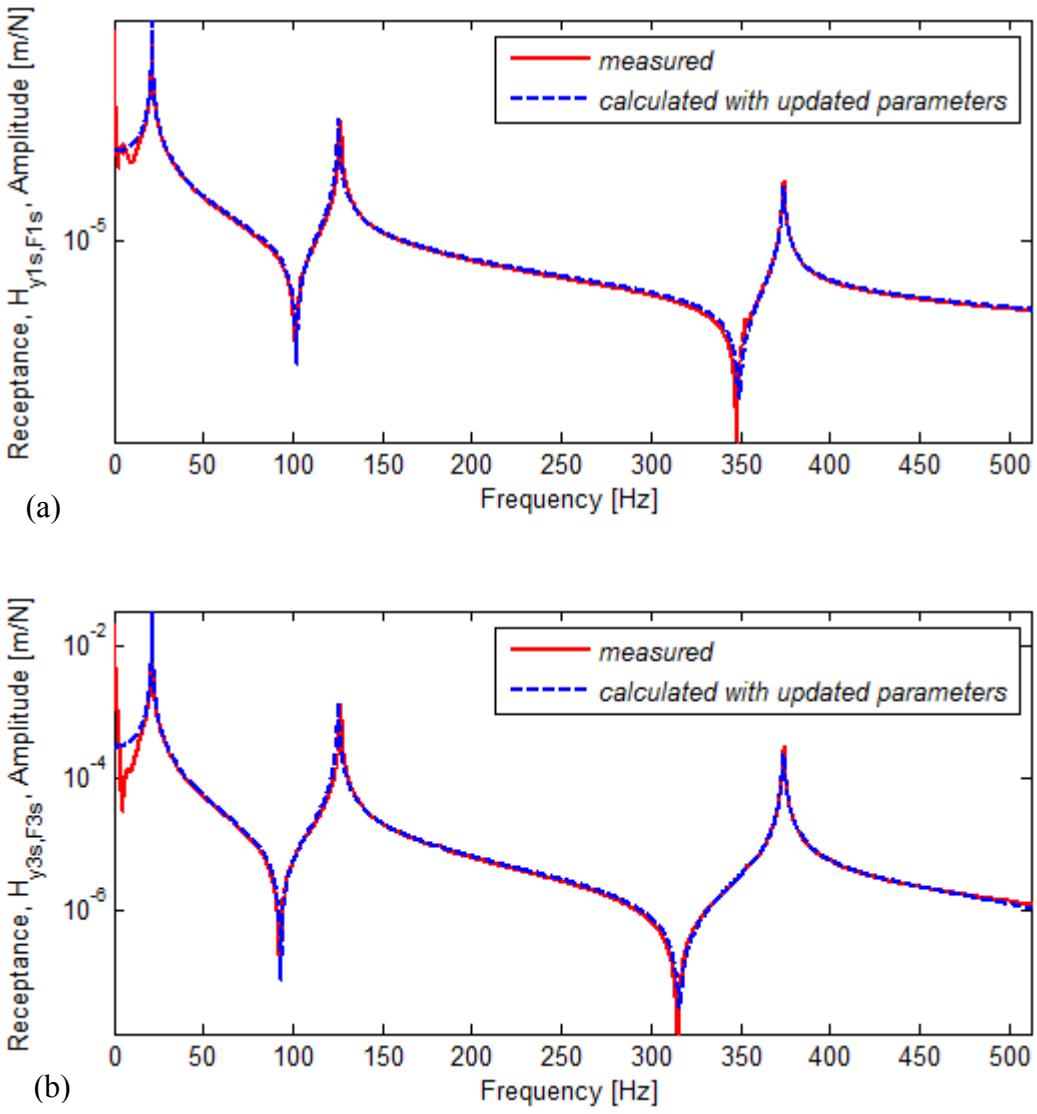

Figure 5.30 Calculated FRFs of the Coupled Structure Using Updated Joint Properties a) $H_{y1s.F1s}$, b) $H_{y3s.F3s}$

5.3.2 Beams Connected with M8x35 Hexagonal Bolt

In this case study, the properties of a joint with M8x35mm hexagon head bolt are determined. Furthermore, in this case study, the identified joint parameters are used to theoretically calculate the FRFs of a different coupled structure obtained with steel

beams and the same bolt, and these FRFs are compared with the measured ones. Moreover, different levels of tightening torques are used in the connection and the effect of torque on the coupled system and the relation between the tightening torque and joint parameters are examined.

5.3.2.1 Measurements and Estimation of FRFs

RDOF related FRFs of substructure A are obtained with the same procedure explained in the previous studies. The required parameters for the FRF synthesis and the synthesized FRFs are given in Appendix A. Moreover, the effect of the difference in the size of the bolt hole on the steel beam cannot be ignored, so substructure B is tested again and the FE model of the free-free beam is calibrated with these data as given in Appendix B.

5.3.2.2 Identification of Bolted Joint

The properties of the bolt are extracted with the identification approach 2, in which only one of the translational FRF measured at the tip point (point 2) of the structure is directly used. The identified joint stiffness and damping values are shown in Figure 5.31 and Figure 5.32, respectively.

Starting with initial estimates from the identified results at the second mode for rotational parameters, at the third mode for translational and cross-coupling parameters, the updated joint parameters are obtained as given in Table 5.6. By using the updated joint parameters, receptances of the assembled system are regenerated and they are compared with the measured receptances in Figure 5.33. It can be seen from the comparison that the receptances regenerated by using the updated joint parameters perfectly match with the measured FRFs.

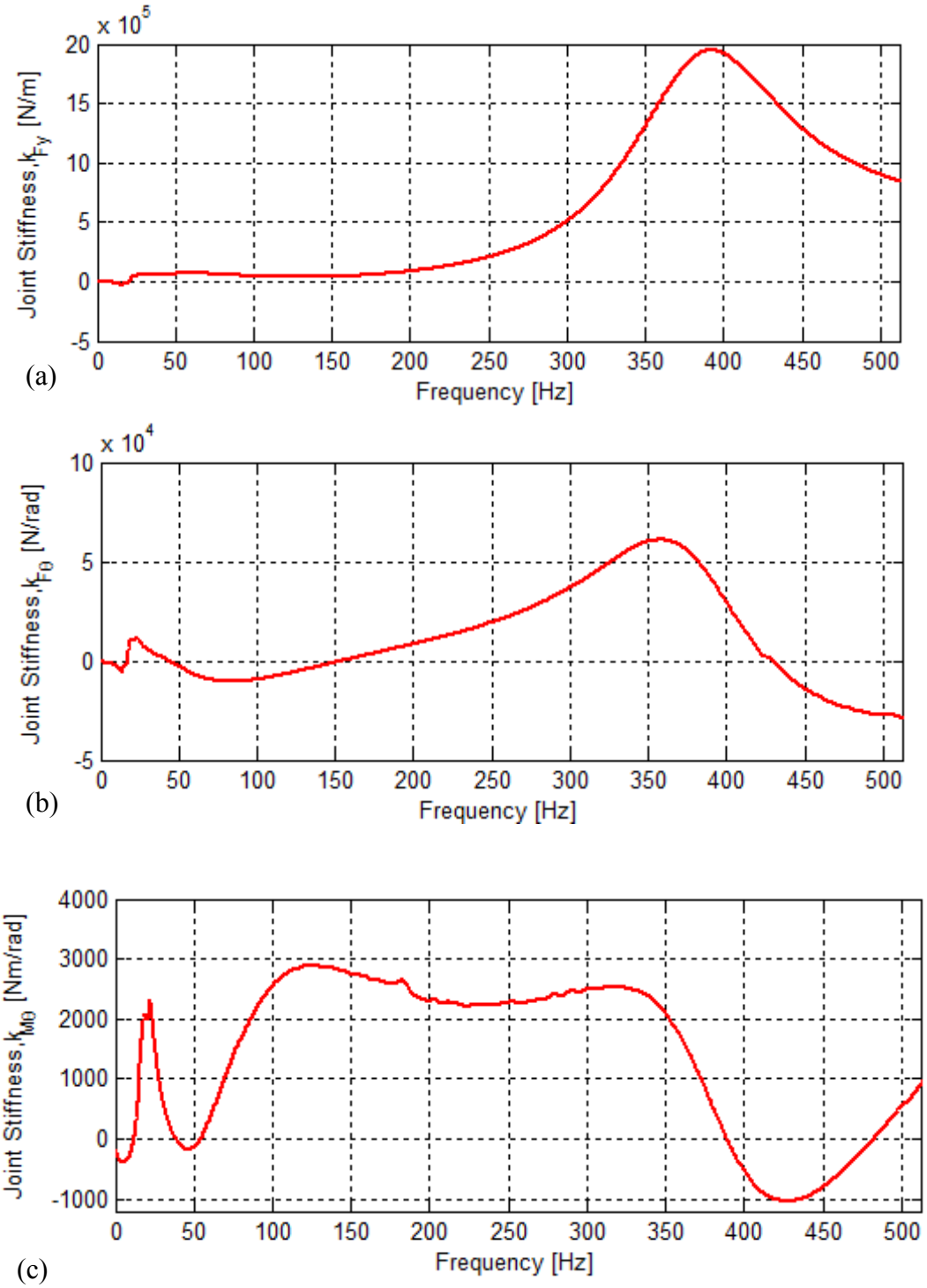

Figure 5.31 Identification of Joint Stiffness (a) Translational Joint Stiffness, (b) Cross-coupling Joint Stiffness, (c) Rotational Joint Stiffness

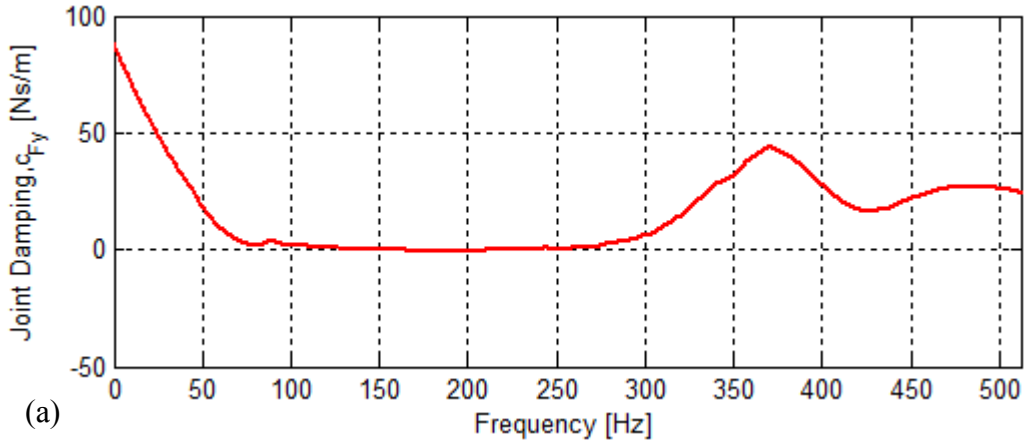

(a)

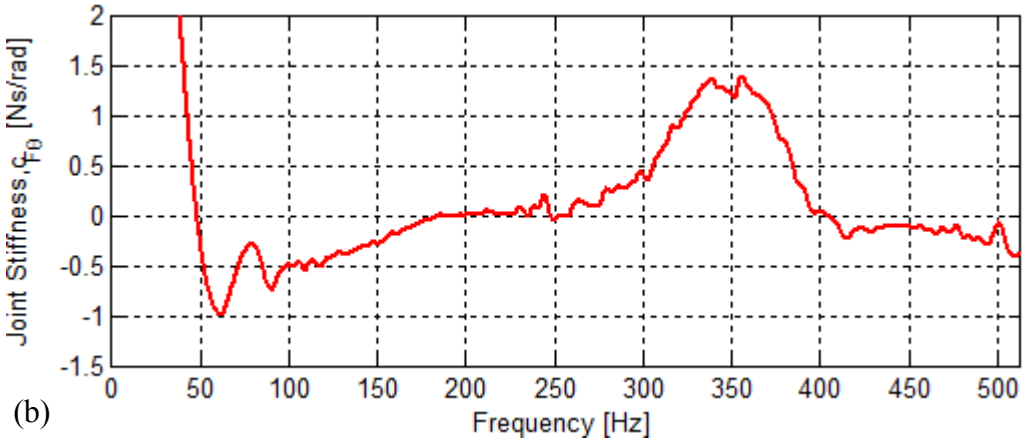

(b)

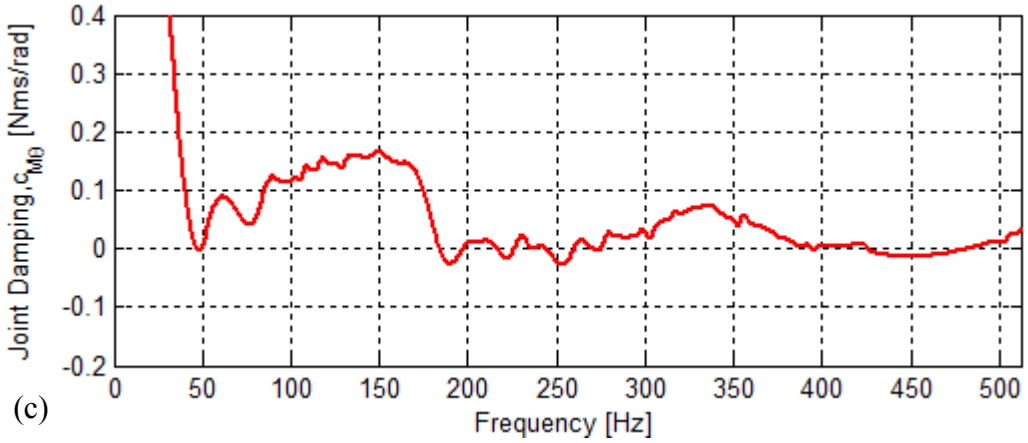

(c)

Figure 5.32 Identification of Joint Damping (a) Translational Joint Damping, (b) Cross-coupling Joint Damping, (c) Rotational Joint Damping

Table 5.6 Joint Parameters of the M8x35 Bolted Connection

	k_{Fy} [N/m]	$k_{F\theta}$ [N/rad]	$k_{M\theta}$ [N.m/rad]	c_{Fy} [N.s/m]	$c_{F\theta}$ [N.s/rad]	$c_{M\theta}$ [N.m.s/rad]
Initial Estimates	$1.83*10^6$	$5.53*10^4$	$2.9*10^3$	42.2	0.848	0.139
Updated	$2.14*10^6$	$2.66*10^4$	$3.2*10^3$	41.2	0.845	0.119

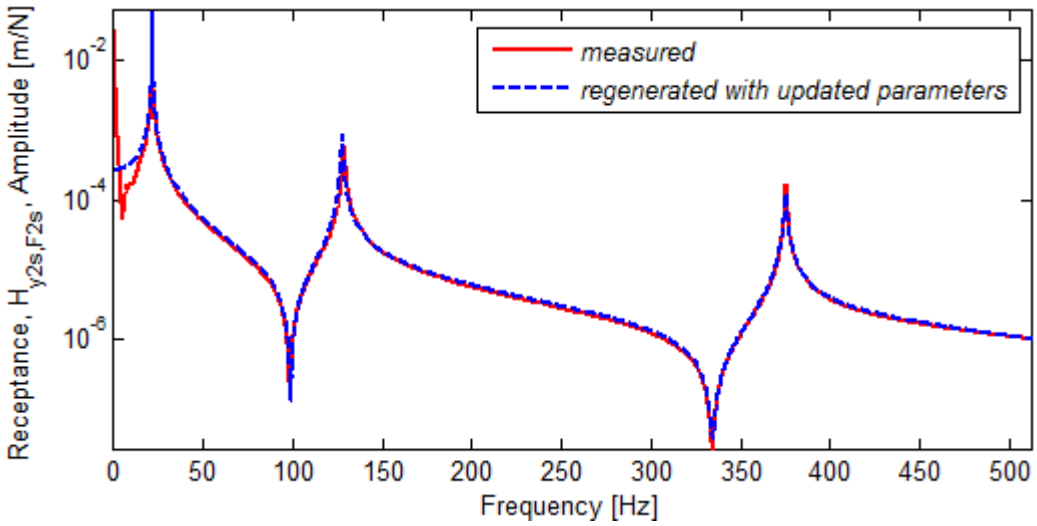

Figure 5.33 Regenerated FRF, $H_{y2s.F2s}$, of the Coupled Structure Using Updated Joint Properties

5.3.2.3 New Structure with M8x35 Bolt

In this verification, a new substructure A with a length of 0.35m (longer than the previous one) is used as shown in Figure 5.34. RDOF related FRFs of the new substructure A are obtained with the same procedure explained in the previous studies. The required parameters for the FRF synthesis and the synthesized FRFs are given in Appendix A. By using the identified joint parameters, receptance of the new

assembled system is calculated and it is compared with the measured receptance in Figure 5.35.

Figure 5.34 New Assembly with M8 Bolt

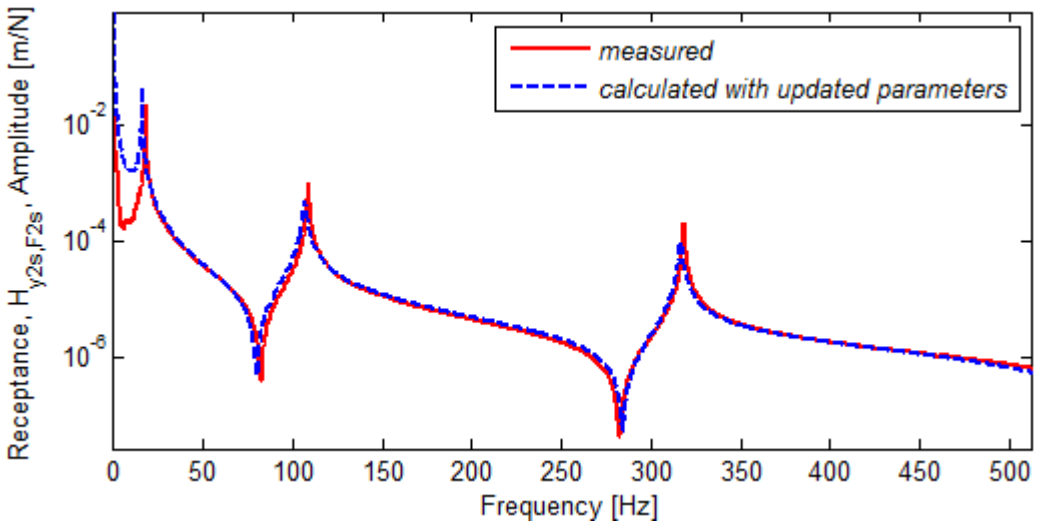

Figure 5.35 Calculated FRF, $H_{y2s.F2s}$, of the New Assembly Using Updated Joint Properties

It can be seen from the comparison that the receptances calculated by using the joint parameters identified from an assembly perfectly match with the measured FRFs of another assembly. Then it can be concluded that, once the joint properties are identified, it can be used for another structure having the same connection, the same material and cross sectional dimensions for the beams and the same bolt.

5.3.2.4 M8 Bolt under Different Levels of Tightening Torque

In this study, the coupled structure with different levels of bolt tightening torques is tested and the relation between the tightening torque and identified joint parameters are studied. The torque levels are taken from the Bossard's catalogue, and the lowest and the highest torque levels for M8 A2 70 type bolt is set to 10Nm and 25Nm, respectively. It is seen from Figure 5.36 that, natural frequencies of the coupled structure increase, as the tightening torque is increased. However, the change is observed to be quite small.

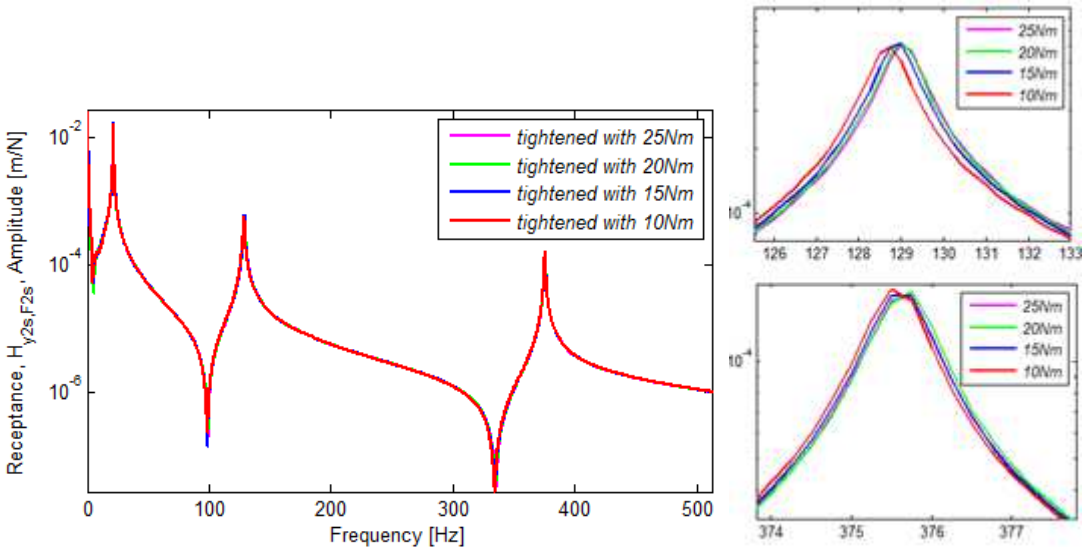

Figure 5.36 Coupled structure FRF, $H_{y2s.F2s}$, with Different Levels of Tightening Torque

From the identification results given in Table 5.7 and Table 5.8 it is seen that, as the tightening torque is increased cross-coupling and rotational joint stiffnesses increase, while translational joint stiffness remains nearly same.

Table 5.7 Identified Joint Stiffness and Damping under Different Levels of Torque

	k_{Fy} ***[N/m]***	$k_{F\theta}$ ***[N/rad]***	$k_{M\theta}$ ***[N.m/rad]***
10Nm	2139415	26641	3209
15Nm	2139413	27574	3231
20Nm	2139412	27956	3302
25Nm	2139410	28401	3341
	c_{Fy} ***[N.s/m]***	$c_{F\theta}$ ***[N.s/rad]***	$c_{M\theta}$ ***[N.m.s/rad]***
10Nm	41.23	0.8449	0.1191
15Nm	41.23	0.8335	0.1291
20Nm	41.23	0.8395	0.1237
25Nm	41.23	0.8399	0.1424

Table 5.8 Percentage Change in the Identified Joint Stiffness under Different Levels of Torque

	$k_{F\theta}$ ***[N/rad]***	$k_{M\theta}$ ***[N.m/rad]***
15Nm	3.5	0.7
20Nm	1.4	2.2
25Nm	1.6	1.2

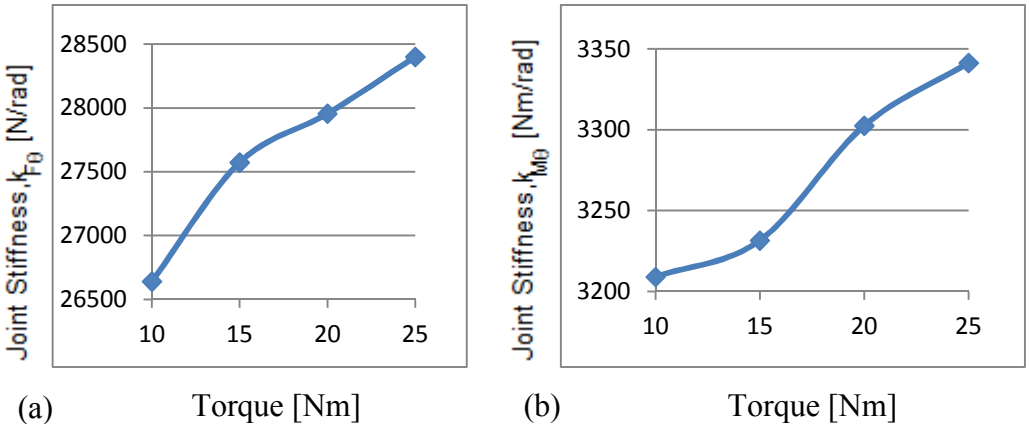

Figure 5.37 Identified Joint Stiffness under Different Levels of Torque (a) Cross-coupling Joint Damping, (b) Rotational Joint Damping

5.3.3 Beams Connected with M6x30 Hexagonal Bolt

In this case study, properties of M6x30mm hexagon head bolt are determined. With the identified joint parameters, the receptances of the structure coupled with a multiple connection are regenerated and compared with the measured receptances of the new assembly. Furthermore, different quality (A2 70 and A4 80 type) M6 bolts are used in the connection and the effect of the bolt quality on the coupled system and joint parameters are examined.

5.3.3.1 Measurements of FRFs

RDOF related FRFs of substructure A are obtained with the same procedure explained in the previous studies. The required parameters for the FRF synthesis and the synthesized FRFs are given in Appendix A. Moreover, the effect of the difference in the size of the bolt hole on the steel beam cannot be ignored, so substructure B is tested again and the FE model of the free-free beam is calibrated with these data as given in Appendix B.

5.3.3.2 Identification of Bolted Joint

The properties of the bolt are extracted with the identification approach 2, in which only one of the translational FRF measured at the tip point (point 2) of the structure is directly used. The identified joint stiffness and damping values are shown in Figure 5.38 and Figure 5.39, respectively.

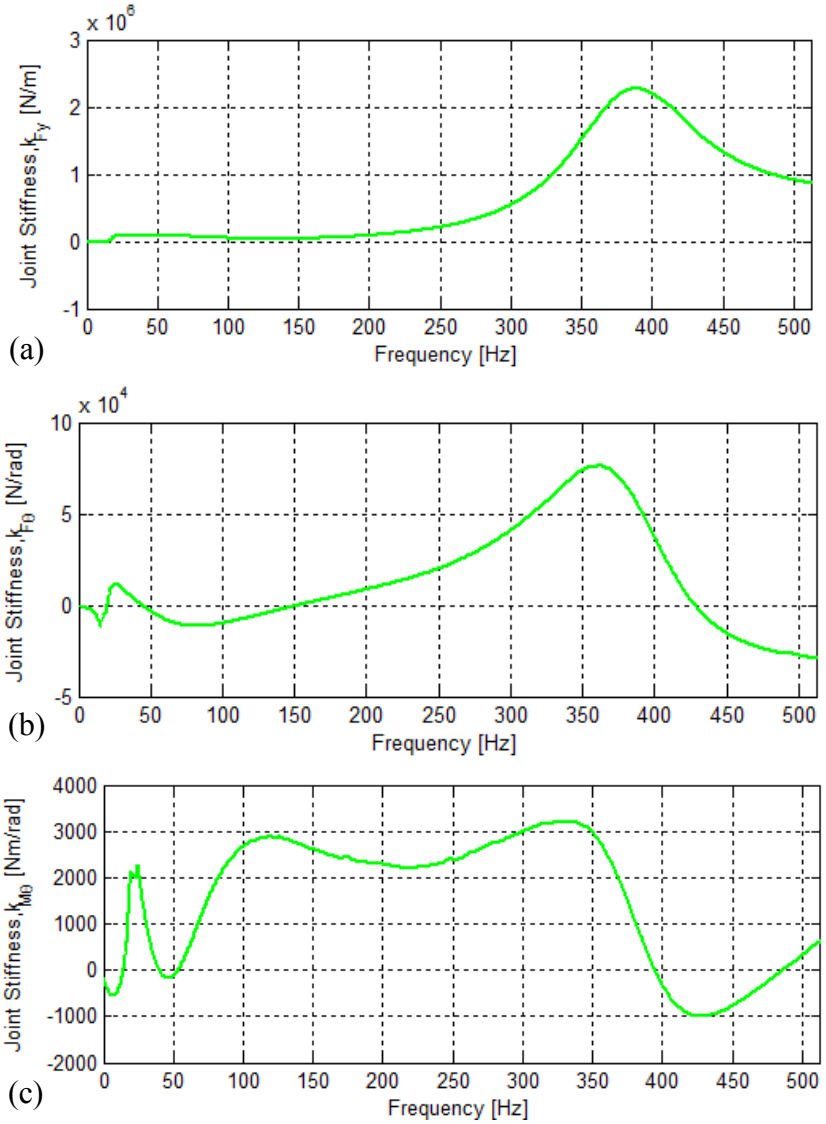

Figure 5.38 Identification of Joint Stiffness (a) Translational Joint Stiffness, (b) Cross-coupling Joint Stiffness, (c) Rotational Joint Stiffness

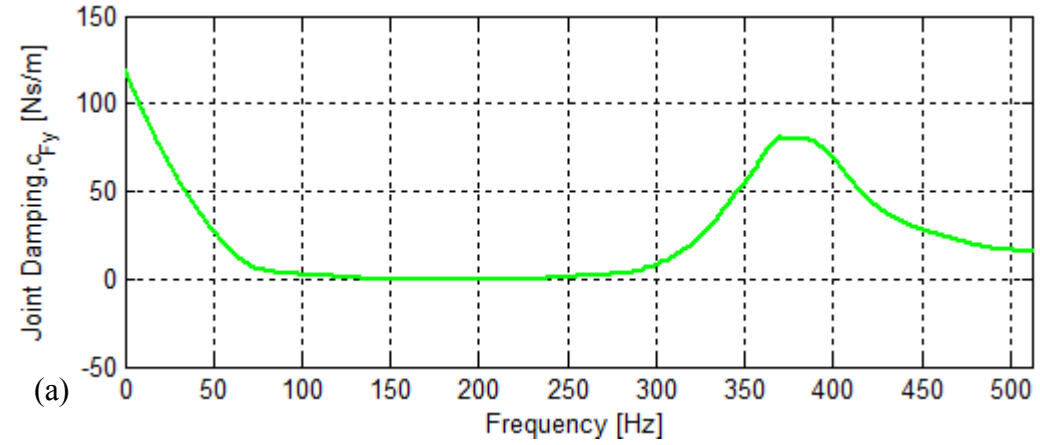

(a)

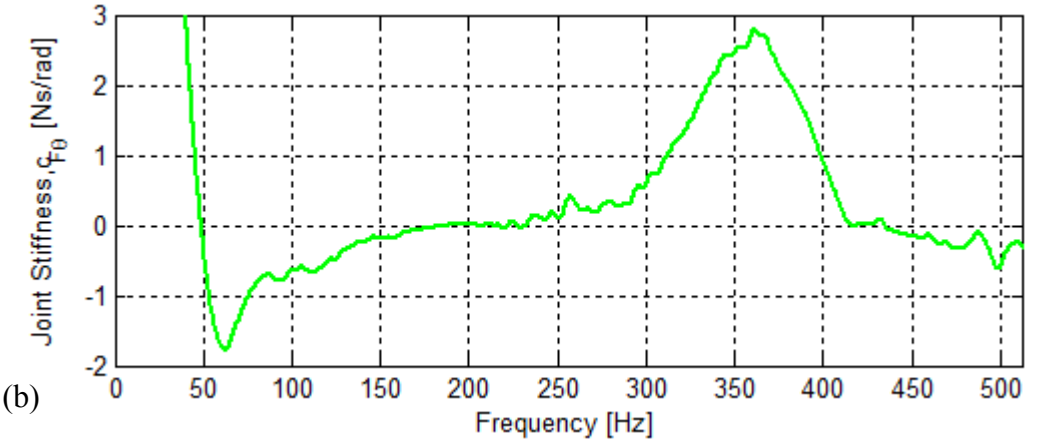

(b)

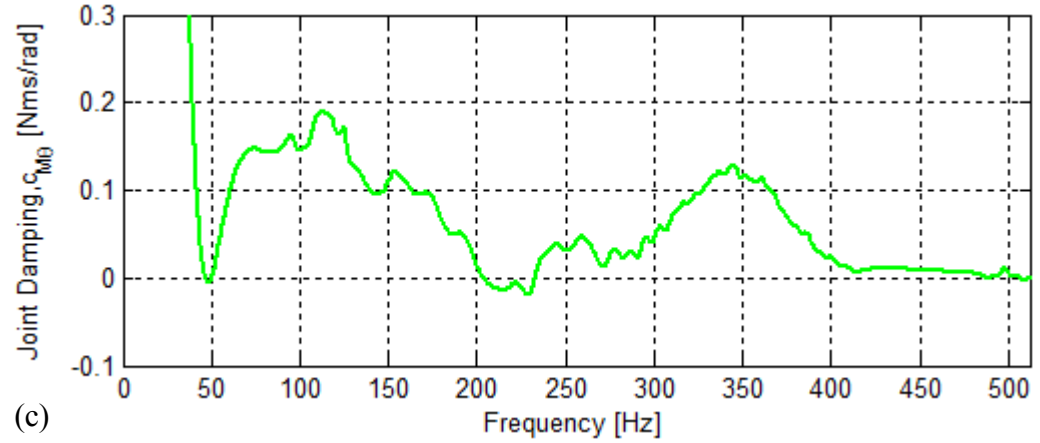

(c)

Figure 5.39 Identification of Joint Damping (a) Translational Joint Damping, (b) Cross-coupling Joint Damping, (c) Rotational Joint Damping

Starting with initial estimates from the identified results at the second mode for rotational parameters, at the third mode for translational and cross-coupling parameters, the updated joint parameters are obtained as given in Table 5.9. By using the updated joint parameters, receptances of the assembled system is regenerated and they are compared with the measured receptances in Figure 5.40. It can be seen from the comparison that the receptances regenerated by using the updated joint parameters perfectly match with the measured FRFs.

Table 5.9 Joint Parameters of the M6x30 Bolted Connection

	k_{Fy} *[N/m]*	$k_{F\theta}$ *[N/rad]*	$k_{M\theta}$ *[N.m/rad]*	c_{Fy} *[N.s/m]*	$c_{F\theta}$ *[N.s/rad]*	$c_{M\theta}$ *[N.m.s/rad]*
Initial Estimates	$2.06*10^6$	$7.40*10^4$	$2.9*10^3$	80.4	2.52	0.139
Updated	$2.27*10^6$	$3.89*10^4$	$3.7*10^3$	75.7	0.94	0.164

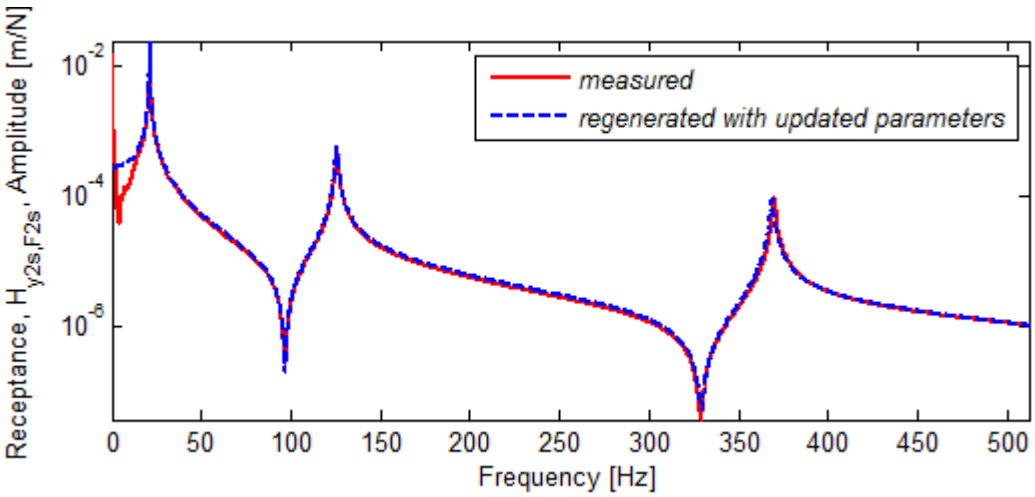

Figure 5.40 Regenerated FRF, $H_{y2s,F2s}$, of the Coupled Structure Using Updated Joint Properties

5.3.3.3 Connection with two M6x30 Bolts

In this verification, two M6 bolts are used in the connection of the substructures as shown in Figure 5.41. By using the identified joint parameters, receptance of the new assembled system is calculated and they are compared with the measured receptance in Figure 5.42. It can be seen from the comparison that the receptance calculated by using the updated joint parameters perfectly match with the measured FRFs. Note that, joint model 3 is used for this type of connection with multiple joints as given in equation (3.27).

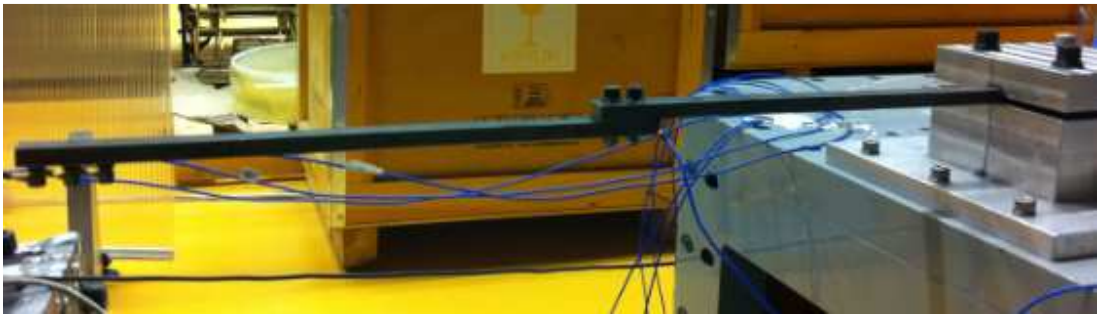

Figure 5.41 Connection with Two Bolts

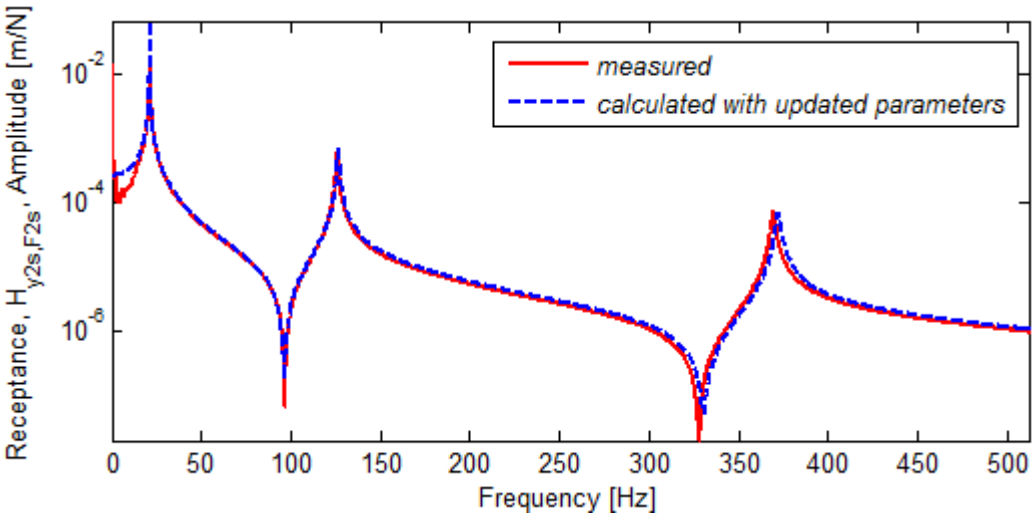

Figure 5.42 Calculated FRF, $H_{y2s.F2s}$, of the Coupled Structure Using Updated Joint Properties

In Figure 5.43 the receptances of the coupled structure with one and two bolts, as well as rigid connection are given, and it is seen that the bolts add some flexibility to the assembly; however, as the number of bolts in the connection increase, assembly becomes more rigid, as expected.

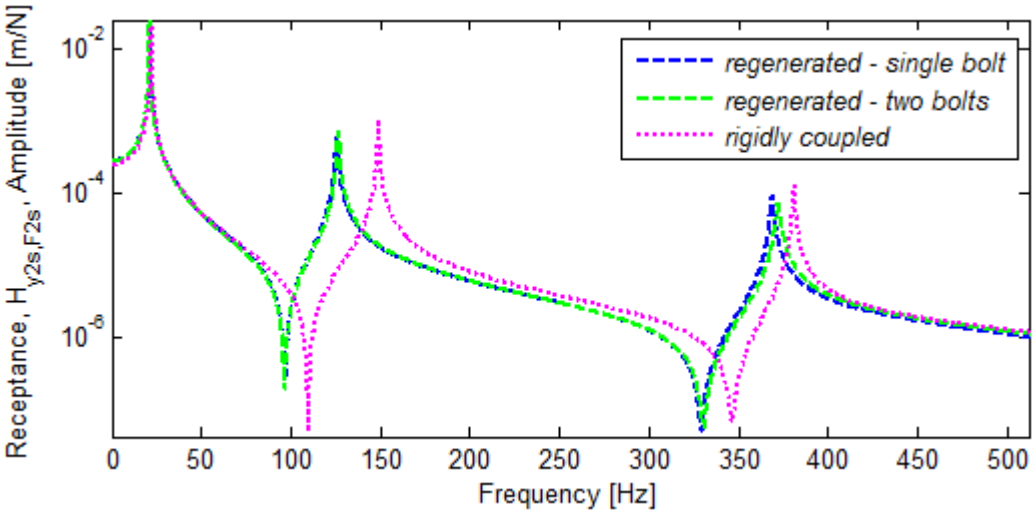

Figure 5.43 FRFs of the Coupled with Single Bolt, Two Bolts and Rigid Connection

5.3.3.4 Effect of Bolt Quality

In this study, the coupled structures which are connected with different quality (A2 70 and A4 80) M6 bolts under different levels of torque are tested and the effect of bolt quality on the identification results is examined. The torque levels are taken from the Bossard's catalogue and set to 8Nm and 12Nm for M6 A2 70 and A4 80 type bolts, respectively. The coupled structure FRFs are given in Figure 5.44.

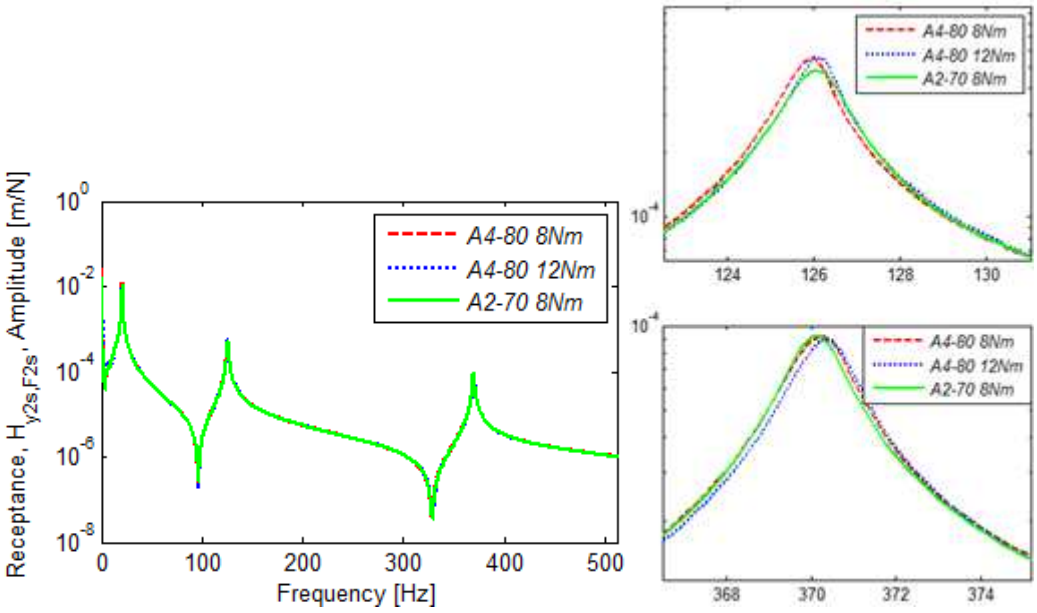

Figure 5.44 Coupled structure FRF, $H_{y2s.F2s}$, with Different Quality Bolts

Using these FRFs of the coupled structure, joint stiffness and damping values are identified as shown in Figure 5.45. From Figure 5.46 and identification results given in Table 5.10 it is seen that, as the tightening torque is increased, translational joint stiffness remains nearly same and the cross-coupling and rotational joint stiffnesses increase as discussed in section 5.3.3.3. Under the same preload level, translational stiffness of the A2 70 type bolt is smaller than that of A4 80's and rotational stiffness of the A2 70 type bolt is higher than that of A4 80's.

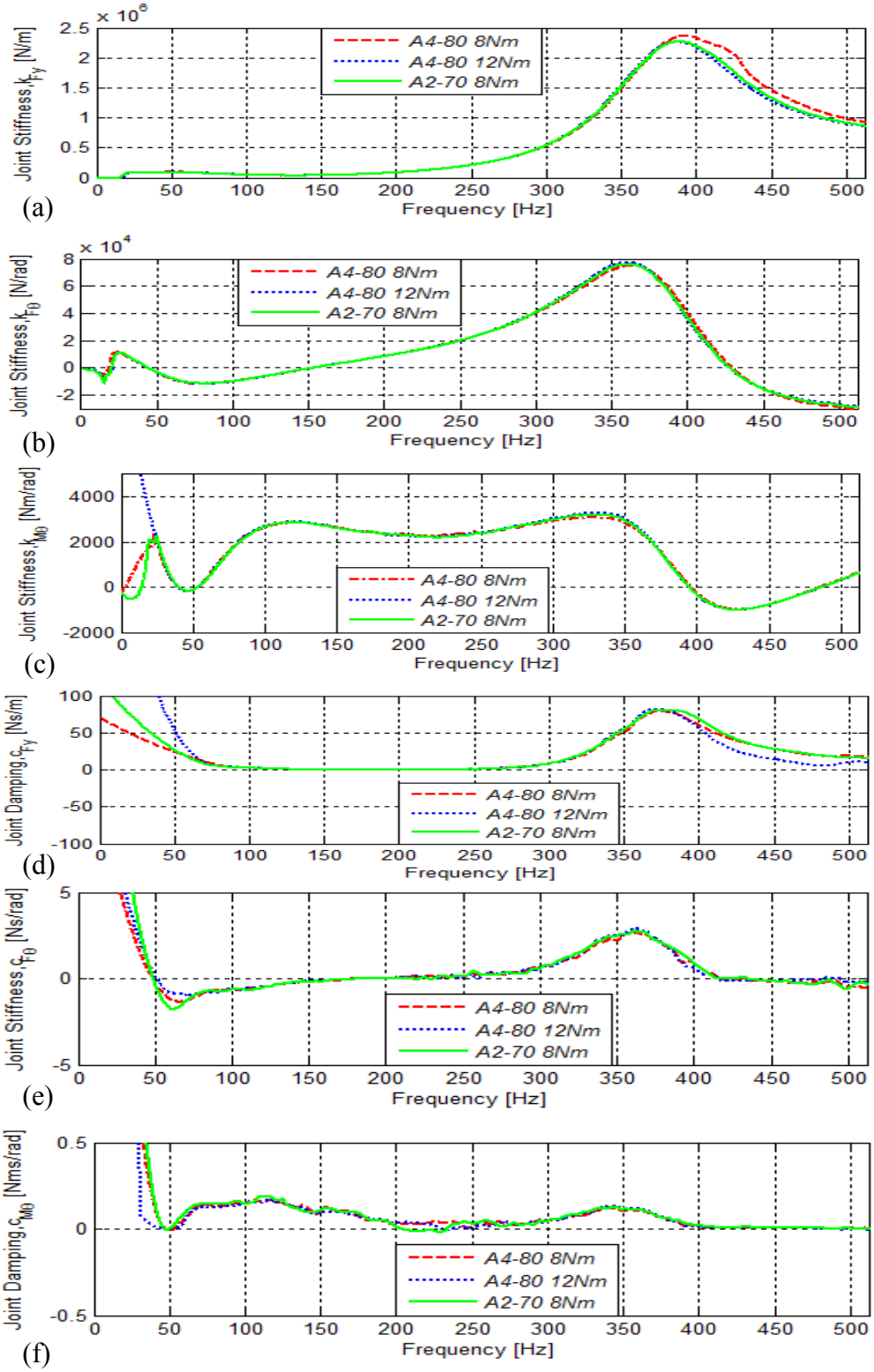

Figure 5.45 Identification of Joint Parameters (a) Translational Joint Stiffness, (b) Cross-coupling Joint Stiffness, (c) Rotational Joint Stiffness (d) Translational Joint Damping, (e) Cross-coupling Joint Damping, (f) Rotational Joint Damping

Table 5.10 Identified Joint Properties using Different Quality Bolts

	k_{Fy} [N/m]	$k_{F\theta}$ [N/rad]	$k_{M\theta}$ [N.m/rad]	c_{Fy} [N.s/m]	$c_{F\theta}$ [N.s/rad]	$c_{M\theta}$ [N.m.s/rad]
A270 8Nm	2265800	38899	3704	75.73101	0.945962	0.164935
A480 8Nm	2265863	36889	3585	75.73106	0.946615	0.158525
A48012Nm	2265812	40004	3769	75.73116	0.947865	0.142518

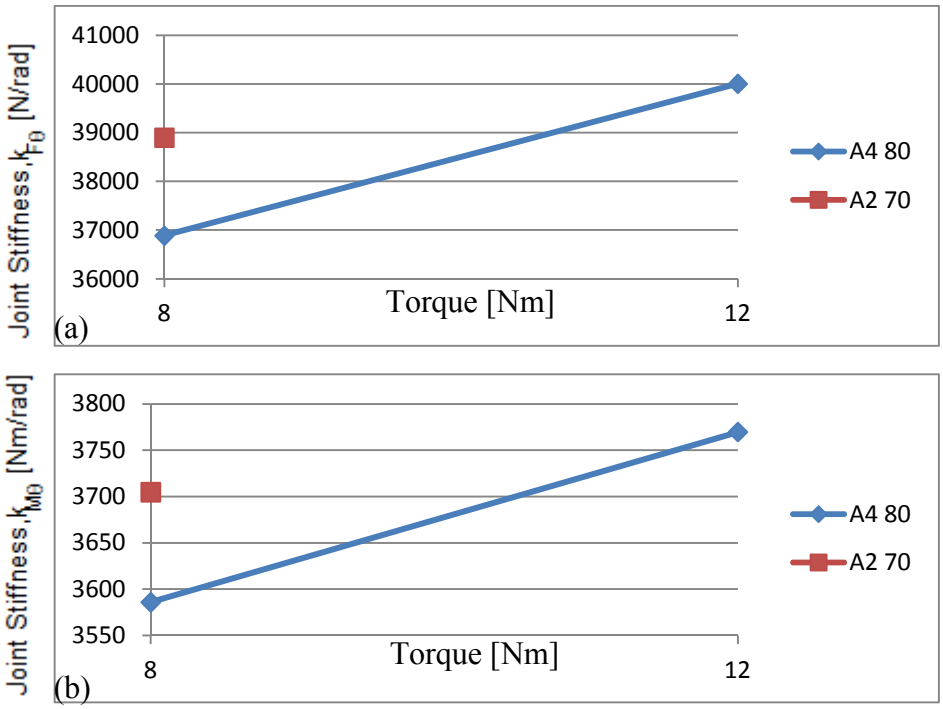

Figure 5.46 Identified Joint Stiffness under Different Levels of Torque (a) Cross-coupling Joint Damping, (b) Rotational Joint Damping

5.4 DISCUSSION OF RESULTS

In this section, results of the identification studies are summarized and some conclusions are to be drawn. The comparison of the identified results obtained with the steel beams using M10, M8 and M6 bolts are given in Figure 5.47, Figure 5.48 and Table 5.11, respectively.

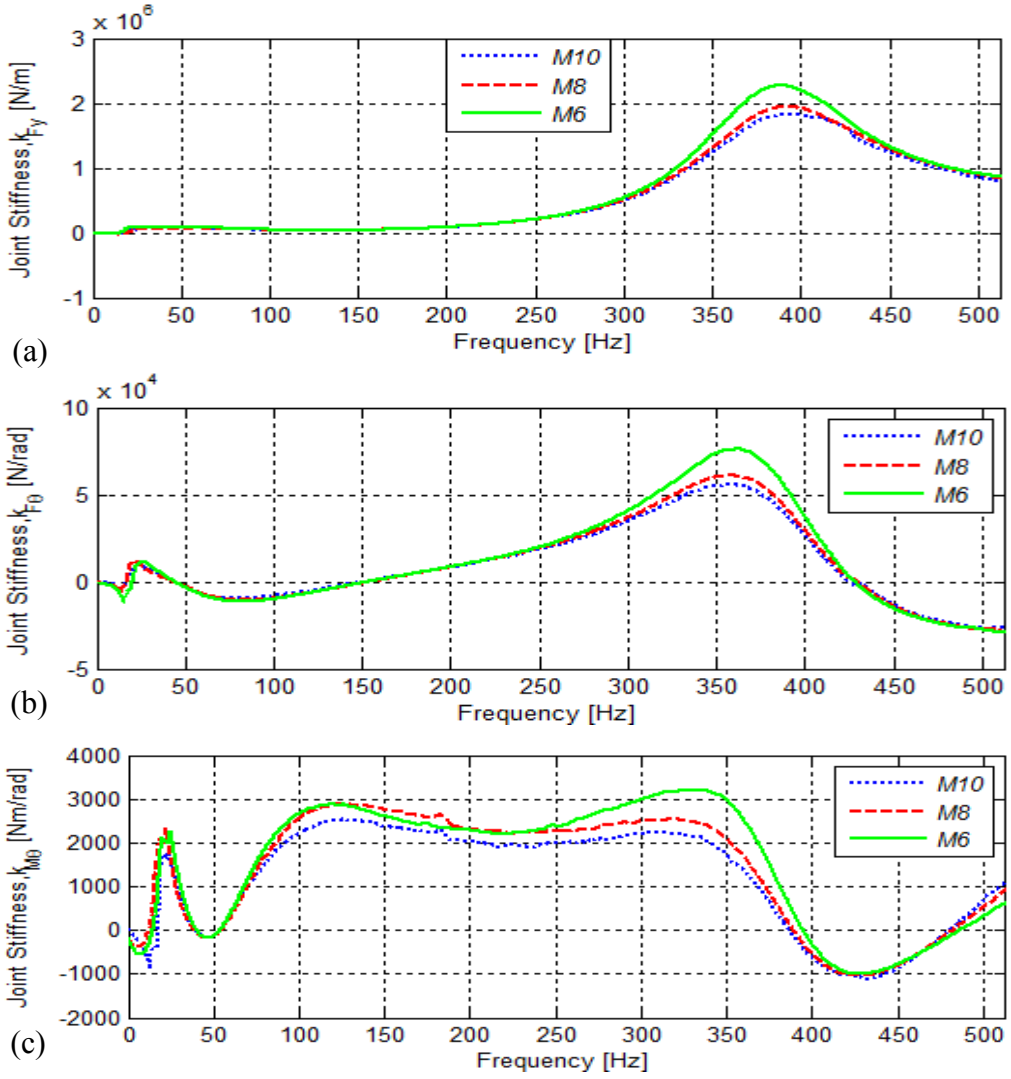

Figure 5.47 Identification of Joint Stiffness (a) Translational Joint Stiffness, (b) Cross-coupling Joint Stiffness, (c) Rotational Joint Stiffness

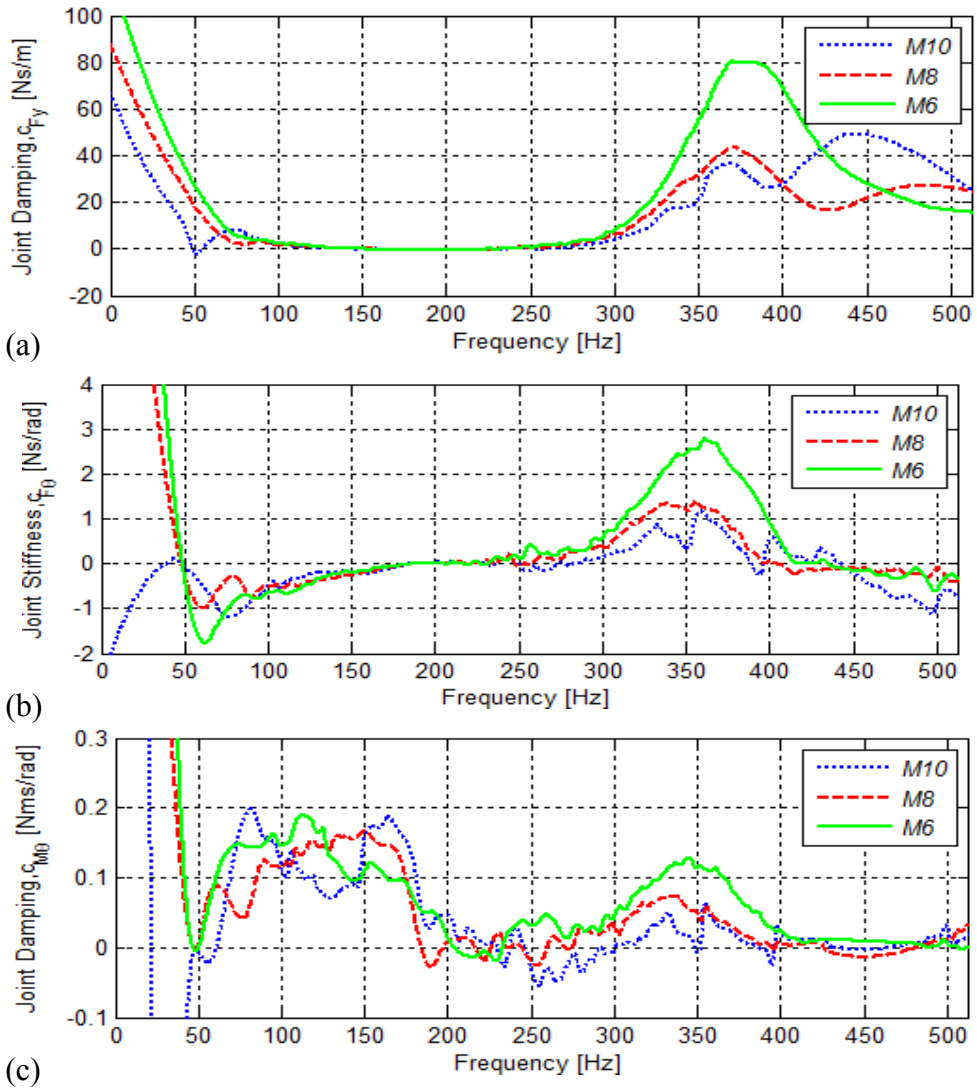

Figure 5.48 Identification of Joint Damping (a) Translational Joint Damping, (b) Cross-coupling Joint Damping, (c) Rotational Joint Damping

Table 5.11 Identified Joint Parameters using Decoupling Equation

	k_{Fy} *[N/m]*	$k_{F\theta}$ *[N/rad]*	$k_{M\theta}$ *[N.m/rad]*	c_{Fy} *[N.s/m]*	$c_{F\theta}$ *[N.s/rad]*	$c_{M\theta}$ *[N.m.s/rad]*
M10	$2.02*10^6$	$2.47*10^4$	$2.8*10^3$	34.41	0.635	0.077
M8	$2.14*10^6$	$2.66*10^4$	$3.2*10^3$	41.2	0.845	0.119
M6	$2.27*10^6$	$3.89*10^4$	$3.7*10^3$	75.7	0.946	0.164

From the results obtained with the steel beams it can be concluded that as the bolt diameter is decreased stiffness parameters are increased. On the other hand, the identified results for the M10 and M8 bolts used with the aluminum beams (given in Table 5.12) show a different trend; as the bolt diameter is decreased the translational stiffness decreases, while the cross-coupling stiffness values increase and rotational joint stiffness values decrease slightly. There is obviously a different trend in the identification obtained from the experiments performed on aluminum and steel beams. This seems to be the effect of different material and thickness of clamped parts. However, a more detailed study is required to generalize this observation.

Table 5.12 Identified Joint Properties using Decoupling Equation

	k_{Fy} *[N/m]*	$k_{F\theta}$ *[N/rad]*	$k_{M\theta}$ *[N.m/rad]*	c_{Fy} *[N.s/m]*	$c_{F\theta}$ *[N.s/rad]*	$c_{M\theta}$ *[N.m.s/rad]*
M10	$5.73*10^5$	$5.82*10^3$	$1.29*10^3$	10.83	-0.83	0.083
M8	$5.04*10^5$	$-1.21*10^4$	$1.22*10^3$	5.04	1.2	0

In this study it is shown by using experimentally obtained results that identification algorithm using the decoupling theory and the joint updating process work very well. Several verification studies are illustrated in this chapter. For example, by using the updated joint parameters, the FRFs of the coupled structure are obtained at a point which is not used in the identification of joint properties, and these receptances perfectly were found to be perfectly matching with the measured FRFs. Moreover, the identified joint parameters are used in the coupling of a new structure and it is seen that the receptances of the new assembly obtained by using the updated joint parameters perfectly match with the measured ones. Lastly, using the identified joint properties in a different configuration of connection and comparing the regenerated

receptances of the coupled system with the measured ones, it is again seen that a perfect match is obtained. Therefore it can be concluded that, once the joint properties are identified, they can be used to in a different assembly even with a different connection type, as long as the clamped parts remain in the same thickness and beams are made of same material with the same cross sectional dimensions.

CHAPTER 6

CONCLUSION AND FUTURE WORK

6.1 CONCLUSION

In this study an experimental identification method is suggested to obtain equivalent dynamic characteristics of bolted joints. In this approach the frequency response functions (FRFs) of substructures and the coupled structure are measured and decoupling method is used to identify equivalent dynamic parameters of joints consisting of stiffness and damping elements. In order study the accuracy of three different joint models presented (models including only translational joint parameters, both translational and rotational parameters, and translational, rotational and cross-coupling joint elements) the dynamic responses of the coupled structure are calculated by using these models, and are studied for accuracy. These joint models represent the connections for transverse vibrations of the beam, and the identification is made by using the experimental studies performed by exciting the coupled structure in transverse direction and by using 2D beam elements including two dofs at each node. Note that, for vibrations in perpendicular direction to joint axis, this joint model should be extended by identifying stiffness and damping terms in other directions. It should be kept in mind that, exciting the structure in perpendicular directions to joint axis may reveal nonlinear behavior of joints. In the ANSYS simulations performed on two beams coupled elastically, it is seen that using only one translational joint does not fully simulate the real case because it lacks of coupling the RDOFs at the connection interface of the beams. Then, it is concluded that rotational joint parameters are very important for beam type structures in order to model the coupled structure behavior in a correct fashion. Hence, a bolted joint is

modeled with translational, rotational and cross-coupling stiffness and damping terms. Since rotational degrees of freedom (RDOF) in connection dynamics plays a significant role, RDOF related FRFs are needed in the identification process. In addition, measuring all the elements of an FRF matrix experimentally is very time consuming and expensive. Hence, FRF synthesis and finite-difference formulations are utilized for the estimation of unmeasured FRFs and RDOF related FRFs, respectively.

In the proposed method four decoupling equations are derived, each giving the equivalent dynamic parameters of a joint. If FRF matrices of the substructures and that of the coupled structure at any frequency are available and accurate, then joint identification can be achieved by using any of the decoupling equations. Theoretically speaking, it does not make any difference which one of the equations are used in the extraction of the joint properties. However, it is observed in the case studies that due to the inaccuracies in the identification of rotational and cross-coupling elements, the performance of each equation is different and the most accurate results are obtained when equation (3.18) is used. Although the most accurate results are obtained with equation (3.18), when this equation is used it is not possible to obtain cross-coupling FRFs including RDOF information between joint and non-joint coordinates. Hence, from the experimental applicability point of view, among the decoupling equations the most practical one is found to be equation (3.21). Furthermore, in order to make the identification more practical for real experiments, rather than using RDOF related FRFs of the coupled structure, only TDOF related ones are measured and used in the identification equation. Hence, in the identification process, the need for the estimation of RDOF related FRFs belonging to the coupled structure is eliminated while keeping joint model (consisting of translational, rotational and cross-coupling elements) unchanged. This approach is observed to increase the accuracy of the identification. Furthermore, it is seen that the accuracy of the identification results increase as the number of measurement points in the non-joint region is increased.

The method proposed is first verified with various simulation studies and very accurate identification is obtained. It is seen from the simulation studies that the error in the identified results of the rotational joint properties is high when compared to that of translational joint properties. Although rotational joint properties are important for the physical completeness of the coupled model, it is concluded that having large errors in the identified values of rotational joint stiffness values does not deteriorate the mathematical model for the joint as long as translational stiffness of the joint is accurately identified. Furthermore, it is observed that joint damping is prone to noise much more than joint stiffness.

In simulation studies simulated experimental values are used, and it is observed that the identification results are prone to high errors due to the matrix inversions included in the identification equations and the noise in measurement results. For that purpose an error analysis is presented. The effect of noise on the identification results is examined by using different noise contamination techniques in the simulation of measured FRFs. It is observed that noise has less effect in the frequency regions which are sensitive to joint parameters. In order to reduce the effect of noise, it is proposed to determine the joint properties by taking the average of the values identified at several frequencies in the frequency regions sensitive to joint parameters. Furthermore, it is important to avoid the substructure natural frequencies while selecting frequency range for the identification. Yet, it is observed in practical applications that experimental errors combine with the measurement noise, and thus the identified values may still not be very accurate. In order to overcome this problem, an update algorithm is proposed. In this approach, the identified dynamic parameters are used as initial estimates and then optimum dynamic parameters representing the joint are obtained by using an optimization algorithm. It is shown with real experimental studies that the proposed method is very successful in identifying bolted joint parameters. The accuracy of the identification results is illustrated by using the same bolt in a new structure, and showing that the calculated FRFs of the structure in which identified joint parameters are used, match perfectly with the experimentally measured ones.

Then, several experimental studies were performed to illustrate the real life application of the suggested method, and to study the change in equivalent dynamic properties of a joint with changing bolt size, bolt quality and bolt torque. Aluminum beams including M10x16 and M8x16 bolts and steel beams including M10x35, M8x35 and M6x30 bolts were used in these experimental studies, and equivalent dynamic properties of bolted connections are successfully determined for various combinations.

In experimental studies, maybe the most interesting one was the use of identified joint parameters for a bolted joint in the coupling of a new structure, and observing that the calculated receptance of the new assembly obtained by using the identified joint parameters perfectly match with the measured receptance. Similarly, using identified joint properties in a different configuration of connection and comparing the calculated receptances of the coupled system with the measured ones showed again a perfect agreement. Thus it is concluded that, once the joint properties are identified, it can be used in a different assembly even with using more joints in the connection, as long as the clamped parts remain in the same thickness and width, and they are made of the same material.

The effect of different size and quality of bolts, as well as the bolt torque on the joint properties are also studied by making a series of experiments and identifying the joint parameters for each case. It is observed from the results obtained with steel beams that as the bolt diameter is decreased stiffness parameters are slightly increased, while the identified results for the M10 and M8 bolts used with the aluminum beams show a different trend: as the bolt diameter is decreased the translational stiffness decreases, while the cross-coupling stiffness values increase and rotational joint stiffness values decrease slightly. From these experimental studies it can be concluded that changing the size of bolt from M10 to M8 has a very slight effect on the equivalent dynamic properties, and the trend is not predictable. Secondly, experiments were performed by using M8 bolt with different levels of bolt tightening torques, it is seen that as the tightening torque is increased cross-coupling

and rotational joint stiffnesses increase, while translational joint stiffness remains nearly the same. Under the same preload level, translational stiffness of the A2 70 type M6 bolt is smaller than those of A4 80's and rotational stiffness of the A2 70 type bolt is higher than those of A4 80's. However, all these changes are not considerable.

Finally, it can be said that the joint identification method developed in this thesis can successfully and efficiently be used to obtain accurate and reliable dynamic models for bolted joints, and to make predictions for the dynamics of assembled structures with bolted connections.

6.2 RECOMMENDATIONS FOR FUTURE WORK

As a further work, the method developed here can be used for complex structures and the method proposed can be validated for a complex system. After identifying joint properties by using a simple set-up including the same type of connection (material, bolt size, bolt quality, etc.), the identified joint parameters can be used to model a complex system in FE software. Then, the predicted response of the system can be compared with the response of the system obtained experimentally.

On the other hand, this study can be extended for 3D joint model to simulate the vibration of the structure in directions perpendicular to joint axis. Since exciting the structure in perpendicular directions to joint axis may reveal nonlinear behavior, first a linearity check is to be performed.

It may also be recommended to study the differences in the joint properties further with a wider range of different sizes and qualities of bolts by using different clamped parts under different levels of torque.

REFERENCES

Ahmadian, H., and Jalali, H., (2007a), "Identification of Bolted Lap Joint Parameters in Assembled Structures", Mechanical Systems and Signal Processing, 21, 1041-1050.

Ahmadian, H., and Jalali, H., (2007b), "Generic Element Formulation for Modelling Bolted Lap Joints", Mechanical Systems and Signal Processing, 21, 2318-2334.

Avitable, P., O'Callahan, J., (2003), "Frequency Response Function Expansion for Unmeasured Translation and Rotation DOFs for Impedance Modelling Applications", Mechanical Systems and Signal Processing 17(4), 723-745.

Batista, F. C., Maia, N. M. M., (2011), "Uncoupling Techniques for the Dynamic Characterization of Sub-structures", Proceedings of 29th International Modal Analysis Conference, Jacksonville, Florida, 383-392.

Beards, C. F., (1983), "The Damping of Structural Vibration by Controlled Interface Slip in Joints", American Society of Mechanical Engineers, Journal of Vibration, Acoustics, Stress analysis, Reliability and Design, 105, 369-373.

Böswald, M., and Link, M., (2005), "Identification of Non-linear Joint Parameters using Frequency Response Functions", Proceedings of 23th International Modal Analysis Conference, Orlando, Florida.

Campbell, R.L., Hambric, S.A., (2004), "Application of Frequency Domain Substructure Synthesis Technique for Plates Loaded with Complex Attachments", Technical Report, Pennsylvania State University Park Applied Research Lab.

Canudas de Wit, C., Olsson, H., Astrom and K.J., Lischinsky, P., (1995), "A New Model for Control of Systems with Friction", IEEE Transaction on Automation Control 40(3), 419-425.

Čelič, D., and Boltežar, M., (2008), "The Influence of the Dynamic Properties of Joints Using Frequency-Response Function", Journal of Sound and Vibration, 317, 158-174.

Čelič, D., and Boltežar, M., (2009), "The Influence of the Coordinate Reduction on the Identification of the Joint Dynamic Properties", Mechanical Systems and Signal Processing, 23, 1260-1271.

Chesson, E. Jr., Munse, W.H., (1964), "Studies of the Behavior of High-Strength Bolts and Bolted Joints", University of Illinois, Experimental Station, Bulletin 469.

De Klerk, D., Rixen, D. J., Voormeeren, S. N., (2008), "General Framework for Dynamic Substructuring: History, Review, and Classification of Techniques", AIAA Journal, 46(5), 1169-1181.

Duarte, M. L. M, (1996), "Experimentally-Derived Structural Models for Use in Further Dynamic Analysis", PhD Thesis, Department of Mechanical Engineering, Imperial College of Science, Technology and Medicine, University of London.

Duarte, M. L. M, Ewins, D. J., (2000), "Rotational Degrees of Freedom for Structural Coupling Analysis Via Finite-Difference Technique with Residual Compensation", Mechanical Systems and Signal Processing 14(2), 205-227.

Gaul, L., Lenz, J., (1997), "Nonlinear Dynamics of Structures Assembled by Bolted Joints", Acta Mechanica, 125, 169-181.

Gaul, L., Nitsche, R., (2000), “Friction control for vibration suppression”, Mechanical Systems and Signal Processing 14(2), 139-150.

Gaul, L., Nitsche, R., (2001), “The Role of Friction in Mechanical Joints”, American Society of Mechanical Engineers, Applied Mechanics Reviews, 54, 93-106.

Groper, M., (1985), “Microslip and Macroslip in Bolted Joints”, Experimental Mechanics, 25, 172-174.

Groper, M., Hemmye, J., (1983), “Partial Slip Damping in High Strength Friction Grip Bolted Joints”, Proceedings of the Fourth International Conference of Mathematical Modeling, Pergamon Press, New York.

Groper, M., Hemmye, J., (1983), “The Dissipation of Energy in High Strength Friction Grip Bolted Joints”, Proceedings of SESA Spring Conference, Cleveland, OH.

Hu, F., Wu, B., Hu, Y., Shi, T., (2009), “Identification of Dynamic Stiffness Matrix of Bearing Joint Region”, Frontiers of Mechanical Engineering in China, 4(3), 289-299.

Hwang, H.Y., (1998), “Identification Techniques of Structure Connection Parameters Using Frequency Response Function”, Journal of Sound and Vibration, 212(3), 469-79.

Ibrahim, R. A., Pettit, C. L., (2005), “Uncertainties and Dynamic Problems of Bolted Joints and Other Fasteners”, Journal of Sound and Vibration, 279, 857-936.

Jalali, H., Ahmadian, H., and Mottershead, J.E., (2007), “Identification of Bolted Lap-Joint Parameters by Force-State Mapping”, International Journal of Solids and Structures, 44, 8087-8105.

Kamal, M. and Wolf, J., (1982), “Modern Automotive Structure Analysis”, Van Norstrand Reinhold Company, 116-194.

Kashani, H., and Nobari, A.S., (2010), “Identification of Dynamic Characteristics of Nonlinear joint Based on the Optimum Equivalent Linear Frequency Response Function”, Journal of Sound and Vibration, 329, 1460–1479.

Kim, T.R., Wu, S.M., and Eman, K.F., (1989), “Identification of Joint Parameters for a Taper Joint”, Transactions of the American Society of Mechanical Engineers, 111, 282-287.

Lee, D.H., and Hwang, W.S., (2007), “An Identification Method for Structural Parameters Using an FRF-based Substructuring Method and an Optimization Technique”, Journal of Mechanical Science and Technology, 21, 2011-2022.

Lenz, J., Gaul, L., (1995), “The Influence of Microslip on the Dynamic Behavior of Bolted Joints”, Proceedings of 13th International Modal Analysis Conference, 248-254, Nashville, Tennesse.

Liu, W., (2000), “Structural Dynamic Analysis and Testing of Coupled Structures”, PhD Thesis, Department of Mechanical Engineering, Imperial College of Science, Technology and Medicine, University of London.

Liu, W., and Ewins, D.J., (2002), “Substructure Synthesis via Elastic Media”, Journal of Sound and Vibration, 257(2), 361-379.

LMS Int., (2000), “LMS Theory and Background”, Technical Report, LMS International Leuven, Belgium.

Magnevall, M., Josefsson, A., and Ahlin, K., (2007), "Parameter Estimation of Hysteresis Elements Using Harmonic Input", Proceedings of 25th International Modal Analysis Conference, Orlando, Florida.

Maia, N. M. M., Silva, J. M. M., Ribeiro, A. M. R., Silva, P. L. C., (1998), "On the Dynamic Characterization of Joints Using Uncoupling Techniques", Proceedings of 16th International Modal Analysis Conference, Santa Barbara, 1132-1138.

Majundar, A., Bhushan, B., (1991), "Fractal Model of Elastic-Plastic Contact between Rough Surfaces", Journal of Tribology, 113, 1 -11.

Manchu, S., (2006), "Parameter Identification for Mechanical Joints", Ms. Thesis, Department of Mechanical Engineering, Blekinge Institude of Technology, Sweden.

Mao, K., Li, B., Wu, J., Shao, X., (2010), "Stiffness Influential Factors-Based Dynamic Modeling and Its Parameter Identification Method of Fixed Joints in Machine Tools", International Journal of Machine Tools and Manufacture, 50, 156–164.

Mayer, M.H., Gaul, L., (2007), "Segment-to-Segment Contact Elements for Modelling Joint Interfaces in Finite Element Analysis", Mechanical Systems and Signal Processing, 21, 724–734.

Moon, F. C. and Li, G. X., (1990), "Experimental Study of Chaotic Vibration in a Pin-Jointed Space Truss Structure", American Institute of Aeronautics and Astronautics Journal, 28, 915-921.

Nobari, A.S., (1991), "Identification of the Dynamic Characteristics of Structural Joints", PhD Thesis, Department of Mechanical Engineering, Imperial College of Science, Technology and Medicine, University of London.

Oldfield, M.J., Ouyang, H., and Mottershead, J.E., (2005), "Simplified Models of Bolted Joints under Harmonic Loading", Computers and Structures, 84, 25-33.

Olsson, H., (1996), "Control Systems with Friction", PhD Thesis, Department of Automatic Control, Lund Institute of Technology.

Ouyang, H., Oldfield, M.J, and Mottershead, J.E., (2006), "Experimental and Theoretical Studies of a Bolted Joint Excited by a Torsional Dynamic Load", International Journal of Mechanical Sciences, 48, 1447–1455.

Özşahin, O., Ertürk, A., Özgüven, H.N., Budak, E., (2009), "A Closed-Form Approach for Identification of Dynamical Contact Parameters in Spindle- Holder-Tool Assemblies", International Journal of Machine Tools and Manufacture, 49, 25–35.

Park, S.S., Chae, J., (2008), "Joint Identification of Modular Tools Using a Novel Receptance Coupling Method", The International Journal of Advanced Manufacturing Technology, 35, 1251-1262.

Ren, Y., (1992), "The Analysis and Identification of Friction Joint Parameters in the Dynamic Response of Structures", PhD Thesis, Department of Mechanical Engineering, Imperial College of Science, Technology and Medicine, University of London.

Ren, Y., Beards, C.F., (1995a), "On Substructure Synthesis with FRF Data", Journal of Sound and Vibration, 185(5), 845-866.

Ren, Y., Beards, C.F., (1995b), "Identification of Joint Properties of a Structure Using FRF Data", Journal of Sound and Vibration, 186(4), 567-587.

Ren, Y., Beards, C.F., (1998), "Identification of 'Effective' Linear Joints Using Coupling and Joint Identification Techniques", Journal of Vibration and Acoustics, 120, 331-338.

Ren, Y., Lim, T.M., amd Lim, M.K., (1998), "Identification of Properties of Nonlinear Joints Using Dynamic Test Data", Transactions of the American Society of Mechanical Engineers, 120, 324-330.

Segalman, D.J., (2001), "An Initial Overview of Iwan Modeling for Mechanical Joints", Sandia National Laboratories, SAND2001-0811.

Segalman, D.J., Paez, T., Smallwood, D., Sumali, A., and Urbina, A., (2003), "Status and Integrated Road-Map for Joints Modeling Research", Sandia National Laboratories, SAND2003-0897.

Silva, J. M.M., Maia, N. M. M., Riberio, A. M. R., (2000), 'Cancellation of Mass-Loading Effects of Transducers and Evaluation of Unmeasured Frequency Response Functions", Journal of Sound and Vibration, 236(5), 761-779.

Silva, J. M. M., Maia, N. M. M., Ribeiro, P. M. L., (1996), "Dynamic Modeling: Application of Uncoupling Techniques", Proceedings of 14th International Modal Analysis Conference, Dearborn, Michigan, 1165-1171.

Tsai, J.S., Chou, Y.F., (1988), "The Identification of Dynamic Characteristics of a Single Bolt Joint", Journal of Sound and Vibration, 125, 487-502.

Wang, J., and Sas, P., (1990), "A method for Identifying Parameters of Mechanical Joints", Journal of Applied Mechanics, 57, 337-342.

Wang, J.H., and Chuang, S.C., (2004), "Reducing Errors in the Identification of Structural Joint Parameters Using Error Functions", Journal of Sound and Vibration, 273, 295-316.

Wang, J.H., Liou, C.M., (1991), "Experimental Identification of Mechanical Joint Parameters", Journal of Vibration and Acoustics, 113, 28–36.

Willner, K., Gaul, L., (1995), "A Penalty Approach for Contact Description by FEM Based on Interface Physics", Proceedings of Contact Mechanics II, Ferrara, Italy, 257-264.

Yang, K.T., Park, Y.S., (1993), "Joint Structural Parameter Identification Using a Subset of Frequency Response Function Measurements", Mechanical Systems and Signal Processing, 7, 509–30.

Yang, T., Fan, S.H., Lin, C.S., (2003), "Joint Stiffness Identification Using FRF Measurements", Computers and Structures, 81, 2549-2556.

Young, M. S., Tiwari, M., Singh, R., (2007), "Identification of Joint Stiffness Matrix Using a Decomposition Technique", Proceedings of 25th International Modal Analysis Conference, Orlando, Florida.

Yuan, J.X., and Wu, X.M., (1985), "Identification of the Joint Structural Parameters of Machine Tool by DDS and FEM", Transactions of the American Society of Mechanical Engineers, 107, 64-69.

APPENDIX A

PARAMETERS USED IN THE FRF SYNTHESIS

After acquiring test data, LMS modal analysis software is used for the system identification and the required parameters (the mode shapes, the damping ratio for each mode, undamped natural frequency, lower and upper residuals) for the FRF synthesis are obtained.

Aluminum Substructure A with M10x16 Bolt

```
N=2;         %number of modes in the measured frequency range
r=4;         %number of measurement points
zeita=[0.0666841,0.0110599];  %damping ratio
U1=zeros(r,N);                %mode shapes
U1(:,1)=[4.003+1i*6.543e-3;3.675+1i*9.692e-3;3.374+1i*1.214e-
2;1.429+1i*4.929e-3];
U1(:,2)=[2.792+1i*1.77e-2;1.622+1i*1.878e-2;4.94e-1+1i*2.089e-2;-
4.198+1i*1.401e-2];
wr=2*pi*[37.9059,288.3];      %undamped natural frequency
Lor=[4.034e-2;1.739e-2;1.706e-2;2.745e-2];      %lower residual
Upr=[5.195e-7;2.703e-7;9.835e-8;-5.158e-8];     %upper residual
```

Aluminum Substructure A with M8x16 Bolt

```
zeita=[0.0199,0.0040056];     %damping ratio
U1=zeros(r,N);                %mode shapes
U1(:,1)=[4.182+1i*3.796e-2;3.681+1i*4.296e-2;3.559+1i*3.134e-
2;1.506+1i*9.133e-3];
U1(:,2)=[2.978-1i*2.586e-1;1.902-1i*1.67e-1;7.779e-1-1i*7.182e-2;-
4.016+1i*3.388e-1];
wr=2*pi*[40.7402,296.884];    %undamped natural frequency
Lor=[4.034e-2;1.739e-2;1.706e-2;2.745e-2];      %lower residual
Upr=[5.195e-7;2.703e-7;9.835e-8;-5.158e-8];     %upper residual
```

Translational FRFs at the tip point of the substructure A are obtained via FRF synthesis and shown in Figure A.1.

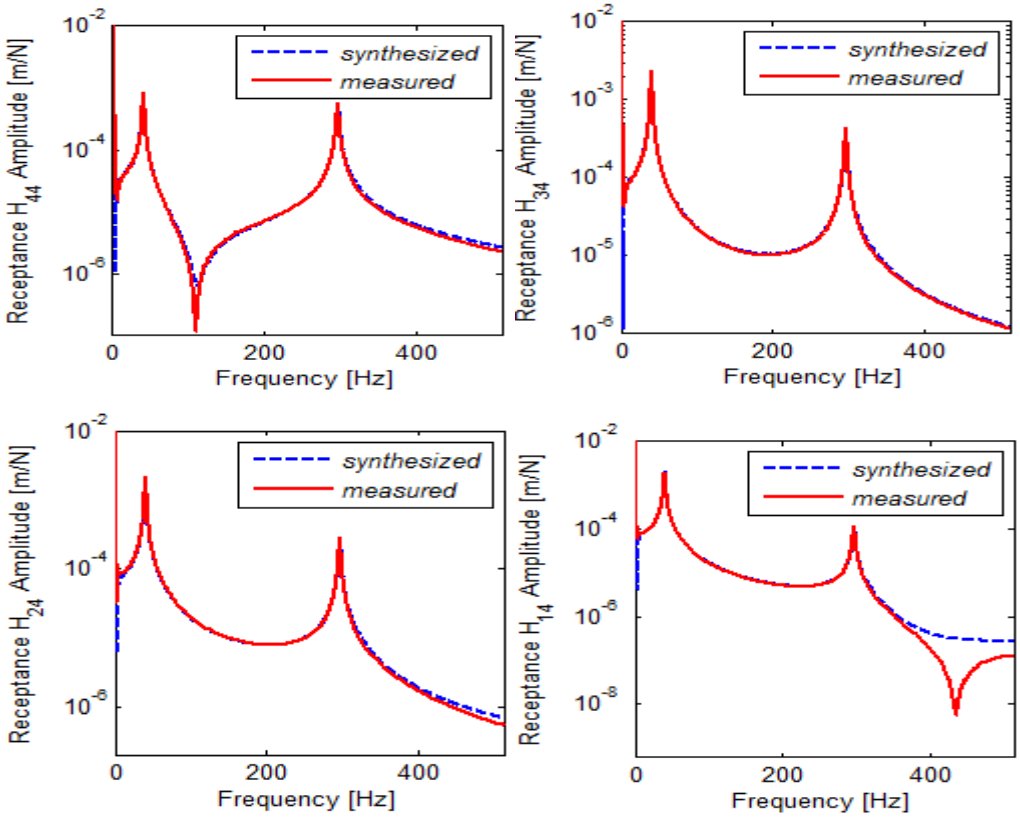

Figure A.1 FRF Synthesis for Substructure A

Steel Substructure A with M10x35 Bolt

```
N=2;        %number of modes in the measured frequency range
r=3;        %number of measurement points
zeita=[0.00240229,0.00236542];      %damping ratio
U1=zeros(r,N);                      %mode shapes
U1(:,1)=[-2.338+1i*1.050e-2;-2.532+1i*1.160e-2;-2.726+1i*1.347e-2];
U1(:,2)=[6.891e-1+1i*5.913e-3;1.268+1i*3.869e-3;1.847+1i*2.923e-3];
wr=2*pi*[75.3828,505.622];          %undamped natural frequency
Lor=[1.042e-2;4.052e-3;-1.915e-2];  %lower residual
Upr=[1.574e-8;3.297e-8;2.244e-8];   %upper residual
```

Steel Substructure A with M8x35 Bolt

```
N=2;        %number of modes in the measured frequency range
r=3;        %number of measurement points
zeita=[0.00384087,0.00254964];      %damping ratio
U1=zeros(r,N);                      %mode shapes
```

```
U1(:,1)=[2.435+1i*2.836e-3;2.630+1i*3.295e-3;2.841+1i*2.179e-3];
U1(:,2)=[8.450e-1+1i*1.516e-2;1.460+1i*1.699e-2;2.126-1i*7.023e-3];
wr=2*pi*[78.3849,514.547];          %undamped natural frequency
Lor=[1.495e-2;-4.592e-3;-1.816e-1]; %lower residual
Upr=[7.057e-9;5.404e-8;4.965e-7];   %upper residual
```

Translational FRFs at the tip point of the substructure A are obtained via FRF synthesis and shown in Figure A.2. After obtaining the translational FRFs at the tip point, using the second order finite difference formula rotational FRFs are estimated at the joint dof (point 2) as shown in Figure A.3.

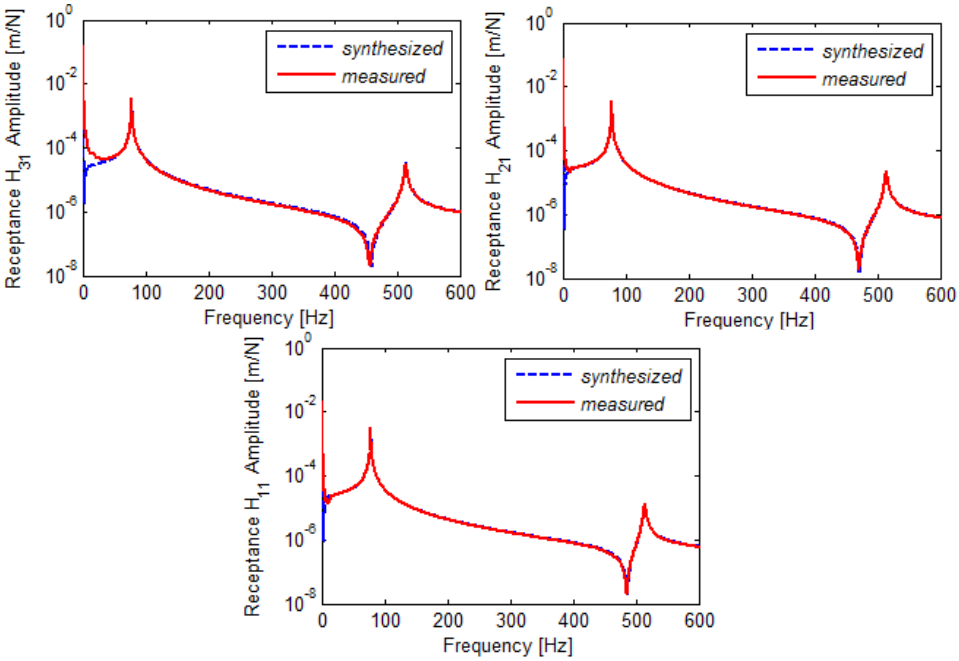

Figure A.2 FRF Synthesis for Substructure A

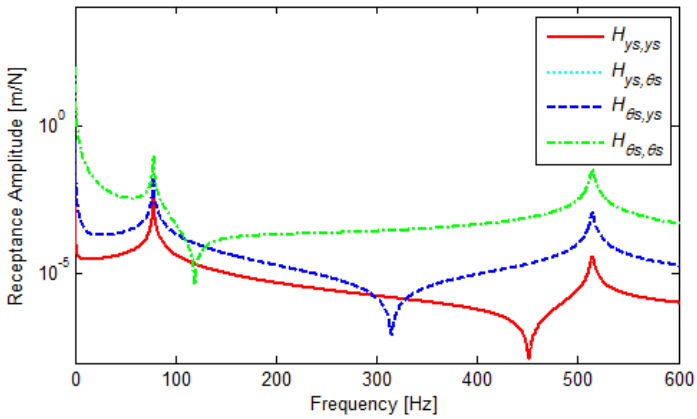

Figure A.3 Rotational FRF Estimation for Substructure A

Long Substructure A with M8x35 Bolt

```
N=2;          %number of modes in the measured frequency range
r=3;          %number of measurement points
zeita=[0.00372436,0.00217269];      %damping ratio
U1=zeros(r,N);                      %mode shapes
U1(:,1)=[-2.378+1i*2.982e-4;-2.544+1i*7.896e-4;-2.705+1i*-3.751e-4];
U1(:,2)=[1.059+1i*1.848e-3;1.576+1i*4.31e-4;2.094-1i*1.024e-3];
wr=2*pi*[57.8667,375.596];          %undamped natural frequency
Lor=[1.199e-2;6.792e-3;-3.752e-3];  %lower residual
Upr=[1.542e-8;2.640e-8;3.351e-8];   %upper residual
```

Translational FRFs at the tip point of the substructure A are obtained via FRF synthesis and shown in Figure A.4. After obtaining the translational FRFs at the tip point, using the second order finite difference formula rotational FRFs are estimated at the joint dof (point 2) as shown in Figure A.5.

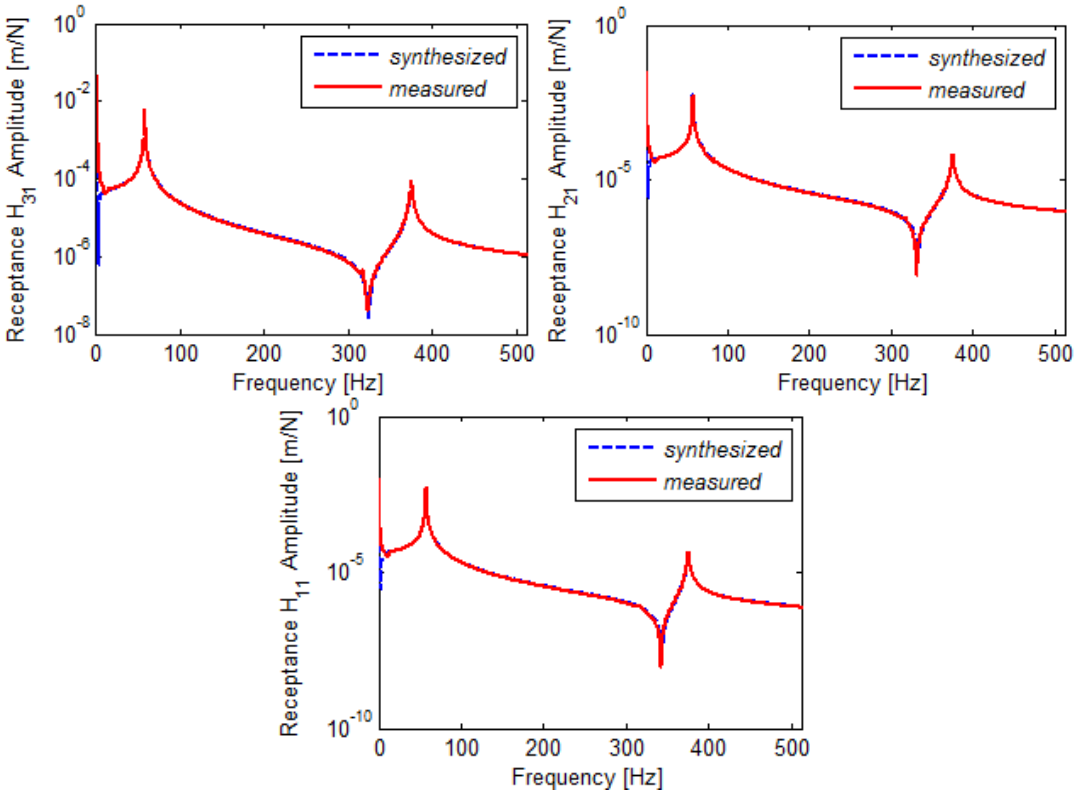

Figure A.4 FRF Synthesis for Long Substructure A

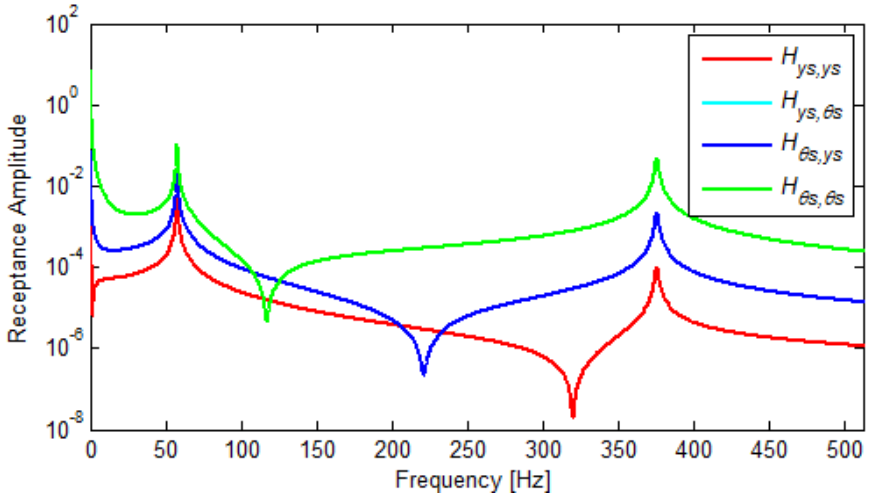

Figure A.5 Rotational FRF Estimation for Substructure A

Substructure A with M6x30 Bolt

```
N=2; %number of modes in the measured frequency range
r=3; %number of measurement points
zeita=[0.00943905,0.00387376];      %damping ratio
U1=zeros(r,N);                      %mode shapes
U1(:,1)=[2.538+1i*1.88e-2;2.758+1i*2.137e-2;2.986+1i*2.772e-2];
U1(:,2)=[9.511e-1+1i*2.225e-2;1.655+1i*2.523e-2;2.398+1i*2.467e-2];
wr=2*pi*[81.1501,523.65];           %undamped natural frequency
Lor=[4.591e-2;-2.236e-2;-2.383e-1]; %lower residual
Upr=[-1.088e-10;-1.869e-8;1.299e-8];%upper residual
```

Translational FRFs at the tip point of the substructure A are obtained via FRF synthesis and shown in Figure A.6. After obtaining the translational FRFs at the tip point, using the second order finite difference formula rotational FRFs are estimated at the joint dof (point 2) as shown in Figure A.7.

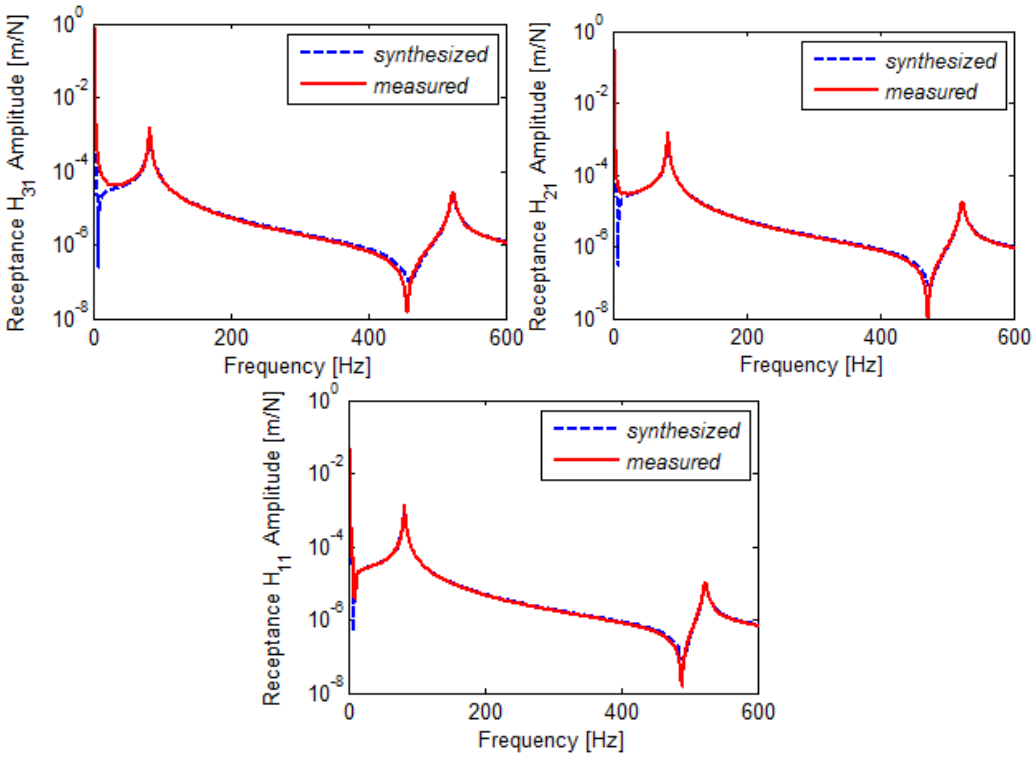

Figure A.6 FRF Synthesis for Substructure A

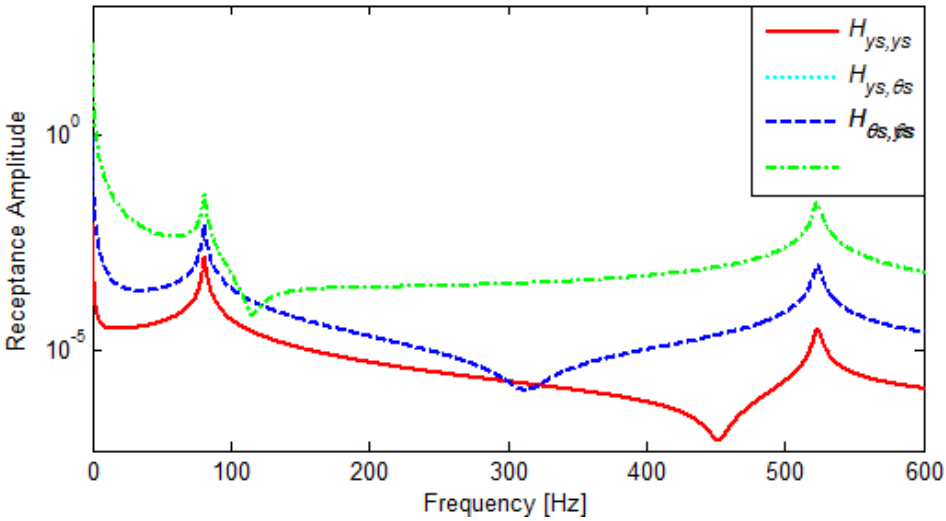

Figure A.7 Rotational FRF Estimation for Substructure A

APPENDIX B

PARAMETERS USED IN THE FE MODEL OF SUBSTRUCTURE B

The FRFs of the substructure B, which has free-free boundary conditions, are obtained theoretically by tuning the modal and structural parameters of the beam with the measured ones.

Steel Substructure B with M8x35 Bolt

```
L=0.335;                        %length of the beam [m]
b=0.015;                        %width of the beam [m]
c=0.010;                        %height of the beam [m]
gg=7604;                        %density [kg/m^3]
E=1.9225*10^11;                 %elastic modulus [Pa]
zeita=[0;0;0.0006;0.0007];      %damping ratio
```

Measured and theoretical receptances of the substructure are given in Figure B.1.

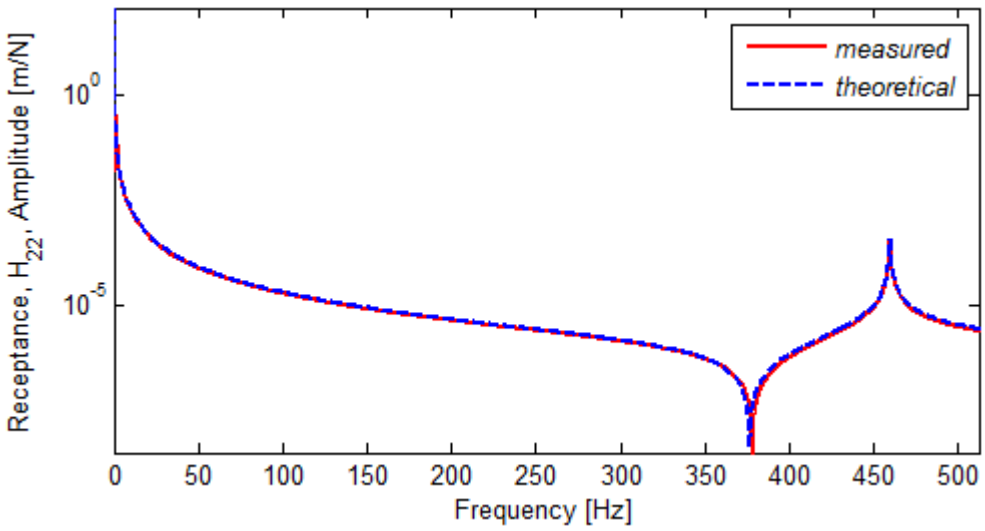

Figure B.1 Tuning of the Substructure B FRF

Steel Substructure B with M6x30 Bolt

```
L=0.340;                        %length of the beam [m]
b=0.015;                        %width of the beam [m]
c=0.010;                        %height of the beam [m]
gg=7604;                        %density [kg/m^3]
E=1.885*10^11;                  %elastic modulus [Pa]
zeita=[0;0;0.00205;0.00165];    %damping ratio
```

Measured and theoretical receptances of the substructure are given in Figure B.2.

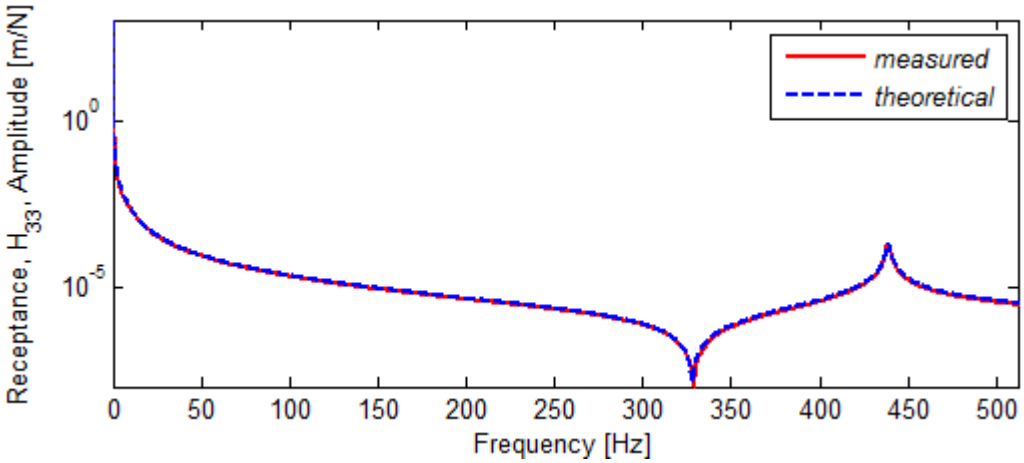

Figure B.2 Tuning of the Substructure B FRF

APPENDIX C

SENSITIVITY ANALYSIS

The sensitivity analysis performed on the steel structure connected with M10x35 bolt is shown in Figure C.1, Figure C.2 and Figure C.3.

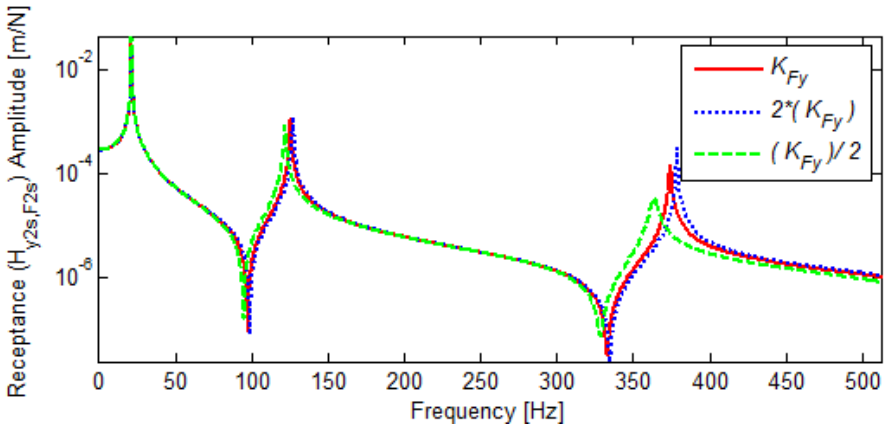

Figure C.1 Sensitivity of the Receptance of the Coupled Structure to Translational Joint Stiffness

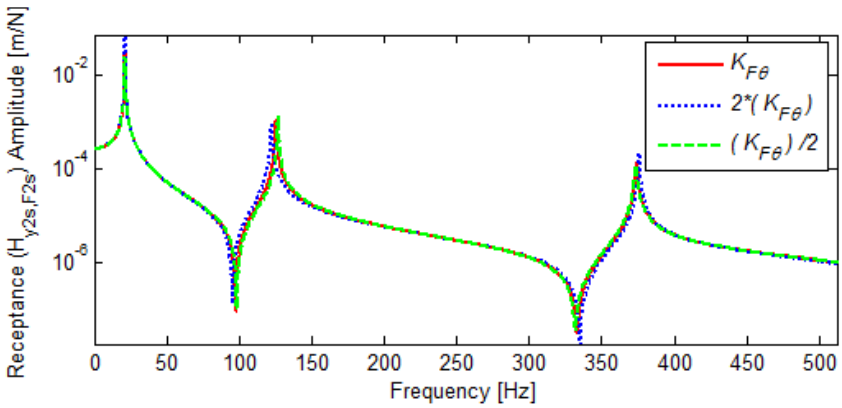

Figure C.2 Sensitivity of the Receptance of the Coupled Structure to Cross-coupling Joint Stiffness

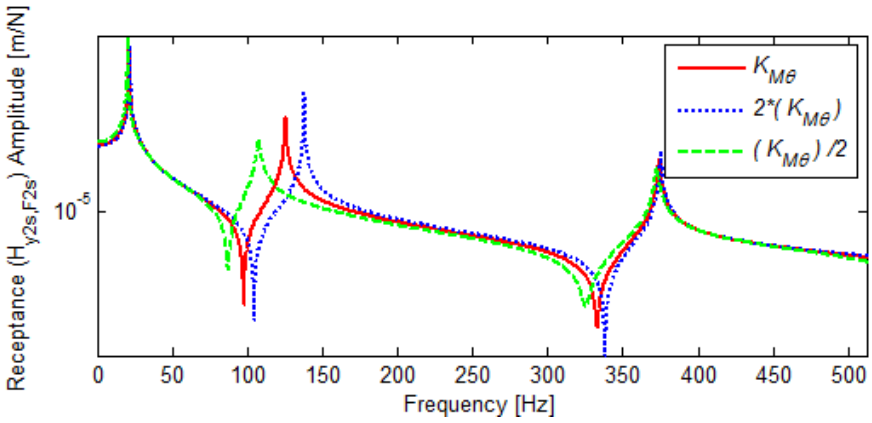

Figure C.3 Sensitivity of the Receptance of the Coupled Structure to Rotational Joint Stiffness

APPENDIX D

Dynamic Characterization of Structural Joints Using FRF Decoupling †

Şerife Tol [1,2], H. Nevzat Özgüven [1]
[1] Department of Mechanical Engineering, Middle East Technical University, Ankara 06800, Turkey
[2] Defense Systems Technologies Division, ASELSAN Inc., Ankara 06172, Turkey

ABSTRACT

Dynamic characteristics of structural systems, in many cases, highly depend on joint properties. In order to predict the dynamic characteristics of assembled structures accurately, joint models are required. Due to the complexity of joints, it is extremely difficult to describe dynamic behavior of joints with analytical models. Reliable models are generally obtained using experimental measurements. In this study, substructure decoupling based on measured and calculated FRFs is used to model a structural joint. In the method proposed the FRFs of two substructures connected with a joint are measured, while the FRFs of the substructures are obtained analytically or experimentally. The joint properties are then calculated in terms of stiffness and damping values by using FRF based substructure decoupling. The method is verified with case studies using simulated experimental data. The limitations of the method in its application to engineering systems are discussed.

1 INTRODUCTION

Most of the mechanical systems are assembled with the use of connection elements, such as bolts and rivets. For individual structures, modeling and response prediction methods have been well developed for decades. However, the prediction of dynamic characteristics of assembled systems is restricted by the capabilities to properly describe joints. Joints add damping and stiffness to the structural system; hence, changing the overall dynamic characteristics of the system. Reliable dynamic models for structural systems are based on the accurate identification of joint parameters.

Due to the complexity of joints, it is extremely difficult to describe dynamic behavior of joints with analytical models. Reliable models are usually obtained by using experimental measurements. Experimental methods can be classified as modal based methods and frequency response function (FRF) based methods. In the former class of methods, modal parameters obtained from modal testing are utilized in the identification of joint properties. However, for structures including closely spaced modes or large modal damping, accurate modal parameters are not easily obtained. Moreover, due to the nature of the modal parameter extraction process, results inevitably contain errors to some degree. In order to overcome this shortcoming, FRF based methods have been proposed in the literature.

The basic strategy in most of the FRF based joint identification methods is to use FRFs of individual substructures without joints and those of the assembled system (which is the structure with joints) to obtain information about the joint properties [1]. Tsai and Chou utilized the substructure FRF synthesis method in the formulation of the joint parameter identification [2]. Wang and Liou [3] improved the work of Tsai and Chou [2]. They avoided inversion of matrices in their algorithm; hence, tried to reduce noise effect in the identification. Hwang [4] used the same formulation and improved the results using an averaging process to exclude highly sensitive regions. Yang and Park proposed a method using subset FRF measurements for the identification of joint parameters [5]. They developed an algorithm to estimate unmeasured FRFs from the measured FRFs. Hence, they eliminated the necessity for joint related and rotational FRF measurements. Ren and Beards developed a generalized coupling method taking into account the physical restrictions of the real structures, and identified joint parameters with this new method [6, 7]. However, they avoided stiff joints in order to avoid ill-conditioned matrices, and used weighting techniques for better accuracy [1]. Celic and Boltezar [8] improved the method developed by Ren and Beards [1, 6, 7] by including the effects of rotational degrees of freedom (RDOFs). Another approach similar to the one presented in [7] is proposed by Batista and Maia [9, 10]. They reformulated the impedance uncoupling technique, and identified joints

† *Published in the Proceedings of the 30th International Modal Analysis Conference, Jacksonville, Florida, 2012.*

without using joint related FRFs. However, this method has not been validated with an experimental study. Yang et al. [11] derived identification equations employing substructural synthesis. They modeled a joint in terms of translational and rotational stiffness values and used singular value decomposition to avoid noise effect. However, joint damping was not included in their work. Later, Hu et al. [12] used this study in order to identify the dynamic stiffness matrix of bearing joint region.

In this study, substructure decoupling based on measured and calculated FRFs is used to model a structural joint. The same approach was successfully used to identify dynamic contact parameters between spindle and holder, and between holder and tool in machine tools [13]. The joints are identified in terms of rotational and translational stiffness and damping elements. An advantage of the proposed method is that the joint related FRFs are not used in the identification equations. The method is verified with simulated test cases.

2 THEORETICAL FORMULATION

2.1 Identification of Dynamic Properties of Joints Using FRF Decoupling

Frequency response function coupling is one of the most widely used methods in the literature in order to couple two structures elastically. Consider substructures A, B and their assembly (structure C) obtained by coupling them with a flexible element as shown in Fig.1.

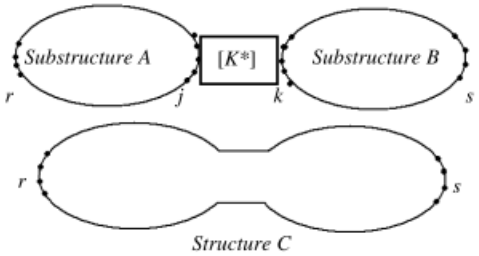

Fig.1 Elastic coupling of two substructures

The coordinates j and k represent joint degrees of freedoms (DOFs), while r and s are the ones that belong to the selected points of substructures A and B, respectively, excluding joint DOFs. Let us partition the receptance matrices of substructures A and B and of the coupled structure C as follows:

$$[H_A(\omega)]=\begin{bmatrix}[H_{rr}(\omega)] & [H_{rj}(\omega)]\\ [H_{jr}(\omega)] & [H_{jj}(\omega)]\end{bmatrix} \quad [H_B(\omega)]=\begin{bmatrix}[H_{kk}(\omega)] & [H_{ks}(\omega)]\\ [H_{sk}(\omega)] & [H_{ss}(\omega)]\end{bmatrix}$$
$$[H_C(\omega)]=\begin{bmatrix}[H^C_{kk}(\omega)] & [H^C_{ks}(\omega)]\\ [H^C_{sk}(\omega)] & [H^C_{ss}(\omega)]\end{bmatrix} \tag{1}$$

Assuming no external forces and moments are acting on joints, the equations representing equilibrium of the forces and compatibility of displacements at connection DOFs can be written as:

$$\{f_j\}+\{f_k\}=0 \tag{2}$$
$$[K^*]\{\{x_j\}-\{x_k\}\}=\{f_k\} \tag{3}$$

where $[K^*]$ is complex stiffness matrix representing the joint dynamics and consists of the stiffness and damping elements that are to be identified.

Using equations (1), (2) and (3), receptance matrices of the assembly can be written as follows (the frequency dependency of the formulation is not included for simplification):

$$\left[H_{rr}^{C}\right]=\left[H_{rr}\right]-\left[H_{rj}\right].\left[\left[H_{jj}\right]+\left[H_{kk}\right]+\left[K^{*}\right]^{-1}\right]^{-1}.\left[H_{jr}\right] \tag{4a}$$

$$\left[H_{rs}^{C}\right]=\left[H_{rj}\right].\left[\left[H_{jj}\right]+\left[H_{kk}\right]+\left[K^{*}\right]^{-1}\right]^{-1}.\left[H_{ks}\right] \tag{4b}$$

$$\left[H_{sr}^{C}\right]=\left[H_{sk}\right].\left[\left[H_{jj}\right]+\left[H_{kk}\right]+\left[K^{*}\right]^{-1}\right]^{-1}.\left[H_{jr}\right] \tag{4c}$$

$$\left[H_{ss}^{C}\right]=\left[H_{ss}\right]-\left[H_{sk}\right].\left[\left[H_{jj}\right]+\left[H_{kk}\right]+\left[K^{*}\right]^{-1}\right]^{-1}.\left[H_{ks}\right] \tag{4d}$$

By using the above equations, it is possible to decouple and thus calculate the complex stiffness matrix representing joint stiffness and damping as shown below:

$$\left[K^{*}\right]=\left[\left[H_{jr}\right].\left[\left[H_{rr}\right]-\left[H_{rr}^{C}\right]\right]^{-1}.\left[H_{rj}\right]-\left[H_{jj}\right]-\left[H_{kk}\right]\right]^{-1} \tag{5a}$$

$$\left[K^{*}\right]=\left[\left[H_{ks}\right].\left[H_{rs}^{C}\right]^{-1}.\left[H_{rj}\right]-\left[H_{jj}\right]-\left[H_{kk}\right]\right]^{-1} \tag{5b}$$

$$\left[K^{*}\right]=\left[\left[H_{jr}\right].\left[H_{sr}^{C}\right]^{-1}.\left[H_{sk}\right]-\left[H_{jj}\right]-\left[H_{kk}\right]\right]^{-1} \tag{5c}$$

$$\left[K^{*}\right]=\left[\left[H_{ks}\right].\left[\left[H_{ss}\right]-\left[H_{ss}^{C}\right]\right]^{-1}.\left[H_{sk}\right]-\left[H_{jj}\right]-\left[H_{kk}\right]\right]^{-1} \tag{5d}$$

If FRF matrices of the substructures and that of the coupled structure at any frequency are available, joint identification can be achieved by using any of the above equations and, theoretically speaking, it does not make any difference which one of the equations are used in the extraction of the joint properties. However, considering the identification of rotational and cross-coupled properties, the most accurate results are obtained when equation (5a) is used as will be demonstrated later. Furthermore, again theoretically, the identification equation can be used with FRFs measured at any frequency. However, as will be discussed in the case studies, the effects of joint dynamics on system response are almost negligible at several frequencies, but very much pronounced at certain other frequencies. Therefore, it is not easy, if not impossible, to use this equation to identify system properties at several frequencies where the equation will be very sensitive to noise that is unavoidable in practical applications. Yet, if the equation is used at any frequency in a mode where joint properties affect the system response considerably, the computations will be insensitive to measurement noise. This point will be discussed further in case studies. After calculating the complex joint stiffness matrix, the stiffness and damping values representing the joint dynamics are obtained from the real and imaginary parts of the matrix elements, respectively. Note that, here we can use any number of points in either of the substructures to take FRF measurements. Thus, orders of the submatrices in equations (5a)-(5d) can be kept very small.

2.2 Estimation of FRFs for RDOF and Unmeasured Coordinates

Analytically, all elements of an FRF matrix can be calculated easily. However, in real life applications, measuring all the elements of an FRF matrix experimentally is very time consuming and expensive; besides, it may not be possible for all cases. Usually, only one column of an FRF matrix can be obtained by exciting the structure from a single point and measuring responses at all the points we are interested in. Furthermore, the measurement of FRFs related to RDOFs is very difficult and requires special equipment. Therefore, in experimental studies it is a general practice to obtain accurate and fast solutions for the estimation of unmeasured FRFs.

The RDOF related FRF estimation procedure is based on the well known technique using finite difference formulations. In this approach, the rotational information is derived from the translational measurements. Duarte and Ewins [14] reviewed the finite difference formulations to establish the best rotational data. In this study, second order central approximation suggested in reference 14 is used. In that approach three measurement points are required (points A, B and C in Fig.2).

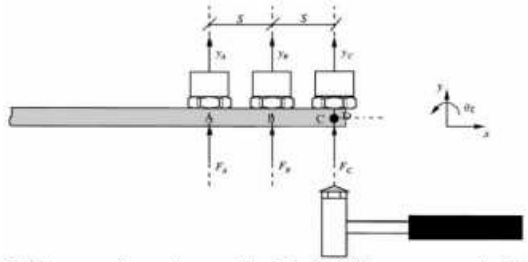

Fig.2 Close-accelerometers method for RDOF measurements [14]

Rotational FRF at point B is calculated by using the second-order-central transformation matrix

$$[T_{2c}] = \frac{1}{2s}\begin{bmatrix} 0 & 2s & 0 \\ -1 & 0 & 1 \end{bmatrix} \tag{6}$$

as follows:

$$[H_{est}] = \begin{bmatrix} H_{yy} & H_{y\theta} \\ H_{\theta y} & H_{\theta\theta} \end{bmatrix} = [T_{2c}].[H_{meas}].[T_{2c}]^T \tag{7}$$

where $[H_{est}]$ represents the estimated FRFs in y and θ directions at point B, and $[H_{meas}]$ denotes the measured translational FRFs at points A, B and C, and is defined as:

$$[H_{meas}] = \begin{bmatrix} H_{AA} & H_{AB} & H_{AC} \\ H_{BA} & H_{BB} & H_{BC} \\ H_{CA} & H_{CB} & H_{CC} \end{bmatrix} \tag{8}$$

In the method proposed we need the full receptance matrix for the DOFs we are interested in. In order to obtain complete FRF matrix the structure should be excited from all points we are interested in. However, in testing usually only one column of the FRF matrix is obtained by exciting the structure from a single point and measuring responses at all other points we are interested in. Then, the incomplete data (in any of the FRF matrices we need to use) can be obtained by using FRF synthesis [15] after extracting modal parameters by modal testing.

3 SIMULATION STUDIES

In this section two case studies are given to verify and illustrate the application of the method suggested. In the first case study a discrete system is used, whereas in the second one two beams bolted to each other is considered. In the case studies, FRFs of the substructures are calculated analytically. In order to simulate experimental FRFs for the coupled structure, the calculated values polluted with 5% noise are used. For the identification of joint parameters equation (5a) is preferred in the first case study, whereas all three equations are used in the second case study in order to compare performances of these equations (note that equations (5b) and (5c) are the same).

3.1 Case Study I: Lumped Parameter Model

In the first case study, two 2 DOF discrete systems connected with a damped elastic element is used in order to demonstrate and validate the joint identification method. Here, joint complex stiffness is modeled with a translational stiffness and a viscous damping element as illustrated in Fig.3. Properties of the substructures and joints are tabulated in Table 1.

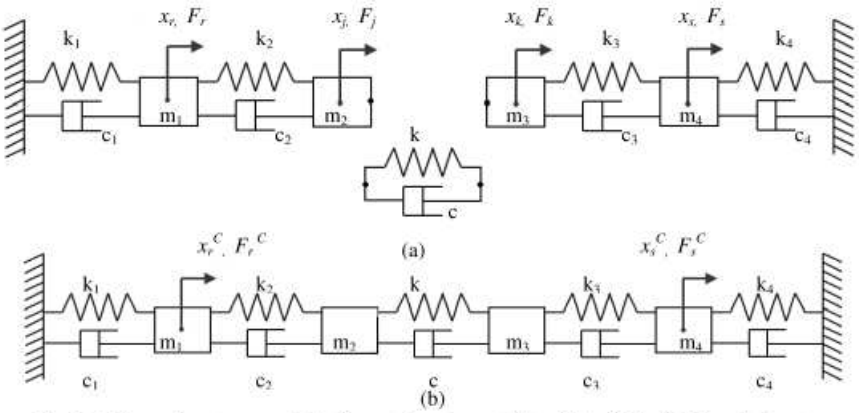

Fig.3 (a) Two subsystems and elastic coupling element $k^* = (k + j\omega c)$, **(b)** Coupled system

Table 1 Dynamic properties of the lumped coupled system

Index	Mass, m [kg]	Stiffness, k [N/m]	Damping, c [N.s/m]
1	5	2500	3
2	3	3500	4
3	4	2000	2
4	2	2500	1
joint	-	2000	3

After calculating all required FRFs for identification (FRFs of subsystems and of the coupled system), FRFs of the coupled system are polluted with 5% noise to simulate experimental measurements. The noise is generated with the "normrnd" function of MATLAB with zero mean, normal distribution and standard deviation of 5% of the maximum amplitude of the system response. As the noise becomes more effective when the response of the structure is low, it is believed that this is a more realistic way of simulating noise in FRF measurements. The receptances of the coupled system at the 1st DOF (shown in Fig.4) are used for identification.

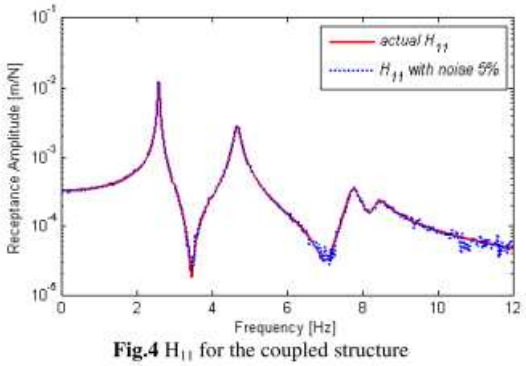

Fig.4 H_{11} for the coupled structure

The joint identification can be made by using the related equations at any frequency in the range. Theoretically it is expected to find the exact values of the stiffness and damping in each case. However, due to noise in measurements and the system response having different sensitivity to the joint properties at different frequencies, the calculated values deviate from the actual values considerably at some frequencies. The identified joint stiffness (k) and joint damping (c) values obtained by employing FRFs measured at each frequency in the range covering all four modes are given in Fig.5 and Fig.6, respectively.

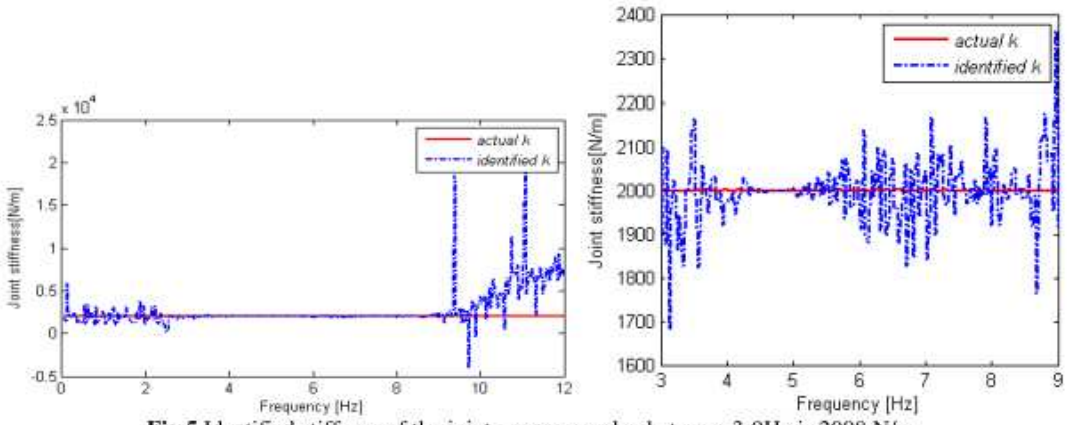

Fig.5 Identified stiffness of the joint - average value between 3-9Hz is 2008 N/m

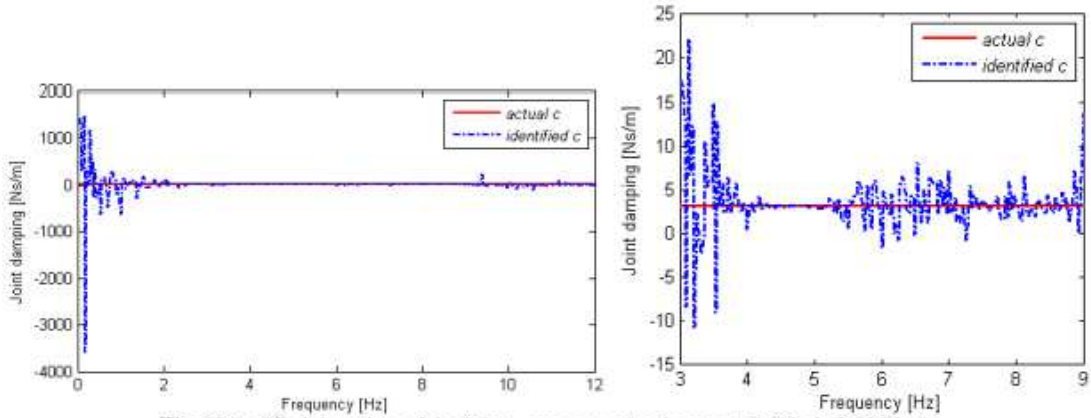

Fig.6 Identified damping of the joint - average value between 3-9Hz is 3.52 N.s/m

It is observed that exact values are calculated for joint stiffness and damping when the exact FRF values are used for the coupled system. However, when polluted FRFs are used, although very accurate values are obtained at some frequencies, the results are deteriorated and deviations from the actual values are drastic at some other frequencies. In order to demonstrate the reason for this behavior, the sensitivity of the receptance of the coupled system to the joint properties is investigated. It can be seen from Fig.7 that, the joint stiffness is effective in the second, third and fourth modes. The receptance values are not affected from the change in joint stiffness, approximately up to 2~3Hz and after 9 Hz. Hence, it does not make any sense to use the identification results calculated by using the FRFs measured in these regions. The results show that the FRF decoupling method works well in the sensitive frequency range, which is between 3-9 Hz for this case. When the average of the values identified in the frequency range of 3-9 Hz are calculated, the identification results are found to be 2008 N/m for stiffness and 3.52 N.s/m for damping (deviations from the actual values are 0.4% and 17%, respectively).

Thus it is concluded that, in the identification of the joint properties, FRFs measured at frequencies where connection stiffness has less effect on the response of the coupled system should be avoided; instead, any set of FRFs, measured at any frequency in the modes at which connection dynamics affect coupled system dynamics considerably, can be used and very accurate identification can be made as can be seen from Fig.5 and Fig.6. Since it is not known in advance at which mode the joint dynamics will affect the coupled system dynamics considerably, it is the best to identify joint properties in a range of frequency and take the average of the values in a region where deviations from a constant value is minimum.

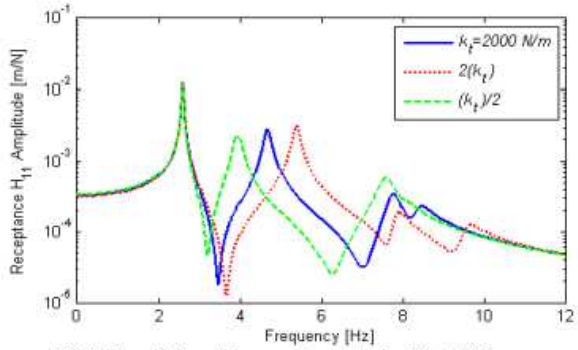

Fig.7 Sensitivity of the receptance to the joint stiffness

3.2 Case Study II: Bolted Beams

In the second case study, two identical beams; substructure A having fixed-free boundary condition and substructure B having free-free boundary condition, are coupled elastically with a joint as shown in Fig.8. Each substructure is modeled with beam elements using finite element method (FEM). Displacements at each node are modeled with one translational and one rotational DOF.

The following data are used for the beams:
Beam length: $L=0.3\ m$; modulus of elasticity: $E=2.07\ 10^{11}\ N/m^2$; moment of inertia of the cross-sectional area: $I=1.0667\ 10^{-9}\ m^3$; mass per unit length of the beams: $m=1.5094\ kg/m$; damping of the beams: structural damping with a loss factor of 0.05.

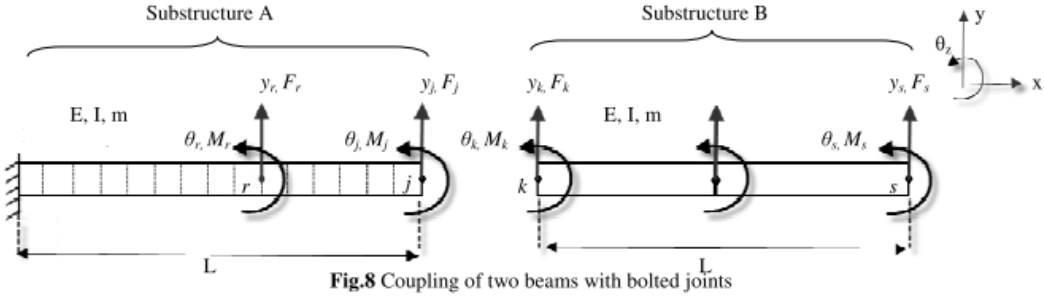

Fig.8 Coupling of two beams with bolted joints

Here, it is assumed that the bolted joint can be modeled with a complex stiffness matrix with translational and rotational stiffnesses, and translational and rotational viscous damping elements, as shown below:

$$[K^*]=\begin{bmatrix} k_{tt}+j\omega c_{tt} & k_{tr}+j\omega c_{tr} \\ k_{rt}+j\omega c_{rt} & k_{rr}+j\omega c_{rr} \end{bmatrix} \tag{9}$$

The following data are used for the joint:
Translational stiffness: $k_{tt}=10^6\ N/m$; rotational stiffness: $k_{rr}=10^3\ N.m/rad$; cross-coupled term between the translational and rotational stiffness: $k_{tr}=10^4\ N/rad$ and $k_{rt}=10^4\ N.m/m$; translational damping: $c_{tt}=25\ N.s/m$; rotational damping, $c_{rr}=5\ N.m.s/rad$; cross-coupled term between the translational and rotational damping: $c_{tr}=8\ N.s/rad$ and $c_{rt}=8\ N.m.s/m$.

Before the identification process, for simulating experimental data, the calculated FRFs of the coupled structure are contaminated with 5% noise as described in the previous case study. In order to compare the performances of four decoupling equations (equations (5a)-(5d)), the joint identification is performed using each equation by following the procedure described before, and the accuracy of the joint parameters identified from each equation are compared. The joint parameters

identified by using each equation and the percentage differences from the actual values are given in Table 2. As it can be seen from the table the best performance is obtained from equation (5a).

Table 2 Joint parameters identified by using different decoupling equations (equations (5a), (5b) and (5d))

	k_{tt} [N/m]	k_{rr} [N.m/rad]	k_{tr} [N/rad]	c_{tt}[N.s/m]	c_{rr} [N.m.s/rad]	c_{tr} [N.s/rad]
Actual values	10^6	10^3	10^4	25	5	8
Identified values (5a)	$1.01*10^6$	$1.11*10^3$	$9.03*10^3$	25.2	4.83	5.60
Error (%)	*1.3*	*11*	*-9.7*	*0.8*	-3.4	-30
Identified values (5b)	$9.91*10^5$	178	$8.60*10^3$	43.2	3.52	8.19
Error (%)	*-1*	*-82*	*-14*	72	-30	3
Identified values (5d)	$9.02*10^6$	$9.66*10^2$	$2.38*10^4$	76.3	3.36	13.5
Error (%)	*10*	*-4*	*138*	205	-32	68

It should be noted that, in the identification of joint parameters, FRFs for RDOF can be taken either from the computational model (thus, it can be assumed that in real life applications they will be directly measured), or else they can be estimated from three translational FRF values. Here, both approaches are simulated separately and thus the effect of estimating FRFs for RDOF is observed. In the latter approach, simulated experimental values for translational FRFs around node *r* are used in equation (7) in order to find FRFs related with RDOF. Identified joint stiffness and damping values are given in Fig.9 and Fig.10, respectively.

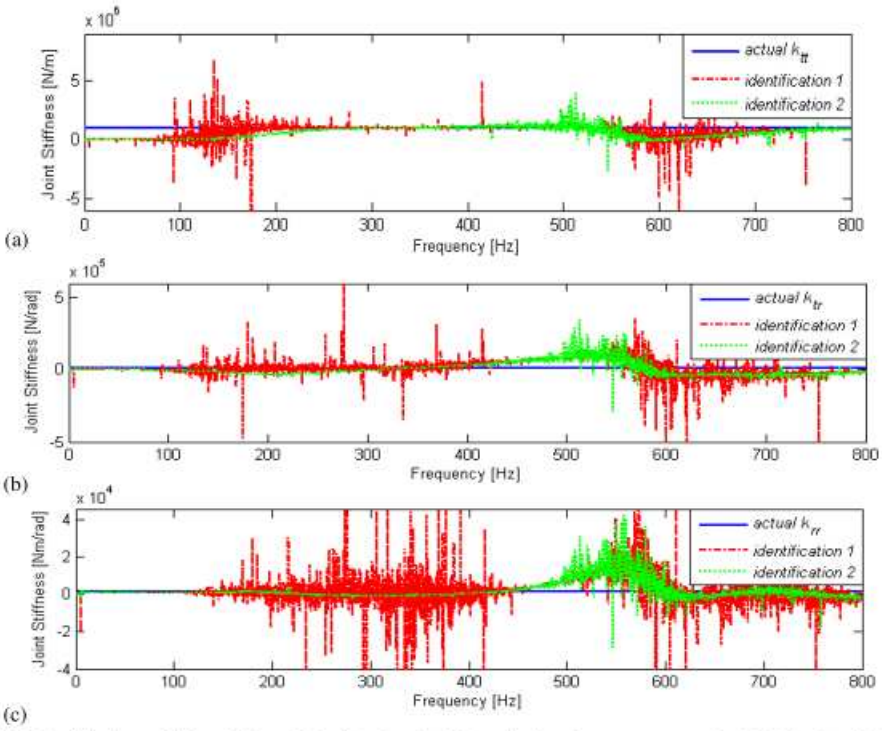

Fig.9 Identification of joint stiffness. Identification 1: Using simulated measurements for RDOF related FRFs; Identification 2: Using estimated RDOF related FRFs. (a) Translational joint stiffness k_{tt}, (b) Cross-coupled joint stiffness k_{tr}, (c) Rotational joint stiffness k_{rr}

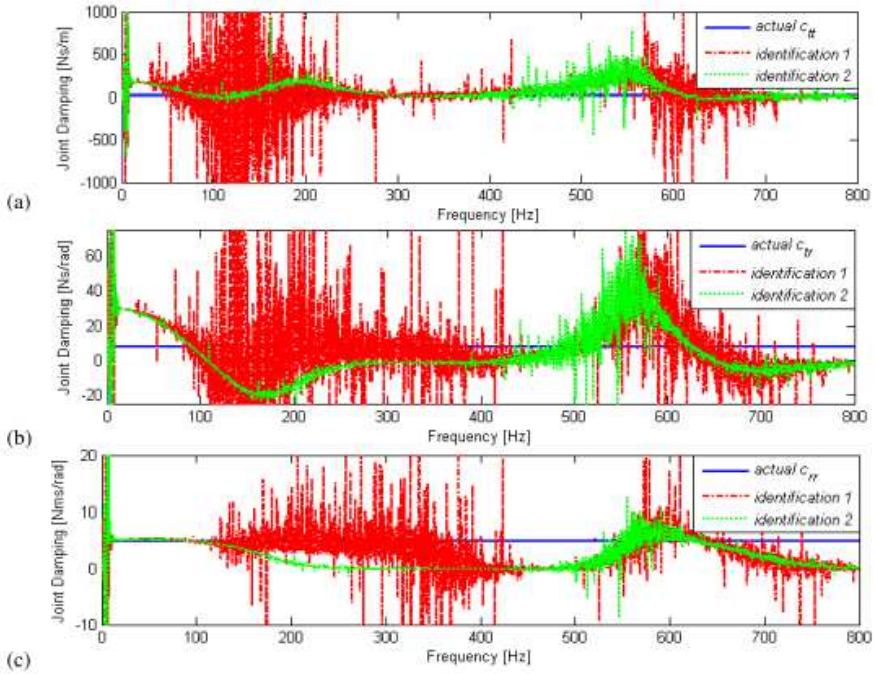

Fig.10 Identification of joint damping. Identification 1: Using simulated measurements for RDOF related FRFs; Identification 2: Using estimated RDOF related FRFs. (a) Translational joint damping k_{tt}, (b) Cross-coupled joint damping k_{tr} (c) Rotational joint damping k_{rr}

As discussed above, at frequencies where the connection parameters have less effect on the response of the coupled system, the identified values deviate from the actual values considerably. Although it is not known in advance at which mode the joint dynamics will affect the coupled system dynamics considerably, the joint properties are identified in a range of frequency and the average of the values are taken in a region where deviations from a constant value is minimum. In this case study, the following ranges are used in the identification of the joint properties: 200-400 Hz for the translational joint properties, 15-300 Hz for the rotational joint properties and 150-310 Hz for the cross-coupled joint properties. Note that, the damping properties prone to noise much more than the stiffness properties, since their effects on the coupled system dynamics is much less than those of joint stiffness values. For the damping terms, the frequency ranges used for identification of stiffness values are employed. The average values of the identification results in these ranges are given in Table 3. Note that when cross-coupled terms are identified as negative values, they are taken as zero.

Table 3 Identified joint properties and percentage errors in these values

	k_{tt} *[N/m]*	k_{rr} *[N.m/rad]*	k_{tr} *[N/rad]*	c_{tt}*[N.s/m]*	c_{rr} *[N.m.s/rad]*	c_{tr} *[N.s/rad]*
Actual values	10^6	10^3	10^4	25	5	8
Identification 1	$1.01*10^6$	$1.11*10^3$	$9.03*10^3$	25.2	4.83	5.60
Error (%)	*1.3*	*11*	*-9.7*	*0.8*	-3.4	-30
Identification 2	$9.02*10^5$	$5.30*10^2$	0	47.6	2.79	0
Error (%)	*-9.8*	*-47*	*-100*	90	-44	-100

From Table 3 it can be observed that when the simulated measurement values for RDOF related FRFs are used in the identification, the maximum error in the identified translational stiffness and damping values is 1.3%. The error in rotational and/or cross-coupled stiffness and damping values can reach to -30%. However, when the estimated RDOF related FRFs are used in the identification, the error in identified translational stiffness and damping values reaches to about -10% and 90%, respectively, whereas the error in rotational and cross-coupled values can be completely erroneous. At this stage, it may be concluded that using estimated FRFs will yield unacceptable errors. However, before reaching to such a conclusion, the effect of the errors in the identified properties of the joints on the regenerated response of the system is to be studied. It is

quite possible that major effect of the joint dynamics on system response is represented by the translational stiffness of which identified value deviates from the actual one less than -10% in the worst case, in this case study. For this purpose, firstly the sensitivity of system response to each joint parameter is investigated. Fig.11 shows the sensitivity of the receptance $H_{yr,yr}$ of the coupled structure to joint stiffness values. It is observed that, the translational joint stiffness is very effective at the third and fourth modes and rotational joint stiffness has some effect at the second mode, while the cross-coupled joint stiffness has negligible effect on the receptance of the coupled system. Hence, it can be concluded that having large errors in the identified values of rotational and especially cross-coupled joint stiffness values will not deteriorate the mathematical model for the joint, as long as translational stiffness of the joint is accurately identified.

Secondly, by using the two sets of identified joint parameters, FRFs of the assembled system are regenerated and they are compared with the actual FRFs in Fig.12.

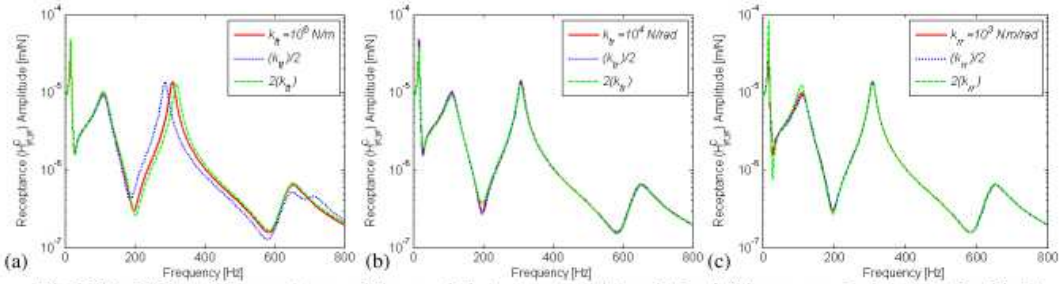

Fig.11 Sensitivity of the receptances of the coupled structure to: (a) translational, (b) cross-coupled, (c) rotational joint stiffness

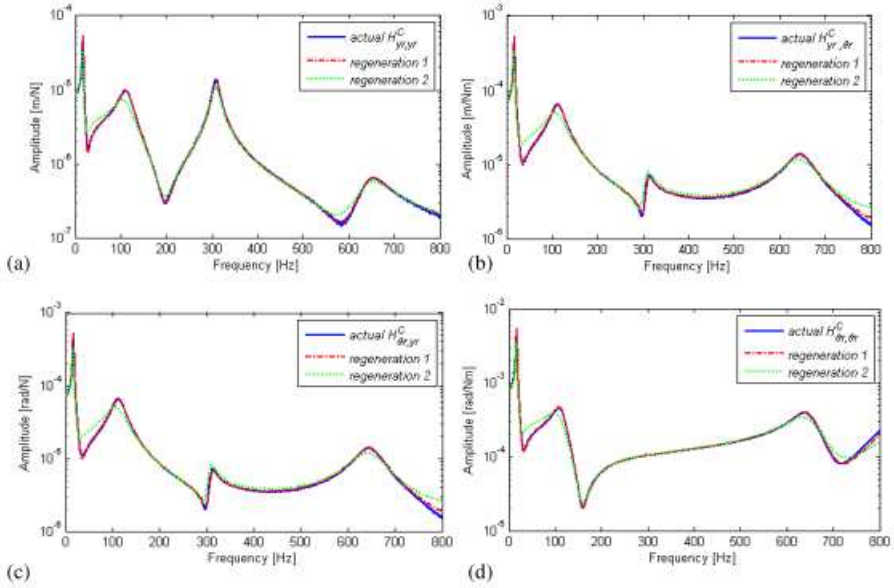

Fig.12 Regenerated FRFs of the coupled structure by using identified joint properties.
(a) $H^C_{yr,yr}$, (b) $H^C_{yr,\theta r}$, (c) $H^C_{\theta r,yr}$, (d) $H^C_{\theta r,\theta r}$

It can be seen from the comparison that the FRFs regenerated by using the joint parameters obtained from identification 1 perfectly match with the actual FRFs. On the other hand, the FRFs regenerated by using the joint parameters obtained from identification 2 have some slight deviations from the actual FRFs, especially at the second and fourth modes. Thus, it can be

concluded that although the accuracy of the identified values for some joint parameters are not so good (when estimated FRFs for RDOF are used), their effect on the system dynamics is not so significant, and therefore the identification method proposed in this study can be used in practical applications for the identification of joint dynamics by using only translational FRF measurements.

4 DISCUSSIONS AND CONCLUSIONS

Substructure decoupling method based on measured and calculated FRFs is used to identify dynamic properties of structural joints. In the approach proposed, FRFs of two substructures connected with a joint are measured, while FRFs of the substructures are obtained analytically. The joint properties expressed in terms of rotational and translational stiffness and damping elements are identified by using FRF based substructure decoupling equations. Three equations are presented for joint identification, each using a different set of FRFs but yielding the same joint properties. If we could have the exact FRF matrices for substructures and coupled structure at any frequency, any of the joint identification equations would give exactly the same and correct result. However, due to using different sets of FRFs in each equation and due to having different measurement noise levels in each type of FRF, it is expected to have different performance from each equation. Indeed, in the case studies presented it is observed that each equation yields different results, and the most accurate results are obtained with the first decoupling equation (equation (5a)). Yet, as expected, when simulated experimental values are used without any pollution, it is shown that all three equations give exactly the same results.

The identification equations can be used with FRFs measured at any frequency, and theoretically the equations are expected to yield the same result at any frequency. However, as the effects of joint dynamics on system response are almost negligible at several frequencies and very much pronounced at some other frequencies, when the equation is used at a frequency where joint properties affect the system response considerably, the computations will be much less sensitive to noise in measurements, and accurate identifications can be made. Since it is not known in advance at which mode the joint dynamics will affect the coupled system dynamics considerably, it is recommended to identify joint properties in a range of frequency and take the average of the values in a region where deviations from a constant value is minimum. It is demonstrated with case studies that quite accurate results can be obtained this way.

An advantage of the proposed method is that identification can be made without using the joint FRFs, which is very useful in practical applications. Yet, the equation which gives the best values for the joint properties is observed to be the one which use joint FRFs (equation 5a) in the case study. In the method proposed, although only the DOFs for selected points of the substructures are used in the formulation, which would reduce the computational effort considerably, all the FRFs for the nodes considered are required. That means we need to measure FRFs for some RDOF. Alternatively, they can be predicted from translational FRFs of the same point and neighbor points. From the case study presented in this work it is observed that using predicted FRFs for RDOF deteriorates the accuracy of the joint parameters identified, especially the accuracy of the rotational and cross-coupled values of the joint stiffness. However, it is further shown in the case study that rotational joint stiffness has small effect, while the cross-coupled joint stiffness has negligible effect on the calculated receptance of the coupled system. Thus, it is concluded that having large errors in the identified values of rotational and especially cross-coupled joint stiffness values will not deteriorate the mathematical model for the joint, as long as translational stiffness of the joint is accurately identified. Note that the maximum error in the translational stiffness value of the joint is found to be less than -10% in the case study presented. Consequently, it can be said that the identification method proposed in this study can be used in practical applications for the identification of joint dynamics from translational FRF measurements taken on the coupled system, along with calculated FRFs of two connected substructures. In the case studies simulated experimental results are used. Although the calculated FRFs for the coupled system are polluted in the examples given here, the theoretical FRFs for substructures are exact values which may not be so in practical applications. Therefore, although the method proposed in this study is very promising to model a structural joint, this conclusion needs to be supported with real experiments.

REFERENCES

[1] Ren Y., Beards C. F., Identification of effective linear joints using coupling and joint identification techniques, Journal of Vibration and Acoustics, v.120, pp.331–338, 1998.

[2] Tsai J. S., Chou Y. F., The identification of dynamics characteristics of a single bolt joint, Journal of Sound and Vibration, v.125(3), pp.487–502, 1988.

[3] Wang J. H., Liou C. M., Experimental identification of mechanical joint parameters, Journal of Vibration and Acoustics, v.113, pp.28–36, 1991.
[4] Hwang H. Y., Identification techniques of structure connection parameters using frequency response functions, Journal of Sound and Vibration, v.212(3), pp.469–79, 1998.
[5] Yang K. T., Park Y. S., Joint structural parameter identification using a subset of frequency response function measurements, Mechanical Systems and Signal Processing, v.7, pp.509–30, 1993.
[6] Ren Y., Beards C. F., On substructure synthesis with FRF data, Journal of Sound and Vibration, v.185(5), pp.845–66, 1995.
[7] Ren Y., Beards C. F., Identification of joint properties of a structure using FRF data, Journal of Sound and Vibration, v.186(4), pp.567–587, 1995.
[8] Celic D., Boltezar M., Identification of the dynamic properties of joints using frequency–response functions, Journal of Sound and Vibration, v.317, pp.158–174, 2008.
[9] Batista F. C., Maia N. M. M., Uncoupling techniques for the dynamic characterization of sub-structures, Conference Proceedings of the Society for Experimental Mechanics Series, v.4, pp.383–392, 2011.
[10] Maia N.M. M., Silva J. M. M., Ribeiro, A. M. R, Silva, P. L.C. G. C., On the dynamic characterization of joints using uncoupling techniques, Proceedings of the 16th International Modal Analysis Conference, pp.1132–1138, 1998.
[11] Yang T., Fan S.H. , Lin C.S., Joint stiffness identification using FRF measurements, Computers and Structures, v.81, pp.2549–2556, 2003.
[12] Hu F., Wu B., Hu Y., Shi T., Identification of dynamic stiffness matrix of bearing joint region, Frontiers of Mechanical Engineering in China, 4(3), 289–299, 2009.
[13] Özşahin O., Ertürk A., Özgüven H. N. and Budak, E., A closed-form approach for identification of dynamical contact parameters in spindle-holder-tool assemblies, International Journal of Machine Tools and Manufacture, v.49, pp.25–35, 2009.
[14] Duarte M. L. M., Ewins D.J., Rotational degrees of freedom for structural coupling analysis via finite-difference technique with residual compensation, Mechanical Systems and Signal Processing, v.14(2), pp.205–227, 2000.
[15] Maia, N. M. M., Silva, J. M. M. (Editors), Theoretical and Experimental Modal Analysis, Research Studies Press, Distribution John Wiley and Sons, 480, 1997.